The Role of TIRR in DNA Damage and Repair



Ruth Frances Ketley
St Anne's College
University of Oxford

A thesis submitted for the degree of
Doctor of Philosophy
Michaelmas 2022

Abstract

The integrity of our DNA genetic code is constantly under threat from a variety of different endogenous and exogenous sources. Failure to accurately repair damage to our DNA can lead to the development of diseases such as cancer. In order to maintain genomic stability, cells possess a network of highly regulated cellular processes which act together to repair DNA, known as the DNA damage response. Many different factors contribute to the repair of DNA lesions, including different proteins and RNA species. A central player in the repair of DNA double strand breaks, a particularly toxic type of DNA damage, is a protein known as 53BP1. The recruitment of 53BP1 to double strand breaks is a highly regulated process, and 53BP1 is constitutively bound by the inhibitor protein TIRR. When a double strand break occurs, TIRR and 53BP1 dissociate, allowing 53BP1 to engage chromatin at the break and function in repair. In Chapter 3 of this thesis, we explore the mechanism of this dissociation, identifying a role for RNA which is transcribed at double strand break itself. We also further characterise the role of TIRR in the wider DNA damage response, firstly in Chapter 4, where we explore the function of TIRR RNA binding in the regulation of RNA processing, and in Chapter 5, where we perform a proximity labelling experiment to identify novel interactors of TIRR. Taken together, this thesis characterises the function of the DNA repair factor TIRR, both as a 53BP1 negative regulator, and as an RNA-binding protein.

Acknowledgements

I would firstly like to thank my supervisor Monika Gullerova for her support and mentorship throughout this DPhil. Thank you for taking a chance on me almost 5 years ago at my DPhil interview, and for your constant understanding, encouragement, and enthusiasm, which has kept me motivated even in the most difficult of times.

I would like to thank Dr Irina Chelysheva for performing all the bioinformatics analysis on the RNA sequencing datasets used in this thesis - without you we would be lost, thank you for all your time, expertise, and helpful discussions. I would also like to thank Dr Marjorie Fournier in the Mass Spectrometry facility for running the protein samples and analysing the mass spectrometry data, and for being patient with my endless questions. Thank you also to Federica for performing the Molecular Dynamics simulations, Esra for helping with the protein purification, and Clémence and Florence for performing the HTRF and SPR assays, which were all important in moving this project forward. Thank you to everyone at the Dunn School who has lent reagents, provided technical assistance, and generally made the department a great place to work.

To the members of the Gullerova lab, thank you for all your input and for making the lab a fun and collaborative environment. In particular, thank you to Adele, my lab wifey, cloning wizard, and provider of snacks. I am grateful to you not just for all your experimental help (especially with cloning and FISH-PLA), but also for listening to me, never making me feel silly for asking questions, and always believing in me even when I didn't believe in myself.

Thank you to my wonderful friends for all their love and support. Naomi, thank you for your kindness and encouragement; Bertina, thank you for all the evenings of good food and laughter; Malitha, thank you for being my cinema buddy for some escapism. My Divinity 15 family, Mei, Selena, and Vineeth. From day one I felt at home with you all – I have so many memories of all the pizza and biryani nights in our run-down living room, trips out for dessert in Mei's car, formal dinners, and even a trip to Sweden. Thank you for being there for me, sharing your wisdom, and always lifting me up. Sanja, from discussions about RNA-binding proteins, to watching countless hours of trashy TV together, you've been an unwavering source of support. Your friendship means the world to me.

Ben, you have been my partner in life for nearly 8 years, even since we met in the first term of our undergraduate degrees. Thank you for always making me laugh after a hard day, for going on adventures with me, and for being there every single step of the way. I would not have been able to do this without you.

To my family, John, Maureen, and James, thank you for all you have done for me. I grew up knowing I would always have the support of my family no matter what I chose to do. I dedicate this thesis to you.

Declaration

I declare that this thesis is entirely my own work unless otherwise stated. Experiments which have been performed by others as part of collaborations have been clearly indicated in **Chapter 2, Materials and Methods**, and in figure legends throughout.

Sections of **Chapter 1, Introduction**, have been taken from publications of which I am either first author and/or have been solely responsible for writing. Specifically, sections from publications 3 and 4 (as listed below) have been adapted/reproduced in this thesis (in **Sections 1.1, 1.2, 1.5,** and **3.3.1**). The data presented in **Chapter 3** has been accepted for publication in Cell Reports (publication 1, as listed below), and data presented in **Chapters 4 and 5** is being prepared as a manuscript for publication. Sections of **Chapter 2, Materials and Methods**, also form part of publication 1.

Word count: 50k (excluding references, appendices, tables, and diagrams).

Publications

1. *DNA double strand break derived RNA drives TIRR/53BP1 complex dissociation.*

   Ketley, R. F., Battistini, F., Alagia A., Mondielli, C., Iehl, F., Balıkçı, E., Huber, K. V. M., Orozco, M., and Gullerova, M. **Cell Reports, 2022.** doi.org/10.1016/j.celrep.2022.111526. This paper contains all data presented in Chapter 3.

2. *Small non-coding vault RNA1-2 modulates expression of cell membrane proteins through nascent RNA silencing.*

   Terenova, J., Alagia A., **Ketley, R. F.**, Chelysheva, I., and Gullerova, M. **BioRxiv, 2022.** doi: 10.1101/2022.08.12.503724.

3. *Proximity Ligation Assay for Detection of R-Loop Complexes upon DNA Damage.*

   Alagia, A., **Ketley, R. F.**, and Gullerova, M. **Methods in Molecular Biology, 2022**. doi: 10.1007/978-1-0716-2477-7_19.

4. *Jack of all trades? The versatility of RNA in DNA double-strand break repair.*

   Ketley, R. F., and Gullerova, M. **Essays in Biochemistry, 2020.** doi: 10.1042/EBC20200008.

5. *Beyond the Trinity of ATM, ATR, and DNA-PK: Multiple Kinases Shape the DNA Damage Response in Concert with RNA Metabolism.*

   Burger, K.*, **Ketley, R. F.***, and Gullerova, M. **Frontiers in Molecular Biosciences, 2019.** doi: 10.3389/fmolb.2019.00061. *Co-first

List of Figures

Figure 1.1: Examples of sources of DNA damage, types of DNA lesions, and different repair pathways which exist in cells.

Figure 1.2: Key steps and proteins involved in NHEJ- and HR-mediated pathways of DSB repair.

Figure 1.3: 53BP1 domain structure and interactors.

Figure 1.4: Crystal structure of TIRR bound to 53BP1 Tudor domain.

Figure 1.5: Overlay of the TIRR monomer with the NUDT16 monomer.

Figure 1.6: Summary of known roles of TIRR within the cell across different cellular compartments.

Figure 1.7: Mechanisms of transcriptional silencing *in cis* to DSBs in transcriptionally active regions of the genome.

Figure 1.8: *De novo* break induced transcription by RNAPII or RNAPIII.

Figure 1.9: Potential mechanisms of R-loop/RNA:DNA hybrid formation at DSBs.

Figure 1.10: The biogenesis and functions of DDRNA.

Figure 2.1: Construction of the plasmids: WT and K10E Neongreen TIRR, 1-211 and 6-211 His-TIRR, and siRNA resistant TIRR.

Figure 2.2: RNA and DNA sequences/structures used in *in vitro* and *in vivo* experiments.

Figure 2.3: Initial unsuccessful purification of 1-211 and 6-211 His-tagged TIRR.

Figure 2.4: Final purification of His-tagged TIRR.

Figure 3.1: The mapped RNA binding site on TIRR from published crosslinking data.

Figure 3.2: The proximity ligation assay to study the TIRR/53BP1 complex.

Figure 3.3: RNA Polymerase II Transcription is required for TIRR/53BP1 dissociation.

Figure 3.4: PLA of TIRR/53BP1 and in the presence of a RNAPIII inhibitor.

Figure 3.5: Surface Plasmon Resonance (SPR) assay with TIRR.

Figure 3.6: EMSA assays with TIRR and 53BP1 Tudor.

Figure 3.7: RNA isolated from damaged cells promotes TIRR/53BP1 separation *in vitro.*

Figure 3.8: Homogeneous Time Resolved Fluorescence (HTRF) assay with TIRR and 53BP1.

Figure 3.9: Transfection of a Cy3 labelled RNA hairpin.

Figure 3.10: The influence of RNA:DNA hybrids on TIRR/53BP1 *in vivo.*

Figure 3.11: Dicer and Drosha, but not DGCR8, are required for TIRR/53BP1 dissociation.

Figure 3.12: TIRR is recruited to DSBs.

Figure 3.13: The interaction of 53BP1 with TIRR is important for the recruitment of TIRR to damage sites.

Figure 3.14: TIRR recruitment to damage sites is dependent on RNA Polymerase II transcription.

Figure 3.15: TIRR and 53BP1 separation is impaired by ATM inhibition.

Figure 3.16: Diagram showing the location of DS1 and DS2, and the design of the FISH PLA assay.

Figure 3.17: FISH-PLA of TIRR and 53BP1 at DS1 and DS2.

Figure 3.18: HADDOCK modelling of TIRR with hairpin RNA.

Figure 3.19: Molecular Dynamics simulations of the TIRR dimer with the RNA hairpin.

Figure 3.20: Molecular Dynamics simulations of the TIRR monomer with the RNA hairpin.

Figure 3.21: Influence of TIRR knockdown on NHEJ and HR as assessed by E5J-GFP and DR-GFP reporter constructs.

Figure 3.22: TIRR is amplified in breast cancers.

Figure 3.23: Model of RNA-mediated TIRR/53BP1 dissociation.

Figure 4.1: Knockdown of TIRR using Sigma Predesigned siRNA in different cell lines.

Figure 4.2: Knockdown of TIRR using Thermo siRNA in different cell lines.

Figure 4.3: Knockdown of TIRR using different RNAi strategies.

Figure 4.4: Rescue of cell death and cell cycle phenotypes using a plasmid expressing an siRNA resistant version of TIRR in Hela cells both transiently and stably.

Figure 4.5: RIP-Seq of RNA bound to TIRR in damage and non-damage conditions.

Figure 4.6: GO analysis of RNA identified in TIRR RIP-Seq.

Figure 4.7: Further analysis of RNAs identified in TIRR RIP-Seq.

Figure 4.8: RNA-Seq in TIRR knockdown with and without damage.

Figure 4.9: GO analysis of differentially expressed (upregulated) RNAs in TIRR knockdown.

Figure 4.10: TIRR contains a predicted NES motif and interacts with XPO1 after damage.

Figure 4.11: Immunofluorescence microscopy of TIRR-GFP and LSM14A after IR.

Figure 4.12: Immunofluorescence microscopy of LSM14A in TIRR knockdown after IR.

Figure 4.13: Immunofluorescence microscopy of TIRR-GFP and G3BP1 after sodium arsenite treatment.

Figure 4.14: Western blot of shGFP and shTIRR samples sent for WCL mass spectrometry analysis.

Figure 4.15: Volcano plots of differentially expressed proteins in WCL mass spectrometry in TIRR knockdown after IR.

Figure 4.16: GO analysis of differentially expressed proteins in TIRR knockdown conditions compared to the GFP control.

Figure 4.17: Overlay of 53BP1 Tudor and TIRR annotated with candidate NES motifs.

Figure 4.18: Potential functions of TIRR in RNA export and RNA processing.

Figure 5.1: Principles of the biotin proximity labelling assay (BioID/TurboID).

Figure 5.2: Overlap of three available datasets/databases of TIRR interactors from Drané et al (2017), Avolio et al (2018), and the BioGRID database.

Figure 5.3: Design of the Flag-tagged TIRR-TurboID (C-terminal) construct and initial expression.

Figure 5.4: Design of the V5-tagged miniTurboID-TIRR (N-terminal) construct and initial expression.

Figure 5.5: Antibiotic selection of miniTurboID and miniTurboID-TIRR expressing Hela cells with 100µg/ml Zeocin.

Figure 5.6: Stable selection of miniTurboID and miniTurboID-TIRR expressing Hela cells after 3 weeks of 100µg/ml or 200µg/ml Zeocin selection.

Figure 5.7: Design of the V5-tagged TurboID-TIRR (N-terminal) construct and initial expression.

Figure 5.8: Stable selection of TurboID only and TurboID-TIRR expressing Hela cells after selection with Hygromycin.

Figure 5.9: Colony screening of TurboID only and TurboID-TIRR cells.

Figure 5.10: Optimisation of biotin concentration and labelling time for Turbo only colony 21 and Turbo-TIRR colony 20.

Figure 5.11: Localisation of Turbo-TIRR in colony 20 cells as assessed by IF.

Figure 5.12: Optimisation of TurboID pull down with streptavidin beads.

Figure 5.13: Enrichment of biotin labelled proteins with streptavidin beads for mass spectrometry.

Figure 5.14: Volcano plot representation of TIRR TurboID samples in –IR and +IR conditions.

Figure 5.15: Comparison of the identified TIRR interactors in TurboID in -IR or +IR conditions.

Figure 5.16: GFP pulldown on GFP and TIRR-GFP expressing Hela cells to identify interactors.

Figure 5.17: Overlap of proteins identified by TIRR-GFP pull-down and mass spectrometry in damage and non-damage conditions.

Figure 5.18: STRING network for proteins bound to TIRR in non-damage and damage in AP-MS.

Figure 5.19: STRING interaction network for proteins identified to interact with TIRR in non-damage conditions in TurboID.

Figure 5.20: STRING interaction network for proteins identified to interact with TIRR in damage conditions in TurboID.

Appendix Figure 1: Control for live laser striping using doxycycline inducible Hela cells expressing GFP only.

Appendix Figure 2: Western blot control and PCA plot of siNeg and siTIRR (Thermo) RNA-Seq samples.

Appendix Figure 3: STRING analysis on downregulated RNAs in siTIRR (Thermo) RNA-Seq.

Appendix Figure 4: STRING analysis on upregulated RNAs in siTIRR (Thermo) RNA-Seq.

List of Tables

Table 1.1: Summary of published literature on TIRR regulation of 53BP1.

Table 1.2: Examples of DSB repair factors and miRNAs which target them.

Table 1.3: Examples of lncRNAs and their functions in DNA repair.

Table 1.4: Summary of proteins involved in DSB-induced transcriptional silencing.

Table 1.5: Summary of proteins with roles in RNA:DNA hybrid/R-loop formation or processing/removal at DSBs.

Table 1.6: Summary of dilncRNA/DART transcription at DSBs and DDRNA processing.

Table 2.1: List of buffers used in this thesis.

Table 2.2: List of primary antibodies used in this thesis.

Table 2.3: List of secondary antibodies used in this thesis.

Table 2.4: List of DNA primers used in this thesis.

Table 2.5: List of plasmids used in this thesis.

Table 2.6: List of siRNA used in this thesis.

Table 2.7: List of RNA and DNA oligonucleotides used in this thesis.

Table 2.8: List of commercially available reagents used in this thesis.

Table 2.9: Typical Q5 Polymerase PCR reaction conditions.

Table 2.10: Typical GoTaq Polymerase PCR reaction conditions.

Table 2.11: Cell lines used in this thesis.

Table 2.12: Cell culture drugs used in this thesis.

Table 2.13: Cell numbers seeded into each well of a 12-well plate for colony formation assays.

Table 2.14: Sequences of DNA probes used in FISH-PLA for DS1 and DS2.

Table 2.15: T4 PNK reaction for radiolabelling RNA and DNA substrates.

Table 3.1: HADDOCK modelling parameters and inputs.

Table 4.1: Differentially expressed proteins identified in whole cell mass spectrometry analysis of TIRR knockdown in damage and non-damage conditions.

Table 5.1: Interactors with TIRR identified using TurboID in damage and non-damage conditions.

Table 5.2: Proteins identified as TIRR interactors in non-damage and damage conditions by GFP affinity pulldown of TIRR-GFP.

List of Abbreviations

IR	Ionising Radiation
4-OHT	4-Hydroxytamoxifen
53BP1	Tumour Suppressor p53-binding Protein 1
Ab	Antibody
AGO2	Argonaute RISC Catalytic Component 2
AID	Activation-Induced Cytidine Deaminase
A-NHEJ	Alternative-NHEJ
AP-MS	Affinity purification mass spectrometry
ARE	AU-rich element
ASOs	Antisense Oligonucleotides
ATM	Ataxia-telangiectasia-mutated
ATR	ATM- and Rad3-Related
BER	Base Excision Repair
BioGRID	Biological General Repository for Interaction Datasets
BIR	Baculovirus IAP repeat
BRCA1	Breast Cancer Gene 1
BRCA2	Breast Cancer Gene 1
BRCT	BRCA1 C-terminal) domains
Bru-Seq	labelling of RNA with Bromouridine followed by sequencing
CAMKKβ	Calcium/calmodulin-dependent protein kinase beta
CBP	CREB Binding Protein
CCR4-NOT	Carbon catabolite repression 4 (CCR4)–negative on TATA-less (NOT) complex
CDS	Coding Sequence
ChIP-Seq	Chromatin Immunoprecipitation and Sequencing
Co-IP	Co-Immunoprecipitation
CPD	Cyclobutane Pyrimidine Dimer
CSB	Cockayne syndrome B
CSR	Class Switch Recombination
CTD	C-terminal domain
CtIP	C-terminal binding protein 1
DARTs	Damage-associated RNA transcripts
DCP1/2	Decapping Protein 1/2
DDR	DNA Damage Response
DDRNA	DNA damage-dependent small RNA
DDX1	DEAD-Box Helicase 1
Depmap	Dependency Map
DGCR8	DiGeorge syndrome critical region 8
diRNA	Dicer-like protein-dependent small RNA
DISC	Double Strand Break Induced Silencing in Cis
DISE	Death induced by survival gene elimination
DMSO	Dimethyl Sulfoxide
DNA	Deoxyribonucleic acid
DNA2	DNA Replication Helicase/Nuclease 2
DNA-PK	DNA-dependent protein kinase
Dox	Doxycycline
DSB	Double Strand Break
dsDNA	Double-strand DNA
dsRNA	Double-stranded RNA
DYNLL1	Dynein Light Chain LC8-Type 1
ELM	Eukaryotic Linear Motif
EMSA	Electrophoretic Mobility Shift Assay
ER	Oestrogen Receptor
ER	Endoplasmic Reticulum
Eto	Etoposide

EU	5-ethynyluridine
EXO1	Exonuclease 1
EXOSC10	Exosome Component 10
EZH2	Enhancer of zeste homolog 2
FASP	Filter Aided Sample Preparation
FC	Fold Change
FDA	Food and Drug Administration
FDR	False Discovery Rate
FISH-PLA	Fluorescence *in situ* Hybridisation Proximity Ligation Assay
FOXK1	Forkhead Box K1
FRAP	Fluorescence Recovery After Photobleaching
FRET	Fluorescence Resonance Energy Transfer assay
FT	Flowthrough
GFP	Green fluorescent protein
GO	Gene Ontology
Gy	Gray (unit)
H2AX	H2A.X Variant Histone
HDAC2	Histone Deacetylase 2
HITT	HIF-1a inhibitor at translational level
HNRNP	Heterogeneous Nuclear Ribonucleoprotein
HR	Homologous Recombination
HTRF	Homogeneous Time Resolved Fluorescence
HU	Hydroxyurea
HuR/ELAV1	Human antigen R / ELAV-like protein 1
IAP	Inhibitors of Apoptosis
iCLIP-Seq	Individual-nucleotide resolution Cross-Linking and Immunoprecipitation
IDP/ITP	Inosine di/triphosphate
IF	Immunofluorescence
Ig	Immunoglobulin
IPTG	Isopropyl β- d-1-thiogalactopyranoside
IRIF	Ionising Radiation Induced Foci
JMJD2A	Jumonji domain-contain protein 2A
kb	Kilobase
Kd	Binding Affinity
KIF18B	Kinesin Family Member 18B
L3MBTL1	Lethal(3)Malignant Brain Tumour-Like Protein 1
LIG1	DNA ligase 1
LIG3	DNA ligase 3
LIG4	DNA Ligase 4
LINP1	LncRNA in non-homologous end joining pathway
LMB	Leptomycin B
lncRNA	Long non-coding RNA
m^1A	N1-methyladenosine
m^5C	5-methylcytosine
m^6A	N6-methyladenosine
MD	Molecular Dynamics
MDC1	Mediator Of DNA Damage Checkpoint 1
miRNA	MicroRNA
MMSET	Multiple Myeloma SET Domain
mRNA	Messenger RNA
MS	Mass Spectrometry
MWCO	Molecular Weight cut-off
NBS1	Nibrin
ncRNA	Non-coding RNA
NER	Nucleotide Excision Repair
NES	Nuclear Export Sequence
NHEJ	Non-homologous End Joining
NLS	Nuclear Localisation Sequence

NMD	Nonsense-mediated RNA decay
NPC	Nuclear Pore Complex
NSAF	Normalised Spectral Abundance
nt	Nucleotide
NUDIX	Nucleoside Diphosphate linked to another moiety X
NUDT16	Nudix Hydrolase 16
NUDT16L1	Nudix Hydrolase 16 Like 1
NuMA	Nuclear Mitotic Apparatus Protein
NUP153	Nucleoporin 153
OD	Oligomerisation Domain
ORCS	Open Repository of CRISPR screens
p53	Tumour protein P53
PABP	Poly(A) binding protein
PAR	Poly(ADP-ribose)
PARP1	Poly(ADP-Ribose) Polymerase 1
PARPi	PARP inhibitors
PBS	Phosphate Buffered Saline
PBs	Processing bodies (P-bodies)
PCA	Principal Component Analysis
PCR	Polymerase Chain Reaction
PDB	Protein Data Bank
PIC	Pre-Initiation Complex
PKC	Protein Kinase C
PLA	Proximity Ligation Assay
POI	Protein of Interest
PP4C	Protein phosphatase 4 catalytic subunit
PPI	Protein-protein interaction
PRC1/2	Polycomb repressive complex 1/2
pri-miRNA	Primary microRNA
PRLH1	P53-regulated lncRNA for HR repair 1
PTEN	Phosphatase And Tensin Homolog
PTM	Post-translational modification
RAN	Ras-related nuclear protein
RBP	RNA-binding protein
RIF1	Replication Timing Regulatory Factor 1
RIP-Seq	RNA immunoprecipitation sequencing
RISC	RNA-induced silencing complex
Rmax	Maximum Response
RMSD	Root Mean Square Deviation
RNA	Ribonucleic acid
RNAi	RNA interference
RNAPII	RNA Polymerase II
RNAPIII	RNA Polymerase III
RNA-Seq	RNA sequencing
RNF8/168	Ring Finger Protein 8/168
ROS	Reactive oxygen species
RPA	Replication protein A
rRNA	Ribosomal RNAs
RU	Response Units
SA	Sodium Arsenite
SCAI	Suppressor Of Cancer Cell Invasion
scaRNA2	Small Cajal body-associated RNA 2
SD	Standard Deviation
SDOS	Syndesmos
SEC	Super Elongation Complex
SENP1	SUMO Specific Peptidase 1
SET8	SET domain-containing protein 8
SETX	Senataxin

SGs	Stress granules
shRNA	Short hairpin RNA
siRNA	Short interfering RNA
SnoRNA	Small nucleolar RNA
SPR	Surface Plasmon Resonance
SSA	Single Strand Annealing
ssDNA	Dingle-strand DNA
ssRNA	Single-stranded RNA
STRING	Search Tool for the Retrieval of Interacting Genes/Proteins
T4 PNK	T4 polynucleotide kinase
TIRR	Tudor-interacting repair regulator
TRAP1	TNF Receptor Associated Protein 1
TRE	Tetracycline Response Element
TREX	Transcription-Export complex
TRiC	T-complex protein Ring Complex
tRNA	Transfer RNA
UDR	Ubiquitin-Dependent Recruitment
USP28	Ubiquitin Specific Peptidase 28
UTR	Untranslated Region
UV	Ultraviolet
VCP	Valosin-containing protein
VDJ	Variability, Diversity, and Joining
WCL	Whole Cell Lysate
XLF	XRCC4-like factor
XPO1/CRM1	Exportin-1
XPO5	Exportin-5
XRCC1	X-ray repair cross-complementing protein 1
XRCC4	X-Ray Repair Cross Complementing 4
YFP	Yellow fluorescent protein
Ψ	Pseudouridine

Table of Contents

ABSTRACT
ACKNOWLEDGEMENTS
DECLERATION
PUBLICATIONS
LIST OF FIGURES
LIST OF TABLES
LIST OF ABBREVIATIONS
TABLE OF CONTENTS

CHAPTER 1: INTRODUCTION 1

1.1 THE DNA DAMAGE RESPONSE 1
1.2 DNA DOUBLE STRAND BREAKS 3
1.2.1 Non-Homologous End Joining 3
1.2.2 Homologous Recombination 4
1.2.3 Single Strand Annealing and Alternative End Joining 5
1.3 P53-BINDING PROTEIN 1 (53BP1) 6
1.3.1 53BP1 domain structure and function 6
1.3.2 Regulation of 53BP1 recruitment to DSBs 8
1.3.3 53BP1 Downstream Regulation 13
1.3.4 53BP1 and PARP inhibitor resistance 14
1.4 TUDOR INTERACTING REPAIR REGULATOR (TIRR) 16
1.4.1 TIRR is a 53BP1 binding partner and regulates 53BP1 functions 16
1.4.2 TIRR is a paralogue of NUDT16 20
1.4.3 The role of TIRR at the plasma membrane 22
1.4.4 TIRR is an RNA binding protein involved in translation 22
1.5 THE RNA-DEPENDENT DNA DAMAGE RESPONSE 24
1.5.1 MicroRNA in DSB Repair 24
1.5.2 Long Non-Coding RNA in DSB Repair 26
1.5.3 Transcriptionally active regions: HR vs NHEJ 29
1.5.4 Double Strand Break Induced Silencing in cis 30
1.5.5 Transcription initiation at DSBs 37
1.5.6 R-loops and RNA:DNA hybrids in DSB repair 41
1.5.7 Non-canonical roles of Dicer and Drosha in the RNA-dependent DDR 50
1.5.8 RNA-templated DSB Repair 60
1.5.9 RNA modifications in DSB Repair 61
1.5.10 RNA may promote phase separation of DSB foci 62
1.6 SUMMARY AND OVERVIEW OF THIS THESIS 63
1.7 REFERENCES 64

CHAPTER 2: MATERIALS AND METHODS 70

2.1 MATERIALS 70
2.1.1 Buffers 70
2.1.2 Primary Antibodies 70
2.1.3 Secondary Antibodies 71
2.1.4 Primers 71
2.1.5 Plasmids 73
2.1.6 Short Interfering RNA (siRNA) 75
2.1.7 RNA and DNA oligonucleotides 75
2.1.8 Other commercially available reagents 76
2.2 METHODS 79
2.2.1 Bacterial Transformation and Culture 79
2.2.2 Preparation of Plasmid DNA 79
2.2.3 Restriction Enzyme Digestion 79
2.2.4 Agarose Gel Electrophoresis 79
2.2.5 Gel Extraction 80
2.2.6 Gibson Assembly 80
2.2.7 Polymerase Chain Reaction (PCR) 80

2.2.8 DpnI treatment and ligations 80
2.2.9 Colony PCR 81
2.2.10 Sanger Sequencing 81
2.2.11 Tissue Culture and Drug incubations 82
2.2.12 Ionising Radiation 83
2.2.13 RNA transfection using Lipofectamine RNAimax 83
2.2.14 Plasmid transfection using Lipofectamine 3000 83
2.2.15 Colony Formation Assays 84
2.2.16 Edu Labelling 85
2.2.17 Cell Cycle Analysis by Flow Cytometry 85
2.2.18 Live cell imaging and laser striping 85
2.2.19 Whole Cell Lysis and Protein Quantification 86
2.2.20 Nuclear Fractionation 86
2.2.21 RNA Extraction 86
2.2.22 Bleach Agarose Gel 87
2.2.23 RNA sequencing 87
2.2.24 Western Blotting 87
2.2.25 Co-Immunoprecipitation (Co-IP) 88
2.2.26 Immunofluorescence (IF) 88
2.2.27 Proximity Ligation Assay (PLA) 89
2.2.28 Fluorescence in situ Hybridisation Proximity Ligation Assay (FISH-PLA) 90
2.2.29 E5J-GFP and DR-GFP Reporter Cells Lines 92
2.2.30 RNA Immunoprecipitation and sequencing (UV RIP-Seq) 92
2.2.31 TurboID Proximity Ligation Assay and On-Bead Digestion 93
2.2.32 TIRR-GFP Affinity Pull-down Mass Spectrometry and digestion 94
2.2.33 Whole cell lysate preparation for Mass Spectrometry 95
2.2.34 Filter Aided Sample Preparation, Trypsin Digestion, and LC-MS/MS 95
2.2.35 5' End Labelling of RNA and DNA substrates 97
2.2.36 Annealing of RNA and DNA substrates 97
2.2.37 Electrophoretic Mobility Shift Assay (EMSA) 97
2.2.38 In vitro RNA separation assays 98
2.2.39 Homogeneous Time Resolved Fluorescence (HTRF) 98
2.2.40 Surface Plasmon Resonance (SPR) 100
2.2.41 Protein purification of 1-211 and 6-211 Thrombin His-TIRR 100
2.2.42 Protein purification 1-211 His-TIRR (final) 103
2.2.43 HADDOCK modelling 105
2.2.44 Molecular Dynamics Simulations 105
2.2.45 Data and Statistical Analysis 106
2.3 REFERENCES 110

CHAPTER 3: THE ROLE OF RNA IN THE SEPARATION OF TIRR AND 53BP1 AFTER DNA DOUBLE STRAND BREAKS 112

3.1 SUMMARY 112
3.2 INTRODUCTION 113
3.3 RESULTS 115
3.3.1 TIRR and 53BP1 separate after damage 115
3.3.2 RNA Polymerase II transcription, but not RNA polymerase III, is required for TIRR and 53BP1 dissociation after damage 116
3.3.3 TIRR binds preferentially to single strand and hairpin RNA 120
3.3.4 TIRR binds to single strand and hairpin RNA, but 53BP1 Tudor does not 122
3.3.5 RNA extracted from cells can separate the TIRR/53BP1 complex 126
3.3.6 Hairpin RNA can dissociate the TIRR and 53BP1 complex 127
3.3.7 Hairpin RNA can separate TIRR and 53BP1 in vivo 129
3.3.8 RNA:DNA hybrids do not appear to play a role in TIRR/53BP1 dissociation in vivo 133
3.3.9 Dicer and Drosha, but not DGCR8, are required for TIRR/53BP1 dissociation 136
3.3.10 TIRR is recruited to the sites of DNA damage 138
3.3.11 The interaction of 53BP1 with TIRR is required for the recruitment of TIRR to damage sites 142
3.3.12 TIRR recruitment to damage sites is dependent on RNA Polymerase II transcription 145
3.3.13 Coordination with ATM signalling 148
3.3.14 TIRR is in proximity to DSB-derived RNA 149

3.3.15 HADDOCK modelling of TIRR with RNA 155
3.3.16 Molecular Dynamics simulations of TIRR with hairpin RNA 159
3.3.17 TIRR knockdown impairs HR 164
3.4 DISCUSSION 166
3.4.1 RNA can play a role in the dissociation of TIRR and 53BP1 166
3.4.2 How does RNA outcompete 53BP1 binding to TIRR? 167
3.4.3 Would breaks produced in any genomic location result in RNA-mediated separation of TIRR and 53BP1? 168
3.4.4 What exactly RNA produced at breaks looks like remains enigmatic 169
3.4.5 What role do Dicer and Drosha play in TIRR/53BP1 dissociation? 171
3.4.6 Dissociation of the TIRR/53BP1 complex likely happens in proximity to the break, but what signalling pathways are involved in their recruitment? 173
3.4.7 How does other RNA in the cell not influence TIRR and 53BP1 binding: A possible role for RNA modifications? 174
3.4.8 The significance of understanding TIRR/53BP1 separation: TIRR is amplified in breast cancers .. 175
3.4.9 Outstanding questions and limitations of the study 177
3.5 REFERENCES 180

CHAPTER 4: THE WIDER INFLUENCE OF TIRR ON DNA DAMAGE AND REPAIR 183

4.1 SUMMARY 183
4.2 INTRODUCTION 184
4.3 RESULTS 189
4.3.1 Optimising the knockdown of TIRR 189
4.3.2 TIRR binds RNA involved in RNA metabolism and RNAPII transcription 199
4.3.3 TIRR does not broadly influence steady state RNA levels in damage and non-damage conditions 205
4.3.4 TIRR contains a predicted nuclear export signal and interacts with XPO1 in damage conditions .. 210
4.3.5 TIRR regulates the formation of Stress Granules and P-Bodies 213
4.3.6 TIRR can regulate the protein levels of proteins involved in RNA metabolism and DNA damage 219
4.4 DISCUSSION 228
4.4.1 Considerations when selecting appropriate knockdown methods for a protein of interest 228
4.4.2 TIRR binds to many different RNA in damaged cells 230
4.4.3 TIRR can interact with XPO1 after damage 231
4.4.4 TIRR can regulate the formation of cytoplasmic RNA granules after stress 235
4.4.5 TIRR broadly does not influence steady state levels of RNA 239
4.4.6 TIRR can regulate the protein levels of proteins involved in RNA metabolism and DNA damage 240
4.4.7 Future work 242
4.5 REFERENCES 245

CHAPTER 5: IDENTIFYING NOVEL BINDING PARTNERS OF TIRR IN NON-DAMAGE AND DAMAGE CONDITIONS 248

5.1 SUMMARY 248
5.2 INTRODUCTION 249
5.3 RESULTS 255
5.3.1 Optimising the expression of TIRR with a Biotin Ligase 255
5.3.2 Generating stable cell lines expressing TurboID-TIRR and TurboID only 261
5.3.3 Optimisation of TurboID experimental conditions 264
5.3.4 Mass Spectrometry of Turbo-TIRR 269
5.3.5 Affinity Pulldown Mass Spectrometry with TIRR-GFP 275
5.4 DISCUSSION 278
5.4.1 Considerations when designing a biotin proximity labelling assay to identify interaction partners 278
5.4.2 Comparing TurboID and AP-MS 280
5.4.3 Identification of novel binding partners of TIRR in non-damage and damage using TurboID 283
5.4.4 What do the identified binding partners or proteins in proximity tell us about TIRR functions in non-damage and damage? 286
5.4.5 Future work 288
5.5 REFERENCES 291

CHAPTER 6: OVERALL DISCUSSION AND PERSPECTIVES 293

6.1 A DIVERSE ARRAY OF DIFFERENT RNAS AND RNA BINDING PROTEINS CAN FUNCTION IN THE DNA DAMAGE RESPONSE 293

6.2 SUMMARY OF EXPERIMENTAL FINDINGS 295
6.3 REMAINING QUESTIONS 297
6.4 FINAL REMARKS 300
6.5 REFERENCES 301
APPENDIX 302

Chapter 1: Introduction

1.1 The DNA Damage Response

Our genome is constantly exposed to both exogenous and endogenous genomic threats, such as ionising radiation (IR), Ultraviolet (UV) radiation, reactive oxygen species (ROS), and stalled replication forks, which can lead to a variety of different DNA lesions. These lesions include DNA crosslinks, mismatches, and single and double strand breaks. Failure to repair DNA damage can result in detrimental consequences for the cell, such as disrupted DNA replication, transcription, and cell division, which can lead to mutations, cell death, and diseases such as cancer. In order to deal with DNA damage, a highly regulated and complex network of processes known collectively as the DNA Damage Response (DDR) acts to sense and repair DNA damage[1,2]. Different DNA lesions activate specific pathways to repair the damage and accurately restore genomic information[1] (**Figure 1.1**).

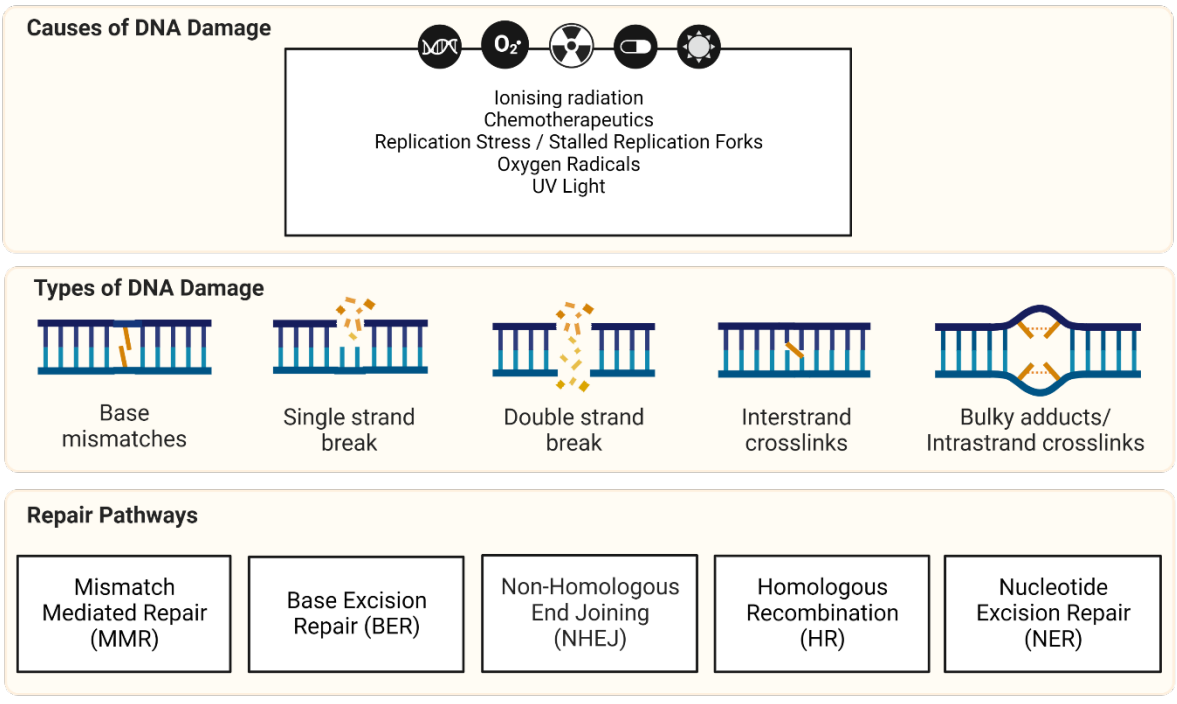


Figure 1.1: *Examples of sources of DNA damage, types of DNA lesions, and different repair pathways which exist in cells. DNA damage by endogenous and exogenous sources can result in lesions such as mismatches, crosslinks, and single and double strand breaks. Many different pathways exist to repair DNA damage depending on the type of lesion, including Mismatch Repair, Base Excision Repair, and Non-Homologous End Joining and Homologous Recombination. Image created with BioRender.com.*

1.2 DNA Double Strand Breaks

DNA double strand breaks (DSBs), where both strands of the DNA double helix are broken, are considered to be one of the most harmful forms of DNA damage. In order to repair genomic insults such as DSBs, the cell possesses two key pathways, Homologous Recombination (HR) and Non-Homologous End Joining (NHEJ) (**Figure 1.2**)[2,3]. The critical difference between HR and NHEJ pathway choice is the requirement of 5' → 3' DNA end resection at the break ends for HR, and the prevention of end resection for NHEJ. Antagonism between Tumour Suppressor p53-binding Protein 1 (53BP1, anti-resection) and Breast Cancer Gene 1 (BRCA1, pro-resection), coupled with the cell cycle phase, and other factors such as transcriptional status, dictates by which pathway the break is repaired[4].

1.2.1 Non-Homologous End Joining

NHEJ is a repair pathway active in the G1, S, and G2 phases of the cell cycle. Initially, Ku, a heterodimer of Ku70/Ku80, binds to the dsDNA ends of the DSB, recruiting DNA-PKc, forming the DNA-PK complex. DNA-PK can then recruit end-processing and ligation factors, including Polymerases μ and λ, Artemis, XRCC4, PAXX, LIG4, and XLF, which facilitate re-joining of the DSB end (**Figure 1.2**)[5]. Many DSB ends are unable to be directly ligated together without end processing by nucleases such as Artemis and polymerases, as ends often contain modifications or overhangs. Consequently, end processing can lead to loss of genetic information[6].

The majority of DSBs in cells, around 70%, are repaired by Ku-mediated NHEJ in a rapid manner, including in S/G2. This rapid repair is thought to be enabled by the high abundance of Ku within cells, and the ability of Ku and DNA-PKc to act a barrier to end resection[7]. The remaining DSBs in G1, around 20%, are repaired by a slower process of NHEJ, dependent on

Artemis, and in G2, around 30% of DSBs are repaired by HR. 53BP1 is considered to be pro-NHEJ and act as a barrier to end resection required for HR (**Section 1.3**), however the kinetics of IR-induced DSB repair mediated by Ku and DNA-PKc are largely unaffected by 53BP1 depletion[8]. Nevertheless, 53BP1 can be recruited to DSB ends in G1 and G2 and is suggested to promote Ku maintenance at DSBs, prevent end-resection, and can be displaced by BRCA1 in S/G2 (**Section 1.3.3**)[9].

1.2.2 Homologous Recombination

HR is an active DSB repair pathway in the S and G2 phases of the cell cycle, when a sister chromatid repair template with sufficient homology is present, and is a more accurate pathway of DSB repair compared to NHEJ[10]. HR requires 5' → 3' end resection generating 3' single stranded DNA overhangs. MRE11 activity, part of the MRN complex (MRE11-RAD50-NBS1), results in removal of Ku from DSB ends[7]. MRE11 possesses both endonuclease and 3' → 5' exonuclease activity, and MRE11 can therefore nick downstream of the DSB using endonuclease activity, followed by 3' → 5' exonucleolytic degradation towards the break end. CtIP is an interacting partner and licensing factor of MRE11, and stimulates MRE11 endonuclease activity[9]. EXO1 and DNA2, 5' → 3' exonucleases, are then recruited by the MRN complex and perform longer-range end-resection away from the break. Replication protein A (RPA) binds the 3' ssDNA overhangs generated by end resection. Subsequently, BRCA1 and BRCA2 help facilitate RAD51 displacement of RPA and the loading of RAD51 onto the ssDNA[5,11]. The RAD51-ssDNA nucleofilament then searches for homology and invades the homologous DNA duplex, which then undergoes resolution for accurate DSB repair (**Figure 1.2**)[11].

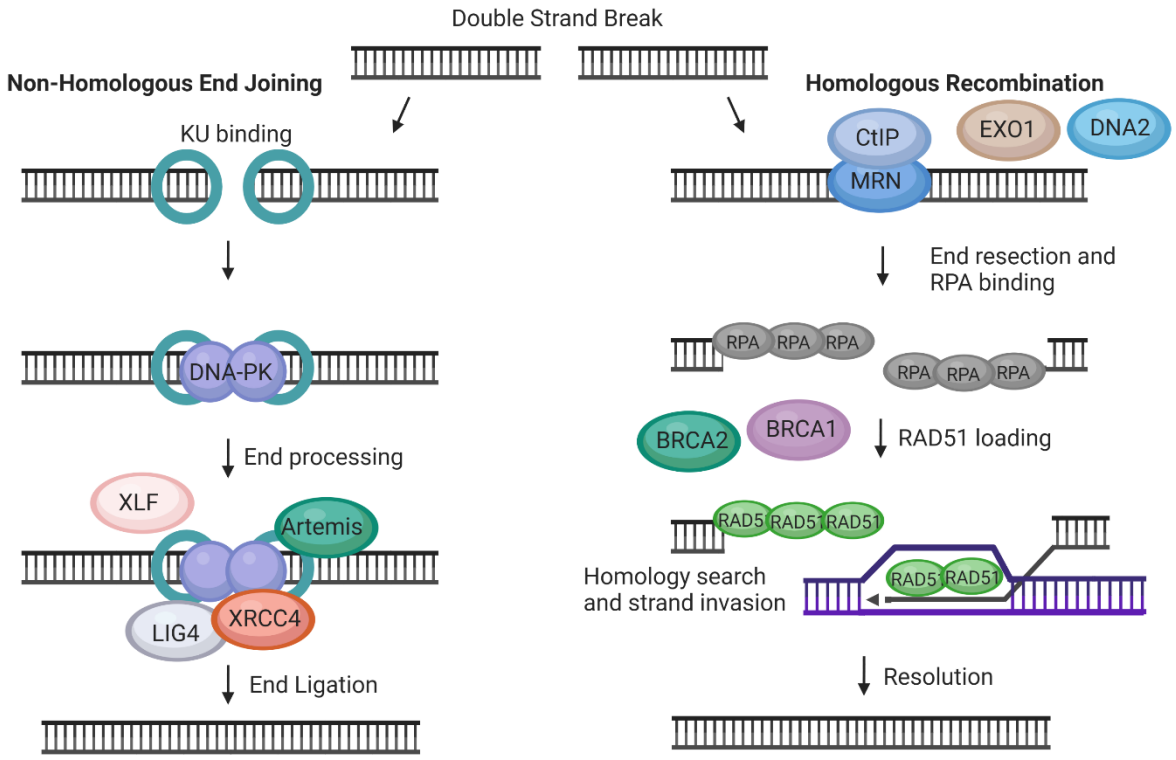


Figure 1.2: *Key steps and proteins involved in NHEJ- and HR-mediated pathways of DSB repair*[2]*. Image created with BioRender.com.*

1.2.3 Single Strand Annealing and Alternative End Joining

In addition to HR and NHEJ, cells are also able to utilise 'alternative' error-prone pathways of DSB mediated repair. Alternative-NHEJ (A-NHEJ), which requires short-range end resection, and single strand annealing (SSA), which requires more extensive end resection, can also be used instead of HR[12]. A-NHEJ involves short range resection by MRE11, and the activities of XRCC1, LIG1/3, Polymerase θ, and PARP1, can then promote annealing through microhomologies[5]. When HR is compromised, SSA is facilitated through long range resection by MRE11, EXO1, and DNA2 activities. In SSA, unlike HR, no strand invasion occurs resulting in a RAD51-independent process, with RAD52 responsible for the annealing step[5].

1.3 P53-binding protein 1 (53BP1)

1.3.1 53BP1 domain structure and function

In response to DSBs, the MRN complex senses DNA damage and activates Ataxia-Telangiectasia mutated (ATM) kinase. ATM kinase is autophosphorylated at S1981 and phosphorylates the MRN complex and H2AX at S139 (γH2AX). This results in the recruitment of MDC1, followed by RNF8 and RNF168. RNF8 and RNF168 are ubiquitin ligases, which ubiquitinate H2AK15[11]. 53BP1, despite having no enzymatic activity, contains multiple domains which mediate 53BP1 function through interactions with other proteins[11]. 53BP1 is recruited to DSBs and recognises two chromatin marks; the constitutive H4K20me2 through the Tudor domain, and the damage-dependent H2AK15Ub through the Ubiquitin-Dependent Recruitment (UDR) domain. 53BP1 also has 28 S/TQ ATM phosphorylation sites at the N-terminus, the first eight of which are required for the interaction with PTIP, which recruits the nuclease Artemis for DSB end processing for NHEJ[4,13]. Sites nine to fifteen are required for RIF1 interaction, which recruits downstream factors to prevent end resection, such as Shieldin (**Section 1.3.3**)[9,11]. The BRCT domains at the 53BP1 C-terminus mediate 53BP1 interactions with p53, but are not required for recruitment to DSBs, and instead promote p53 transcriptional responses after IR[14]. The minimum region required for 53BP1 recruitment to DSBs, known as the minimum focus forming region or ionising radiation induced foci (IRIF) region, is composed of the LC8, the oligomerisation domain (OD), the tandem Tudor domains, and the UDR[11] (**Figure 1.3**).

The balance of 53BP1 and BRCA1 is considered key to the choice of repair pathway, although both 53BP1 and BRCA1 recruitment to DSBs is mediated by the same upstream pathway involving RNF168 ubiquitination of H2AK15Ub[15]. Using super-resolution microscopy, analysis of individual IRIF allows the observation of 53BP1 and BRCA1 recruitment

dynamics[16]. Consistent with NHEJ activity in G1 of the cell cycle, 53BP1, but not BRCA1, is recruited to DSBs predominantly in G1 phase. During S and G2, BRCA1 is also recruited to the DSB, resulting in 53BP1 'repositioning', that is 53BP1 exclusion from the centre of IRIF to the periphery, and increased occupancy of BRCA1 at the centre of IRIF, illustrating the antagonistic relationship between BRCA1 and 53BP1[16].

53BP1 plays a general role in limiting end resection, not only in G1 to promote NHEJ, but also in S/G2 phase to prevent hyper-resection which favours mutagenic SSA over the more accurate HR[12]. Inhibition of 53BP1 results in hyper-resection of DSB ends, which actually promotes RAD52-mediated single strand annealing, rather than HR[12], and somewhat paradoxically, 53BP1 appears to actually be required for RAD51 foci formation. Therefore, it is suggested that 53BP1 can limit hyper-resection and RAD52 loading and allows RAD51-mediated HR[12].

53BP1 therefore plays an important role in DNA end joining at pathological DSBs such as those induced by IR. However, 53BP1 is essential for programmed pathways of DSB generation which facilitate the diversification of the antigen receptors; Class Switch Recombination (CSR)[17] and long range VDJ recombination. Briefly, CSR occurs when activation-induced cytidine deaminase (AID) induces DSBs in the immunoglobulin heavy-chain (IgH) locus at multiple sites, leading to deletions and diversification of the antibody repertoire[10]. In VDJ recombination, RAG-1 and RAG-2 cleave at sites flanking the variable (V), diversity (D), and joining (J) segments in IgG heavy and light chains, and T cell receptor α, β, and δ chains[18].

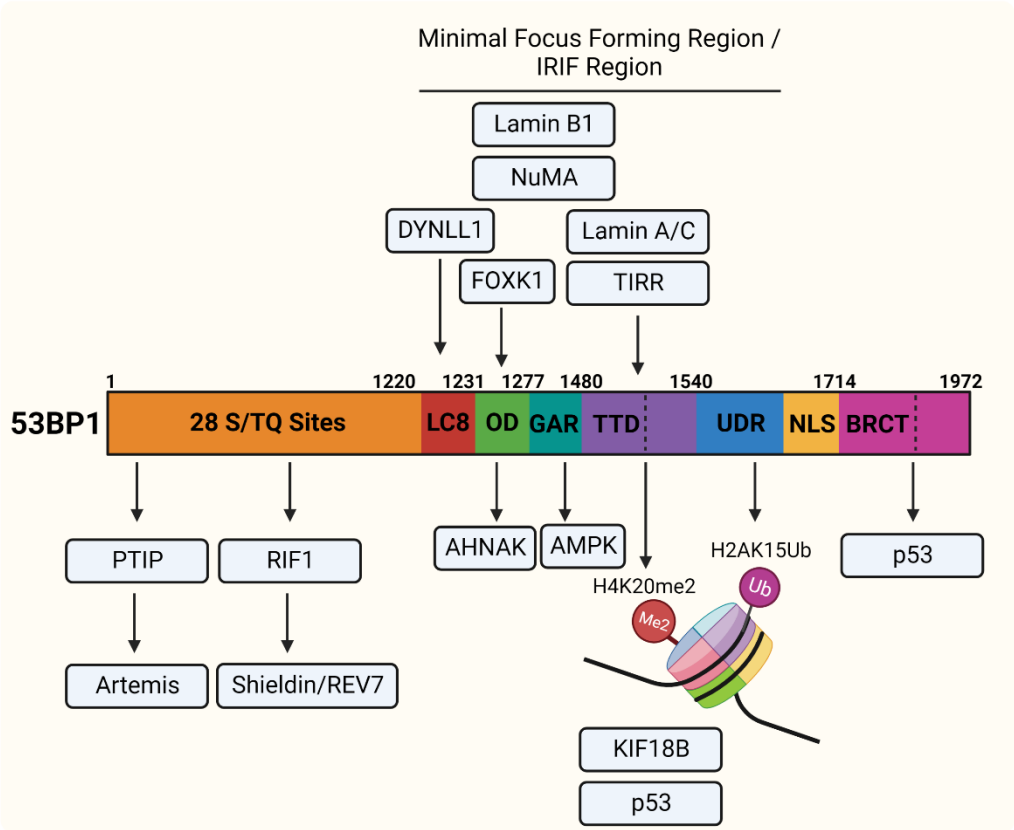


Figure 1.3: *53BP1 domain structure with the minimal focus forming region highlighted. Examples of 53BP1 interactors with each of these domains are shown*[19]*. Image created with BioRender.com.*

1.3.2 Regulation of 53BP1 recruitment to DSBs

Regulation of 53BP1 recruitment to chromatin at DSBs is tightly controlled at multiple levels, including chromatin modification status, 53BP1 post-translational modification, and interaction with 53BP1-binding partners[20].

Chromatin Status

53BP1 binding to both H4K20me2 and H2AK15Ub is critical for 53BP1 association with chromatin. Regulation of 53BP1 access to chromatin can be influenced by proteins which mask H4K20me2, other chromatin marks which reduce the interaction of the 53BP1 Tudor domain with H4K20me2, and coupling of H4K20me2 levels to the cell cycle.

H4K20me2 is a constitutive chromatin mark which is broadly not influenced by DNA damage[21]. However, it has been shown that the histone methyltransferase MMSET is recruited to DSBs through interaction with MDC1 mediated by the ATM phosphorylation of MMSET. MMSET can methylate H4K20 at DSB sites, increasing the local concentration of H4K20me2 to promote 53BP1 recruitment, while the global H4K20me2 levels remain consistent in non-damage and damage conditions[21]. Jumonji domain-contain protein 2A (JMJD2A/KDM4A) and Lethal(3)Malignant Brain Tumour-Like Protein 1 (L3MBTL1) bind H4K20me2 in the absence of DNA damage, masking H4K20me2 and preventing 53BP1 binding to chromatin. In response to DSBs, the recruitment of RNF8 facilitates ubiquitination of L3MBTL1. The ATPase VCP and cofactors NPL4 and UFD1 are recruited to DSBs by the ubiquitination activity of RNF8, and can then evict ubiquitinated L3MBTL1 from H4K20me2 chromatin, allowing 53BP1 to bind[22]. JMJD2A is ubiquitinated by RNF8 and RNF168 in response to DSBs, triggering proteasomal degradation of JMJD2A and subsequent unmasking of H4K20me2[23].

The levels of H4K20me2 are also linked to the cell cycle. As the genome is replicated and cells progress from G1 into S/G2 phases of the cell cycle, the relative amount of H4K20me2 declines, which correlates with 53BP1 and RIF1 foci accumulation, despite ɣH2AX and H2AK15Ub levels remaining unchanged across G1 to S. The methyltransferase SET8, which methylates H4K20, is degraded as cells progress into S phase and therefore limits H4K20me2 deposition on newly replicated chromatin. An increase in BRCA1 accumulation after IR can also be seen during S phase, highlighting the relationship between H4K20me2 levels and the balance between 53BP1 and BRCA1 recruitment[24].

Moreover, the acetyltransferase TIP60/KAT5, part of the NuA4 chromatin remodelling complex, acetylates histone H4 at K16, which disrupts the interaction of the 53BP1 Tudor with H4K20me2. Acetylation can also promote BRCA1 recruitment, and as such acetylation can contribute to the regulation of both 53BP1 and BRCA1 recruitment. At shorter time points after DNA damage, deacetylation of H4K16 by deacetylases HDAC1 and HDAC2 allows the recruitment of 53BP1 to H4K20me2, but acetylation increases at longer time points after damage, paralleling the recruitment of BRCA1. Interestingly, H4K16Ac is also associated with regions of active transcription, and DSBs occurring in transcriptionally active regions showed increased levels of H4 acetylation and BRCA1[25], linking transcriptional status with repair pathway choice (**Section 1.5.3**).

Post-Translational Modification

53BP1 is an extensively post-translationally modified protein both in non-damage and damage conditions, including by phosphorylation[26], acetylation[25], ubiquitination[27], and sumoylation[28], regulating recruitment of 53BP1 to chromatin. For example, in non-damage conditions, 53BP1 can be acetylated by the acetyltransferase CBP in the UDR at residues K1626/1628, which prevents 53BP1 interaction with chromatin. However, in response to IR, HDAC2 is phosphorylated by ATM and can deacetylate 53BP1, releasing this barrier to recruitment[29]. The interaction of HDAC2 and 53BP1 is also cell cycle regulated and enhanced in G1, and consequently 53BP1 acetylation is highest in S phase and lower in G1[29].

Increasing evidence has also suggested a role for the nuclear pore complex (NPC) in DNA repair[28]. Nucleoporin NUP153 is important for nuclear import of 53BP1, as well as for sumoylation of 53BP1, a PTM which is required for 53BP1 recruitment to DSBs[28]. Mechanistically, NUP153 interacts with SENP1, a SUMO protease, which modifies 53BP1

with SUMO1. SUMO1 modification of 53BP1, and subsequently foci formation, is reduced when NUP153 is depleted. Therefore, NUP153 at the nuclear pore regulates 53BP1 function in DSB repair via both promoting nuclear import and sumoylation for recruitment[28].

53BP1 Binding Partners

A variety of different 53BP1 binding partners have been identified as interacting with 53BP1 to either promote recruitment to DSBs or restrain 53BP1 binding to chromatin. The binding partners discussed below and the regions on 53BP1 with which they interact are summarised in **Figure 1.3**.

Examples of negative regulators of 53BP1 which act through direct interaction include Lamin B1, Lamins A/C, NuMA, AHNAK, and FOXK1. Lamin B1, a nuclear structural protein, interacts with 53BP1 via the IRIF region in non-damage conditions, and this interaction is reduced after IR by ATM phosphorylation of 53BP1. The overexpression of Lamin B1 prevents 53BP1 foci formation, and impairs NHEJ[20]. Additionally, Lamins A/C also bind to 53BP1 via the Tudor domain, and this interaction is reduced after IR, also dependent on ATM phosphorylation. Lamin A/C depletion also leads to decreased 53BP1 protein stability due to proteasomal degradation, and consequently Lamin A/C depletion results in increased cellular sensitivity to IR[30]. NuMA, another nuclear structural protein, also binds 53BP1 in non-damage conditions via the focus forming region of 53BP1. The 53BP1/NuMA interaction is reduced after IR, dependent on ATM phosphorylation of NuMA, and NuMA depletion promotes 53BP1 foci formation after IR[31]. Furthermore, the scaffolding protein AHNAK interacts with 53BP1 via the OD in G1, however this interaction is increased by IR and is also ATM-mediated. AHNAK acts to restrain 53BP1 accumulation on chromatin, including in non-damage conditions, but this is enhanced after DNA damage[32]. The transcription factor FOXK1

negatively regulates 53BP1 independently of its transcription regulation function by interacting with the 53BP1 oligomerisation domain predominantly in S-phase of the cell cycle. This interaction is enhanced by IR mediated by ATM, and prevents 53BP1 accumulation at DSBs. The overexpression of FOXK1 also impairs 53BP1 foci formation and promotes HR[33].

Not all 53BP1 interactors are negative regulators of recruitment, with many binding partners helping facilitate or stabilise 53BP1 binding on chromatin, such as AMPK and KIF18B. The kinase AMPK interacts with 53BP1 after IR and acts to promote 53BP1 recruitment to chromatin. AMPK is phosphorylated and activated after DSBs by CAMKKβ, and AMPK then subsequently phosphorylates 53BP1 at S1317, located in the 53BP1 focus forming region, promoting 53BP1 DSB accumulation and NHEJ mediated DSB repair[34]. In addition, kinesin KIF18B also promotes 53BP1 recruitment to H4K20me2 by interacting with the 53BP1 Tudor domain. KIF18B enhances binding between 53BP1 and H4K20me2 by interacting with the 53BP1 Tudor adjacent to the H4K20me2 binding pocket, forming a trimeric complex. Consequently, KIF18B knockdown also impairs NHEJ[35].

53BP1 functions also require 53BP1 oligomerisation, however 53BP1 recruitment to DSBs is not dramatically impacted by deletion of the oligomerisation domain, suggesting 53BP1 oligomerisation can be facilitated independently of the OD. DYNLL1 binds constitutively to 53BP1 via a region just N-terminal to the OD domain, residues 1107-1219 known as LC8 motifs. Deleting the LC8 motifs in OD mutant conditions prevents 53BP1 foci formation, suggesting DYNLL1 helps facilitate 53BP1 oligomerisation at DSBs. DYNLL1 or the OD individually are unable to support proper 53BP1 DNA repair activities, but instead act together to promote 53BP1 oligomerisation and DSB repair[36]. Interestingly, DYNLL1 has also been

implicated in preventing DNA end resection at DSBs through interaction with MRE11 of the MRN complex, and therefore promotes NHEJ[37].

Taken together, this non-exhaustive summary of 53BP1-binding partners, coupled with chromatin context and post-translational modification, illustrates the importance of regulated chromatin interaction and the fine-tuning of 53BP1 accumulation at DSBs. In addition to the repair proteins discussed above, Tudor interacting repair regulator (TIRR), was recently discovered as an important regulator of 53BP1 (**Section 1.4**).

1.3.3 53BP1 Downstream Regulation

At DSBs, 53BP1 acts to prevent end resection to promote NHEJ, but how does 53BP1 exert this function? 53BP1 was recently identified to cooperate with the Shieldin complex, composed of the subunits SHLD1/RINN3/C20orf196, SHLD2/RINN2/FAM35A, and SHLD3/RINN1, along with REV7/MAD2L2 to restrict end resection. Shieldin is a downstream effector of 53BP1[38], acting in the 53BP1-RIF1-REV7 axis[17,38,39]. The SHLD3 subunit and RIF1 interact, and Shieldin complex recruitment to DSBs depends on RIF1, linking 53BP1 with Shieldin[40].

Mechanistically, the Shieldin complex facilitates the counteraction of end resection. SHLD2 preferentially binds ssDNA over dsDNA[38,40], which is in contrast to Ku70/80 heterodimer which binds to blunt dsDNA ends at DSBs, suggesting Shieldin may act to prevent end resection at partially resected DSB ends[40]. The SHLD2 DNA binding activity is important for Shieldin function, and cells with mutations in the SHDL2 DNA-binding region form fewer SHLD2 foci[39]. Shieldin interacts with the CTC1-STN1-TEN1 (CST) complex, which recruits Polymerase-α-primase. Therefore, 53BP1 and Shieldin act together with CST and Polymerase-α-primase to fill in resected DSB ends[41], through a mechanism of DNA synthesis at 3' ssDNA overhangs[42]. Additionally, 53BP1 and Shieldin can block EXO1 and DNA2 nuclease activity[42].

Together, the blocking exonucleases and the synthesis of DNA at partially resected ends allows 53BP1 to counteract end resection.

Finally, how 53BP1 is repositioned from IRIF? 53BP1 activity at DSB can be counteracted by the activity of BRCA1. In S/G2, 53BP1 can still be phosphorylated by ATM and recruited with RIF1 to DSBs. However, 53BP1 is rapidly dephosphorylated at T543 by the phosphatase PP4C dependent on BRCA1, which reduces RIF1 interaction with 53BP1 and results in 53BP1 repositioning. Depletion of PP4C impairs EXO1 recruitment, which can be rescued by co-depletion with 53BP1, indicating 53BP1 repositioning by dephosphorylation is essential for end resection. Together, the actions of BRCA1 and PP4C relieve the barrier to end resection in S/G2 and allow repair of DSBs by HR[26]. In addition, SCAI also acts to inhibit RIF1 by binding to phosphorylated 53BP1, promoting BRCA1 foci formation, and facilitating HR[43].

1.3.4 53BP1 and PARP inhibitor resistance

Synthetic lethality occurs when simultaneous defects in the two genes result in cell death, but defects in each gene individually have minimal impact on cell fitness[44]. BRCA1/2 cancers are highly sensitive to the inhibition of PARP1 due to the resultant inhibition of the BER pathway for repair of single strand breaks (for which PARP1 is required) leading to DSBs which cannot be repaired by HR. Additionally, PARP inhibitors (PARPi) trap PARP1 on DNA, leading to stalled replication forks, which require HR for repair. These and other mechanisms make cancers with HR defects, like BRCA1/2 mutation, sensitive to PARPi[45]. PARPi have been approved for clinical use by the FDA for treatment of BRCA mutant breast and ovarian cancers[44]. However, whilst PARPi are clinically promising, the development of resistance limits their success[45]. BRCA1/2 mutant cells can develop PARPi resistance through different mechanisms, including restoration of BRCA1/2 function, loss of PARP1, and increased export of PARPi via upregulation of drug export machinery[45]. Additionally, loss of 53BP1 or its

downstream effectors such as RIF1 and REV7, results in restoration of HR and PARPi resistance[45]. Multiple screens for PARPi resistance factors identify 53BP1 and its binding partners and downstream effectors as prominent hits[17,39]. Therefore, deregulation of end resection via 53BP1 loss of function is suggested to be another clinically relevant mechanism of PARPi resistance development[45]. Consequently, understanding how 53BP1 is regulated is vital for fully elucidating further mechanisms of PARPi resistance, and for the development of novel therapeutics to target 53BP1 regulatory pathways.

1.4 Tudor interacting repair regulator (TIRR)

1.4.1 TIRR is a 53BP1 binding partner and regulates 53BP1 functions

Tudor-interacting repair regulator (TIRR/NUDT16L1/SDOS/Syndesmos) has been identified as a 53BP1-binding protein, binding 53BP1 in non-damage conditions via the Tudor domain. The complex of 53BP1/TIRR is constitutive in non-damage conditions, however after a DSB occurs, the complex dissociates. TIRR therefore acts as a negative regulator of 53BP1. TIRR is part of the Nucleoside Diphosphate linked to another moiety X (NUDIX) family, a family of hydrolases which are found across different organisms[46]. NUDIX proteins contain a characteristic NUDIX box, composed of the motif $GX_5EX_7REUXEEXGU$, where X is any amino acid and U is a hydrophobic amino acid[46]. However, TIRR is not a canonical NUDIX protein as it does not contain the classical NUDIX box, instead containing glycine and leucine amino acids instead of the three glutamic acid residues[47].

One TIRR dimer and two 53BP1 tandem Tudor domains (part of one 53BP1 dimer) interact in the nucleus of cells, in the soluble fraction, with a binding affinity (Kd) of around 1μM[48,49], preventing 53BP1 binding to dimethylated H4K20 (Kd ~20μM)[50]. The binding interface of TIRR with the 53BP1 Tudor domain is more extensive than 53BP1 with H4K20me2[50], due to additional interactions of TIRR with the second Tudor of the tandem Tudor domain[49]. H4K20me2 is the most abundant histone methyl lysine mark in cells and is found on around 85% of H4[50], and therefore careful regulation of 53BP1 binding to H4K20me2 is needed (**Section 1.3**)[50].

Structurally, the TIRR monomer comprises seven alpha helices and seven beta strands, and both the TIRR and 53BP1 structures are globally similar between the unbound and bound forms[51]. However, the 53BP1 aromatic binding cage of the Tudor domain (comprising W1495,

Y1502, F1519, Y1523, and D1521) undergoes conformational changes upon TIRR binding. Residues found on TIRR central to the 53BP1 binding interaction include the N-terminal 10-24 region and a loop containing residues 105, 106, and 107 (**Figure 1.4**)[51]. In the structure of unbound TIRR, residues K10 and 103-107 are highly flexible and display low electron density in the TIRR crystal structure, with these residues becoming more structured upon binding to 53BP1[51]. Interestingly, the NUDIX motif on TIRR, residues 60-90, has also been implicated in the interaction with 53BP1[52].

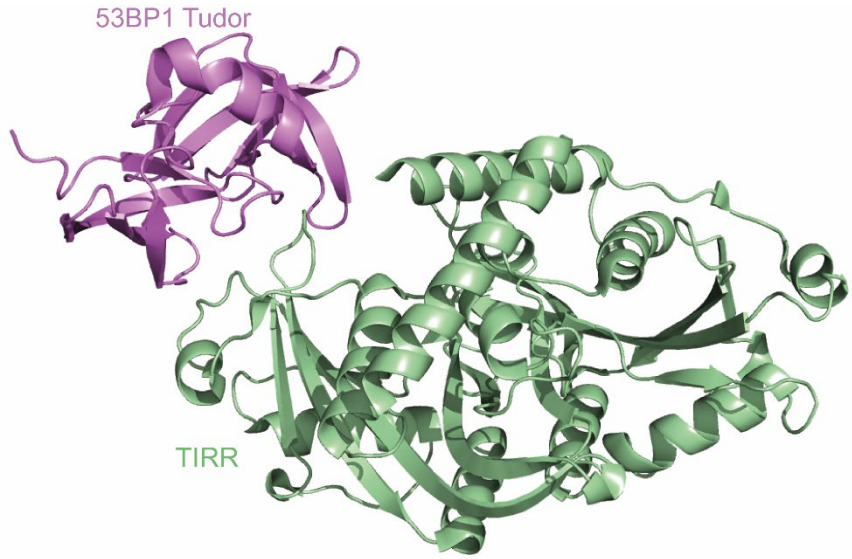


Figure 1.4: *Crystal structure of TIRR bound to 53BP1 Tudor domain (PDB: 6CO1)* [51].

Functionally, TIRR can restrain 53BP1 activities and alter the cellular response to DSBs. The depletion of TIRR sensitises cells to IR[48,49,52]. TIRR may also regulate 53BP1 stability, with TIRR depletion observed to result in reduced total 53BP1 levels[49], increased association of 53BP1 with chromatin[48], and increased interaction of 53BP1 with other 53BP1-binding parters[48]. This appears to be a co-regulation, as 53BP1 knockout also leads to reduced TIRR protein[52]. This suggests TIRR is important for 53BP1 functions, regulating 53BP1 stability, localisation, and protein-protein interactions. The overexpression of TIRR also prevents 53BP1 foci formation in response to IR[48,50,52], as well as increasing the resistance of BRCA mutant

cells to PARPi[48,50]. In agreement with this, in TIRR KO cells, RPA foci are reduced due to a lack of negative regulation of 53BP1, resulting in 'hyperactivation'[49], and conversely, overexpression of TIRR promotes RPA and RAD51 foci formation[50]. Contrastingly, one study suggested that BRCA mutant cells may be more resistant to PARPi after TIRR depletion, and RPA and RAD51 foci formation may be promoted, due to reduced 53BP1 stability in TIRR KO conditions[52]. TIRR was also able to reduce the interaction of 53BP1 Tudor with KIF18B *in vitro*, which stimulates 53BP1 Tudor interaction with H4K20me2 (**Section 1.3.2**)[35]. Taken together, this body of literature suggests that TIRR is an important regulator of 53BP1 in response to DSBs (**Table 1.1**).

The mechanism of dissociation of TIRR and 53BP1 after IR is not yet fully understood, however ATM inhibition prevents complex dissociation[48,52], and mutation of 53BP1 ST/Q (ATM phosphorylation) sites to alanine also reduces separation after damage[48]. Moreover, RIF1 depletion, but not PTIP, impairs TIRR and 53BP1 dissociation, suggesting ATM phosphorylation and RIF1 interaction with 53BP1 may be important in this mechanism[48]. Additionally, IMP and RNA have been suggested to play a role in this dissociation[51] (**Chapter 3**).

Aside from DSB repair at break sites, TIRR can also influence 53BP1 interaction with p53, altering p53-dependent cellular functions[53]. 53BP1 (in complex with USP28) can interact with p53 via either the BRCT domains[14], or the Tudor domains[53] (**Figure 1.3**). The 53BP1 Tudor domain can interact with p53 dimethylated at K382 by the methyltransferase SET8. TIRR can therefore compete with p53K382me2 for binding to the 53BP1 Tudor domain. Depletion of TIRR leads to an increase in transcription of p53-target transcripts, such as p21 and MDM2, due to increased binding of p53 at p53 promoter response elements after cell stress, including

IR. This results in p21-mediated cell cycle arrest, a reduction in the number of cells in S-phase, and increased cellular senescence after IR. Therefore, TIRR can influence 53BP1 functions outside of H4K20me2 association, such as through regulating p53 transcriptional stress responses[53].

Overexpression/Depletion of TIRR?	Phenotype	Reference
Overexpression	Prevents 53BP1 foci formation after IR	Drané *et al* 2017 Dai *et al* 2018 Wang *et al* 2018 Zhang *et al* 2017
Overexpression	BRCA mutant cells are more resistant to PARPi	Drané *et al* 2017 Wang *et al* 2018
Depletion	53BP1 binding mutant (does not bind TIRR, phenocopies TIRR depletion) results in increased sensitivity to PARPi	Botuyan *et al* 2018
	BRCA mutant cells are resistant to PARPi (attributed to lack of 53BP1 stability)	Zhang *et al* 2017
Overexpression	Impairs CSR due to impaired 53BP1 function	Drané *et al* 2017
	TIRR may not impact CSR: 53BP1 binding mutant (does not bind TIRR) rescues CSR to WT levels	Botuyan *et al* 2018
Depletion	Increases chromatin bound 53BP1	Drané *et al* 2017
Depletion	Increased interaction of 53BP1 with binding partners such as MDC1	Drané *et al* 2017
Depletion	Sensitises cells to IR	Drané *et al* 2017 Dai *et al* 2018 Zhang *et al* 2017
Depletion	Reduced 53BP1 protein levels / stability	Dai *et al* 2018

		Zhang *et al* 2017
Depletion	Reduction in RPA foci	Drané *et al* 2017 Dai *et al* 2018
	Restored RPA and RAD51 foci (attributed to lack of 53BP1 stability)	Zhang *et al* 2017
Overexpression	Promotes RPA and RAD51 foci formation	Wang *et al* 2018
Depletion	Increases p53 activation	Parnandi *et al* 2021

Table 1.1: *Summary of TIRR regulation of 53BP1 functions.*

1.4.2 TIRR is a paralogue of NUDT16

NUDT16 is a close paralogue of TIRR, and TIRR shares 47.9% amino acid similarity with NUDT16[51], yielding a highly similar structure with a Root Mean Square Deviation (RMSD) of 1.86Å (**Figure 1.5**). TIRR arose from a gene duplication of NUDT16 in the tetrapod lineage[54]. However, there are several key differences between NUDT16 and TIRR which give them unique cellular functions. NUDT16 lacks the H106 found in the 53BP1 binding loop of TIRR, and as a result cannot bind to 53BP1[49]. Addition of H106 in NUDT16 allows 53BP1 binding[49], and replacing residues 101-107 in TIRR with corresponding residues in NUDT16 prevents 53BP1 binding[51], highlighting the importance of this loop in TIRR for 53BP1 interaction. Interestingly however, TIRR can Co-IP with NUDT16 suggesting they may interact, or even form a heterodimer due to their structural similarity[50]. Additionally, unlike NUDT16, TIRR does not have NUDIX catalytic activity as the NUDIX box glutamic acids are replaced by glycine/leucines[55]. These glutamic acid residues are central for the coordination of divalent metal ions Mn^{2+} or Mg^{2+}, which confer catalytic activity[47].

NUDT16 displays catalytic hydrolase activity on a diverse range of substrates including RNA 5' caps, IDP/ITP, and ADP-ribose. NUDT16 can regulate RNA stability by functioning as a RNA decapping enzyme, acting on U8 snoRNA and mRNA[56]. NUDT16 was initially thought

to act in the nucleus[54], but has also been implicated in cytoplasmic RNA decapping[57]. Moreover, NUDT16 removes ADP-ribosylation on both poly- and mono-ADP ribosylated proteins[58], and RNA[59]. NUDT16 also acts as a 'house-keeping' protein, hydrolysing ITP and IDP into IMP, ensuring (d)ITP/IDP levels in the nucleotide pool are kept low, in order to stop incorporation of inosine/deoxyinosine into RNA/DNA. As a result, the knockdown of NUDT16 results in an increase in single strand breaks and cell cycle arrest in S phase, increased incorporation of inosine into RNA, and reduced cell proliferation[60].

NUDT16 catalytic activity has also been shown to play a role in regulating 53BP1 stability after IR[27]. Similarly to TIRR[52], loss of NUDT16 can lead to reduced 53BP1 at the protein level, suggesting NUDT16 regulates 53BP1 stability[27]. 53BP1 can be ADP-ribosylated by RNF146 in response to IR, which leads to increased ubiquitination of 53BP1 by RNF146 and subsequently 53BP1 degradation. However, NUDT16 is able to remove PAR chains from 53BP1, and therefore promotes 53BP1 stability after IR. Consequently, expression of a catalytic mutant of NUDT16 impairs 53BP1 binding to H4K20me2, and loss of NUDT16 increases cellular sensitivity to IR[27].

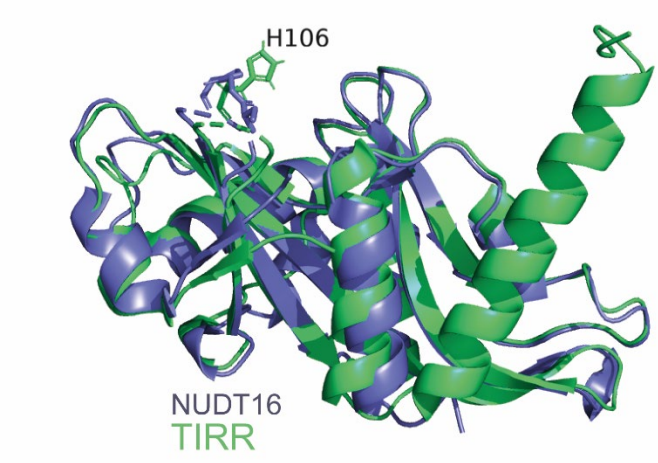


Figure 1.5: *Overlay of a TIRR monomer (PDB: 6D0L) with a NUDT16 monomer (PDB: 3COU), yielding a RMSD value of 1.86, suggesting a highly similar structure. Reside H106 is highlighted on TIRR and shown in liquorice, and corresponding residues on NUDT16 are shown in liquorice*

.

1.4.3 The role of TIRR at the plasma membrane

Before being implicated as a DSB repair protein acting as a negative regulator of 53BP1, TIRR was identified as an interactor of the cytoplasmic domain of the transmembrane protein Syndecan-4[47,61,62]. Syndecan-4 is a cell surface proteoglycan, involved in focal adhesion formation and stress fibre assembly[61]. TIRR also interacts with Paxillin, a focal adhesion adaptor protein, which is enhanced by Protein Kinase C (PKC) signalling and mediates the interaction of Syndecan-4 with Paxillin[62]. TIRR and Syndecan-4 localise together in focal adhesion complexes. Through interactions with Syndecan-4, TIRR overexpression was found to promote cell spreading and the formation of focal contacts[61]. TIRR can also interact with PTEN, and knockdown of TIRR increased cell migration[63].

1.4.4 TIRR is an RNA binding protein involved in translation

Furthermore, whilst TIRR does not retain NUDT16 catalytic activity, TIRR retains RNA binding activity[55]. TIRR can localise to the endoplasmic reticulum (ER) with a TIRR-interactor, TRAP1, and associates with actively translating polyribosomes, regulating translation[55]. Although TIRR overexpression does not dramatically alter RNA at a transcriptional level, the overexpression of TIRR impairs protein synthesis, suggesting TIRR can regulate cell functions at a translational level[55]. TIRR can bind a variety of different RNAs in cells, with the majority of RNA identified in iCLIP-Seq experiments in non-damage conditions being messenger RNA (66%), and around 8% of bound RNA being long non-coding RNAs[55]. TIRR was proposed to act as a repressor of translation of mRNA through direct RNA interactions[55], and a portion of TIRR bound RNAs were found to play a role in cilia biogenesis. Consequently, depletion of TIRR was found to promote cilia formation[55]. A summary of TIRR functions is shown in **Figure 1.6.**

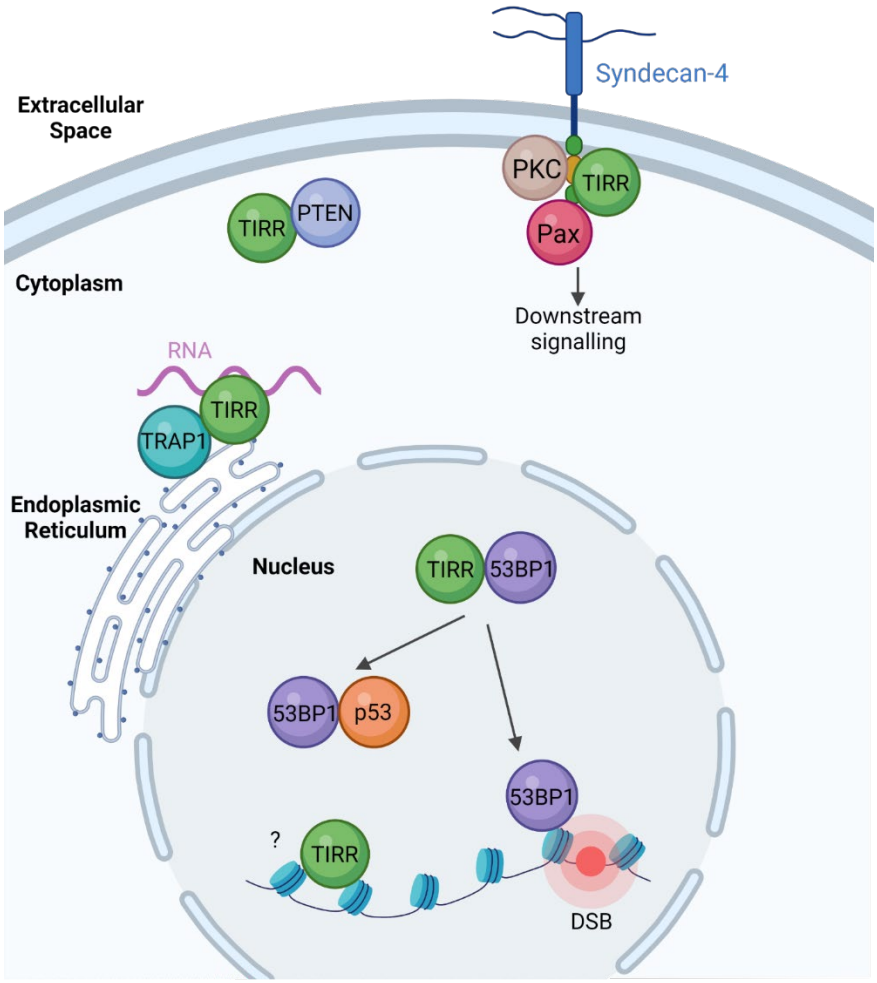


Figure 1.6: *Summary of known TIRR roles within the cell across different cellular compartments. Interestingly, TIRR is also bound on chromatin in non-damage and damage conditions with unknown function*[48]*. Image created with BioRender.com.*

1.5 The RNA-dependent DNA damage response

Over the last decade, it has emerged that RNA has many functions in the repair of DNA damage, including in DSB repair. RNAPII transcribed RNA can be either coding messenger RNA (mRNA), which is translated into proteins, or non-coding RNA (ncRNA). These ncRNA can be further divided into the classes long non-coding RNA (lncRNA, >200 bp), or short ncRNA. Short ncRNAs include, but are not limited to, microRNA (miRNA), and the recently identified DNA damage-dependent small RNA (DDRNA)[2].

1.5.1 MicroRNA in DSB Repair

MicroRNAs are ~22 nucleotide small ncRNAs which have sequence complementarity to specific mRNAs, and are involved in RNA post-transcriptional silencing. Dicer and Drosha are ribonucleases which are central in miRNA processing and maturation. MiRNAs are first transcribed as primary transcripts (pri-miRNA) and processed by Drosha and the cofactor DiGeorge syndrome critical region 8 (DGCR8) in the nucleus into pre-miRNA. The pre-miRNAs are then exported via Exportin-5 and RAN-GTP into the cytoplasm, where Dicer and TRBP cleave pre-miRNA into mature miRNA, which then are loaded into AGO2 to form the RNA-induced silencing complex (RISC). MiRNAs can downregulate the expression of mRNAs in a process known as RNA interference (RNAi), by guiding RISC to an mRNA with sequence complementarity. RNA degradation machinery can then be recruited which either disrupts the translation of the mRNA or degrades the target mRNA[2,64]. The majority of mRNA (over ~60%) are predicted to be targeted by miRNAs[65], and one type of miRNA can target many different genes[66].

Many miRNAs are now known to play key roles in DSB repair, regulating the levels of a variety of DSB repair factors[67], and miRNA processing is also known to be influenced in response to

DSB induction. For example, in response to DNA damage, ATM phosphorylates and activates KSRP (a protein which contributes to miRNA maturation) to promote miRNA processing and expression by increasing KSRP binding to pri-miRNA[68]. Moreover, proteins with functions in DNA repair can interact with miRNA processing machinery, for example BRCA1 can interact with Drosha and bind to pri-miRNAs, promoting processing of pri-miRNAs including let-7a-1 and miR-34a[69].

Examples of miRNAs regulating DSB repair factors include: miR-421, miR-100, and miR-181a/b regulation of ATM[70–72], miR-24 and miR-138 regulation of H2AX[73,74], miR-34 family regulation of RAD51[75], and miR-15a and miR-16 regulation of BMI1[76]. MiRNAs miR-1255b, miR-148b*, and miR-193b can also suppress HR in G1 through the targeting of HR factors BRCA1, BRCA2, and RAD51[77]. These and other examples of miRNAs targeting DNA repair proteins are shown in **Table 1.2**. Taken together, the wide variety of miRNAs known to target different DSB repair proteins to regulate their protein levels highlights the importance of this class of short RNA in influencing DNA repair outcomes.

DSB Repair Protein	Targeted by	Reference
H2AX	miR-138 miR-24	73,74
ATM	miR-421 miR-100 miR-101 miR-181a/b	70-72,78
CtIP	miR-130b miR-335	79,80
MRE11	miR-493-5p	81
MDC1	miRNA-22	82
53BP1	miRNA-34a	83
BRCA1	miR-1255b miR-193b* miR-182	77,84
BRCA2	miR-1255b miR-193b* miR19-a miR19-b	77,85
RAD51	miR-148b* miR-34	75,77

	miR-193b*	
DNA-PKc	miR-101 miR-874-3p	78,86
Ku80	miR-526b miR-622	87,88
Ku70	miR-622 miR-502 miR-545	88-90
LIG4	miR-1246 miR-4727-5p	91,92
XLF	miR-502	89
BMI1	miR-15a miR-16	76

Table 1.2: *Examples of DSB repair factors and miRNAs which target them*[2].

1.5.2 Long Non-Coding RNA in DSB Repair

There are estimated to be tens of thousands of lncRNAs encoded in the human genome[93]. A vast array of lncRNAs have been implicated in the DSB response, including in chromatin organisation, cell cycle regulation, and gene expression regulation (a non-exhaustive summary of lncRNAs characterised in DNA repair can be found in **Table 1.3**)[2]. Furthermore, the expression of various lncRNAs can be modulated in response to IR. LncRNAs can also bind directly to repair proteins to regulate DSB repair and influence the choice between HR and NHEJ. Examples of such lncRNAs involved in DSB repair are summarised below, including PRLH1, scaRNA2, LINP1, and HITT.

LncRNA HITT (HIF-1a inhibitor at translational level) is an example of a direct DSB regulator. HITT is up-regulated following DSB induction[94], and can augment DSB repair through interaction with ATM. Overexpression of HITT reduces p-ATM foci and ATM recruitment to chromatin after DSB induction by binding to ATM at the site of NBS1 interaction (part of the MRN complex), blocking ATM and NBS1 association. Consequently, the expression of HITT sensitises cells to DSB inducing agents and results in delayed DNA repair[94]. HITT has been suggested to be a mechanism of restraining ATM activity in certain cellular contexts, for example after completion of repair, as HITT is up-regulated at later time points after damage

(1h after doxorubicin treatment, a topoisomerase II inhibitor and inducer of DSBs) relative to ATM activation (5 minutes) in the DSB response[94].

PRLH1 (p53-regulated lncRNA for HR repair 1) is another example of a direct regulator of DSB repair. PRLH1 expression is increased after doxorubicin treatment[95]. PRLH1 can regulate DSB repair pathway choice through binding to RNF169, an E3 ubiquitin ligase and a paralogue of the RNF168[95]. The complex of PRLH1 and RNF169 competes with 53BP1 for binding to RNF168 ubiquitinated H2AK15 chromatin. The overexpression of PRLH1 increases the recruitment of RNF169 to DSBs, and consequently reduces 53BP1 foci formation. Knockdown of PRLH1 also reduces RNF169 protein levels, suggesting PRLH1 can regulate HR-mediated DSB repair through both stabilisation of RNF169 and blocking of 53BP1 recruitment[95].

LINP1 (LncRNA in non-homologous end joining pathway) associates with another repair factor at DSBs, the Ku70/80 heterodimer[96]. LINP1 expression was found to increase after DSB induction. Mechanistically, LINP1 can act in DSB repair by binding Ku heterodimers to bridge DNA ends, promoting Ku multimerisation and increasing the lifetime of the DNA synaptic complex compared to the complex of Ku-PAXX[96]. Additionally, LINP1 promotes DSB repair by scaffolding Ku80 and DNA-PKc. Consequently, LINP1 knockdown results in the reduced interaction of Ku80 and DNA-PKc, delayed clearance of γH2AX, and increased sensitivity to IR[97,98].

Small Cajal body-associated RNA 2 (scaRNA2) is a lncRNA which localises to DSB sites. Mechanistically, scaRNA2 binds DNA-PKc, weakening the interaction of DNA-PKc with the Ku70/80 heterodimer and therefore preventing DNA-PK assembly and activation at DSBs[99]. This is in contrast to LINP1 lncRNA, which promotes the interaction of Ku80 and DNA-PKc,

and stimulates DNA-PK autophosphorylation[97–99]. Interestingly, scaRNA2 depletion also enhances the interaction of DNA-PKc with LINP1, suggesting a competition between LINP1 and scaRNA2 in DNA-PK activation. Through acting as an inhibitor of DNA-PK, scaRNA2 promotes recruitment of HR factors such as BRCA1 and RAD51, promoting repair by HR[99].

Aside from direct binding to DSB repair proteins, lncRNAs can also act as indirect regulators of DNA repair through sponging miRNA, competing with endogenous mRNA targets for miRNA binding to regulate gene expression. For example, Lnc-RI can compete with miR-4727-5p to regulate LIG4, with Lnc-RI knockdown resulting in reduced NHEJ due to reduced LIG4 protein[92]. Additionally, Lnc-RI also has an opposing role in promoting HR by sponging miR-193a-3p which targets RAD51 mRNA[100].

LncRNA	Function/Associated Phenotype in DSB Repair	Reference
GUARDIN	Scaffolds BRCA1 and BARD1, preventing proteasomal degradation of BRCA1.	101
HOTAIR	Knockdown of HOTAIR leads to cell sensitivity to IR and accumulation of endogenous DNA damage.	102
LIRR1	LIRR1 is upregulated upon DSB induction. The overexpression of LIRR1 results in reduced Ku70/80 expression, and increased γH2AX foci.	103
MALAT1	Promotes A-NHEJ by binding to PARP1 and LIG3, and is needed for LIG3 recruitment to DSBs. Knockdown of MALAT1 induces γH2AX.	104
ANRIL	Knockdown of ANRIL reduces p-ATR foci. ANRIL promotes HR by binding to ATR and preventing ubiquitin-mediated degradation.	105
HITT	Interacts with ATM and restrains HR-mediated DSB repair.	94
ScaRNA2	Promotes HR by reducing the interaction of DNA-PKc and Ku70, and enhancing recruitment of HR factors to DSBs, including BRCA1 and RAD51.	99
DINO	Interacts with p53 in response to DSB induction, stabilising p53 and promoting p53 transcriptional program activation.	106
PCAT-1	Represses expression of BRCA2 post-transcriptionally and therefore impairs HR.	107
PANDA	Upregulated in response to DSB induction. Knockdown of PANDA induced apoptosis after DNA damage.	108
LINP1	Scaffolds Ku80 and DNA-PKc, enhancing DNA-PK activation and promoting NHEJ.	97–99
DDSR1	Interacts with BRCA1 to promote HR.	109
Lnc-RI	Stabilises RAD51 mRNA to promote HR by sequestering miR-193a-3p. Also competes with LIG4 mRNA for miR-4727-5p to promote LIG4 expression and NHEJ.	92,100
CUPID1 and CUPID2	CUPID1/2 depletion results in reduced RAD51 recruitment to DSBs. Promotes HR.	110

BGL3	Binds to BARD1 and PARP1 and is recruited to DSBs. BGL3 depletion reduces recruitment of BARD1 and BRCA1 to DSBs. Promotes HR.	111

Table 1.3: *Non-exhaustive list of examples of lncRNAs and their functions in DNA repair*[2].

1.5.3 Transcriptionally active regions: HR vs NHEJ

Increasing evidence suggests that DSBs which occur in transcriptionally active regions may be repaired by different mechanisms to those occurring in transcriptionally silent regions. In addition to the need to shutdown active transcription *in cis* to DSBs (**Section 1.5.4**), the choice of DSB repair pathway may be influenced by the transcriptional status of the region where the break occurs.

Mapping of specific DSB sites suggests that DSBs occurring in transcriptionally active regions are preferentially repaired by the HR repair pathway over NHEJ[112]. Analysis of DSBs induced by the A*si*SI endonuclease, which cuts at specific sequences across the genome, revealed that in G2, DSBs in regions of the genome with chromatin marks typically associated with active transcription (such as H3K36me3 and H3K9Ac) were associated with RAD51 binding, indicative of HR-mediated repair[112]. Meanwhile, DSBs in regions with chromatin marks associated with repressed transcription (such as H3K27me3 and H3K9me3) were bound by XRCC4, indicative of repair by NHEJ. XRCC4 was also predominantly bound to most DSBs in G1, consistent with repair by NHEJ being the main repair pathway in G1[112]. Inhibiting transcription was also found to reduce RAD51 bound at DSBs, but does not impact XRCC4 recruitment, suggesting DSBs in actively transcribing regions favour repair by HR[112].

Interestingly, DSBs which occur in transcriptionally active regions of the genome in G1, where HR is inactive, may cluster together with DSBs on the same or different chromosomes in order to delay repair from G1 until S/G2[113]. This clustering was found to be dependent on the MRN complex, and the cytoskeletal organisation factors FMN2 and the LINC complex[113]. DSBs

which displayed more clustering were found to exhibit higher levels of transcription and higher RAD51 binding, suggesting repair by HR. In contrast, DSBs which were considered 'NHEJ-prone' (XRCC4 bound), did not exhibit high levels of clustering and were repaired more rapidly in G1[113].

However, it should be noted that transcriptionally active regions were also found to preferentially recruit NHEJ factors such as 53BP1, through a direct interaction with RNAPII, to promote RNA-templated DNA repair (**Section 1.5.8**)[114]. HR factors such as RAD51 were also found to associate with RNAPII, although as part of distinct complexes[114]. Together this suggests that the cells may regulate DSB repair pathway choice dependent on the transcriptional status at the location where the DSB occurs. These mechanisms may serve to promote more accurate DSB repair by HR in transcriptionally active regions in S/G2 phases of the cell cycle[112], or more rapid repair by NHEJ to promote cell survival[114].

1.5.4 Double Strand Break Induced Silencing *in cis*

Aside from influencing the choice of repair pathway, DSBs occurring within or nearby genes which are actively transcribed appear to elicit a transient response which serves to silence transcription *in cis* to the break, known as Double Strand Break Induced Silencing in Cis (DISC)[115]. DISC is orchestrated through multiple pathways which act to pause active transcription either through remodelling of the surrounding chromatin, or through post-translational modification of RNAPII resulting in eviction of the total RNAPII from the gene body. The kinases ATM and DNA-PK, as well as PARP1, have been implicated in distinct transcriptional silencing pathways.

DISC was first described using a transcriptional reporter in the vicinity of an inducible DSB[115]. The transcriptional reporter consists of: 1) a lac operator array which is bound by a lac repressor

fused to the FokI endonuclease and mCherry (for visualisation of the DSB induced by FokI), 2) 4kb of tandem tetracycline response elements (TREs) followed by a CMV promoter, which after the addition of doxycycline/tetracycline, will transcribe 3) MS2 stem loop repeats found in the transcription unit (bound by YFP-MS2 as a readout of transcription)[115]. DSBs induced by FokI 4kb upstream of the CMV promoter result in reduced transcription, which suggests that reduced transcriptional activity was a result of DSB signalling and not necessarily the DSB itself 'blocking' transcription[115]. This reduced transcription was also accompanied by a reduction in the elongating form of RNAPII (C-terminal domain (CTD) phosphorylation at S2) at the reporter locus dependent on ATM. However, total RNAPII occupancy was not reduced, suggesting that RNAPII is not evicted from the gene, but rather ATM signalling regulates RNAPII transcription activity[115]. Moreover, inducing DSBs globally at sites not *in cis* to the reporter did not result in transcriptional silencing, indicating that transcriptional silencing occurs only *in cis* to the DSB[115].

Furthermore, a more comprehensive analysis of DISC across the genome was performed by profiling of DSBs induced by the A*si*SI endonuclease[116]. Chromatin Immunoprecipitation and Sequencing (ChIP-Seq) of ɣH2AX (to monitor break induction by A*si*SI) was coupled with ChIP-Seq to monitor the occupancy of total and elongating (S2) RNAPII, RNA sequencing (RNA-Seq) to monitor steady state RNA levels, and metabolic pulse-labelling of RNA with Bromouridine followed by sequencing (Bru-Seq) to determine the rate of RNA synthesis. After A*si*SI cutting, the total levels of RNA produced by genes within 2kb of the break sites were decreased, which was not influenced by the location within the gene where the DSB was found (promoter, intron, and so on), but more global silencing of gene expression was not observed as assessed by RNA-Seq[116], in agreement with the DISC model proposed using the reporter system[115]. The changes in total RNA levels from genes with A*si*SI induced DSBs was a result

of a reduction in S2 RNAPII and decreased RNA synthesis as measured by Bru-Seq. However, the total RNAPII levels remained unchanged, as previously observed[115,116]. DISC was observed to be dependent on the distance away from the break, with genes downregulated to a greater extent the closer they are found to the break, with no changes in gene expression observed at a distance of 1Mb from the break. The observed silencing was also once again found to be dependent on ATM signalling[116].

How does ATM silence RNAPII transcription *in cis* to DSBs? The silencing of transcription observed using the reporter construct[115] was found to be a result of ATM-dependent ubiquitination of H2AK119[115,117]. Many different protein complexes have been found to contribute to transcriptional silencing through H2AK119 ubiquitination, including the SWI/SNF complex PBAF components BAF180 and BRG1[118]. BAF180 and BRG1 are recruited to DSB sites, and BAF180 is phosphorylated by ATM and ubiquitinates H2AK119[118]. The Cohesin complex was also found to be needed for DISC via H2AK119Ub, functioning in the same pathway as PBAF. Depletion of PBAF and cohesin was found to result in the mis-rejoining of DNA ends, suggesting repressing transcription at DSBs in active genes may be required to prevent genomic rearrangements of active genes[119]. H2AK119Ub is also facilitated at DSBs in transcriptionally active regions by the Polycomb repressive complexes 1 and 2 (PRC1 and PRC2). The EZH2 subunit of PRC2 promotes H3K27me3, which is recognised by PRC1, and the BMI1 subunit of PRC1 ubiquitinates H2AK119[118]. Additionally, ENL, a transcription elongation factor (part of the super elongation complex (SEC) which is associated with RNAPII), was found to be phosphorylated by ATM in response to DSBs, allowing interaction with and recruitment of BMI1 of the PRC1 complex, leading to H2AK119Ub[117]. The ubiquitin ligase complex FRRUC (FBXL10, RNF68, and RING1B) also contributes to H2AK119 ubiquitination and is also required for PRC1 recruitment. However, FRRUC

recruitment was found to be dependent on PARP1 but not ATM[120]. The recruitment of CDYL1 to DSBs in transcriptionally active regions was also found to be dependent on PARP1 but not ATM, which in turn promotes the recruitment of EZH2, the methyltransferase subunit of PRC2, promoting H3K27me3 and subsequent recruitment of PRC1 for ubiquitination of H2AK119[121]. Additional factors also likely contribute to DISC through PARP1 dependent recruitment, such as the NELF complex. NELF-E is recruited to DSBs in a manner independent of ATM signalling but dependent on RNAPII and PARP activity[122]. The ADP-ribosylation of RNAPII after DSBs allows NELF association[122]. PARP1 activity is also required for the recruitment of KDM5A, which is recruited to DSBs in actively transcribed loci and demethylates H3K4me3, a chromatin mark known to be associated with active transcription[123]. KDM5A recruits the ZMYND8-NuRD complex, which contributes to the repression of transcription[123]. This suggests both ATM and PARP1 mediated pathways are important in DISC (**Figure 1.7**).

However, aside from the ATM-dependent ubiquitination of H2AK119, and PARP1 dependent recruitment of FRRUC and the NELF and ZMYND8-NurD complexes, a DNA-PK dependent pathway involving direct RNAPII ubiquitination also plays a role in DISC. Transcriptional silencing of I-PpoI endonuclease induced DSBs was found to be independent of ATM signalling, and instead was dependent on DNA-PK. RNAPII found in both genes bodies and promoter regions was decreased after DSBs, and this was reversed after DNA-PK inhibition, suggesting that the break itself is not responsible for reduced RNAPII, but rather the action of DNA-PK signalling which is required for DISC[124]. The activity of DNA-PK was found to be mediated by the ubiquitin ligase WWP2, which is recruited to DSBs in transcriptionally active genes and ubiquitinates RNAPII, followed by the recruitment of the proteasome for RNAPII eviction. The depletion of WWP2 was also found to impair NHEJ, suggested to be due to the

impaired recruitment of NHEJ proteins to DSBs such as Ku70/80 and XRCC4, which was attributed to collisions of NHEJ factors with RNAPII[125] (**Figure 1.7**).

It is clear that many different factors contribute to the repression of transcription after a DSB has occurred within or *in cis* to a transcriptionally active gene (summarised in **Table 1.4** and **Figure 1.7**), although how exactly these different pathways, i.e. ATM-dependent, PARP1-dependent, and DNA-PK dependent, function together is still enigmatic. Transcriptional silencing and repressive chromatin formation appears to be a protective mechanism by the cell to prevent aberrant RNA transcript production[126], keep DSB ends in close proximity for repair[126], prevent chromosome translocations due to mis-rejoining of DSB ends[119], or to prevent RNAPII collisions with DSB machinery to allow faithful repair[125]. Having said that, while it is assumed that transcriptional silencing is required for proper DSB repair, recent evidence has challenged the requirement of silencing of transcription for both HR and NHEJ by uncoupling transcriptional silencing from DSB repair[126]. CDYL1 possess lysine decrotonylation activity. H3K9cr is a marker of active transcription, and therefore CDYL1 can contribute to transcriptional silencing after DSBs by reducing H3K9cr[126]. The observed reduction in lysine crotonylation after DSBs dependent on CDYL1 was observed to occur at both HR-prone and NHEJ-prone DSBs in A*si*SI cells, indicating decrotonylation and transcriptional silencing is a feature of both NHEJ and HR prone DSBs, although CDYL1 depletion only impaired HR[121,126]. However, expression of a decrotonylation defective mutant of CDYL1 was able to rescue the HR defect observed in CDYL1-deficient cells, despite not being able to promote transcriptional silencing at DSBs, indicating transcriptional silencing is not a prerequisite for repair by HR[126].

Nevertheless, transcriptional silencing of active loci induced by DSBs *in cis* or within a gene

appears to be a feature of the DNA damage response, protecting genomic integrity and allow faithful repair. However, a surprising aspect of DNA repair which is seemingly contradictory to DISC, is the observation that *de novo* transcription appears to initiate at DSB ends (**Section 1.5.5**).

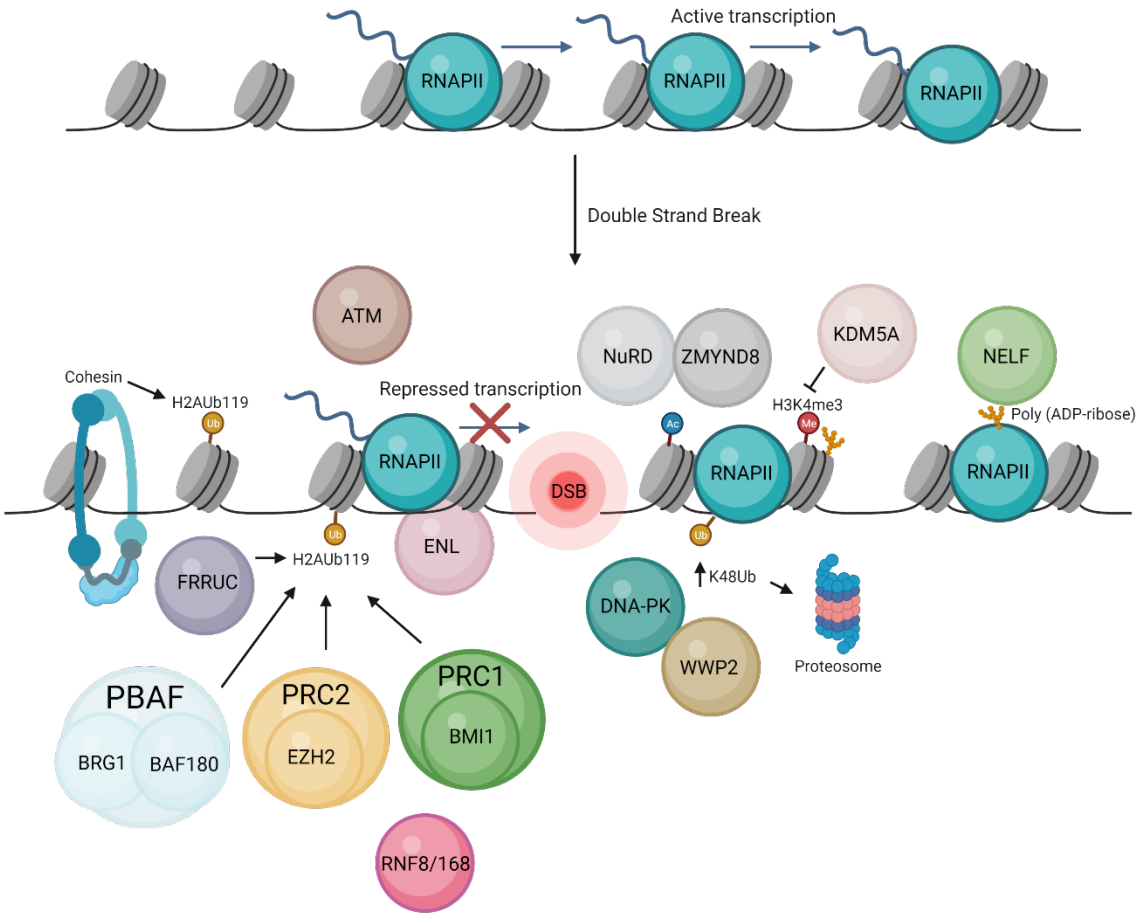


Figure 1.7: *Different mechanisms of transcriptional silencing in cis to DSBs in transcriptionally active genes. Figure adapted from*[128]*. Image created with BioRender.com.*

Protein	Activity	Function in transcriptional silencing at DSBs	Ref
DNA-PK and WWP2	WWP2: E3 Ubiquitin Ligase	• DNA-PK is involved in removal of total RNAPII at promoter and gene bodies of damage genes • WWP2 is an effector of DNA-PK, and interacts with DNA-PK and RNAPII, mediating K48 ubiquitination of RNAPII and eviction from damaged genes by the proteasome • Promotes NHEJ-mediated DSB repair	124,125
USP16	Deubiquitinase	• Removes H2A119Ub to restore transcription after repair	115

PRC1 (BMI1, RING1B)	E3 Ubiquitin Ligase	• H3K27me3 is recognised by PRC1 • The BMI1 subunit of PRC1 promotes transcriptional repression by promoting H2AK119Ub	118
PRC2 (EZH2)	EZH2: Methyltransferase	• EZH2 promotes H3K27me3, which is recognised by PCR1 to promote H2AK119Ub	118
Dicer and Drosha	Ribonuclease activity	• Process DDRNA which can bind and recruit BMI1 to DSBs, resulting in H2AK119Ub (**Section 1.5.7**).	127
PBAF (BRG1, BAF200, BAF180, BRD7)	SWI/SNF chromatin remodelling complex	• BAF180 and BRG1 are recruited to DSBs to promote H2AK119Ub, and this is ATM mediated through BAF180 phosphorylation • Facilitates NHEJ repair	118
Cohesin	Loop extrusion	• Acts with PBAF and promotes H2AK119Ub in both G1 and G2 • BAF180 and SA2 (cohesin subunit specific for centromeres) are independently recruited to DSBs and are needed to prevent the mis-rejoining of DSB ends	119
ZMYND8-NurD (HDAC1, HDAC2, CHD4) complex and KDM5A	KDM5A: Histone demethylase ZMYND8: bromodomain binding acetylation NuRD: Chromatin remodelling and histone deacetylase	• Recruitment of KDM5A and ZMYND8-NuRD to DSBs depends on PARP1 • KDM5A demethylates H3K4me3 near DSBs, which is required for ZMYND8-NuRD binding to chromatin to repress transcription • H4 acetylation by TIP60 promotes ZMYND8-NurD recruitment • Promotes HR	123
NELF complex	Negative elongation factor complex	• Recruited by PARP1 to transcriptionally active DSBs, but recruitment is not dependent on ATM • RNAPII is ADP-ribosylated after DSBs, and this is required for the interaction with NELF-E • Promotes HR and NHEJ	122
ENL	Transcription elongation factor, present in super elongation complex	• ENL is associated with RNAPII • ENL is phosphorylated by ATM which results in interaction with and recruitment of PRC1 (BMI1), which ubiquitinates H2AK119 • Knockdown of ENL or BMI1 reduces Ku recruitment • ENL can be evicted from DSBs by CDYL1 decrotonylation activity	117,126
FRRUC (FBXL10-RNF68-RNF2/RING1B)	Ubiquitin Ligase Complex	• FRRUC is recruited to DSBs dependent on PARP1 (but not ATM or DNA-PK) and ubiquitinates H2AK119 • Promotes HR • Required for recruitment of BMI1 and RING1B (PRC1)	120
CDYL1	Crotonyl-CoA hydratase	• PARP1 dependent but ATM independent recruitment • Promotes EZH2 (subunit of PRC2) recruitment to promote H3K27me3 to repress transcription	121,126

	• CDYL1 promotes lysine decrotonylation at DSBs, which promotes ENL eviction and transcriptional silencing • Promotes HR (may be independent of decrotonylation activity and transcriptional silencing)

Table 1.4: *Summary of proteins involved in DSB-induced transcriptional silencing and their activities.*

1.5.5 Transcription initiation at DSBs

Seemingly paradoxical to DISC, mounting evidence suggests a mechanism of *de novo* transcription at the DSB ends by RNAPII. Colocalisation of γH2AX and EU, which detects nascent RNA, was observed in immunofluorescence microscopy experiments[129,130], and nascent transcripts mapping to DSBs were detected by sequencing[131,132]. Furthermore, RNAPII recruitment/accumulation at breaks has been observed using various methods, including immunofluorescence microscopy and ChIP[133,134]. Specifically, RNAPII phosphorylated at the CTD at S2 and S5, associated with active transcription, was shown to be recruited to DSBs, colocalising with γH2AX foci[134]. Additionally, RNAPII co-immunoprecipitates with the MRN complex[129]. RNAPII, phosphorylated at Y1 on the CTD by c-Abl, was also seen to accumulate at DSBs induced by A*si*SI, dependent on MRN and ATM activity[133]. Functionally, RNAPII appears to play a role in DSB repair through repair factor recruitment, as RNAPII inhibition results in reduced 53BP1 foci, but not γH2AX foci[134].

A reporter system designed to monitor transcription at DSBs provides further compelling evidence for a mechanism of break induced transcription. The reporter system features an I-SceI endonuclease cut site in either an exon or promoter proximal region of a doxycycline-inducible IgM gene, flanked by MS2 sequences (sense) upstream (bound by MS2-RFP), and PP7 sequences downstream (sense, bound by PP7-GFP), as a readout for transcription[135]. After cutting by I-SceI, DISC was observed both up and downstream of the break in the sense orientation. Transcriptional recovery of the DSB in the exon occurred on the order of 30-40

minutes, consistent with NHEJ-mediated repair, in around half of the cells. However, in the other ~50% cells, transcription downstream of the DSB occurred rapidly after transcriptional shutdown, suggesting transcription initiation occurring at the break[135]. Using a modified reporter with a MS2 sequence in the antisense upstream direction, revealed that this transcription also occurs in the antisense upstream direction as well as the sense downstream direction[135]. However, sense downstream and antisense upstream transcription was not observed to occur concurrently, suggesting only one end of the DSB may initiate *de novo* transcription[135]. Interestingly, the DSB induced in the promoter proximal region did not recover throughout the duration of the assay (50 minutes), suggesting DSBs may be repaired differently depending on their location within genes, or break-induced transcription may not be a feature of all DSBs[135].

The transcription by RNAPII at breaks results in the formation of long-noncoding RNAs, known as damage-induced long non-coding RNA (dilncRNA)[134] or damage-responsive transcripts (DARTs)[133]. Both divergent transcription (away from the break in the antisense and sense directions) and to a lesser extent convergent transcription (towards the break), was observed by RNAPII (phosphorylated at S2 and S5) at DSBs generated in both genic and intergenic regions[134], suggesting RNAPII is actively recruited to DSBs. However, unlike S2 and S5 RNAPII initiating transcription at DSBs in both genic and intergenic regions[134], RNAPII phosphorylated at Y1 was found to transcribe at promoter-associated DSBs only, and not DSBs in intergenic regions, which could suggest a model where RNAPII must already be present on the gene for *de novo* transcription initiation, rather than *de novo* recruitment[133]. This Y1P RNAPII associated transcription was also observed to be divergent away from the break (sense downstream and antisense upstream), with Y1P dependent sense upstream transcripts

also observed, which was suggested to occur as a result of antisense transcription promoted by R-loop formation (**Section 1.5.6**)[133].

Long non-coding RNA transcripts were also detected in a separate study using the I-PpoI endonuclease which has cut sites in the 28S locus and the genic RYR2 locus[131]. Transcripts were observed only in the antisense upstream direction from the break (divergent transcription) [131]. These transcripts were sensitive to RNAPII inhibition, which indicates that RNAPII is responsible for break induced transcription, even at loci which are not canonically transcribed by RNAPII, such as the 28S locus[131]. Bidirectional divergent transcription resulting from transcription in the sense downstream direction couldn't be confirmed in this system, due to high levels of sense downstream transcripts detected resulting from pre-existing transcription[131]. However, knockdown of EXOSC10, which processes/degrades dilncRNA (**Section 1.5.6**), resulted in an increase in transcripts in both the sense downstream and antisense upstream directions at the RYR2 locus, as well as an additional locus cut by A*si*SI (RBMXL1), confirming divergent transcription from both ends of the break[132]. *De novo* break-induced transcription has also been observed in other organisms such as Drosophila[136] and *Arabidopsis*[137] (**Table 1.6**). In Drosophila, DSBs trigger RNAPII stalling/pausing, which results in spliceosome-mediated recruitment of RNAPII for antisense transcription. These transcripts then hybridise with the pre-existing mRNA transcript, forming dsRNA (**Section 1.5.7**)[136].

An interesting question arises from the notion of *de novo* break-induced transcription, namely, can RNAPII actually use a DNA end generated at a DSB without a promoter for transcription initiation? *In vitro*, RNAPII was found to be able to associate with free DNA ends on a plasmid cut by I-SceI, forming RNA products resulting from bidirectional divergent transcription (sense

downstream and antisense upstream), suggesting free DNA ends at a DSB can be used for transcription initiation[134]. Furthermore, the RNAPII Pre-Initiation Complex (PIC (TFIIA, TFIIB, TFIID, TFIIE, TFIIF, and TFIIH)), and associated factors CDK9 and MED1, were found to be recruited to DSBs[129]. The knockdown of PIC components impairs the recruitment of RNAPII to DSB ends and reduces the formation of 53BP1 foci, suggesting that the PIC complex plays a role in RNAPII transcription initiation at breaks. This recruitment of RNAPII and the PIC complex is also dependent on MRN[129]. MRN interacts with RNAPII and PIC, and has been suggested to tether them to DSB ends[129]. MRN and RNAPII together were found to be the minimal components required for transcription at DNA ends, with MRN promoting RNAPII activity when free DNA ends (either blunt ends or with overhangs) are available, by DNA end melting/strand separation, independent of MRN nuclease activity, to facilitate transcription initiation[138]. This suggests DSBs can act as promoters of *de novo* break induced transcription facilitated by MRN, and additionally also suggests end resection is not a prerequisite for dilncRNA transcription by RNAPII[138].

A study also found that RNA Polymerase III (RNAPIII) is recruited to DSBs by MRN (with a requirement of short range end resection by MRN for *de novo* transcription) [130]. In this study, RNAPII recruitment was not detected[130]. The observed involvement of RNAPIII, with no role for RNAPII, is unexpected and seems to contradict the large body of evidence for RNAPII recruitment and/or activity at DSBs[129,133,134,139]. Nevertheless, RNAPIII may also play a role in the RNA dependent DDR, potentially in conjunction with RNAPII. This could also suggest differential usage of RNA Polymerases, perhaps depending on the type of locus which is damaged.

Taken together this body of literature suggests that RNAPII, and potentially also RNAPIII, can

transcribe long non-coding RNA transcripts at DSBs which serve functional roles in repair (**Figure 1.8**). However, some remaining questions arising from conflicting evidence need to be resolved, for example regarding the location of the DSB within the genome influencing *de novo* transcription or recruitment. The mechanistic details of *de novo* break-induced transcription and the repair factors which process these transcripts are summarised in **Table 1.6**.

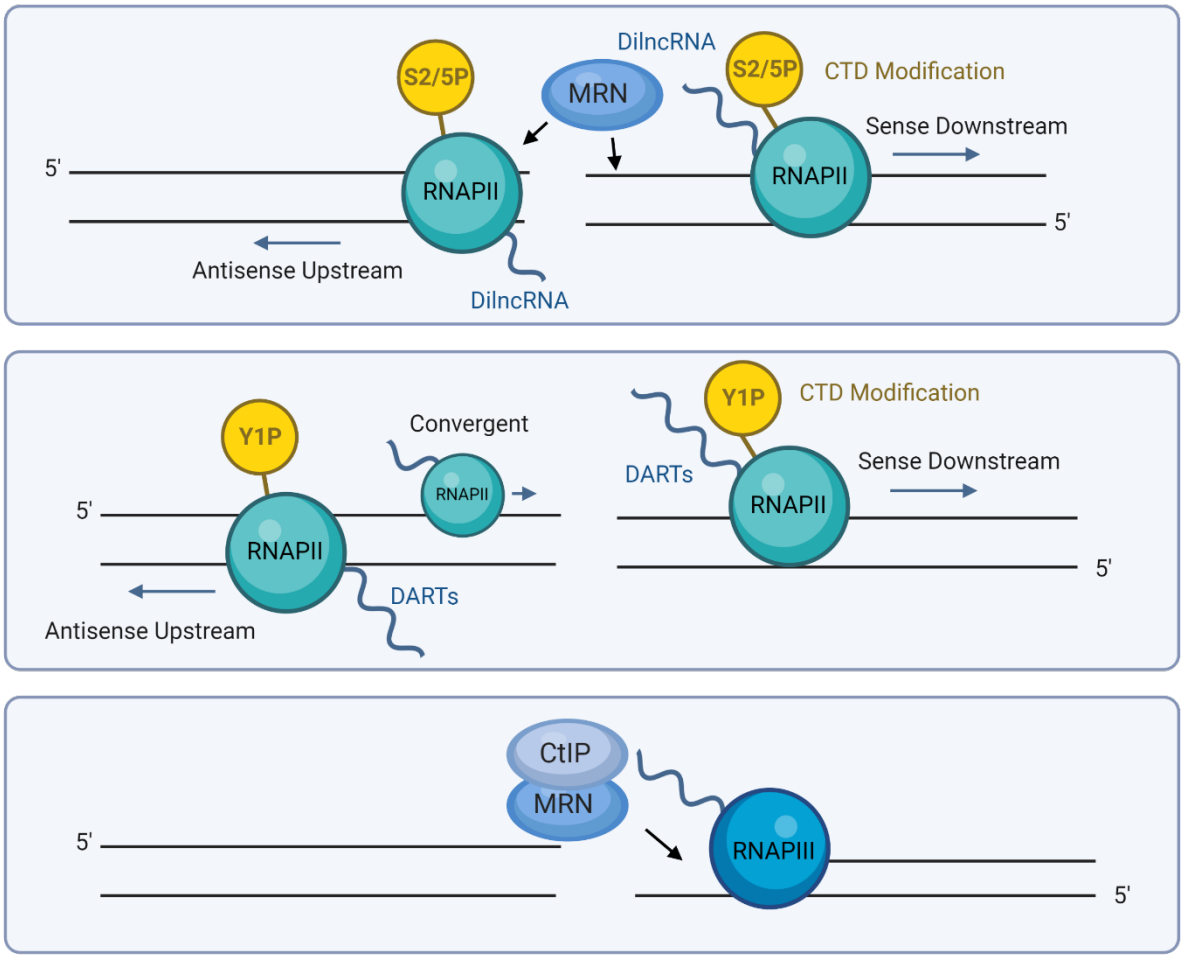


Figure 1.8: *Different models of de novo break induced transcription by RNAPII (or RNAPIII). Image created with BioRender.com.*

1.5.6 R-loops and RNA:DNA hybrids in DSB repair

R-loops, three stranded structures with an RNA:DNA hybrid and a displaced single DNA strand, and/or RNA:DNA hybrids, have been suggested to form as a consequence of

transcription around DSBs. However, it is less clear if RNA:DNA hybrid/R-loop formation at breaks is either a result of *de novo* break-induced transcription[134,140,141], or from pre-existing transcription in transcriptionally active regions[142,143] (**Figure 1.9**). It is also not yet understood if these structures play an important role as repair intermediates or are simply consequences of active transcription or pausing around DSBs, and need to be removed for repair to occur. Furthermore, the distinction between hybrids/R-loops formation is not always apparent, for example, commonly utilised experimental tools like the S9.6 antibody (an antibody which recognises RNA:DNA hybrid structures) in immunofluorescence or pull-down and sequencing (DRIP-Seq), or catalytically inactive RNaseH1 (an RNA:DNA hybrid processing enzyme), don't allow differentiation between R-loops or RNA:DNA hybrids[144].

Evidence of RNA:DNA hybrid formation at DSBs

In general, the formation of RNA:DNA hybrids and/or R-loops at DSBs is relatively well described. Various techniques have eluded to RNA:DNA hybrid formation at DSBs, including the recruitment of RNaseH1 to laser induced DNA damage[145], DRIP-Seq at A*si*SI induced DSBs[140,145], DRIP-Seq at I-PpoI induced DSBs[140,141,146], Chromatin Immunoprecipitation (ChIP) of RNaseH1 in A*si*SI cells[133], S9.6 immunofluorescence microscopy at damage sites[130], and in a cell free *in vitro* transcription system[138]. However, the formation of these hybrids may be influenced by the location of the DSB in different regions of the genome. Analysis of DRIP-Seq data generated in the A*si*SI cell line found the occurrence of RNA:DNA hybrids at DSBs correlated mainly with the transcriptional activity of the locus[112,147], implying there may be a requirement for pre-existing transcription in RNA:DNA hybrid formation at DSBs. However, this was not always the case, with some RNA:DNA hybrids detected at regions with very low pre-existing transcriptional activity, indicating *de novo* RNAPII recruitment/transcription may contribute at least partially to RNA:DNA hybrid formation at DSBs[147]. Further support for a

model of *de novo* transcription at breaks leading to RNA:DNA hybrid formation comes from *in vitro* experiments using linear DNA in a minimally reconstituted system with RNAPII and MRN without pre-existing transcription[138]. The RNA products generated initially were sensitive to RNaseA (mainly digesting ssRNA), but became RNaseA resistant and RNaseH sensitive over time, suggesting RNA transcripts (dilncRNA) resulting from *de novo* transcription at breaks have the potential to form RNA:DNA hybrids[138].

Functional roles of RNA:DNA hybrids in repair: Repair factor recruitment, promoting end resection, protecting resected ends, and dsRNA formation

RNA:DNA hybrids may function as important DSB repair intermediates, acting as platforms for the recruitment of repair factors, such as BRCA1[140,148], to promote or restrain DNA end resection[145,148], and to protect ssDNA generated after DNA end resection from degradation by nucleases[130].

In agreement with this, the overexpression of RNaseH1 was shown to impair both HR and NHEJ mediated DSB repair[145], although in some cases hybrid formation was found to preferentially influence one pathway over the other (**Table 1.5**). Drosha, and to an extent Dicer, through their non-canonical roles outside of miRNA processing (**Section 1.5.7**), were needed for the formation of RNA:DNA hybrids/R-loops and recruitment of RNaseH1 at A*si*SI induced breaks[145]. Functionally, RNA:DNA hybrids/R-loops promoted efficient end resection, as the overexpression of RNaseH1 led to reduced end resection[145].

Conversely, RNA:DNA hybrids have been suggested to form as a consequence of end resection. RNA:DNA hybrids were observed in non-genic regions at I-PpoI and A*si*SI induced breaks, as well as in genic regions (consistent with a model of *de novo* transcription generating

RNA:DNA hybrids)[140]. RNA:DNA hybrids were formed as a result of nascent RNA pairing to resected DNA ends, and RNA:DNA hybrid levels were reduced when end resection was inhibited[140]. The overexpression of RNaseH1 impaired BRCA1 and BRCA2 recruitment to DSBs, suggesting RNA:DNA structures are required for repair factor recruitment to resected DNA ends. Furthermore, BRCA2 also facilitated RNA:DNA hybrid processing to allow RAD51 binding by recruiting RNaseH2[140]. Therefore, RNA:DNA hybrids formed at resected ends act to recruit repair factors like BRCA1 and BRCA2, but are then removed by the action of RNaseH2 to allow repair by HR to proceed[140]. Moreover, RNA:DNA hybrids may protect resected ends from degradation by nucleases[130]. RNAPIII was found to utilise the 3' DNA end at the DSB which is exposed after minimal end resection (by the action of MRN and CtIP) to transcribe and synthesise dilncRNA, which hybridises with the resected DNA end to form an RNA:DNA hybrid[130], protecting the 3' DNA overhangs from degradation and preventing the loss of genetic information[130]. Additionally, in *S. pombe*, the overexpression of RNaseH1/2 increased end resection and RPA spreading, and led to loss of repeat regions in the 28S locus after I-PpoI-induced DSBs[141]. Therefore, RNA:DNA hybrids are also required to restrain end resection in order to prevent loss of genetic information[141]. However, the timely removal of RNA:DNA hybrids was important for RPA recruitment to resected DNA ends due to pairing of nascent RNA to the ssDNA, and consequently the knockdown of RNaseH1 also impaired HR[141].

While RNA:DNA hybrid formation appears to influence / be influenced by end resection, which is an important step in HR, RNA:DNA hybrids have also been found to promote repair by NHEJ[145,146]. RNA:DNA hybrid formation at I-PpoI-induced DSBs at both genic and intergenic regions was shown to depend on the RNA binding protein RBM14, which promotes RNAPII recruitment to DSBs for *de novo* transcription[146]. The depletion of RBM14 was found

to impair NHEJ, suggesting RNA:DNA hybrids generated by RNAPII transcription are also needed for NHEJ-mediated repair[146].

R-loops formed at DSBs as a consequence of Y1P RNAPII break-induced transcription were also found to facilitate dsRNA generation by promoting antisense transcription[133]. The resulting dsRNA can then be processed by Dicer (**Section 1.5.7**) and can function in the recruitment of 53BP1 and MDC1[133].

Processing/Removal of RNA:DNA hybrids is required for DSB repair

As already touched on above with the action of RNase H1[141] and RNaseH2[140], whilst RNA:DNA hybrids may have functional roles in DSB repair, their timely processing/removal is an important step to ensure the fidelity of DSB repair[148]. Impaired RNA:DNA hybrid processing/removal potentially has deleterious consequences on genome integrity[149]. Processing factors including Senataxin[144], the RNA exosome component EXOSC10[132], DHX9[150], DDX1[151], XPF[149], and the RNA-editing enzyme ADAR2[152], are known to be recruited to RNA:DNA hybrids/R-loops to aid in their resolution.

For example, the RNA helicase DDX1 is recruited to DSBs and functions to remove RNA:DNA hybrids at resected DNA ends to maintain ssDNA and allow RPA and RAD51 binding, to promote HR repair[151]. Moreover, the RNA exosome subunit, EXOSC10, is required to limit the formation of RNA:DNA hybrids between *de novo* transcribed dilncRNA and resected ssDNA, by degrading the dilcRNA and allowing RAD51 and RPA recruitment for HR[132]. Consequently, the depletion of EXOSC10 results in 'hyper'-end resection and impaired RPA recruitment[132].

Moreover, Senataxin, which unwinds RNA:DNA hybrids, is also recruited to DSBs[144]. The depletion of Senataxin increases the formation of RNA:DNA hybrids/R-loops at DSBs, and impairs RAD51 recruitment (but not end resection) and HR[144]. Additionally, depletion of Senataxin increased the improper re-joining of DSB ends resulting in translocations, which was rescued by RNaseH1 overexpression, suggesting that RNA:DNA hybrids need to be resolved to prevent translocations at DSBs and preserve genome integrity[144]. Furthermore, Senataxin depletion increased deletions observed at DSBs as a result of XPF activity, suggesting RNA:DNA hybrids contribute to loss of genetic information at DSBs and need to be removed[149]. In addition, a role for RNA editing in R-loop resolution by Senataxin was also recently suggested[152]. Adenine-to-Inosine editing of RNA in the hybrid by the deaminase ADAR2 is required for end resection[152]. ADAR2 interacts with Senataxin, suggesting RNA editing may facilitate the removal of R-loops by Senataxin to allow HR repair[152].

To summarise, RNA:DNA hybrids/R-loops appear to form at DSBs occurring predominantly in transcriptionally active regions of the genome[147], although not without exception[140,146]. Whether RNA:DNA hybrids form as consequences of active transcription prior to DSB-induction, as 'signals' for HR-mediated repair of transcriptionally active regions[148], or are products of *de novo* transcription at DSBs in active and inactive regions of the genome[140], is not yet clear. Similarly, it is also not conclusive at which step in repair RNA:DNA hybrids/R-loops act/form, for example, post-end resection (RNA:DNA hybrids forming due to RNA pairing with resected DNA ends[132,144,151]), or pre-end resection (due to displacement of the DNA double strand forming an R-loop which then influences DNA end resection[145,148,152]). However, it seems that RNA:DNA hybrids/R-loops can, at least in certain regions of the genome, act as important structures in DSB repair, recruiting repair factors such as BRCA1/2 and protecting resected DNA ends, but their proper processing and removal by RNA processing

enzymes, such as EXOSC10[132], Senataxin[144,153], and ADAR2[152], is needed for repair and maintenance of genome integrity after a DSB (**Table 1.5**). In addition, RNA:DNA hybrid formation may facilitate RNA-templated DSB repair (**Section 1.5.8**).

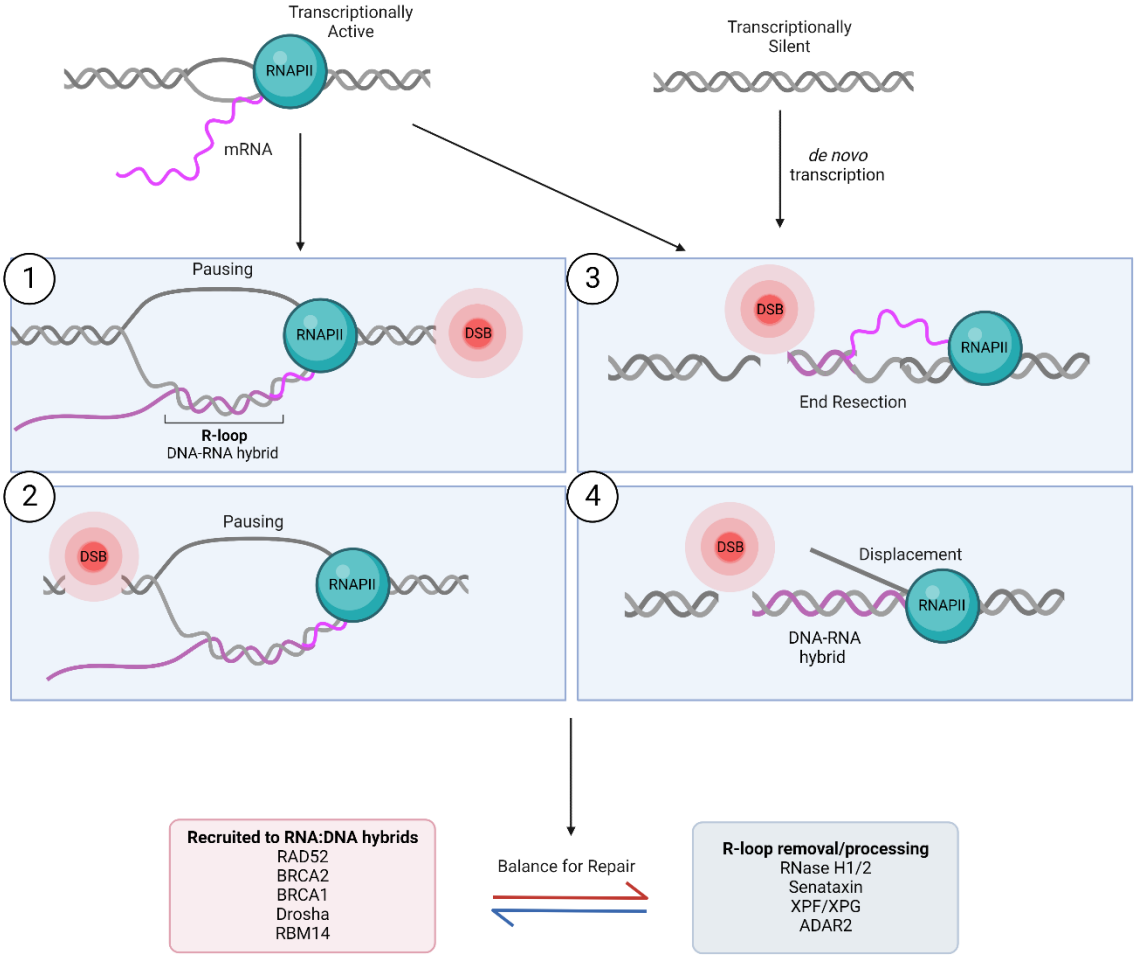


Figure 1.9: *Examples of potential mechanisms of R-loop/RNA:DNA hybrid formation at DSBs. Figure adapted from*[143]*. References for each model; Model 1*[144,148]*, Model 2*[144,145,148]*, Model 3*[130,140,141,144,151]*, Model 4*[130,132,141,145]*. Note: some references may support more than one model. For details, see* ***Table 1.5****. Image created with BioRender.com.*

Protein	Function at DSBs	Genomic context	Repair Pathway	Pre- or post-resection?	Ref
RBM14	Needed for RNAPII-dependent generation of RNA:DNA hybrids - may be involved in transcription initiation at DSBs	RBM14, Ku80, RNA:DNA hybrids, and RNAPII detected at both intergenic (devoid of pre-existing transcription)	NHEJ	N/A	146

	RBM14 interacts with Ku (Ku needed for RBM14 recruitment) and binds RNA:DNA hybrids	and genic regions at I-PpoI induced breaks, which is impaired by transcription inhibition			
SETX	Promotes RNA:DNA hybrid/R-loop resolution	SETX is recruited to DSB in transcriptionally active genomic regions (but some RNA:DNA hybrids still detected in untranscribed regions)	HR	Post-end resection: Senataxin activity promotes RAD51 recruitment without affecting end-resection (measured using ssDNA assay), suggesting RNA:DNA hybrids prevent RPA/RAD51 loading. Senataxin needed to prevent DNA translocations as a result of RNA:DNA hybrid formation	144
	SETX is required to prevent large deletions (loss of proximal gene) at DSBs caused by the flap endonuclease XPF processing of RNA:DNA hybrids/R-loops (could be via SSA?)	RNA:DNA hybrids/R-loops form at DSB in an integrated transcriptionally active reporter locus	Not explored	Not explored	149
EXOSC10	EXOSC10 degrades/processes dilncRNA generated at DSBs to prevent RNA:DNA hybrid formation	Transcriptionally active regions	HR	Pre-end resection: *De novo* transcription produces dilncRNA and promotes end resection. The depletion of EXOSC10 hyperactives end resection (SMART assay), which can be rescued by RNAPII inhibition. DilncRNA hybridises with resected DNA ends, generating RNA:DNA hybrids, which prevents RPA binding and HR. EXOSC10 is required to degrade dilncRNA, reducing RNA:DNA hybrid formation and allowing RPA binding	132

DDX1	Resolves RNA:DNA hybrids at DSBs at active loci	Not explored, used DR-GFP I-SceI site	HR	Post-end resection: Maintains ssDNA after end-resection by removing RNA:DNA hybrids, but does not influence end resection itself, and is therefore needed for RPA and RAD51 foci formation. Consequently, DDX1 knockdown leads to an accumulation of RNA:DNA hybrids.	151
BRCA2 and RNaseH2	BRCA2 is recruited to RNA:DNA hybrids (by BRCA1) and recruits RNaseH2 in S/G2 to degrade RNA:DNA hybrids	RNA:DNA hybrids formed at both genic and nongenic regions (in both I-PpoI and A*si*SI systems).	HR	Post-end resection: dilncRNA hybridise with resected DNA ends in S/G2, but dilncRNA generation (or RNAPII transcription) is not required for end resection RNA:DNA hybrids formed by dilncRNA needed for BRCA1 and BRCA2 recruitment, and subsequent RNaseH2 recruitment and processing, allowing RAD51 binding	140
Drosha (and Dicer)	Required for the formation of RNA:DNA hybrids/R-loops at DSBs (through invasion of the DNA duplex) and the recruitment of RNaseH1 to DSBs	RNA:DNA hybrids/R-loops formed mainly at transcriptionally active regions	RNaseH1 overexpression and Drosha KD impaired both HR and NHEJ	Pre-end resection: RNA:DNA hybrids/R-loops and Drosha are needed to promote end resection. Depletion of Drosha and Dicer, and over-expression of RNaseH1, results in reduced end resection and RNA:DNA hybrid formation/R-loop at DSBs	145
RNaseH1 (Rnh1 in S. *pombe*)	Rnh1 resolves RNA:DNA hybrids at DSBs to allow RPA binding	RNAPII recruited to DSBs and RNA:DNA hybrids formed at I-PpoI cleavage site in 28S	HR (both overexpression and depletion of RNaseH1 impairs HR)	Pre- or Post-end resection: Loss of RNaseH1 prevents RPA binding to ssDNA. RNAPII transcribes on resected DNA ends, and RNA hybridises with the ssDNA - needs to be removed to allow RPA binding	141

				Overexpression of RNaseH1 led to loss of repeat regions due to 'hyper'-end resection as a result of DNA:RNA hybrid removal	
RAD52 and XPG	RAD52 is recruited to DSBs by RNA:DNA hybrids/R-loops and in turn recruits BRCA1 RAD52 promotes resolution of RNA:DNA hybrids by recruiting XPG	Transcriptionally active loci	HR, prevents genomic alterations by NHEJ in transcriptionally active regions	Pre-end resection: RNA:DNA hybrids/R-loops are required for RAD52 recruitment. RAD52 recruits XPG which processes RNA:DNA hybrids/R-loops to facilitate end resection and RAD51 binding.	148
ADAR2	Deaminase / RNA editing (A → I) of hybrids/R-loops and removal of hybrids needed for end resection and subsequently HR ADAR2 interacts with SETX	Not explored	HR	Pre-end resection: ADAR2 depletion and RNA:DNA/R-loop hybrid accumulation impairs DNA end resection (SMART assay) and RPA foci formation. Overexpression of RNaseH1 leads to RPA foci formation, suggesting RNA:DNA hybrids/R-loops prevent end resection. ADAR2 is recruited to DSBs and is required for removal of RNA:DNA hybrids/R-loops, potentially by editing RNA:DNA hybrids for subsequent removal by SETX	152

Table 1.5: *Summary of proteins with activity in RNA:DNA hybrid/R-loop formation or processing/removal at DSBs. The context in which RNA:DNA hybrids/R-loops were observed is also highlighted, as well as the contribution to a specific repair pathway. Whether or not the RNA:DNA hybrids/R-loops were observed to form pre- or post-end resection is also highlighted.*

1.5.7 Non-canonical roles of Dicer and Drosha in the RNA-dependent DDR

Transcription at DSBs and dilncRNA production may also result in the formation of short non-coding RNA known as DNA damage RNAs (DDRNA) through Dicer and Drosha activity,

outside of their canonical miRNA processing roles (**Section 1.5.1**). In response to DSBs, Dicer, a mainly cytoplasmic enzyme, can be phosphorylated on residue S1016 and residues S1728 and S1852, in order to facilitate nuclear translocation and dsRNA processing respectively[154]. Drosha and Dicer are recruited to DSBs sites[145,155], however the exact step at which Dicer and Drosha act in DSB repair is not completely clear. Mutations in Dicer residues S1016 or S1728/S1852 results in impaired 53BP1 foci formation[154]. In agreement with this, Dicer and Drosha were proposed to act downstream of γH2AX, ATM, and MDC1, but upstream of 53BP1, as Dicer and Drosha knockdown impairs 53BP1 foci, but not pATM or γH2AX[145]. However, other studies have suggested Dicer and Drosha may function further upstream in DSB repair, with knockdown resulting in impaired 53BP1 foci, as well as MDC1 and p-ATM foci, but not γH2AX[156]. The knockdown of Dicer and Drosha also does not affect MRN recruitment to DSBs[157].

It appears that Dicer and Drosha act in DSB repair independently of the miRNA pathway as TNRC6A knockdown, which interacts with AGO2 in miRNA-dependent silencing, had no impact on 53BP1 foci formation, implicating Dicer and Drosha in the RNA dependent DDR at DSB sites outside of their canonical miRNA roles[145]. Mechanistically, the impact of Dicer on repair factor foci is suggested to be due to the endonuclease activity of Dicer on dilncRNA, as an endonuclease-mutant Dicer cannot rescue 53BP1 foci formation in Dicer depleted cells[156]. In addition, Dicer RNA products of 22-23nt were observed mapping to sites around a DSB generated at an integrated I-SceI locus, suggesting that Dicer processes the transcribed dilncRNA into DDRNA[134]. Furthermore, Drosha knockdown also reduced DDRNA production, and a concurrent increase in dilncRNA was observed, indicating DDRNA are processed from dilncRNA by both Dicer and Drosha[134].

Functionally, Dicer and Drosha may regulate repair factor recruitment through DDRNA production. 53BP1 foci have previously been shown to be sensitive to RNase A treatment[158]. The exogenous addition of short RNA sequences corresponding to DDRNA was able to restore 53BP1 focus formation in cells treated with RNase A, indicating 53BP1 foci formation depends on small RNA which originate from the break itself[156]. Interestingly, DDRNA and dilncRNA were also found in 53BP1 RIP-Seq, indicating RNA may regulate DDR foci formation by directly interacting with repair factors[134]. DDRNA themselves localise to DSBs at sites from where they originate, which is impaired by RNAPII inhibition, but not RNaseH1 expression, suggesting DDRNA can localise to specific sites by hybridisation with dilncRNA transcribed at breaks. This gives dilncRNA two roles in DSB repair, as both signals for site-specific DDRNA recruitment, and as substrates for biogenesis of DDRNA by Dicer and Drosha[134]. An alternate mechanism of DDRNA production was suggested to occur dependent on R-loop formation[133]. Y1P RNAPII antisense transcription resulting from R-loops formed by DARTS/dilncRNA, leads to the generation of longer dsRNA (**Section 1.5.6**)[133]. The knockdown of Dicer increased the presence of these longer dsRNA (detected by the J2 antibody), suggesting Dicer may process these longer Y1P transcribed dsRNA into shorter DDRNA[133]. Additionally, small damage-responsive RNA produced at breaks was also detected in plants. In *Arabidopsis,* Dicer-like proteins were found to be required for DSB repair at an integrated I-SceI cut site, and the production of Dicer-like protein-dependent small RNA (diRNA) was detected both sense and antisense up- and down-stream from the I-SceI cut site, which were bound by AGO2[137]. Interestingly, DDRNA were also found bound to Argonaute in RIP-Seq in human cells, suggesting another functionality of DDRNA in repair[131].

The activity of Dicer and Drosha in DDRNA production may also be required for other repair-related processes, such as DISC and chromatin remodelling[127,159]. Depletion of Dicer and

Drosha was observed to lead to reduced RNAPII transcriptional repression induced by DSBs (DISC), due to reduced recruitment of BMI1, part of the PRC1 complex, to DSBs and subsequently reduced H2AK119Ub (**Section 1.5.4**). DDRNA mapping to an I-SceI cut site was found to bind BMI1 by RIP-Seq, suggesting DDRNA contribute to DISC through recruitment of BMI1[127]. In addition to DISC, DDRNA may play a role in chromatin modification and remodelling for repair factor recruitment[159]. MMSET and TIP60 are responsible for histone methylation and acetylation respectively, which are important for repair factor recruitment to chromatin. Knockdown of Dicer and Drosha results in reduced H4K20me2 and H4K16Ac at DSBs as a consequence of reduced MMSET and TIP60 respectively, which can be rescued by addition of short RNA mapping to the I-PpoI cut site. AGO2 was found to interact with both MMSET and TIP60 for recruitment to DSBs, dependent on AGO2 binding to small RNA, and subsequently promoted recruitment of BRCA1 to DSBs. This additionally implicates small RNA in the regulation of DNA repair through chromatin remodelling[159]. Interestingly, RNA itself may promote a more open chromatin structure through interaction with histone tails[160].

However, DDRNA may not be produced at every DSB site across the genome[139]. Short RNA transcripts were detected at the 28S repetitive locus, but not non-repetitive genic or intergenic regions, despite the same study observing dilncRNA generation at unique genic regions at the same cut site, implying not all dilncRNA are processed into DDRNA[131]. Furthermore, analysis of small RNA-Seq at A*si*SI induced DSBs resulted in the observation of no small RNA products mapping to the cut sites tested, despite a defect in HR and NHEJ resulting from Dicer and Drosha depletion being observed in the same study[145]. This could potentially reflect differences in DDRNA production or detection between repetitive loci (e.g. 28S cut by I-PpoI[131]) and non-repetitive loci (e.g. those mainly cut by A*si*SI[145]) or exogenous integrated sites without physiological chromatin status[161] (e.g. I-SceI[134,156]). This also suggests that

Drosha and Dicer may have other functions in the RNA-dependent DDR which results in the repair defect phenotypes observed.

In agreement with this, the requirement of both Dicer and Drosha for DDRNA production has been challenged[131]. Small RNA of 21-22nt were detected mapping to the 28S I-PpoI cut site, which were sensitive to RNAPII inhibition[131]. However, Drosha or DGCR8 knockout had no impact on the production of these small RNA[131]. In contrast, Dicer knockout impaired the production of only a portion (~50%) of these small RNA, suggesting some DDRNA may be produced by Dicer cleavage, whereas others are produced through different mechanisms, such as by other nucleases[131].

Taken together, it appears that Dicer and Drosha can influence DSB repair independently of miRNA biogenesis in the RNA dependent DDR. Where exactly Dicer and Drosha act in DSB repair has not reached a consensus in the literature, and whilst Dicer and Drosha may be required to process (a least a subset of) dilncRNA, the observation of small DDRNA generated from longer dilncRNA has not been unanimously confirmed[145]. It has also been suggested that Dicer and Drosha may act in distinct pathways in repair[131], instead of in the same RNA cleavage pathway[134]. Furthermore, it is possible that Dicer and Drosha have roles in repair outside of RNA processing, contributing to NHEJ or HR repair and/or dilncRNA formation independently of RNA cleavage activity, such as through promoting transcription at DSBs or RNA:DNA hybrid/R-loop formation. Indeed, Drosha has been found to interact with RNAPII and is associated with promoter-proximal regions of genes, positively regulating gene expression independently of RNA cleavage[162], and Dicer can promote transcription termination at sites of transcription-replication conflict in S. *pombe*[163]. The involvement of RNA and

transcription in DNA repair is summarised in **Table 1.6**, and DDRNA biogenesis and functions are summarised in **Figure 1.10**.

Notably, other miRNA factors other than Dicer and Drosha have been shown to be involved in the DDR outside of their canonical miRNA processing roles, including AGO2 and DGCR8. AGO2 has been shown to bind DDRNA/diRNA[131,164], and facilitates RAD51 recruitment to DSBs to promote HR[164]. DGCR8 can act in DNA repair, independently of RNA processing and Drosha binding, through promoting the recruitment of RNF168 to DSBs. After DSB induction, DGCR8 is phosphorylated by ATM, which results in deubiquitination and stabilisation of DGCR8. DGCR8 is then recruited with binding partner RNF168 to MDC1 and RNF8 at DSBs. Consequently, the knockdown of DGCR8 impairs both HR and NHEJ[165].

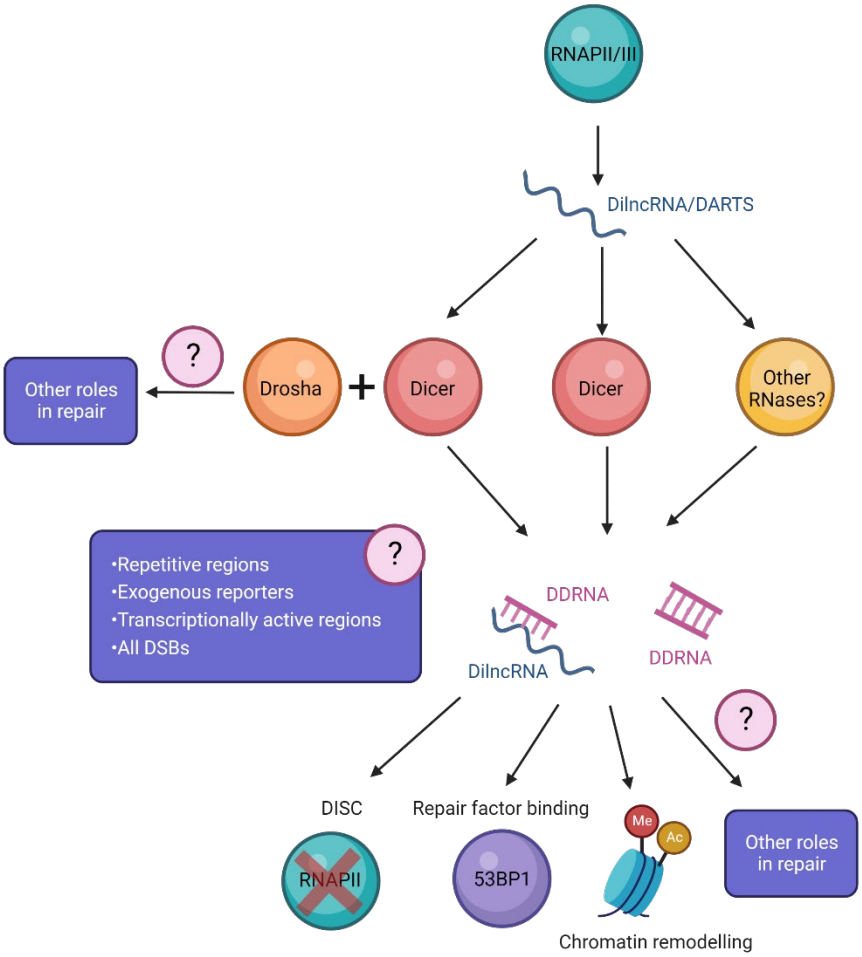


Figure 1.10: *The possible mechanisms of DDRNA biogenesis and their functional roles in DSB repair. Image created with BioRender.com.*

Reference	Transcription at DSB?	Genomic context	NHEJ or HR?	Proteins involved	Methods/Cellular Systems
Vítor 2019 (Almeida)[135]	Either antisense upstream or sense downstream (not both at the same time)	DSB in promoter proximal region did not initiate transcription but an intragenic DSB (in exon) showed *de novo* transcription from the break	Not explored	Not explored	Novel MS2/PP7 I-SceI reporter in HEK293 Live cell imaging and single transcript detection
Bonath *et al* 2018 (Visa)[131]	Antisense upstream (can't rule out sense downstream because sequence is identical to mRNA)	diRNA (DDRNA): Repetitive regions (28S) not genic or intergenic dilncRNA: 28S and genic RYR2 loci (both repetitive and non-repetitive)	Not explored	Dicer (one diRNA subtype) but not Drosha or DGCR8. DiRNA are bound by AGO proteins	I-PpoI (endogenous loci) in Hela and mESC (mouse) cells Small RNA-Seq, RT-qPCR, AGO RIP-Seq

Domingo-Prim *et al* 2019 (Visa)[132]	EXOSC10 depleted cells had higher dilncRNA levels in the antisense upstream and downstream sense In 28S, observe diRNA (DDRNA) mapping antisense upstream, which are increased after EXCOS10 depletion	A*si*SI cut site in the promoter of RBMXL1, and I-PpoI cut sites in 28S repetitive locus and RYR2 genic	EXOSC10 promotes HR by degrading dilncRNA EXOSC10 promotes RPA and RAD51 recruitment, but cells depleted of EXOSC10 show hyper-end resection	EXOSC10 is recruited to DSBs dependent on RNAPII transcription	A*si*SI and I-PpoI Small RNA-Seq, laser microirradiation, end resection assay (Brdu/SMART), qPCR, DRIP-qPCR
Lu *et al* 2018 (Bushell)[145]	Indirectly: observe RNA:DNA hybrids at DSB. No small RNA detected at regions cut by A*si*SI, but dilncRNA transcription not assessed	RNA:DNA hybrids formed mostly in transcriptionally active regions	Dicer and Drosha depletion impairs both NHEJ and HR	Dicer and Drosha KD impaired 53BP1 recruitment (but not ɣH2AX) and RNA:DNA hybrid formation	A*si*SI RNaseH1 laser stripes, S9.6 DRIP-Seq, IF, laser microirradiation, small RNA-Seq
D'Alessandro *et al* 2018 (d'Adda di Fagagna)[140]	Indirectly: Observed RNA:DNA hybrids in upstream antisense and sense downstream direction, dependent on RNAPII	DAB1 weakly transcribed gene and also a nongenic site cut by I-PpoI Saw DRIP signal and dilncRNA production also in nongenic A*si*SI site Observed enrichment of RNASEH2A by ChIP at A*si*SI site in nongenic region	ASOs targeting dilncRNA impaired both HR and NHEJ in traffic light reporter system but dilncRNA promote HR by pairing to resected ends to form RNA:DNA hybrids to recruit BRCA1	DilncRNA recruit BRCA1, BRCA2, and RAD51. BRCA1 interacts with RNaseH2 to control RNA:DNA hybrid levels in S/G2	A*si*SI U2OS and in I-PpoI in Hela cells DRIP-qPCR, RNaseH2A ChIP, IF, EMSA
Francia *et al* 2012 (d'Adda di Fagagna)[156]	Not explored	Not explored	Not explored	Dicer and Drosha are required for RNA synthesis from breaks RNase A treatment impaired pATM, 53BP1, and MDC1 foci formation	NIH2/4 exogenous I-SceI locus flanked by Lac and Tet repeats IF, small RNA-Seq, RT-qPCR

Francia *et al* 2016 (d'Adda di Fagagna)[157]	Not explored	Not explored	Not explored	RNase A treatment and Dicer and Drosha KD impaired 53BP1 and MDC1 recruitment, but not NBS1 of the MRN complex	U2OS/TRE/I-SceI-19 cells Laser stripes and IF
Michelini *et al* 2017 (d'Adda di Fagagna)[134]	Observed divergent transcription (sense downstream and antisense upstream) and convergent transcription (sense upstream and antisense downstream, 5' → 3') RNA S5, S2, and total RNAPII localises to breaks Using plasmid cut with I-SceI: observed transcription was a bidirectional divergent transcription (sense downstream, antisense upstream)	Measured dilncRNA formation on strand lacking pre-existing transcription in different systems: integrated locus (I-SceI), A*si*SI cleavage in intergenic region, I-PpoI cleavage in DAB1 and in an intergenic region, and Cas9 cleavage at Myc gene	Not explored	RNAPII inhibition, but not ATM inhibition, impairs dilncRNA formation MRN interacted with RNAPII in irradiated cells, and MRN knockdown results in a decrease in dilncRNA production, due to decreased RNAPII association with DSBs 53BP1 associated with DDRNA and dilncRNA	A*si*SI and I-PpoI, I-SceI integrated NIH2/4 cells smFISH, Cell-free extracts with I-SceI recognition site containing plasmid, IF, RT-qPCR, chromatin fibres, RIP-qPCR
Burger *et al* 2019 (Gullerova)[133]	DilncRNA (DART) synthesis away from the break (divergent, sense downstream and antisense upstream) by Y1P RNAPII, which forms R-loops to allow reverse oriented transcription towards the break (convergent)	Promoter associated DSBs in A*si*SI, but not intergenic sites	Not explored	c-Abl phosphorylates RNAPII on Y1P for DSB recruitment DART synthesis, RNA:DNA hybrids, and dsRNA formation from Dicer processing of DARTs, needed for 53BP1 and MDC1 foci formation	A*si*SI mNET small RNA-Seq, S5/S2/Y1/total RNAPII ChIP, IF, RNaseH1 ChIP, DRIP-qPCR, J2-RIP
Wei *et al* 2012 (Qi)[137]	Detection of short RNA (diRNA) both antisense and sense upstream	Integrated I-SceI cut site in *Arabidopsis* and	Not explored	DiRNA are produced dependent on Dicer-like	I-SceI Small RNA sequencing,

	and downstream (*Arabidopsis* and human U2OS)	DR-GFP/U2OS cells		proteins which are then bound by AGO2 Requires Pol IV and V (*Arabidopsis*)	AGO (small) RIP-Seq and northern blot
Böttcher *et al* 2022 (Föstermann)[136]	DilncRNA transcription in the antisense upstream direction (can hybridise with coding RNA), forms dsRNA and processed into damage induced-siRNA for Ago2 binding (Drosophila)	Intron containing genes, but not intronless genes	Not explored	Stalled RNAPII and spliceosome recruits RNAPII for antisense transcription, which forms dsRNA by hybridising to the mRNA strand	Cas9 cleavage in S2 cells and NET small RNA-seq
Wang 2016 (Goldstein)[159]	Not explored	Not explored	HR	Dicer and Drosha promote HR via production of diRNA which are bound by AGO2 and promotes recruitment of MMSET and TIP60 for chromatin remodelling This promotes recruitment of BRCA1 and RAD51	I-SceI and I-PpoI IF, ChIP-qPCR
Liu *et al* 2021 (Kong)[130]	Indirectly; RNAPIII recruited to DSBs and results in RNA:DNA hybrid formation	A*si*SI cut sites at both transcribed and untranscribed regions	HR	RNAPIII transcribes dilncRNA which hybridise with the 3' DNA overhang to prevent end degradation, promoting HR	I-SceI and A*si*SI Laser microirradiation, IF, RNAPIII ChIP-qPCR, DNA sequencing around DSBs, MRE11 pull down mass spectrometry
Gómez-Cabello *et al* 2022 (Bartek)[166]	Nascent RNA transcription observed in S and G2 phases after IR Indirectly in S9.6 SMART (RL-SMART): saw RNA:DNA hybrids increase after damage on resected DNA	N/A	HR	Nascent RNA expression and RNA:DNA hybrid formation after IR depends on CtIP, RAD52, and BRCA1, but not 53BP1 RNAPII inhibition resulted in decreased CtIP, MRE11, and	IF, laser microirradiation, R-SMART = EU and Brdu, RL-SMART = S9.6 and Brdu

		RPA accumulation and increased 53BP1 accumulation Suggest transcription at DSBs promotes end resection through formation of hybrids

Table 1.6: *Summary of dilncRNA/DART transcription at DSBs and DDRNA processing. The genomic context, whether or not dilncRNA transcription promotes HR or NHEJ, the proteins involved, and the methods/cellular systems used in the study are also highlighted.*

1.5.8 RNA-templated DSB Repair

Aside from the functions described above, RNA has also been suggested to have further functionality in repair, acting as a template allowing error-free repair of DSBs in transcribed regions of the genome, dependent on RNA:DNA hybrid formation, through a HR-like pathway. In *S. cerevisiae,* Rad52 promotes annealing of RNA to the DSB end for DNA synthesis[167]. Human post-mitotic neurons, which don't replicate their DNA and therefore do not have a sister chromatid available for HR, can undergo HR-mediated repair of DSBs dependent on RNAPII transcription and RNA:DNA hybrid formation via RAD52 activity[168]. Furthermore, HR proteins RAD51, RAD52, and RPA were found to be recruited to DSBs in transcriptionally active regions in G0/G1 dependent on Cockayne syndrome B (CSB) [169]. RNaseH treatment reduced the recruitment of RAD52, suggesting an RNA:DNA hybrid is needed for recruitment[169]. Interestingly, tethering of RNA, which has an identical sequence to that of the DNA across the break site, in proximity to a DSB generated by I-SceI using dCas9, was able to restore HR repair when the locus was transcriptionally inactive, which was not enhanced by restoring transcription, indicating RNA molecules themselves can be used for HR repair[170]. Moreover, 53BP1 was found to be preferentially associated with DSBs in transcriptionally active regions and nascent mRNA, suggesting that nascent RNA may influence DNA repair by NHEJ as well as HR[114]. This RNA was suggested to act as a repair template by forming an

RNA:DNA hybrid via strand invasion, and RNaseH treatment reduced the association of 53BP1 with nascent mRNA[114]. In *in vitro* experiments, an RNA oligonucleotide was also able to act as a repair template for two DNA oligonucleotides with a 4nt gap, allowing error-free NHEJ[114].

1.5.9 RNA modifications in DSB Repair

It is now understood that RNA itself, much like DNA and proteins, can be modified post-transcriptionally. These RNA modifications possess the ability to alter a diverse array of cellular processes, including cell cycle progression and apoptosis, by altering the stability and structure of RNAs, and protein–RNA interactions[2]. Modifications of RNA include; N6-methyladenosine (m^6A), N1-methyladenosine (m^1A), 5-methylcytosine (m^5C), and pseudouridine (Ψ), however over 150 RNA modifications have been identified. Many different RNAs can be modified, such as transfer RNAs (tRNAs), ribosomal RNAs (rRNAs), mRNAs, and lncRNAs. Recently, various RNA modifications have also been shown to play a role in the cellular response to DNA damage[2].

The RNA m^6A modification is reversible, and has several writers (the METTL3–METTL14 complex, METTL16, and WTAP), and erasers (ALKBH1/3/5, and FTO), and has been implicated in the cellular response to DSBs. In response to DSBs, METTL3 is phosphorylated by ATM and recruited to breaks through an interaction with RNAPII[171]. METTL3 modifies DSB associated RNA with m^6A methylation, which forms RNA:DNA hybrids stabilised by the recruitment of the m^6A reader YTHDC1[171]. Consequently, knockdown of METTL3 results in increased γH2AX foci, reduced recruitment of RAD51, and impaired HR[171]. Interestingly, in non-damaged cells, m^6A has been shown to be present on RNA:DNA hybrids predominantly in S and G2/M phases of the cell cycle[172]. However, it is not yet clear if this could impact the DDR, in particular the DSB response[172]. Interestingly, an RNA-mediated interaction of

METTL16 and MRE11 (MRN complex) was also reported[173]. The interaction represses end resection, and is reduced after DSB induction and ATM phosphorylation of METTL16[173]. This allows end resection and promotes HR, although this appears to be independent of METTL16 function as a m^6A writer[173].

Modification of RNA with m^5C has also been shown to play a role in DSB repair. The m^5C writer TRDMT1 modifies RNA in RNA:DNA hybrids at DSB sites, which results in the recruitment of RAD52 and RAD51, and therefore favours repair by HR[174].

1.5.10 RNA may promote phase separation of DSB foci

RNA is known to promote phase separation, forming membrane-less compartments within cells which can regulate the inclusion/exclusion of specific proteins/RNA[161], such as the cytoplasmic compartments stress granules[175]. RNA may also influence phase separation for DNA repair. 53BP1 has been shown to have liquid-like behaviour and form phase separated foci, which can be reduced by RNAPII inhibition[129,161]. Targeting dilncRNA using antisense oligonucleotides (ASOs) impairs 53BP1 foci formation/liquid-like behaviour, suggesting RNA, particularly RNA transcribed at breaks, may facilitate phase separation of DDR foci to promote repair[129,161].

1.6 Summary and Overview of this Thesis

The accurate and timely repair of DSBs is critical for genome integrity and cell survival. This is orchestrated in cells through a cascade of signalling events and the carefully coordinated selection of the repair pathway, predominantly between NHEJ and HR. Therefore, understanding how each step of DSB repair is regulated is of great importance and has applications in the treatment of diseases, including cancers. 53BP1 is key in the choice between NHEJ and HR. 53BP1 activity is highly regulated through mechanisms such as restriction of H4K20me2 binding by TIRR, an enigmatic RNA binding protein. RNA has emerged as an important component of DSB repair at many levels, including repair factor regulation by miRNA, lncRNA scaffolding at DSBs, and *de novo* transcription of dilncRNA at breaks. Identifying new functionalities of damage-responsive RNA and RNA binding proteins in coordinating repair can expand our understanding of the DNA damage response.

TIRR is a poorly characterised RNA-binding protein, especially in response to IR, and how TIRR and 53BP1 separation after IR is regulated is an open question. In **Chapter 3** we provide evidence for a DSB-induced RNA-mediated separation of TIRR and 53BP1. In **Chapter 4**, we look further at the RNA binding and processing roles of TIRR in the DNA damage response. In **Chapter 5**, we expand on our observations in Chapter 4 and aim to identify novel interactors of TIRR in both non-damage and damage conditions using complementary TurboID and affinity pull-down approaches.

1.7 References

1. Jackson, S. P. & Bartek, J. The DNA-damage response in human biology and disease. *Nature* (2009) doi:10.1038/nature08467.
2. Ketley, R. F. & Gullerova, M. Jack of all trades? The versatility of RNA in DNA double-strand break repair. *Essays Biochem.* **64**, 721–735 (2020).
3. Burger, K., Ketley, R. F. & Gullerova, M. Beyond the Trinity of ATM, ATR, and DNA-PK: Multiple Kinases Shape the DNA Damage Response in Concert With RNA Metabolism. *Front. Mol. Biosci.* **6**, 61 (2019).
4. Her, J. & Bunting, S. F. How cells ensure correct repair of DNA double-strand breaks. *J. Biol. Chem.* **293**, 10502–10511 (2018).
5. Ceccaldi, R., Rondinelli, B. & D'Andrea, A. D. Repair Pathway Choices and Consequences at the Double-Strand Break. *Trends Cell Biol.* **26**, 52–64 (2016).
6. Pannunzio, N. R., Watanabe, G. & Lieber, M. R. Nonhomologous DNA end-joining for repair of DNA double-strand breaks. *J. Biol. Chem.* **293**, 10512–10523 (2018).
7. Shibata, A. & Jeggo, P. A. Roles for the DNA-PK complex and 53BP1 in protecting ends from resection during DNA double-strand break repair. *J. Radiat. Res. (Tokyo)* **61**, (2020).
8. Shibata, A. & Jeggo, P. A. Roles for 53BP1 in the repair of radiation-induced DNA double strand breaks. *DNA Repair* **93**, 102915 (2020).
9. Shibata, A. Regulation of repair pathway choice at two-ended DNA double-strand breaks. *Mutat. Res. Mol. Mech. Mutagen.* **803–805**, 51–55 (2017).
10. Chapman, J. R., Taylor, M. R. G. & Boulton, S. J. Playing the End Game: DNA Double-Strand Break Repair Pathway Choice. *Mol. Cell* (2012) doi:10.1016/j.molcel.2012.07.029.
11. Panier, S. & Boulton, S. J. Double-strand break repair: 53BP1 comes into focus. *Nat. Rev. Mol. Cell Biol.* **15**, 7–18 (2014).
12. Ochs, F. *et al.* 53BP1 fosters fidelity of homology-directed DNA repair. *Nat. Struct. Mol. Biol.* **23**, 714–721 (2016).
13. Wang, J. *et al.* PTIP associates with Artemis to dictate DNA repair pathway choice. *Genes Dev.* **28**, 2693–2698 (2014).
14. Cuella-Martin, R. *et al.* 53BP1 Integrates DNA Repair and p53-Dependent Cell Fate Decisions via Distinct Mechanisms. *Mol. Cell* **64**, 51–64 (2016).
15. Becker, J. R. *et al.* BARD1 reads H2A lysine 15 ubiquitination to direct homologous recombination. *Nat. 2021* **596**, 1–5 (2021).
16. Chapman, J. R., Sossick, A. J., Boulton, S. J. & Jackson, S. P. BRCA1-associated exclusion of 53BP1 from DNA damage sites underlies temporal control of DNA repair. *J. Cell Sci.* **125**, 3529–3534 (2012).
17. Gupta, R. *et al.* DNA Repair Network Analysis Reveals Shieldin as a Key Regulator of NHEJ and PARP Inhibitor Sensitivity. *Cell* **173**, 972-988.e23 (2018).
18. Khan, F. A. & Ali, S. O. Physiological Roles of DNA Double-Strand Breaks. *J. Nucleic Acids* (2017) doi:10.1155/2017/6439169.
19. Lei, T., Du, S., Peng, Z. & Chen, L. Multifaceted regulation and functions of 53BP1 in NHEJ-mediated DSB repair (Review). *Int. J. Mol. Med.* **50**, 90 (2022).
20. Etourneaud, L. *et al.* Lamin B1 sequesters 53BP1 to control its recruitment to DNA damage. *Sci. Adv.* **7**, eabb3799 (2021).
21. Pei, H. *et al.* MMSET regulates histone H4K20 methylation and 53BP1 accumulation at DNA damage sites. *Nature* **470**, 124–128 (2011).
22. Acs, K. *et al.* The AAA-ATPase VCP/p97 promotes 53BP1 recruitment by removing L3MBTL1 from DNA double-strand breaks. *Nat. Struct. Mol. Biol.* **18**, 1345–1350 (2011).
23. Mallette, F. A. *et al.* RNF8- and RNF168-dependent degradation of KDM4A/JMJD2A triggers 53BP1 recruitment to DNA damage sites: RNF8- and RNF168-dependent degradation of KDM4A/JMJD2A. *EMBO J.* **31**, 1865–1878 (2012).
24. Pellegrino, S., Michelena, J., Teloni, F., Imhof, R. & Altmeyer, M. Replication-Coupled Dilution of H4K20me2 Guides 53BP1 to Pre-replicative Chromatin. *Cell Rep.* **19**, 1819–1831 (2017).
25. Tang, J. *et al.* Acetylation limits 53BP1 association with damaged chromatin to promote homologous recombination. *Nat. Struct. Mol. Biol.* **20**, 317–325 (2013).
26. Isono, M. *et al.* BRCA1 Directs the Repair Pathway to Homologous Recombination by Promoting 53BP1 Dephosphorylation. *Cell Rep.* **18**, 520–532 (2017).
27. Zhang, F. *et al.* Nudix hydrolase NUDT16 regulates 53BP1 protein by reversing 53BP1 ADP-ribosylation. *Cancer Res.* canres.2205.2019 (2020) doi:10.1158/0008-5472.can-19-2205.

28. Duheron, V., Nilles, N., Pecenko, S., Martinelli, V. & Fahrenkrog, B. Localisation of Nup153 and SENP1 to nuclear pore complexes is required for 53BP1-mediated DNA double-strand break repair. *J. Cell Sci.* **130**, 2306–2316 (2017).
29. Guo, X. *et al.* Acetylation of 53BP1 dictates the DNA double strand break repair pathway. *Nucleic Acids Res.* **46**, 689–703 (2018).
30. Gibbs-Seymour, I., Markiewicz, E., Bekker-Jensen, S., Mailand, N. & Hutchison, C. J. Lamin A/C-dependent interaction with 53BP1 promotes cellular responses to DNA damage. *Aging Cell* **14**, 162–169 (2015).
31. Moreno, N. S. *et al.* The nuclear structural protein NuMA is a negative regulator of 53BP1 in DNA double-strand break repair. *Nucleic Acids Res.* **47**, 10475–10475 (2019).
32. Ghodke, I. *et al.* AHNAK controls 53BP1-mediated p53 response by restraining 53BP1 oligomerization and phase separation. *Mol. Cell* **81**, 2596-2610.e7 (2021).
33. Tang, M. *et al.* FOXK1 Participates in DNA Damage Response by Controlling 53BP1 Function. *Cell Rep.* **32**, 108018 (2020).
34. Jiang, Y. *et al.* AMPK-mediated phosphorylation on 53BP1 promotes c-NHEJ. *Cell Rep.* **34**, 108713 (2021).
35. Luessing, J. *et al.* The nuclear kinesin KIF18B promotes 53BP1-mediated DNA double-strand break repair. *Cell Rep.* **35**, 109306 (2021).
36. Becker, J. R. *et al.* The ASCIZ-DYNLL1 axis promotes 53BP1-dependent non-homologous end joining and PARP inhibitor sensitivity. *Nat. Commun.* **9**, 5406 (2018).
37. He, Y. J. *et al.* DYNLL1 binds to MRE11 to limit DNA end resection in BRCA1-deficient cells. *Nature* **563**, 522–526 (2018).
38. Noordermeer, S. M. *et al.* The shieldin complex mediates 53BP1-dependent DNA repair. *Nature* **560**, 117–121 (2018).
39. Dev, H. *et al.* Shieldin complex promotes DNA end-joining and counters homologous recombination in BRCA1-null cells. *Nat. Cell Biol.* **20**, 954–965 (2018).
40. Gao, S. *et al.* An OB-fold complex controls the repair pathways for DNA double-strand breaks. *Nat. Commun.* **9**, 3925 (2018).
41. Mirman, Z. *et al.* 53BP1–RIF1–shieldin counteracts DSB resection through CST- and Polα-dependent fill-in. *Nature* **560**, 112–116 (2018).
42. Paiano, J. *et al.* Role of 53BP1 in end protection and DNA synthesis at DNA breaks. *Genes Dev.* **35**, 1356–1367 (2021).
43. Isobe, S.-Y., Nagao, K., Nozaki, N., Kimura, H. & Obuse, C. Inhibition of RIF1 by SCAI Allows BRCA1-Mediated Repair. *Cell Rep.* **20**, 297–307 (2017).
44. Ashworth, A. & Lord, C. J. Synthetic lethal therapies for cancer: what's next after PARP inhibitors? *Nat. Rev. Clin. Oncol.* **15**, 564–576 (2018).
45. D'Andrea, A. D. Mechanisms of PARP inhibitor sensitivity and resistance. *DNA Repair* **71**, 172–176 (2018).
46. McLennan, A. G. The Nudix hydrolase superfamily. *Cell. Mol. Life Sci. CMLS 2006 632* **63**, 123–143 (2005).
47. Kim, H. *et al.* Crystal structure of syndesmos and its interaction with Syndecan-4 proteoglycan. *Biochem. Biophys. Res. Commun.* **463**, 762–767 (2015).
48. Drané, P. *et al.* TIRR regulates 53BP1 by masking its histone methyl-lysine binding function. *Nature* **543**, 211–216 (2017).
49. Dai, Y., Zhang, A., Shan, S., Gong, Z. & Zhou, Z. Structural basis for recognition of 53BP1 tandem Tudor domain by TIRR. *Nat. Commun.* **9**, (2018).
50. Wang, J. *et al.* Molecular basis for the inhibition of the methyl-lysine binding function of 53BP1 by TIRR. *Nat. Commun.* **9**, (2018).
51. Botuyan, M. V. *et al.* Mechanism of 53BP1 activity regulation by RNA-binding TIRR and a designer protein. *Nat. Struct. Mol. Biol.* **25**, 591–600 (2018).
52. Zhang, A., Peng, B., Huang, P., Chen, J. & Gong, Z. The p53-binding protein 1-Tudor-interacting repair regulator complex participates in the DNA damage response. *J. Biol. Chem.* **292**, 6461–6467 (2017).
53. Parnandi, N. *et al.* TIRR inhibits the 53BP1-p53 complex to alter cell-fate programs. *Mol. Cell* **81**, (2021).
54. Taylor, M. J. & Peculis, B. A. Evolutionary conservation supports ancient origin for Nudt16, a nuclear-localized, RNA-binding, RNA-decapping enzyme. *Nucleic Acids Res.* **36**, 6021 (2008).
55. Avolio, R. *et al.* Protein Syndesmos is a novel RNA-binding protein that regulates primary cilia formation. *Nucleic Acids Res.* **46**, 12067 (2018).
56. Lu, G. *et al.* hNUDT16: A universal decapping enzyme for small nucleolar RNA and cytoplasmic mRNA. *Protein Cell* **2**, 64–73 (2011).
57. Song, M.-G., Li, Y. & Kiledjian, M. Multiple mRNA Decapping Enzymes in Mammalian Cells. *Mol. Cell* **40**, 423 (2010).
58. Palazzo, L. *et al.* Processing of protein ADP-ribosylation by Nudix hydrolases. *Biochem. J.* **468**, 293–301 (2015).
59. Munnur, D. *et al.* Reversible ADP-ribosylation of RNA. *Nucleic Acids Res.* **47**, 5658–5669 (2019).

60. Iyama, T., Abolhassani, N., Tsuchimoto, D., Nonaka, M. & Nakabeppu, Y. NUDT16 is a (deoxy)inosine diphosphatase, and its deficiency induces accumulation of single-strand breaks in nuclear DNA and growth arrest. *Nucleic Acids Res.* **38**, (2010).
61. Baciu, P. C. *et al.* Syndesmos, a protein that interacts with the cytoplasmic domain of syndecan-4, mediates cell spreading and actin cytoskeletal organization. *J. Cell Sci.* **113 Pt 2**, 315–24 (2000).
62. Denhez, F. *et al.* Syndesmos, a syndecan-4 cytoplasmic domain interactor, binds to the focal adhesion adaptor proteins paxillin and Hic-5. *J. Biol. Chem.* **277**, 12270–12274 (2002).
63. Gunaratne, J. *et al.* Protein interactions of phosphatase and tensin homologue (PTEN) and its cancer-associated G20E mutant compared by using stable isotope labeling by amino acids in cell culture-based parallel affinity purification. *J. Biol. Chem.* **286**, 18093–18103 (2011).
64. Pong, S. K. & Gullerova, M. Noncanonical functions of microRNA pathway enzymes - Drosha, DGCR8, Dicer and Ago proteins. *FEBS Lett.* **592**, 2973–2986 (2018).
65. Chowdhury, D., Choi, Y. E. & Brault, M. E. Charity begins at home: Non-coding RNA functions in DNA repair. *Nat. Rev. Mol. Cell Biol.* **14**, 181–189 (2013).
66. Rybak-Wolf, A. *et al.* A variety of dicer substrates in human and C. elegans. *Cell* **159**, (2014).
67. Thapar, R. Regulation of DNA Double-Strand Break Repair by Non-Coding RNAs. *Molecules* **23**, 2789 (2018).
68. Zhang, X., Wan, G., Berger, F. G., He, X. & Lu, X. The ATM Kinase Induces MicroRNA Biogenesis in the DNA Damage Response. *Mol. Cell* **41**, 371–383 (2011).
69. Kawai, S. & Amano, A. BRCA1 regulates microRNA biogenesis via the DROSHA microprocessor complex. *J. Cell Biol.* **197**, 201–208 (2012).
70. Hu, H., Du, L., Nagabayashi, G., Seeger, R. C. & Gatti, R. A. ATM is down-regulated by N-Myc-regulated microRNA-421. *Proc. Natl. Acad. Sci. U. S. A.* **107**, 1506–1511 (2010).
71. Sun, Y., Wang, H. & Luo, C. MiR-100 regulates cell viability and apoptosis by targeting ATM in pediatric acute myeloid leukemia. *Biochem. Biophys. Res. Commun.* **522**, 855–861 (2020).
72. Bisso, A. *et al.* Oncogenic miR-181a/b affect the DNA damage response in aggressive breast cancer. *Cell Cycle* **12**, 1679–1687 (2013).
73. Lal, A. *et al.* MiR-24-mediated downregulation of H2AX suppresses DNA repair in terminally differentiated blood cells. *Nat. Struct. Mol. Biol.* **16**, 492–498 (2009).
74. Wang, Y. *et al.* MicroRNA-138 modulates DNA damage response by repressing histone H2AX expression. *Mol. Cancer Res.* **9**, 1100–1111 (2011).
75. Chen, S. *et al.* MiR-34s negatively regulate homologous recombination through targeting RAD51. *Arch. Biochem. Biophys.* **666**, 73–82 (2019).
76. Patel, N. *et al.* miR-15a/miR-16 down-regulates BMI1, impacting Ub-H2A mediated DNA repair and breast cancer cell sensitivity to doxorubicin. *Sci. Rep.* **7**, 4263 (2017).
77. Choi, Y. E. *et al.* MicroRNAs down-regulate homologous recombination in the G1 phase of cycling cells to maintain genomic stability. *eLife* **2014**, (2014).
78. Yan, D. *et al.* Targeting DNA-PKcs and ATM with miR-101 Sensitizes Tumors to Radiation. *PLoS ONE* **5**, e11397 (2010).
79. Yang, L. *et al.* The CTIP-mediated repair of TNF-α-induced DNA double-strand break was impaired by miR-130b in cervical cancer cell. *Cell Biochem. Funct.* **37**, 534–544 (2019).
80. Martin, N. T. *et al.* ATM-Dependent MiR-335 Targets CtIP and Modulates the DNA Damage Response. *PLoS Genet.* **9**, e1003505 (2013).
81. Meghani, K. *et al.* Multifaceted Impact of MicroRNA 493-5p on Genome-Stabilizing Pathways Induces Platinum and PARP Inhibitor Resistance in BRCA2-Mutated Carcinomas. *Cell Rep.* **23**, 100–111 (2018).
82. Lee, J.-H. *et al.* c-Fos-dependent miR-22 targets MDC1 and regulates DNA repair in terminally differentiated cells. *Oncotarget* **8**, 48204–48221 (2017).
83. Kofman, A. *et al.* microRNA-34a promotes DNA damage and mitotic catastrophe. *Cell Cycle* **12**, 3500–3511 (2013).
84. Moskwa, P. *et al.* MiR-182-Mediated Downregulation of BRCA1 Impacts DNA Repair and Sensitivity to PARP Inhibitors. *Mol. Cell* **41**, 210–220 (2011).
85. Mogilyansky, E. *et al.* Post-transcriptional regulation of BRCA2 through interactions with miR-19a and miR-19b. *Front. Genet.* **7**, 143 (2016).
86. Piotto, C., Biscontin, A., Millino, C. & Mognato, M. Functional validation of miRNAs targeting genes of DNA double-strand break repair to radiosensitize non-small lung cancer cells. *Biochim. Biophys. Acta - Gene Regul. Mech.* **1861**, 1102–1118 (2018).
87. Zhang, Z. Y. *et al.* By downregulating Ku80, hsa-miR-526b suppresses non-small cell lung cancer. *Oncotarget* **6**, 1462–1477 (2015).
88. Choi, Y. E. *et al.* Platinum and PARP Inhibitor Resistance Due to Overexpression of MicroRNA-622 in BRCA1-Mutant Ovarian Cancer. *CellReports* **14**, 429–439 (2016).

89. Smolinska, A. *et al.* MiR-502 is the first reported miRNA simultaneously targeting two components of the classical non-homologous end joining (C-NHEJ) in pancreatic cell lines. *Heliyon* **6**, (2020).
90. Liao, C. *et al.* MicroR-545 enhanced radiosensitivity via suppressing Ku70 expression in Lewis lung carcinoma xenograft model. *Cancer Cell Int.* **15**, (2015).
91. Mo, L. J. *et al.* Exosome-packaged mir-1246 contributes to bystander dna damage by targeting lig4. *Br. J. Cancer* **119**, 492–502 (2018).
92. Liu, R. *et al.* Long noncoding RNA lnc-RI regulates DNA damage repair and radiation sensitivity of CRC cells through NHEJ pathway. *Cell Biol. Toxicol.* 1–15 (2020) doi:10.1007/s10565-020-09524-6.
93. Jankowsky, E. & Harris, M. E. Specificity and nonspecificity in RNA-protein interactions. *Nat. Rev. Mol. Cell Biol.* **16**, (2015).
94. Zhao, K., Wang, X., Xue, X., Li, L. & Hu, Y. A long noncoding RNA sensitizes genotoxic treatment by attenuating ATM activation and homologous recombination repair in cancers. *PLOS Biol.* **18**, e3000666 (2020).
95. Deng, B. *et al.* An LTR retrotransposon-derived lnc RNA interacts with RNF 169 to promote homologous recombination. *EMBO Rep.* **20**, (2019).
96. Thapar, R. *et al.* Mechanism of efficient double-strand break repair by a long non-coding RNA. *Nucleic Acids Res.* **48**, (2020).
97. Zhang, Y. *et al.* Long noncoding RNA LINP1 regulates repair of DNA double-strand breaks in triple-negative breast cancer. *Nat. Struct. Mol. Biol.* **23**, 522–530 (2016).
98. Wang, X. *et al.* LINP1 facilitates DNA damage repair through non-homologous end joining (NHEJ) pathway and subsequently decreases the sensitivity of cervical cancer cells to ionizing radiation. *Cell Cycle* (2018) doi:10.1080/15384101.2018.1442625.
99. Bergstrand, S. *et al.* Small Cajal body-associated RNA 2 (scaRNA2) regulates DNA repair pathway choice by inhibiting DNA-PK. *Nat. Commun.* **13**, 1015 (2022).
100. Shen, L. *et al.* LncRNA lnc-RI regulates homologous recombination repair of DNA double-strand breaks by stabilizing RAD51 mRNA as a competitive endogenous RNA. *Nucleic Acids Res.* **46**, 717–729 (2018).
101. Hu, W. L. *et al.* GUARDIN is a p53-responsive long non-coding RNA that is essential for genomic stability. *Nat. Cell Biol.* **20**, 492–502 (2018).
102. Hu, X., Ding, D., Zhang, J. & Cui, J. Knockdown of lncRNA HOTAIR sensitizes breast cancer cells to ionizing radiation through activating miR-218. *Biosci. Rep.* **29**, (2019).
103. Jiao, Y. *et al.* Long intergenic non-coding RNA induced by X-ray irradiation regulates DNA damage response signaling in the human bronchial epithelial BEAS-2B cell line. *Oncol. Lett.* **9**, 169–176 (2015).
104. Hu, Y. *et al.* Targeting the MALAT1/PARP1/LIG3 complex induces DNA damage and apoptosis in multiple myeloma. *Leukemia* **32**, 2250–2262 (2018).
105. Liu, L. *et al.* Long non-coding RNA ANRIL promotes homologous recombination-mediated DNA repair by maintaining ATR protein stability to enhance cancer resistance. *Mol. Cancer* **20**, 94 (2021).
106. Schmitt, A. M. *et al.* An inducible long noncoding RNA amplifies DNA damage signaling. *Nat. Genet.* **48**, 1370–1376 (2016).
107. Prensner, J. R. *et al.* PCAT-1, a long noncoding RNA, regulates BRCA2 and controls homologous recombination in cancer. *Cancer Res.* **74**, 1651–1660 (2014).
108. Hung, T. *et al.* Extensive and coordinated transcription of noncoding RNAs within cell-cycle promoters. in *Nature Genetics* vol. 43 621–629 (NIH Public Access, 2011).
109. Sharma, V. *et al.* A BRCA 1-interacting lnc RNA regulates homologous recombination. *EMBO Rep.* **16**, 1520–1534 (2015).
110. Betts, J. A. *et al.* Long Noncoding RNAs CUPID1 and CUPID2 Mediate Breast Cancer Risk at 11q13 by Modulating the Response to DNA Damage. *Am. J. Hum. Genet.* **101**, 255–266 (2017).
111. Hu, Z. *et al.* BGL3 lncRNA mediates retention of the BRCA1/BARD1 complex at DNA damage sites. *EMBO J.* (2020) doi:10.15252/embj.2019104133.
112. Aymard, F. *et al.* Transcriptionally active chromatin recruits homologous recombination at DNA double-strand breaks. *Nat. Struct. Mol. Biol.* **21**, 366–374 (2014).
113. Aymard, F. *et al.* Genome-wide mapping of long-range contacts unveils clustering of DNA double-strand breaks at damaged active genes. *Nat. Struct. Mol. Biol.* **24**, 353–361 (2017).
114. Chakraborty, A. *et al.* Classical non-homologous end-joining pathway utilizes nascent RNA for error-free double-strand break repair of transcribed genes. *Nat. Commun.* **7**, 13049 (2016).
115. Shanbhag, N. M., Rafalska-Metcalf, I. U., Balane-Bolivar, C., Janicki, S. M. & Greenberg, R. A. ATM-Dependent Chromatin Changes Silence Transcription In cis to DNA Double-Strand Breaks. *Cell* **141**, 970–981 (2010).
116. Iannelli, F. *et al.* A damaged genome's transcriptional landscape through multilayered expression profiling around in situ-mapped DNA double-strand breaks. *Nat. Commun.* **8**, 15656 (2017).
117. Ui, A., Nagaura, Y. & Yasui, A. Transcriptional Elongation Factor ENL Phosphorylated by ATM Recruits Polycomb and Switches Off Transcription for DSB Repair. *Mol. Cell* **58**, 468–482 (2015).

118. Kakarougkas, A. *et al.* Requirement for PBAF in Transcriptional Repression and Repair at DNA Breaks in Actively Transcribed Regions of Chromatin. *Mol. Cell* **55**, (2014).
119. Meisenberg, C. *et al.* Repression of Transcription at DNA Breaks Requires Cohesin throughout Interphase and Prevents Genome Instability. *Mol. Cell* **73**, 212-223.e7 (2019).
120. Rona, G. *et al.* PARP1-dependent recruitment of the FBXL10-RNF68-RNF2 ubiquitin ligase to sites of DNA damage controls H2A.Z loading. *eLife* **7**, e38771 (2018).
121. Abu-Zhayia, E. R., Awwad, S. W., Ben-Oz, B. M., Khoury-Haddad, H. & Ayoub, N. CDYL1 fosters double-strand break-induced transcription silencing and promotes homology-directed repair. *J. Mol. Cell Biol.* **10**, 341–357 (2018).
122. Awwad, S. W., Abu-Zhayia, E. R., Guttmann-Raviv, N. & Ayoub, N. NELF-E is recruited to DNA double-strand break sites to promote transcriptional repression and repair. *EMBO Rep.* **18**, 745–764 (2017).
123. Gong, F., Clouaire, T., Aguirrebengoa, M., Legube, G. & Miller, K. M. Histone demethylase KDM5A regulates the ZMYND8–NuRD chromatin remodeler to promote DNA repair. *J. Cell Biol.* **216**, 1959–1974 (2017).
124. Pankotai, T., Bonhomme, C., Chen, D. & Soutoglou, E. DNAPKcs-dependent arrest of RNA polymerase II transcription in the presence of DNA breaks. *Nat. Struct. Mol. Biol.* **19**, 276–282 (2012).
125. Caron, P. *et al.* WWP2 ubiquitylates RNA polymerase II for DNA-PK-dependent transcription arrest and repair at DNA breaks. *Genes Dev.* **33**, 684–704 (2019).
126. Abu-Zhayia, E. R. *et al.* CDYL1-dependent decrease in lysine crotonylation at DNA double-strand break sites functionally uncouples transcriptional silencing and repair. *Mol. Cell* **82**, 1940-1955.e7 (2022).
127. Sofia Francia *et al.* DROSHA and DICER RNA products control BMI1-dependent transcriptional repression at DNA damage sites. *ResearchSquare* (2022) doi:https://doi.org/10.21203/rs.3.rs-1214613/v1.
128. Puget, N., Miller, K. M. & Legube, G. Non-canonical DNA/RNA structures during Transcription-Coupled Double-Strand Break Repair: Roadblocks or Bona fide repair intermediates? *DNA Repair* **81**, 102661 (2019).
129. Pessina, F. *et al.* Functional transcription promoters at DNA double-strand breaks mediate RNA-driven phase separation of damage-response factors. *Nat. Cell Biol.* **21**, 1286–1299 (2019).
130. Liu, S. *et al.* RNA polymerase III is required for the repair of DNA double-strand breaks by homologous recombination. *Cell* **184**, 1314-1329.e10 (2021).
131. Bonath, F., Domingo-Prim, J., Tarbier, M., Friedländer, M. R. & Visa, N. Next-generation sequencing reveals two populations of damage-induced small RNAs at endogenous DNA double-strand breaks. *Nucleic Acids Res.* **46**, (2018).
132. Domingo-Prim, J. *et al.* EXOSC10 is required for RPA assembly and controlled DNA end resection at DNA double-strand breaks. *Nat. Commun.* **10**, 1–13 (2019).
133. Burger, K., Schlackow, M. & Gullerova, M. Tyrosine kinase c-Abl couples RNA polymerase II transcription to DNA double-strand breaks. *Nucleic Acids Res.* (2019) doi:10.1093/nar/gkz024.
134. Michelini, F. *et al.* Damage-induced lncRNAs control the DNA damage response through interaction with DDRNAs at individual double-strand breaks. *Nat. Cell Biol.* **19**, 1400–1411 (2017).
135. Vítor, A. C. *et al.* Single-molecule imaging of transcription at damaged chromatin. *Sci. Adv.* **5**, eaau1249 (2019).
136. Böttcher, R., Schmidts, I., Nitschko, V., Duric, P. & Förstemann, K. RNA polymerase II is recruited to DNA double-strand breaks for dilncRNA transcription in *Drosophila*. *RNA Biol.* **19**, 68–77 (2022).
137. Wei, W. *et al.* A Role for Small RNAs in DNA Double-Strand Break Repair. *Cell* **149**, 101–112 (2012).
138. Sharma, S. *et al.* MRE11-RAD50-NBS1 Complex Is Sufficient to Promote Transcription by RNA Polymerase II at Double-Strand Breaks by Melting DNA Ends. *Cell Rep.* **34**, (2021).
139. Domingo-Prim, J., Bonath, F. & Visa, N. RNA at DNA Double-Strand Breaks: The Challenge of Dealing with DNA:RNA Hybrids. *BioEssays* 1900225 (2020) doi:10.1002/bies.201900225.
140. D'Alessandro, G. *et al.* BRCA2 controls DNA:RNA hybrid level at DSBs by mediating RNase H2 recruitment. *Nat. Commun. 2018 91* **9**, 1–17 (2018).
141. Ohle, C. *et al.* Transient RNA-DNA Hybrids Are Required for Efficient Double-Strand Break Repair. *Cell* (2016) doi:10.1016/j.cell.2016.10.001.
142. Marnef, A. & Legube, G. R-loops as Janus-faced modulators of DNA repair. *Nat. Cell Biol.* **23**, (2021).
143. Petermann, E., Lan, L. & Zou, L. Sources, resolution and physiological relevance of R-loops and RNA–DNA hybrids. *Nat. Rev. Mol. Cell Biol.* (2022) doi:10.1038/s41580-022-00474-x.
144. Cohen, S. *et al.* Senataxin resolves RNA:DNA hybrids forming at DNA double-strand breaks to prevent translocations. *Nat. Commun.* **9**, 1–14 (2018).
145. Lu, W.-T. *et al.* Drosha drives the formation of DNA:RNA hybrids around DNA break sites to facilitate DNA repair. *Nat. Commun. 2018 91* **9**, 1–13 (2018).
146. Jang, Y. *et al.* Intrinsically disordered protein RBM14 plays a role in generation of RNA:DNA hybrids at double-strand break sites. *Proc. Natl. Acad. Sci. U. S. A.* (2020) doi:10.1073/pnas.1913280117.
147. Bader, A. S. & Bushell, M. DNA:RNA hybrids form at DNA double-strand breaks in transcriptionally active loci. *Cell Death Dis.* **11**, (2020).

148. Yasuhara, T. *et al.* Human Rad52 Promotes XPG-Mediated R-loop Processing to Initiate Transcription-Associated Homologous Recombination Repair. *Cell* **175**, 558-570.e11 (2018).
149. Brustel, J., Kozik, Z., Gromak, N., Savic, V. & Sweet, S. M. M. Large XPF-dependent deletions following misrepair of a DNA double strand break are prevented by the RNA:DNA helicase Senataxin. *Sci. Rep.* **8**, 1–12 (2018).
150. Chakraborty, P. & Hiom, K. DHX9-dependent recruitment of BRCA1 to RNA promotes DNA end resection in homologous recombination. *Nat. Commun.* **12**, 4126 (2021).
151. Li, L. *et al.* DEAD Box 1 Facilitates Removal of RNA and Homologous Recombination at DNA Double-Strand Breaks. *Mol. Cell. Biol.* **36**, 2794–2810 (2016).
152. Jimeno, S. *et al.* ADAR-mediated RNA editing of DNA:RNA hybrids is required for DNA double strand break repair. *Nat. Commun.* **12**, 5512 (2021).
153. Cohen, S. *et al.* A POLD3/BLM dependent pathway handles DSBs in transcribed chromatin upon excessive RNA:DNA hybrid accumulation. *Nat. Commun.* **13**, 2012 (2022).
154. Burger, K. & Gullerova, M. Nuclear re-localization of Dicer in primary mouse embryonic fibroblast nuclei following DNA damage. *PLoS Genet.* **14**, e1007151 (2018).
155. Burger, K. *et al.* Nuclear phosphorylated Dicer processes double-stranded RNA in response to DNA damage. *J. Cell Biol.* **216**, 2373–2389 (2017).
156. Francia, S. *et al.* Site-specific DICER and DROSHA RNA products control the DNA-damage response. *Nature* **488**, 231–5 (2012).
157. Francia, S., Cabrini, M., Matti, V., Oldani, A. & d'Adda di Fagagna, F. DICER, DROSHA and DNA damage response RNAs are necessary for the secondary recruitment of DNA damage response factors. *J. Cell Sci.* **129**, 1468–76 (2016).
158. Pryde, F. *et al.* 53BP1 exchanges slowly at the sites of DNA damage and appears to require RNA for its association with chromatin. *J. Cell Sci.* **118**, 2043–2055 (2005).
159. Wang, Q. & Goldstein, M. Small RNAs Recruit Chromatin-Modifying Enzymes MMSET and Tip60 to Reconfigure Damaged DNA upon Double-Strand Break and Facilitate Repair. *Cancer Res.* **76**, 1904–1915 (2016).
160. Dueva, R. *et al.* Neutralization of the Positive Charges on Histone Tails by RNA Promotes an Open Chromatin Structure. *Cell Chem. Biol.* **26**, (2019).
161. Fijen, C. & Rothenberg, E. The evolving complexity of DNA damage foci: RNA, condensates and chromatin in DNA double-strand break repair. *DNA Repair* **105**, 103170 (2021).
162. Gromak, N. *et al.* Drosha Regulates Gene Expression Independently of RNA Cleavage Function. *Cell Rep.* **5**, 1499–1510 (2013).
163. Castel, S. E. *et al.* Dicer Promotes Transcription Termination at Sites of Replication Stress to Maintain Genome Stability. *Cell* **159**, 572–583 (2014).
164. Hu, X. *et al.* Phosphorylation of Ago2 is required for its role in DNA double-strand break repair. *J. Genet. Genomics* **48**, (2021).
165. Hang, Q. *et al.* Non-canonical function of DGCR8 in DNA double-strand break repair signaling and tumor radioresistance. *Nat. Commun.* **12**, (2021).
166. Gómez-Cabello, D., Pappas, G., Aguilar-Morante, D., Dinant, C. & Bartek, J. CtIP-dependent nascent RNA expression flanking DNA breaks guides the choice of DNA repair pathway. *Nat. Commun.* **13**, 5303 (2022).
167. Keskin, H. *et al.* Transcript-RNA-templated DNA recombination and repair. *Nature* **515**, 436–439 (2014).
168. Welty, S. *et al.* RAD52 is required for RNA-templated recombination repair in post-mitotic neurons. *J. Biol. Chem.* **293**, 1353–1362 (2018).
169. Wei, L. *et al.* DNA damage during the G0/G1 phase triggers RNA-templated, Cockayne syndrome B-dependent homologous recombination. *Proc. Natl. Acad. Sci.* **112**, (2015).
170. Ouyang, J. *et al.* RNA transcripts stimulate homologous recombination by forming DR-loops. *Nature* **594**, (2021).
171. Zhang, C. *et al.* METTL3 and N6-Methyladenosine Promote Homologous Recombination-Mediated Repair of DSBs by Modulating DNA-RNA Hybrid Accumulation. *Mol. Cell* **79**, 425-442.e7 (2020).
172. Abakir, A. *et al.* N 6-methyladenosine regulates the stability of RNA:DNA hybrids in human cells. *Nat. Genet.* (2020) doi:10.1038/s41588-019-0549-x.
173. Zeng, X. *et al.* METTL16 antagonizes MRE11-mediated DNA end resection and confers synthetic lethality to PARP inhibition in pancreatic ductal adenocarcinoma. *Nat. Cancer* **3**, 1088–1104 (2022).
174. Chen, H. *et al.* m5C modification of mRNA serves a DNA damage code to promote homologous recombination. *Nat. Commun.* **11**, 2834 (2020).
175. Campos-Melo, D., Hawley, Z. C. E., Droppelmann, C. A. & Strong, M. J. The Integral Role of RNA in Stress Granule Formation and Function. *Front. Cell Dev. Biol.* **9**, 621779 (2021).

Chapter 2: Materials and Methods

2.1 Materials

2.1.1 Buffers

A list of buffers used in this thesis can be found in **Table 2.1**.

Name	Composition
Freezing Media (1X)	10% DMSO in FBS
TAE Buffer (50X)	2M Tris, 50mM EDTA, 1M Glacial Acetic Acid
TGEN150 Buffer	20mM Tris pH 7.65, 150mM NaCl, 3mM $MgCl_2$, 10% Glycerol, 0.01% NP40, Protease inhibitors
RIP Lysis Buffer	100mM NaCl, 15mM $MgCl_2$, 10mM Tris pH 7.5, 0.5% NP40, 0.5% Sodium Deoxycholate, 1mM DTT, Protease inhibitors
RIP High Salt Buffer	500mM NaCl, 1mM $MgCl_2$, 20mM Tris pH 7.5, 0.05% NP40, 0.1% SDS, Protease inhibitors
RIP Low Salt Buffer	150mM NaCl, 20mM Tris pH 7.5, 1mM $MgCl_2$, 0.01% NP40
RIP Proteinase K Buffer	100mM Tris pH 7.5, 50mM NaCl, 10mM EDTA
Cell Lysis Buffer	50mM Tris pH 8, 150mM NaCl, 1mM EDTA, 5mM $MgCl_2$, 0.5% NP40, Protease inhibitors and Phosphatase inhibitors, Pierce Universal Nuclease
Co-IP Wash Buffer	50mM Tris pH 8, 150mM NaCl, 1mM EDTA, 5mM $MgCl_2$, Protease inhibitors and Phosphatase inhibitors
UB8 Buffer	8M Urea, 100mM Ammonium bicarbonate
UB1 Buffer	1M Urea, 25mM Ammonium bicarbonate
Annealing buffer (1X)	50mM HEPES pH7.6, 50mM NaCl
EMSA Reaction buffer (1X)	50mM HEPES, 50mM NaCl, 5% Glycerol, 20mM $MgCl_2$, 0.01% Tween 20
Hypotonic Lysis buffer	10mM HEPES pH 7.9, 60mM KCl, 1.5mM $MgCl_2$, 1mM EDTA, 1mM DTT, 0.075% NP40, Protease inhibitors
NiNTA Buffer A (lysis)	37mM Na_2HPO_4, 13mM NaH_2PO_4, 500mM NaCl, 1mM DTT, Protease inhibitors
NiNTA Buffer High Salt	37mM Na_2HPO_4, 13mM NaH_2PO_4, 1M NaCl, 1mM DTT, Protease inhibitors
NiNTA buffer high imidazole	37mM Na_2HPO_4, 13mM NaH_2PO_4, 500mM NaCl, 1mM DTT, 500mM imidazole, Protease inhibitors
Dialysis Buffer	37mM Na_2HPO_4, 13mM NaH_2PO_4, 300mM NaCl, 1mM DTT, 10mM imidazole
SEC Buffer	37mM Na_2HPO_4, 13mM NaH_2PO_4, 300 mM NaCl, 1 mM DTT

Table 2.1: *List of buffers used in this thesis.*

2.1.2 Primary Antibodies

A list of primary antibodies used in this thesis can be found in **Table 2.2.**

Name	Supplier	Application
53BP1 Antibody	Novus Biologicals	WB PLA
6*his, His tag RB Polyclonal antibody	Proteintech	WB
Anti-53BP1, Clone BP13	Merck	WB PLA
Anti-anti-Cy3 Antibody (A-6)	Santa Cruz	PLA
Anti-ATM (phospho S1981) antibody	Abcam	WB
Anti-Dicer antibody [13D6]	Abcam	WB

Anti-beta Tubulin antibody - Loading Control	Abcam	WB
Anti-DNA-RNA Hybrid Clone S9.6	Sigma	IF
ANTI-FLAG antibody	Sigma	WB
Anti-gamma H2A.X (phospho S139) Antibody	Abcam	WB IF PLA
Anti-NUDT16L1 antibody	Atlas Antibodies	WB PLA
Anti-phospho-Histone H2A.X (Ser139) Antibody, clone JBW301	Millipore	PLA IF
Anti-RNA polymerase II CTD repeat YSPTSPS antibody	Abcam	WB
Anti-V5 tag antibody [SV5-P-K]	Abcam	WB
DGCR8 C-terminal Polyclonal antibody	Proteintech	WB
Drosha (D28B1) Rabbit mAb	Cell Signalling Technologies	WB
G3BP1 Polyclonal antibody	Proteintech	IF
GFP Monoclonal antibody (3H9)	Chromotek	WB
LSM14A Polyclonal antibody	Proteintech	IF
mNeonGreen antibody [32F6]	Proteintech	PLA WB
NUDT16L1 Antibody	Novus Biologicals	PLA
Purified Mouse Anti-Human 53BP1	BD BioSciences	PLA
SDOS antibody (100ug) Unconjugated	Biorbyt Ltd	PLA

Table 2.2: *A full list of primary antibodies used in this thesis.*

2.1.3 Secondary Antibodies

A list of secondary antibodies used in this thesis can be found in **Table 2.3**.

Name	Supplier	Application	Dilution
Anti-Rabbit IgG (whole molecule)–Peroxidase antibody produced in goat	Sigma	WB	1:5000
Anti-Mouse IgG (whole molecule)–Peroxidase antibody produced in goat	Sigma	WB	1:5000
Goat Anti-Rat IgG Antibody, HRP conjugate	Merck	WB	1:5000
Donkey anti-Rabbit IgG (H+L) Highly Cross-Adsorbed Secondary Antibody, Alexa Fluor™ 488	Thermo Fisher	IF	1:1000
Donkey anti-Mouse IgG (H+L) Highly Cross-Adsorbed Secondary Antibody, Alexa Fluor™ 555	Thermo Fisher	IF	1:1000
Goat anti-Rabbit IgG (H+L) Cross-Adsorbed Secondary Antibody, Alexa Fluor™ 555	Thermo Fisher	IF	1:1000

Table 2.3: *A full list of secondary antibodies used in this thesis.*

2.1.4 Primers

A list of DNA primers used in cloning, PCR reactions, and Sanger Sequencing used in this thesis can be found in **Table 2.4**. DNA primers were purchased from either IDT or Sigma.

Name	Sequence (5'→3')
CMV_PROM_FWD	GCTATTACCATGGTGATGCG

bGH polyA REV	GACACCTACTCAGACAATGCG
V5_MT_TIRR_BLEO_REV	AGCTCTGCTTATATAGACCTCCCACCGTACACGCCTACCG
V5_MT_TIRR_BLEO_FWD	CTGGAGAAGTTGCTCCCGGCCTCCTCTTAACTGTGCCTTCTAGTTGCCAGCCATC
JUST_MINITURBO_FWD	TAACTGTGCCTTCTAGTTGCCAGCCATCT
JUST_MINITURBO_REV	CTTTTCGGCAGACCGCAGACTGA
V5_miniturbo_TIRR_right_FWD	GTACGCCGCCAACCCTGGGCAG
V5_miniturbo_TIRR_right_REV	TTAAGAGGAGGCCGGGAGCAACTTCTCCAG
TIRR_bGHpolyA_REV	GAGGGGCAAACAACAGATGGCTGGCAACTAGAAGGCACAGTTAAGAGGAGGCCGGGAGCAAC
GB_tirr_fwd	TCCACGGAGTCCCAGCAGCCATGTCGACGGCGGCGGTT
GB_tirr_rev	CCAGAACCTCCGCCTCCACCAGAGGAGGCCGGGAGCAAC
TIRR_fwd	ATGTCGACGGCGGCGGTT
TIRR_rev	AGAGGAGGCCGGGAGCAACT
GB_TIRR_vector_turbo_rev	GGAACCGCCGCCGTCGACATGGCTGCTGGGACTCCGTG
GB_TIRR_vector_turbo_fwd	AGTTGCTCCCGGCCTCCTCTGGTGGAGGCGGAGGTTCTG
TURBO_REV_SEQ	GTGCTTGTTGATAGCGGCCC
hygro_trrtb2nd_fwd	ACAAAAATTTAACGCGAATTATGACACAAACCCCGCCC
hygro_trtb2nd_rev	GCTGGCACGACAGGTTTCCCGAACAAACGACCCAACACC
turbo2nd_hygro_rev	CTGGGCGGGGTTTGTGTCATAATTCGCGTTAAATTTTTGTTAAATC
turbo2nd_hygro_fwd	GGGTGTTGGGTCGTTTGTTCGGGAAACCTGTCGTGCCAG
ori REV	CCACCTCTGACTTGAGCGTC
F1ori FWD	GTGGACTCTTGTTCCAAACTGG
just_turbo_2nd_rev	CTTTTCGGCAGACCGCAGACT
just_turbo_2nd_fwd	TAACTGTGCCTTCTAGTTGCCAGC
NEON GREEN_fwd	CTGGTGGAGGCGGAGGTTCTGTCAGCAAAGGCGAAGAAGAC
NEON GREEN_rev	CTGGCAACTAGAAGGCACAGTTACTTATAGAGTTCGTCCATGCC
TIRR_K10E_FWD	TCCGGAGCTGGAGCAGATCAGCC
TIRR_K10E_rev	GGCTGATCTGCTCCAGCTCCGGA
TIRR+G4S_fwd	CAGGTTGGACCGGTGCCACCATGTCGACGGCGGCGGTTCC
TIRR+G4S_rev	TCTTCTTCGCCTTTGCTGACAGAACCTCCGCCTCCACCAG
VECTOR_NSUN2_FLAG_fwd	TGGACGAACTCTATAAGTAACTGTGCCTTCTAGTTGCCAGCC
VECTOR_NSUN2_FLAG_rev	GGAACCGCCGCCGTCGACATGGTGGCACCGGTCCAACCTG
Nde1 1-211 His-TIRR	TAAGCAGAATTCATGAGCACCGCGGCGGTGCC
BamH1 1-211 His-TIRR	TGCTTAGCGGCCGTCAGCTGCTCGCCGGCAGCA
1-211 His-TIRR F Seq Primer	GCATAGGCTTGGTTATGCCG
1-211 His-TIRR R Seq Primer	GCATGCAAGGAGATGGCGC
6-211 Primer 1 (5' Phos)	GTGCCGGAACTGAAGCAGATTAGCCGT

6-211 Primer 2 (5' Phos)	CATATGGCTGCCGCGCGGCACC
6-211 SDM Point Mutation 1 (5'Phos)	CCGCGCGGCACCAGGCCGCTG
6-211 SDM Point Mutation 2 (5'Phos)	CAGCCATATGGTGCCGGAACTGAAGC
Tirr_si(R)_fwd	AGGTCTATATAAGCAGAGCTGGTTTAGTGAACCGTCAGATCCGC
Tirr_si(R)_rev	CTGGCAACTAGAAGGCACAGTCGAGGCTGATCAGCGAGCC
Vector_Tirr_si(R)_fwd	GGCTCGCTGATCAGCCTCGACTGTGCCTTCTAGTTGCCAG
Vector_Tirr_si(R)_rev	ATCTGACGGTTCACTAAACCAGCTCTGCTTATATAGACCTCC

Table 2.4: *A full list of DNA primers used in this thesis.*

2.1.5 Plasmids

A list of plasmids used in this thesis can be found in **Table 2.5**.

Plasmid	Source	Reference
ppyCAG_RNaseH1_D210N	Addgene	1
ppyCAG_RNaseH1_WKKD	Addgene	1
ppyCAG_RNaseH1_WT	Addgene	1
MiniTurbo TIRR	This thesis[a]	-
MiniTurbo only	This thesis[a]	-
TIRR Turbo	This thesis[a]	-
Turbo only	This thesis[a]	-
TIRR Turbo HygroR 2nd	This thesis[a]	-
Turbo only Hygro	This thesis[a]	-
NeonGreen TIRR	This thesis[a]	-
NeonGreen TIRR K10E	This thesis[a]	-
siResistant TIRR	This thesis[a]	-
1-211 His-TIRR	This thesis	-
6-211 His-TIRR	This thesis	-
pCBASceI	Addgene	2
His-TIRR (final)	This thesis[b]	-

Table 2.5: *A full list of plasmids used in this thesis.*
[a]*Generated with the help of Dr Adele Alagia.*
[b]*Generated by Dr Esra Balıkçı.*

Design and sequencing (**Section 2.2.10**) of 1-211 and 6-211 His-TIRR, K10E TIRR-Neongreen, and siRNA resistant TIRR can be found in **Figure 2.1**.

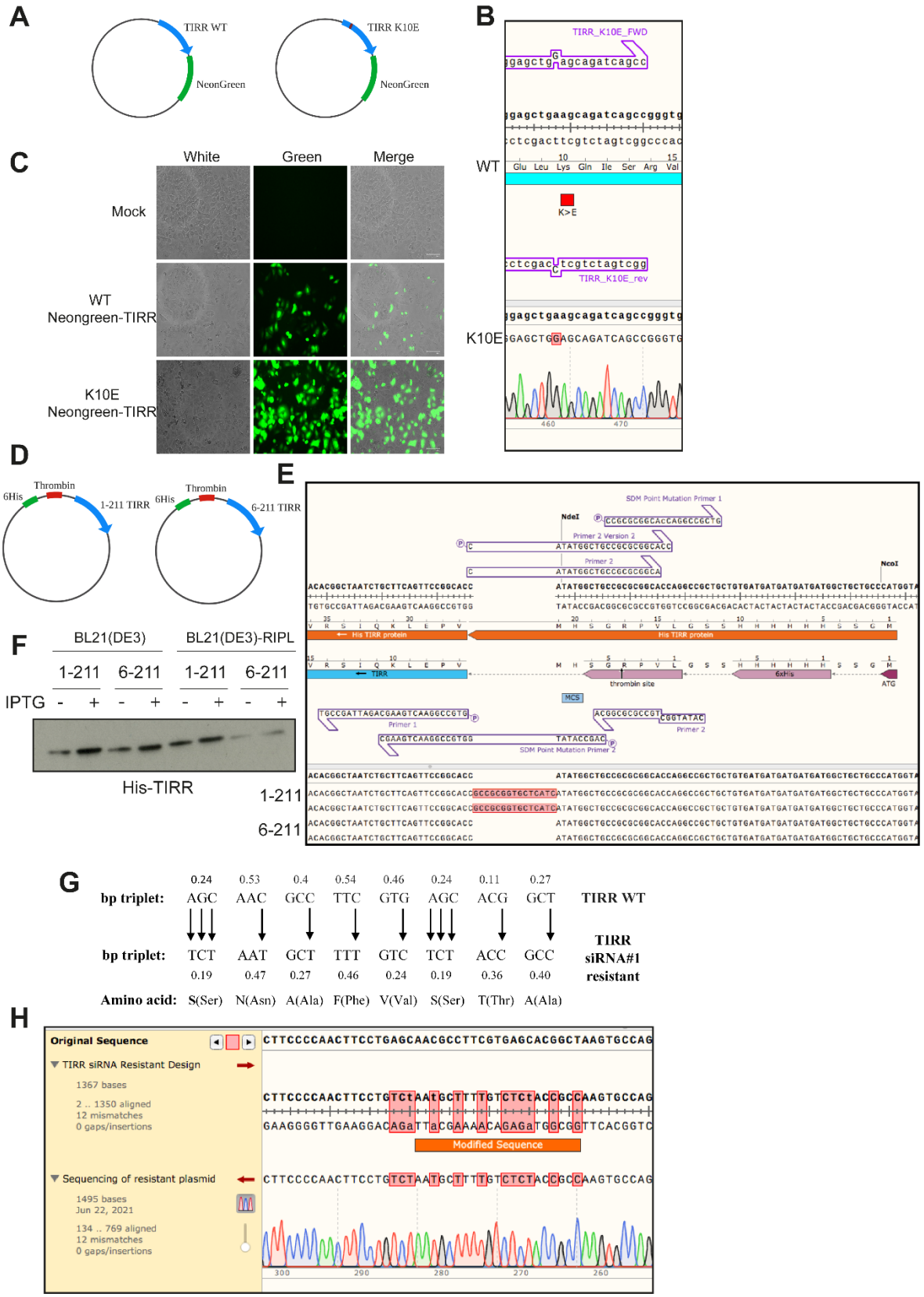


Figure 2.1: ***A)*** *Design of WT and K10 TIRR-Neongreen.* ***B)*** *Sanger sequencing confirming site directed mutagenesis of WT TIRR-Neongreen to create K10E TIRR.* ***C)*** *Expression of WT and K10E TIRR in light microscopy.* ***D)*** *Design of 1-211 and 6-211 His-TIRR for protein purification.* ***E)*** *Sequencing of 1-211 and 6-211 His-TIRR confirming correct deletion of the*

first five amino acids. ***F)*** *Expression of 1-211 and 6-211 TIRR in bacteria induced with IPTG for ~18hours at 18°C.* ***G)*** *Design of siRNA resistant TIRR.* ***H)*** *Sequencing of siRNA resistant TIRR.*

2.1.6 Short Interfering RNA (siRNA)

A list of siRNAs used in this thesis can be found in **Table 2.6**.

Name	Supplier
NUDT16L1 Stealth siRNA (Number 2) (1299001)	Thermo
NUDT16L1 Pre Designed siRNA SASI_Hs01_00138264	Sigma
ON-TARGETplus Non-targeting Control D-001810-01	Dharmacon
ON-TARGETplus Human NUDT16L1 siRNA SMARTpool	Dharmacon
ON-TARGETplus Human NUDT16L1 siRNA J-014872-23-0005	Dharmacon
84309 - NUDT16L1 (human) siPOOL	siTools Biotech
ON-TARGETplus Human DGCR8 siRNA SMARTpool	Dharmacon
ON-TARGETplus Human DICER1 siRNA SMARTpool	Dharmacon
ON-TARGETplus Human DROSHA siRNA SMARTpool	Dharmacon
ON-TARGETplus Human TP53BP1 siRNA J-003548-09-0005	Dharmacon
ON-TARGETplus Human TP53BP1 siRNA SMARTPool L-003548-00-0005	Dharmacon
ON-TARGETplus Human BRCA1 siRNA J-003461-09-0005	Dharmacon

Table 2.6: *A full list of siRNA used in this thesis.*

2.1.7 RNA and DNA oligonucleotides

A list of RNA and DNA oligonucleotides (not inclusive of DNA primers or siRNA) used in this thesis can be found in **Table 2.7** and **Figure 2.2**. RNA and DNA oligonucleotides were purchased from either IDT or Sigma.

Name	Sequence (5'→3')
DNA Sense	GGA CAA GAT GCC TTA TGT GG
DNA Antisense	CCT GTT CTA CGG AAT ACA CC
RNA Sense	GGA CAA GAU GCC UUA UGU GG
RNA Antisense	CCU GUU CUA CGG AAU ACA CC
RNA Hairpin	GGACAAGAUGCCUUAUGUGGACUUCACCACAUAAGGCA UCUUGUCC
RNA Beacon	CGCUCCCAAAAAAAAAAACCGAGCG
Cy3 Labelled RNA Hairpin	Cy3 GCCGGGCGAAGAAUGAAAACGGC

Table 2.7: *A full list of RNA and DNA oligonucleotides used in this thesis.*

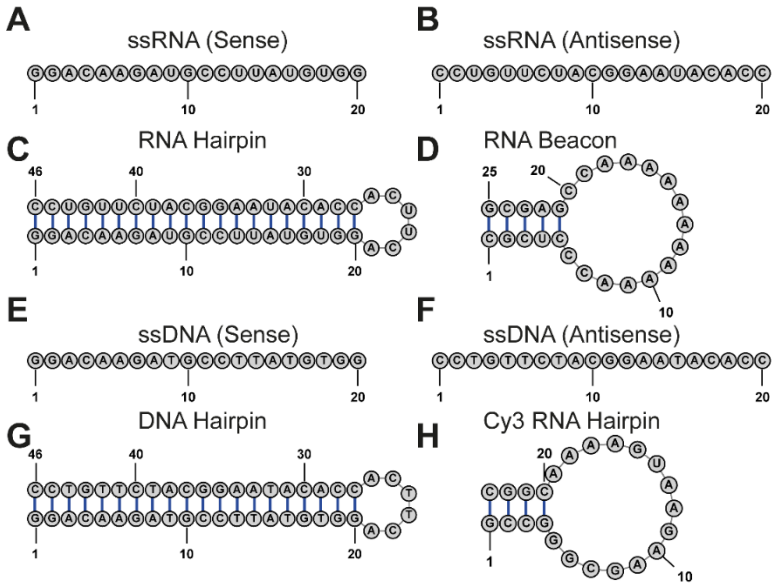


Figure 2.2: *RNA and DNA structures used in in vitro and in vivo experiments.* ***A)*** *ssRNA (1, Sense).* ***B)*** *ssRNA 2 (Antisense to A, annealed with A to form dsRNA).* ***C)*** *RNA Hairpin.* ***D)*** *RNA Beacon.* ***E)*** *ssDNA, annealed with ssRNA to form RNA:DNA hybrid.* ***F)*** *ssDNA (Antisense to E).* ***G)*** *DNA Hairpin.* ***H)*** *RNA hairpin labelled with Cy3 at the 5'.*

2.1.8 Other commercially available reagents

A list of all other commercially available reagents used in this thesis can be found in **Table 2.8**.

Name	Supplier
µ-Dish 35 mm, high Glass Bottom	Ibidi
1 kb Plus DNA Ladder	NEB
10% Tween-20 Solution	BioRad
10X gel loading solution (Native Agarose)	Thermo Fisher
10X Tris/Glycine/SDS Buffer	BioRad
4-15% Mini-Protean TGX gels 10 and 15 well	BioRad
40% Acrylamide/Bis solution 19:1	BioRad
Alexa Fluor 555 Azide, Triethylammonium Salt	Invitrogen
Amersham Hyperfilm MP High performance autoradiography film	Cytiva
Ampicillin	Sigma
Anti-FLAG® M2 magnetic beads	Merck
BamHI-HF	NEB
Binding Control Magnetic Agarose Beads	Chromotek
Bio-Rad Protein Assay Dye Reagent Concentrate	BioRad
Column G-25 Illustra Microspin	VWR
cOmplete Protease Inhibitor Cocktail	Roche
DAPI Solution	BD Biosciences
Deoxyribonuclease I from bovine pancreas	Sigma
DEPC	Sigma
DL-Dithiothreitol Solution	Sigma

DMEM, high glucose, GlutaMAX Supplement, pyruvate	Gibco
DMSO	Sigma
dNTP Set	Bioline
DpnI	NEB
Duolink In Situ Detection Reagents Green	Sigma
Duolink In Situ Detection Reagents Red	Sigma
Duolink In Situ Red Starter Kit Mouse/Rabbit	Sigma
EasyTides Adenosine 5'-triphosphate, [gamma-32P]- 50mM Tricine (pH 7.6), green dye 6000Ci(222TBq)/mmol	Perkinelmer
EdU (5-ethynyl-2'-deoxyuridine)	Invitrogen
Ethidium Bromide solution 1%	PanReac AppliChem
Fetal Bovine Serum (FBS)	Merck
Fluoroshield Mounting Medium With DAPI	Abcam
Gel Loading Dye, Purple (6x)	NEB
GFP-Trap Magnetic Beads	Chromotek
Gibson Assembly Master Mix	NEB
GoTaq Green Master Mix	Promega
HisTrap FF (5ml)	VWR
Hoechst 33342	Life Technologies
Hygromycin B	Cambio
Hyperfilm ECL Amersham Film	VWR
IPTG Solution, ready-to-use	Thermo Fisher
L-Glutamine	Life Technologies
Laemmli SDS sample buffer, reducing (6X)	Alfa Aesar
Lipofectamine 3000	Life Technologies
Lipofectamine RNAiMAX Transfection Reagent	Life Technologies
Lysozyme from chicken egg white	Sigma
M-PER Mammalian Protein Extraction Reagent	Fisher Scientific
Microglass Cover Glasses 20mm	VWR
Monarch DNA Gel Extraction Kit	NEB
Monarch Total RNA Miniprep Kit	NEB
NdeI	NEB
Ni-NTA Agarose	Qiagen
Nitrocellulose membrane	Perkinelmer
Novex™ TBE Running Buffer (5X)	Invitrogen
NP-40 Surfact-Amps Detergent Solution	Fisher Scientific UK
PageRuler Plus Prestained Protein Ladder	Thermo Fisher
Paraformaldehyde, 4% in PBS	Alfa Aesar
Penicillin Streptomycin	Life Technologies
Phosphate Buffered Saline (PBS) (1X)	Sigma
Phosphate Buffered Saline Tablets	Fisher Scientific
PhosSTOP	Roche
Pierce ECL Western Blotting Substrate	Thermo Scientific
Pierce Silver Stain for Mass Spectrometry	Thermo Scientific

Pierce Universal Nuclease for Cell Lysis	Thermo Scientific
Ponceau S	Merck
Proteinase K	Thermo Fisher
Protran Nitrocellulose Hybridization Transfer Membrane, 0.45µm	Perkin Elmer
Q5 Hot Start High-Fidelity DNA Polymerase	NEB
QIAprep Spin Miniprep Kit	Qiagen
rCutSmart Buffer	NEB
Ribolock RNAse Inhibitor	Life Technologies
RNAse T1	Life Technologies
RNAsin Plus	Promega
Salmon Sperm DNA	Life Technologies
Short Cut RNAse III	NEB
SimplyBlue™ SafeStain	Invitrogen
Streptavidin, Alexa Fluor 488	Life Technologies
Streptavidin HRP	Proteintech
Streptavidin Sepharose® High Performance	Cytiva
SuperSignal Western Blot Enhancer	Life Technologies
T4 DNA Ligase	NEB
T4 Polynucleotide Kinase	NEB
TBE Running Buffer (50X)	Novex
TP53BP1 tudor-like region (human recombinant)	Cayman
Tris-Glycine Transfer Buffer (25X)	Novex
Triton-X100	Sigma
TRIzol LS Reagent	Life Technologies
TrypLE Express	Gibco
TURBO DNase (2 U/µL)	Invitrogen
UltraPure Agarose	Invitrogen
Yeast tRNA	Life Technologies

Table 2.8: *A full list of commercially available reagents used in this thesis.*

2.2 Methods

2.2.1 Bacterial Transformation and Culture

For bacterial transformation, 25µl of DH5α competent cells were incubated with 1pg-100ng (1-5µl) of plasmid DNA for 15 minutes on ice. Bacteria were then transformed by heat shock at 42°C for 30 seconds, followed by incubation on ice for 2 minutes. 400µl of 2XYT was added and bacteria incubated for 1 hour at 37°C. Bacteria were then plated on LB agar plates with the appropriate antibiotic for selection overnight at 37°C to allow colony formation.

For bacterial culture, individual colonies were picked and added to 2XYT culture media supplemented with selection antibiotics. This culture was grown overnight at 37°C at 180rpm. Bacteria were pelleted by centrifugation at 4000g for 10 minutes.

2.2.2 Preparation of Plasmid DNA

Plasmid DNA was prepared from bacterial cell pellets using the QIAprep Spin Miniprep kit according to the manufacturer's instructions and eluted in 30-50µl of water.

2.2.3 Restriction Enzyme Digestion

To perform restriction digests, DNA was incubated with the appropriate restriction enzymes (NdeI and BamHI) in rCutSmart Buffer for ~1 hour at 37°C. Successful digestion was confirmed by agarose gel electrophoresis (**Section 2.2.4**).

2.2.4 Agarose Gel Electrophoresis

Agarose gels were cast to the desired percentage (1-2%) using UltraPure Agarose in 1xTAE buffer. To aid visualisation of DNA fragments, 1µl of 1% Ethidium Bromide solution was added to 10ml of Agarose gel preparation. DNA samples were loaded with 6x Gel Loading

Dye and ran at 100V in 1x TAE buffer. A 1kb Plus DNA Ladder was used as a marker for fragment sizes. DNA was visualised using the Syngene GeneGenius BioImaging System.

2.2.5 Gel Extraction

Gel extraction was used to isolate DNA fragments for cloning. DNA fragments were run on agarose gels and isolated using the Monarch Gel Extraction kit according to the manufacturer's instructions and eluted in 8µl of elution buffer.

2.2.6 Gibson Assembly

Gibson assembly was performed in a final volume of 10µl using the Gibson Assembly Master Mix and the appropriate amount of each DNA fragment. Bacteria were transformed with the reaction product and screened by colony PCR (**Section 2.2.9**).

2.2.7 Polymerase Chain Reaction (PCR)

To amplify regions of plasmid DNA for cloning, Q5 High-Fidelity DNA polymerase was used according to the manufacturer's instructions. NEB Tm calculator was used to select the annealing temperature. Typical PCR conditions for the Q5 PCR reaction can be found in **Table 2.9**, and a full list of DNA primers used in this thesis can be found in **Table 2.4**.

Step	Temperature	Duration	Cycles
Initial Denaturation	98°C	10 seconds	1
Denaturation	98°C	10 seconds	30
Annealing	Variable	30 seconds	
Extension	72°C	30 seconds/kb	
Final Extension	72°C	2 minutes	1

Table 2.9: *Typical Q5 Polymerase PCR reaction conditions.*

2.2.8 DpnI treatment and ligations

For PCR reactions where it is important to remove template plasmid DNA, such as for cloning, 1-2µl of DpnI enzyme and NEB CutSmart Buffer (to 1X final) were added to PCR reactions and incubated at 37°C for 2hours. DpnI was inactivated by incubation at 80°C for 20 minutes.

2.2.9 Colony PCR

To screen bacterial colonies for the presence of a specific plasmid, a small amount of plated bacterial colony was picked, and either added directly to a GoTaq Green PCR reaction, or added to 10µl of water and boiled at 98°C for 5 minutes before centrifugation at 13,000g for 5 minutes, after which the supernatant was collected and 2µl added to the PCR reaction. GoTaq Green Master Mix was used according to the manufacturer's instructions. Typical PCR conditions for the GoTaq PCR can be found in **Table 2.10**. Completed PCR reactions were then run directly on agarose gels (**Section 2.2.4**) to screen the colonies. Selected colonies were grown according to the bacterial culture protocol (**Section 2.2.1**), prepared according to the plasmid DNA preparation protocol (**Section 2.2.2**), and then sent for Sanger sequencing (**Section 2.2.10**).

Step	Temperature	Duration	Cycles
Initial Denaturation	94°C	5 minutes	1
Denaturation	94°C	30 seconds	40
Annealing	42°C	30 seconds	
Extension	72°C	3.5 minutes	
Final Extension	72°C	10 minutes	1

Table 2.10: *Typical GoTaq Polymerase PCR reaction conditions.*

2.2.10 Sanger Sequencing

To verify the sequence of plasmid DNA constructs, plasmid DNA was sent for Sanger sequencing to Source BioSciences and prepared according to their template requirements (Plasmid DNA at 100ng/µl in 5µl, and primers at 3.2pmol/µl in 5µl).

2.2.11 Tissue Culture and Drug incubations

Cells were cultured in appropriate cell culture medium as indicated in **Table 2.11** with 1% L-glutamine, and 10% FBS in 5% CO_2 at 37°C, with or without 1% PenStrep. Cells were passed using TrypLE Express upon reaching ~70% confluency. Cell lines were frozen in freezing media and stored at -80°C or in liquid Nitrogen. A full list of the cell lines used in this thesis can be found in **Table 2.11**.

Cells were incubated where indicated with cell culture drugs diluted to the appropriate working concentration in cell culture media. A full list of the drugs used in this thesis can be found in **Table 2.12**.

Name	Parent	Culture Medium	Notes
Hela (Wild Type)	Hela	DMEM	
TRex Flp-In GFP	Hela	DMEM	A gift from Alfredo Castello
TRex Flp-In TIRR-GFP	Hela	DMEM	A gift from Alfredo Castello
TRex Flp-In shGFP	Hela	DMEM	A gift from Alfredo Castello
TRex Flp-In shSDOS (shTIRR)	Hela	DMEM	A gift from Alfredo Castello
53BP1-GFP	U2OS	DMEM	A gift from Matthias Altmeyer
TurboID-TIRR[a] #20	Hela	DMEM	
TurboID only[a] #21	Hela	DMEM	
siTIRR resistant[a]	Hela	DMEM	
AsiSI-ER	U2OS	DMEM	A gift from Gaëlle Legube
E5J-GFP NHEJ reporter	U2OS	DMEM	A gift from Jeremy Stark
DR-GFP HR reporter	U2OS	DMEM	A gift from Jeremy Stark
MCF7 (Wild Type)	MCF7	DMEM	
HCC1937 (Wild Type)	HCC1937	RPMI	
COV436 (Wild Type)	COV436	DMEM	
MDA436 (Wild Type)	MDA-436	DMEM	

Table 2.11: *Cell Lines used in this thesis.*
[a]*Generated in this thesis.*

Name	Working Concentration	Incubation
ATMi (KU-60019)	10μM	1 hour
Biotin	100-500μM	Variable
Doxycycline (hyclate)	1μg/ml	16-48 hours
DRB	100μM	1 hour
Etoposide	5-10μM	2 hours
Hygromycin	300μg/ml	N/A

RNAPIIIi (ML-60218)	30μM	24 hours
Tamoxifen (4-OHT)	500nM	4 hours
Sodium Arsenite	0.5mM	1 hour
THZ1	100nM	1 hour
Wortmannin	1μM	72 hours (total)
Zeocin Selection Reagent	100-200μg/ml	N/A
α-amanitin	2μg/ml	6-24 hours

Table 2.12: *Cell Culture drugs used in this thesis.*

2.2.12 Ionising Radiation

Ionising Radiation induced damage was delivered at the indicated doses using the Gravatom (GRAVITRON RX 30/55).

2.2.13 RNA transfection using Lipofectamine RNAimax

Short interfering RNA (siRNA) for gene expression knockdown was performed using Lipofectamine RNAimax according to the manufacturer's instructions. Cells were seeded in 6 well plates in antibiotic free media, and forward transfected 24 hours later with 20nM siRNA using 9ul of Lipofectamine RNAimax per well of the 6 well plate. Media without antibiotics was added to a final volume of 2ml per well. Knockdown was achieved 48 hours later as assessed by western blot. A full list of all siRNAs used in this thesis can be found in **Table 2.6**.

For transfection of the Cy3 labelled RNA hairpins (**Table 2.7**), the RNA was annealed at a concentration of 10μM in 1X annealing buffer by heating at 98°C for 3 minutes, followed by slowly cooling to room temperature. Per well of a 6 well plate, 9μl of Lipofectamine RNAimax was used with either 20nM (low) or 100nM (high) RNA and made up to a final volume of 2ml with antibiotic free media per well.

2.2.14 Plasmid transfection using Lipofectamine 3000

DNA plasmids were transfected using Lipofectamine 3000 according to the manufacturer's instructions. Cells were seeded in 6-well plates and 24 hours later forward transfected with 1-5µg of plasmid DNA using 3.75µl of Lipofectamine 3000 reagent per well of a 6-well plate. Antibiotic free media was added to a final volume of 2ml per well. Cells were harvested 24-48 hours later. A full list of all plasmids used in this thesis can be found in **Table 2.5**.

2.2.15 Colony Formation Assays

To assess the impact of knockdown of TIRR on cell survival, colony formation assays were carried out. For cells treated with siRNA, cells were first seeded in 6 well plates and 24 hours later, siRNAs were transfected according to the RNA transfection protocol (**Section 2.2.13)**. Following this, after 24 hours cells were harvested and reseeded into 12-well plates at a low density according to **Table 2.13**. Cells were left for 7-14 days until visible colonies formed. Plates were then washed 1X in PBS and stained in Crystal Violet staining solution for 30 minutes. Plates were washed in water, left to dry, and visualised according to the ColonyArea protocol (**Section 2.2.43**).

For doxycycline inducible shGFP and shTIRR (shSDOS) cells: cells were seeded in 6-well plates and 24 hours later induced with doxycycline. After 24 hours, cells were reseeded in 12-well plates in media with fresh doxycycline. Doxycycline was refreshed every 48 hours.

Cell Type	Cells per well (12-well plate)
Hela	750
shGFP Hela	750
shTIRR/shSDOS Hela	750
MCF7	1000
HCC1973	20,000
MDA-436	5000

Table 2.13: *Cell numbers seeded into each well of a 12-well plate for colony formation assays.*

2.2.16 Edu Labelling

To incorporate Edu into newly replicated DNA, Cells were seeded in 6-well plates (2 wells per condition). At ~70% confluency, cells were washed once in PBS at 37°C, and 10µM Edu in 2ml media added to each well. Cells were incubated with Edu for 30 minutes at 37°C.

2.2.17 Cell Cycle Analysis by Flow Cytometry

Edu labelled cells were washed in PBS and harvested by trypsinisation. 2 wells per sample were combined to achieve the desired cell number. Cells were centrifuged at 1800rpm for 3 minutes, then washed once in PBS, centrifuged at 1800rpm for 3 minutes, and resuspended in 1ml PBS. Cells were counted and diluted to ~400,000 cells in 3ml PBS. Cold 100% Ethanol was slowly added to the cells with vortexing at a low speed to a final volume of 10ml. Cells were placed on a wheel at 4°C overnight for fixation. The following day, fixed cells were pelleted by centrifugation at 1800rpm for 3 minutes and washed in PBS. Cells were resuspended in 500µl of PBSTri-BSA (0.1% Triton X-100, 1% BSA, PBS) and incubated on ice for 15 minutes, followed by centrifugation at 1000g for 5 minutes. Cells were resuspended in PBST-BSA (0.1% Tween 20, 1% BSA, PBS) and washed twice. Cells were resuspended in 250µl Click-IT reaction and incubated in the dark for 1 hour. Cells were washed twice in 500µl of PBST-BSA. Cells were resuspended in 250µl of DAPI staining solution (0.1% BSA, 100µl (10mg/ml) RNase A, 1µg/ml (final) DAPI, PBS to 10ml) and incubated in the dark at RT for 1 hour. Cell cycle phase was determined using a Cytoflex LX flow cytometer.

2.2.18 Live cell imaging and laser striping

Cells were seeded in 35mm glass bottom dishes to reach ~70% confluency at the point of the experiment. If applicable, plasmid transfections were performed according to the plasmid transfection protocol (**Section 2.2.14**), in a final volume of 2ml. Before laser stripping, cells were pre-sensitised using Hoechst 33342 (10µg/ml) at 37°C in phenol red free media. Cells

were imaged using an Olympus SoRa spinning disc confocal microscope using the 405nm FRAP module in a chamber at 37°C and 5% CO_2. To select for cells with similar expression levels, cells were systematically chosen using a 488-nm laser setting. DNA damage was induced by a 405nm laser and recruitment of the fluorescently labelled proteins was monitored by live cell imaging. All images were quantified using FIJI software. Fluorescent intensities were normalised against intensities measured in undamaged parts of nuclei. Laser striping and analysis was performed by Dr Monika Gullerova.

2.2.19 Whole Cell Lysis and Protein Quantification

For whole cell lysis of adherent cells, 150-300µl M-PER Mammalian Protein Extraction Reagent was added directly to a well of a 6-well plate and cells scraped and collected in Eppendorf tubes. Samples were vortexed and sonicated for 10-15s before protein quantification using the Implen NanoPhotometer N60.

2.2.20 Nuclear Fractionation

Cells seeded in 15cm dishes at ~70% confluency were washed 3X in cold PBS and were harvested by scraping from plates in cold PBS. Cells were collected in Eppendorf tubes and centrifuged at 500g for 5 minutes. The cell pellet was lysed gently in 5X the cell pellet volume in hypotonic lysis buffer, and incubated for 10 minutes at 4°C on a wheel. Samples were centrifuged at 800g for 5 minutes and the supernatant removed to obtain the nuclear fraction. The nuclear pellet was washed 3X in hypotonic lysis buffer without NP-40 to remove any contaminating cytoplasmic fraction.

2.2.21 RNA Extraction

Total RNA was extracted by scrapping from plates using either TRIzol or RNA lysis reagent from the Monarch Total RNA Miniprep Kit. RNA lysis reagent was added directly to plates and collected into Eppendorf tubes for use in the Monarch Total RNA Miniprep Kit as per the

manufacturer's instructions. For TRIzol extraction, TRIzol was added to plates and cells scraped, collected into Eppendorf tubes and vortexed. Chloroform was added to the TRIzol sample according to the manufacturer's instructions (200µl of chloroform per 1ml of TRIzol Reagent) and vortexed, before centrifugation at 12,000g for 15 minutes at 4°C. The aqueous phase was collected and used in the Monarch Total RNA Miniprep Kit as per the manufacturer's instructions. RNA was eluted in water and quantified using the Implen NanoPhotometer N60.

2.2.22 Bleach Agarose Gel

For visualisation of RNA integrity, a bleach agarose gel was used[3]. Agarose gels were prepared with the addition of 1% bleach and were run at 100V for 1 hour. RNA was visualised using the Syngene GeneGenius BioImaging System.

2.2.23 RNA sequencing

RNA was quality checked (QC) using a bleach agarose gel according to **Section 2.2.22** and the concentration and 260/230 and 260/280 measured using an Implen NanoPhotometer N60. RNA samples were submitted to the Oxford Genomics Centre for rRNA depletion and paired-end bulk full transcript RNA sequencing on the Illumina NovaSeq6000 was performed.

2.2.24 Western Blotting

Protein samples in 1X Laemmli Buffer were sonicated for 10-30 seconds, followed by incubation for 5 minutes at 98°C. Samples were then loaded in 4-15% Mini-Protean TGX gels and electrophoresed in Tris-Glycine running buffer at 100V for 1 hour. Gels were transferred onto nitrocellulose membranes for 1 hour 30 minutes at a constant voltage of 15V. Successful transfer of protein to the membrane was visualised using Ponceau S. Membranes were blocked in 5% milk or BSA in PBS with 0.1% Triton X100 (PBST) at room temperature for 1 hour. Membranes were then incubated with primary antibodies overnight. Membranes were washed

3 times in PBST and incubated with a secondary antibody for 1 hour at room temperature. Membranes were washed 3 times in PBST, then visualised using ECL and Amersham Hyperfilm ECL film. Some membranes were processed using the Super Signal Western Blot Enhancer kit according to the manufacturer's instructions. A full list of primary and secondary antibodies used for western blotting in this thesis can be found in **Table 2.2** and **Table 2.3**, respectively.

2.2.25 Co-Immunoprecipitation (Co-IP)

Cells were plated in 10cm or 15cm dishes to achieve ~70% confluency at the point of harvest. Cells were washed 3x in cold PBS, harvested by scraping, and centrifuged at 500g for 5 minutes. The cell pellet was lysed in 5 volumes of cell lysis buffer for 30 minutes at 4°C on a wheel with vigorous pipetting every 10 minutes. Lysates were centrifuged at 17,000g for 10 minutes at 4°C of Co-IP wash buffer was added to lysates (1.5x cell lysate volume). GFP-Trap magnetic beads were washed 3x in cold Co-IP wash buffer and added to the lysate on a wheel for 1.5 hours at 4°C. The beads were then washed 3x in cold Co-IP wash buffer and samples were eluted using 2x Laemmli buffer and boiling at 95°C.

2.2.26 Immunofluorescence (IF)

Cells were plated in 6-well plates on glass coverslips for ~70% confluency. Cover slips were washed 3 times in cold PBS and fixed in cold 4% paraformaldehyde in PBS for 10 minutes. Cover slips were then washed 3 times in cold PBS and fixed with cold 0.2% Triton X-100 in PBS for 10 minutes. Slides were then washed 3 times in cold PBS and blocked in 10% FBS in PBS for 2 hours at 4°C. Primary antibodies were diluted to the appropriate concentration in 10% FBS in PBS and incubated overnight at 4°C in a humidified chamber. Cover slips were then washed 3 times in PBS with 0.1% Triton X-100 (PBST). Cover slips were incubated for 2 hours at RT with secondary antibodies diluted in 0.15% FBS in PBS. Coverslips were washed

3 times in PBST in the dark, followed by washing a final time in PBS before mounting on slides with Fluoroshield Mounting Medium with DAPI. Slides were imaged using an Olympus Fluoview FV1200 confocal microscope with a 60X objective lens. A full list of primary and secondary antibodies used for IF in this thesis can be found in **Table 2.2** and **Table 2.3**, respectively.

For S9.6 Immunofluorescence experiments, after fixation permeabilisation with 0.2% Triton X100, cells were treated with RNase pre-treatment solution (0.1% BSA, 3mM $MgCl_2$, RNAse T1 (Thermo) 1:200 (v/v), ShortCut RNAseIII (NEB) 1:200 (v/v) in PBS) for 2 hours at RT[4]. Subsequent blocking and antibody incubation steps were then carried out as above. S9.6 IF experiments were performed by Dr Adele Alagia.

2.2.27 Proximity Ligation Assay (PLA)

Proximity Ligation Assay was performed according to the manufacturer's instructions. Briefly, cells were seeded on cover slips, and fixed and permeabilised according to the immunofluorescence protocol (**Section 2.2.26**). Cover slips were blocked in PLA blocking buffer in a humidity chamber for 1 hour at 37°C. Primary antibodies were diluted in PLA antibody diluent and incubated with cover slips in a humidified chamber at 4°C overnight. Cover slips were then washed 3 times in PLA buffer A at RT, then incubated with PLA probes for 1 hour at 37°C. Cover slips were washed 3 times in PLA buffer A, then incubated with PLA ligase in ligation buffer for 30 minutes at 37°C. Cover slips were washed 3 times in PLA buffer A and incubated with PLA polymerase in polymerase buffer for 100 minutes at 37°C in the dark. Cover slips were washed 3 times in PLA buffer B in the dark, and twice in 0.01X PLA buffer B. Coverslips were mounted on slides using PLA DAPI solution and imaged using an Olympus Fluoview FV1200 confocal microscope with a 60X objective lens. PLA foci were

quantified using CellProfiler[5] and the Speckle Counter pipeline. A full list of antibodies used in this thesis for PLA can be found in **Table 2.2**.

2.2.28 Fluorescence *in situ* Hybridisation Proximity Ligation Assay (FISH-PLA)

A*si*SI U2OS Cells were plated on glass coverslips and 24 hours later incubated with α-amanitin where indicated. 24 hours after addition of α-amanitin, 4-OHT was added where indicated for 4 hours. Coverslips were then washed 3 times in cold PBS and fixed in cold 4% paraformaldehyde in PBS for 15 minutes. Coverslips were then washed 3 times in cold PBS and permeabilised with cold 0.5% Triton X-100 in PBS (PBST) for 10 minutes. Slides were then washed 3 times in cold PBS and blocked in blocking buffer (1x SSC, 20µg/µl yeast tRNA, 20µg/µl salmon sperm DNA, 0.5% Triton-X100, 2% BSA, 1U/µl RNAsin Plus) at 37°C for 1 hour. Probe incubation buffer (1x SSC, 100nM DNA probes) was heated to 98°C for 3 minutes and cooled on ice for 10 minutes before addition of 1% Triton X-100 and 1U/µl RNAsin Plus (final). Coverslips were incubated with probe incubation buffer for 3 minutes at 80°C, and then at 37°C overnight. Coverslips were washed 3x in SSC-T buffer (1x SSC, 0.1% Triton X-100, 1% BSA) and 2x in PBS, before blocking for 1 hour at 37°C with PLA blocking buffer. Primary antibodies were diluted to the appropriate concentrations in PLA antibody diluent and incubated overnight at 4°C in a humidified chamber. Cover slips were then washed 3 times in PLA buffer A at RT, then incubated with a minus rabbit PLA probe for 1 hour at 37°C. The PLA protocol was then followed according to the manufacturer's instructions using the Duolink In Situ Red Starter Kit Mouse/Rabbit (**Section 2.2.27**). The double strand breaks probed were DS1: RBMXL1 (promoter) hg19, chr1:89,458,643 and DS2: VSTM2B (CDS) hg19, chr19:30,019,487. Sequences of the FISH-PLA probes can be found in **Table 2.14.**

Probe	Sequence (5' → 3')
FISH_PLA_DS1_1	CCGGCCGACTCCACAGCCAATGGAGTTCCCTGAGTCCACACCCATAGCCAAAAAAAAAAAAAAAAAAAAAAAAAAAAAAAAAAAAAAATATGACAGAACTAGACAC

FISH_PLA_DS1_2	CCAAATTCCATACCCATATCCAAGTCCCCGCCCCACTAACTCGAGCCCGCAAAAA AAAAAAAAAAAAAAAAAAAAAAAAAAAAAAAAAAATATGACAGAACTAGACAC
FISH_PLA_DS1_3	GCCCATCCTTGCAAACCAGTCCTCGTCCTATAACCTGCCCCAACCCGATCAAAAA AAAAAAAAAAAAAAAAAAAAAAAAAAAAAAAAAAATATGACAGAACTAGACAC
FISH_PLA_DS1_4	CCCTGCCCTCTCTCAGGCACCTTCCAAAGTTATTCCAACCCGATCCCTCCAAAAA AAAAAAAAAAAAAAAAAAAAAAAAAAAAAAAAAAATATGACAGAACTAGACAC
FISH_PLA_DS1_5	GTTCCTTTACGCTTTTTAACCCCACACCCCCATCTCAAATGACAAATGCAAAAAA AAAAAAAAAAAAAAAAAAAAAAAAAAAAAAAAAAATATGACAGAACTAGACAC
FISH_PLA_DS1_6	GTCATTTTTCTTCCTTCTTCAGTCTCACATGTCCCTTTCATTCTTAGTTTAAAAAAA AAAAAAAAAAAAAAAAAAAAAAAAAAAAAAAAAAATATGACAGAACTAGACAC
FISH_PLA_DS1_7	TTCGCTGACACTGCCCTCCCCAAAGAAGTCACCAGTGGTTTCCTTGTTTTAAAAA AAAAAAAAAAAAAAAAAAAAAAAAAAAAAAAAAAATATGACAGAACTAGACAC
FISH_PLA_DS1_8	CCCTCTAGCCTCTCATCCTCTTAAAATAGAAGAGGAAAAATATCCAAACAAAAA AAAAAAAAAAAAAAAAAAAAAAAAAAAAAAAAAAAATATGACAGAACTAGACA C
FISH_PLA_DS1_9	GAAGAGTATATTCCTTTAATCAATGTATACTTTTGTTCCCTCCTTTAGAAAAAAAA AAAAAAAAAAAAAAAAAAAAAAAAAAAAAAAAAAATATGACAGAACTAGACAC
FISH_PLA_DS1_10	CACATCCAGGCTCGCCCCTACCTGTACACAATAATTTCTCCATGCACCTAAAAAA AAAAAAAAAAAAAAAAAAAAAAAAAAAAAAAAAAATATGACAGAACTAGACAC
FISH_PLA_DS1_11	TGAGATGTAGTATGATCACCAATCGCGGGGGACCCCACAGCCAGTGCGCGAAAA AAAAAAAAAAAAAAAAAAAAAAAAAAAAAAAAAAATATGACAGAACTAGACA C
DS2_VSTM2B_FISH_1F	AGGATGCAACTAAAATCAGCGTAAGTGTGGAGCCCAGCGCGGGCCGCGGGAAA AAAAAAAAAAAAAAAAAAAAAAAAAAAAAAAAAAAATATGACAGAACTAGA CAC
DS2_VSTM2B_FISH_2F	CCTTGCCTAAAGGCGGATCCGAGTTCCCCTAGCCAGAAGGCCGCGAGCCTAAAA AAAAAAAAAAAAAAAAAAAAAAAAAAAAAAAAAAAATATGACAGAACTAGAC AC
DS2_VSTM2B_FISH_3F	CTGGGAAACTCTTGGAAAGCCGGACGTCCTTTGTGCCCTCAACCCCCATCAAAAA AAAAAAAAAAAAAAAAAAAAAAAAAAAAAAAAAAAATATGACAGAACTAGACA C
DS2_VSTM2B_FISH_4F	CATCCAGTCTCCCCAGTTCAGCCGGCAGGTGTGCACCAGGGCAGCCACCCAAAA AAAAAAAAAAAAAAAAAAAAAAAAAAAAAAAAAAAATATGACAGAACTAGAC AC
DS2_VSTM2B_FISH_5F	GTCCAGACACAGCGGCCCTCCCTCCAGTTCTTCACGGCTCCCAGTGAGCTAAAAA AAAAAAAAAAAAAAAAAAAAAAAAAAAAAAAAAAAATATGACAGAACTAGACA C
DS2_VSTM2B_FISH_6F	GTCTGCCTCAAAACCCACACTCTCTTACACACTCTAGTGTGCTCGCGTGCAAAAA AAAAAAAAAAAAAAAAAAAAAAAAAAAAAAAAAAAATATGACAGAACTAGACA C
DS2_VSTM2B_FISH_7F	GCCACCAGAAAACCGAGTACCGGAAAGCCGGCAGGACCTCCAGCCCTCAGAAAA AAAAAAAAAAAAAAAAAAAAAAAAAAAAAAAAAAAATATGACAGAACTAGAC AC
DS2_VSTM2B_FISH_8F	TGCTCGCTGGCTGCGGCCCTCTGATGGGTGCTGGGTAGTGAAGGAAGCCCAAAA AAAAAAAAAAAAAAAAAAAAAAAAAAAAAAAAAAAATATGACAGAACTAGAC AC
DS2_VSTM2B_FISH_9F	CAGCAGTGGTTACCCCCAAACCTGTCAATTATTTTGACAGCATCGCTGTTAAAAA AAAAAAAAAAAAAAAAAAAAAAAAAAAAAAAAAAAATATGACAGAACTAGACA C

DS2_VSTM	AGGGAGGGAAGCAGCGGGCTTCACTCGCGCAGGGCGCCGCCCTGTGGCGCAAAA
2B_FISH10F	AAAAAAAAAAAAAAAAAAAAAAAAAAAAAAAAAAAAATATGACAGAACTAGACAC

Table 2.14: *Sequences of DNA probes used in FISH-PLA for DS1 and DS2.*

2.2.29 E5J-GFP and DR-GFP Reporter Cells Lines

For experiments using siRNA knockdown of repair proteins, E5J-GFP (NHEJ) or DR-GFP (HR) cells were seeded in 6-well plates (2 wells per condition) in media without antibiotics, and 24 hours later transfected with siRNA according to **Section 2.2.13**, with the modification of using 4µl of RNAimax per condition. After 24 hours, cells were transfected with 1.5µg of I-SceI plasmid according to **Section 2.2.14**. The following day, the media was replaced with fresh antibiotic free media, and 24 hours later cells were harvested by trypsinisation and collected in 10% FBS in PBS. The percentage of cells expressing GFP was measured using a Cytoflex LX flow cytometer.

For experiments using wortmannin, cells were seeded as above and 24 hours later treated with wortmannin. After 24 hours of incubation, 1.5µg of I-SceI plasmid was transfected with the addition of wortmannin to the media. The following day the transfection reagent was removed and fresh media with wortmannin added. 24 hours later, cells were harvested and processed as above.

2.2.30 RNA Immunoprecipitation and sequencing (UV RIP-Seq)

3 x 15-cm dishes were used per condition and plated to achieve ~70% confluency at the point of harvest. TRex Flp-In TIRR-GFP and TRex Flp-In GFP cells were plated and 24 hours later, induced with 1µg/ml doxycycline for 24 hours. After 24 hours, cells were washed three times in cold PBS and crosslinked at 254nm at 0.15 J/cm2. Cells were lysed in cold RIP lysis buffer with 1 x protease inhibitor and Ribolock, with Turbo DNase. Lysates were sonicated (10s on, 30s off) at level medium. Lysates were centrifuged at 17,000g for 10 minutes and the

supernatant collected. GFP-Trap A beads were washed 3 times in lysis buffer and added to samples for 2 hours on a wheel at 4°C. Beads were collected by centrifugation at 2500g for 2 minutes and washed 2x with RT RIP high salt buffer, 2x with cold RIP low salt buffer, and 2x with RIP Proteinase K buffer. Beads were incubated with Proteinase K in RIP Proteinase K buffer at 37°C for 1 hour with shaking at 1100rpm. RNA was extracted using TRIzol and the Monarch Total RNA Miniprep kit according to the manufacturer's instructions. RNA was quantified using a Bioanalyzer Agilent and sent for sequencing (**Section 2.2.23**).

2.2.31 TurboID Proximity Ligation Assay and On-Bead Digestion

TurboID samples were prepared according to a previously published protocol[6], with a few modifications. TurboID only or TurboID-TIRR expressing cells were seeded in 15cm dishes to achieve ~70% confluency at the point of harvest. 24 hours later, cells were irradiated with 10Gy as indicated. After 45 minutes, Biotin containing media was added (or not as a control) for 30 minutes and incubated at 37°C. Cells were then washed 3X in cold PBS, and harvested by scraping into Eppendorf tubes. Cells were centrifuged at 500g for 5 minutes, and lysed in 900µl of cell lysis buffer. Lysates were placed on a wheel for 30 minutes at 4°C, with vortexing every 10 minutes for 10 seconds at high speed. Cell lysates were then centrifuged at 17,000g for 10 minutes and the supernatant collected. Protein concentration was measured using a Bradford Assay, and 2.5mg of total protein used per sample. Streptavidin Sepharose beads were washed 3X in cell lysis buffer by centrifugation at 1000g for 2 minutes, and 50µl used per sample. Beads were added to lysates and incubated overnight on a wheel at 4°C. Beads were washed twice in 1ml cell lysis buffer, once in 0.1M Na_2CO_3, once in 2M urea in 10mM Tris-HCl (pH 8.0), and twice in cell lysis buffer. Finally, beads were washed 3X in PBS and prepared for mass spectrometry. Silver stains for quality control of streptavidin pull downs

were performed using the Pierce Silver Stain for Mass Spectrometry Kit according to the manufacturer's instructions.

To prepare samples for mass spectrometry, samples were digested and alkylated on-bead. Beads were resuspended in 75µl of 8M Urea in 100mM Ammonium Bicarbonate (AmBic). Cysteines were reduced using 10mM TCEP and incubated at RT for 30 minutes, followed by alkylation of cysteines with 50mM 2-Chloroacetamide in 8M Urea and 100mM AmBic at RT. Beads were pre-digested by incubation with LysC (1µg per 100µg of protein, 0.1µg total per sample) for 2 hours at 37°C with shaking. Urea was then diluted to 2M with 100mM AmBic, and $CaCl_2$ added to 2mM final. Trypsin was added to the beads (1µg per 40µg of protein, 0.25µg total per sample), and incubated for ~16 hours at 37°C with shaking. The reaction was stopped by the addition of 5% formic acid. The supernatant was collected and spun down at 14,000rpm for 30 minutes at 4°C to remove aggregates. The samples were then desalted onto C18 columns.

2.2.32 TIRR-GFP Affinity Pull-down Mass Spectrometry and digestion

TIRR-GFP and GFP Flp-IN cells were seeded into 15cm dishes and 24 hours later, induced with doxycycline for a further 24 hours. Cells were washed 3x in cold PBS, harvested in PBS, and centrifuged at 1800rpm for 5 minutes, before lysis in 500µl of Cell Lysis buffer for 30 minutes on a wheel at 4°C, with pipetting every 10 minutes. Lysates were centrifuged at 17,000g for 10 minutes, and a Bradford assay performed on the supernatant. 2mg of total protein from each sample was diluted in Co-IP dilution buffer to a final volume of 1250µl. 50µl per sample of Control beads and GFP-Trap beads were washed 3x in cold dilution buffer, and samples were precleared for 1 hour at 4°C on a wheel. Supernatant was added to GFP-Trap beads, and samples left on a wheel at 4°C for 2 hours. Beads were washed 2x in cold dilution buffer, and 2x in cold PBS, before being eluted in 1.5x bead volume 0.2M Glycine (pH 2) for

7 minutes at 4°C. Glycine was neutralised using 1M Tris (pH 8). Glycine elution was repeated twice. Samples were then prepared for Mass Spectrometry using Filter Aided Sample Preparation (FASP) and Trypsin Digestion, according to **Section 2.2.34**. Note, volumes for FASP were adjusted for bead elutions, as the eluent volume from the beads is more than for whole cell lysate preparations.

2.2.33 Whole cell lysate preparation for Mass Spectrometry

ShGFP and shTIRR cells were seeded in 6-well plates (2 wells per condition) and 24 hours later, knockdown was induced using doxycycline for 48 hours. After the completion of knockdown, samples were either irradiated with 10Gy and incubated for 6 hours, or incubated for 6 hours without inducing damage. Cells were then washed 3 times in cold PBS and harvested by scraping, followed by centrifugation at 500g for 5 minutes. Cells were then resuspended in 5 volumes of cell lysis buffer and incubated at 4°C on a wheel for 30 minutes, with vortexing every 10 minutes for 10 seconds at high speed. Samples were then centrifuged at 17,000g for 10 minutes and the supernatant collected. The amount of protein was quantified using a Bradford Assay with BioRad Protein Assay Dye Reagent Concentrate.

2.2.34 Filter Aided Sample Preparation, Trypsin Digestion, and LC-MS/MS

The Filter Aided Sample Preparation was performed according to the protocol obtained from Dr Marjorie Fournier. FASP filters (10,000 MWCO) were washed in 300µl of UB8 buffer by centrifugation at 14,000rpm for 30 minutes, and the flow through (FT) discarded. 100µg of total protein per sample was loaded on each filter, and centrifuged at 14,000 rpm for 30 minutes, or until all the sample had passed through the filter. The flow through was discarded and 100µl of 5mM TCEP in UB8 buffer was added to each filter and incubated for 30 minutes at RT. Subsequently, 100µl of 80mM 2-Chloroacetamide (2-CAA) in UB8 buffer was added to filters and incubated at RT for 30 minutes. Samples were spun at 14,000rpm for 30 minutes,

and the FT discarded. Filters were then washed 6 times with 400µl buffer UB8 by centrifugation at 14,000 rpm for 30 minutes and flow through discarded. Filters were then washed twice in buffer UB1, before transferring to fresh collection tubes. 200ng Trypsin in 100µl UB1 buffer was added to filters and incubated overnight at 37°C with gentle shaking. Filters were centrifuged at 14,000rpm for 20 minutes and the flowthrough was saved. 150µl 0.1% TFA was added to filters, followed by centrifugation at 14,00rpm for 20 minutes and the flowthrough saved. 150µl 50% ACN, 0.1% TFA was then added to filters, followed by centrifugation of 14,000rpm for 20 minutes. Flowthroughs were combined, and the sample was then dried and desalted before Mass Spectrometry analysis by Dr Marjorie Fournier according to the following protocol.

Dried peptides were resuspended into 2% acetonitrile / 0.1% formic acid before LC-MS/MS analysis. Peptides were separated by nano liquid chromatography (Thermo Scientific Easy-nLC 1000 or Ultimate RSLC 3000) coupled in line with a QExactive mass spectrometer equipped with an Easy-Spray source (Thermo Fischer Scientific). Peptides were trapped onto a C18 PepMac100 precolumn (300µm i.d.x5mm, 100Å, ThermoFischer Scientific) using Solvent A (0.1% Formic acid, HPLC grade water). The peptides were further separated onto an Easy-Spray RSLC C18 column (75um i.d., 50cm length, Thermo Fischer Scientific) using a 30 (GFP-TIRR samples), 60 (Turbo-TIRR samples) and 120 minutes (Whole cell lysates) linear gradient (15% to 35% solvent B (0.1% formic acid in acetonitrile)) at a flow rate 200nl/min. The raw data were acquired on the mass spectrometer in a data-dependent acquisition mode (DDA). Full-scan MS spectra were acquired in the Orbitrap (Scan range 350-1500m/z, resolution 70,000; AGC target, 3e6, maximum injection time, 50ms for 30 and 60mins gradient or 100ms for 120mins gradient). The 10 (30 and 60mins gradients) and 20 (120mins gradient) most intense peaks were selected for higher-energy collision dissociation

(HCD) fragmentation at 30% of normalised collision energy. HCD spectra were acquired in the Orbitrap at resolution 17,500, AGC target 5e4, maximum injection time of 120ms with fixed mass at 180m/z. Charge exclusion was selected for unassigned and 1+ ions. The dynamic exclusion was set to 5s, 20s and 40s for 30, 60mins gradients and 120mins gradient respectively.

2.2.35 5' End Labelling of RNA and DNA substrates

For 5' end labelling of DNA and RNA substrates with ^{32}P, 10µM of RNA or DNA was incubated with T4 polynucleotide kinase (T4 PNK) according to the reaction detailed in **Table 2.15** and incubated for 1 hour at 37°C. After reaction completion, 30µl of H2O was added to samples to reach a final volume of 50µl, and reactions were ran through a G25 spin column to remove free nucleotides. For single stranded substrates, 50µl of water was added to the sample to reach a final concentration of RNA/DNA of 100nM. For hairpin or double stranded substrates, 40µl of water and 10µl of 10X annealing buffer was added for a final concentration of 100nM.

Component	Volume
10µM RNA/DNA	1µl
[^{32}P] ATP	1µl
10X Kinase Buffer	2µl
T4 PNK	1µl
H_2O	15µl

Table 2.15: *T4 PNK reaction for radiolabelling RNA and DNA substrates.*

2.2.36 Annealing of RNA and DNA substrates

RNA and DNA substrates were annealed at a concentration of 100nM in 1X annealing buffer by heating at 98°C for 3 minutes, followed by slowly cooling to room temperature.

2.2.37 Electrophoretic Mobility Shift Assay (EMSA)

EMSA assays were performed to assess the binding of protein to RNA and DNA substrates. 10nM of radiolabelled RNA or DNA substrate was incubated with increasing concentrations of recombinant protein as indicated in 1X EMSA buffer. Reactions were carried out in a final volume of 10µl. Reactions were incubated for 15 minutes at 37°C, before adding native agarose gel loading solution to 1X final.

Reactions were run on 0.5X TBE 6% native polyacrylamide gels in 0.5X TBE running buffer for 3 hours at 100V. Gels were then dried on Whatman paper for 2 hours at 80°C, and imaged using autoradiography film overnight at -80°C.

2.2.38 *In vitro* RNA separation assays

To perform *in vitro* RNA separation assays for TIRR and 53BP1 with increasing concentrations of nuclear irradiated RNA, 1µg of recombinant Flag-TIRR and 1µg recombinant HA-53BP1 (obtained from Evotec (Toulouse)) were incubated together with 20µl of Anti-FLAG M2 magnetic beads per sample in TGEN150 buffer for 1 hour at 4°C on a wheel. Supernatant was removed and the beads washed 1X in TGEN150 buffer. Nuclear RNA from Hela cells 1h post IR (10Gy) was extracted using TRIzol followed by Monarch Total RNA Miniprep Kit. Increasing amounts of RNA (500ng, 1µg, 5µg, and 10µg) was added to the beads in constant volume of TGEN150 buffer with Ribolock and incubated at RT on a wheel for 1 hour. Beads were washed 2X in TGEN150 buffer, before being eluted in 2X Laemmli SDS sample buffer. Eluent was collected and ran on a western blot to visualise binding.

2.2.39 Homogeneous Time Resolved Fluorescence (HTRF)

HTRF assays were performed by Evotec (Toulouse) as part of our collaboration using the following method. 1536 well plates were thawed at RT and centrifuged at 1800rpm at RT and placed on a rotating Cytomat hotel of a robotic platform. Solutions of proteins (HA-TEV-

53BP1 1484-1603 and 3xFlag-TIRR, 10nM each (final)) and of antibodies (Cryptate donor Anti-Flag TB3+, Cisbio, 61FG2TL, 0.13µg/ml final and Cryptate acceptor Anti-HA XL665, Cisbio, 610HAXL, 2µg/ml final) were prepared in PPI buffer (Terbium detection buffer, Cisbio, 61DB10RDF). An EL406 (Biotek) was used to dispense solutions of proteins into 1536 well plates followed by incubation at RT for 15 minutes. Antibodies were then added and left to incubate for 2 hours at RT. PPI buffer alone was used to measure background signal. The following readings were then taken on a Tecan Spark:

Measurement 1

Excitation filter: 340(20)nm / Emission filter: 620(10)nm / MirrorDichroic: 510

Lag time: 100µs / Integration time: 300µs / Number of reads: 3 / Gain: 170 / Z-Position: 20500 [µm]

Measurement 2

Excitation filter: 340(20)nm / Emission filter: 665(8)nm/ MirrorDichroic: 510

Lag time: 100µs / Integration time: 300µs / Number of reads: 3 / Gain: 160 / Z-Position: 20500 [µm]

Raw data files were processed using Screener Utilities before implementation in Genedata Screener for QC validation, data pre-processing and data analysis. Raw data are uploaded into Genedata Screener and plates or wells that had technical issues are masked. Raw fluorescence of the donor (620 nm) and acceptor (665 nm) is recorded and the HTRF ratio is calculated. The HTRF ratio is normalised on each plate independently using the median of control wells: 100% inhibition (no target proteins in DMSO) and 0% inhibition (proteins with HTRF antibodies in DMSO). The data are expressed as normalised activity (%): an example of 100% inhibition is

represented as a normalised activity of 100%, whereas 0% inhibition in the DMSO vehicle wells is represented as a normalised activity of 0%.

2.2.40 Surface Plasmon Resonance (SPR)

SPR assays were performed by Evotec (Toulouse) as part of our collaboration using the following method. Corresponding RNA or DNA substrates were annealed at 95°C for 5 minutes in annealing buffer (10mM Tris pH 7.5, 50mM NaCl, 1mM EDTA) and slowly cooled to RT. All experiments were conducted on a Biacore 8K+ Device and were performed at 25°C. N_{α},N_{α}-Bis(carboxymethyl)-L-lysine hydrate reagent (Sigma) dissolved in 50mM borate buffer (pH 8.5) was chemically bound to the SPR CM4 sensorchip (Cytiva, BR100534) using an amine coupling kit (Cytiva, BR100050). 6-211 TIRR-His (0.1 µM) was injected via NTA-Capture coupling on the SPR surface during 200s at 5 µL/min to reach ~600 RU of protein immobilised (running buffer for immobilisation: PBS-P (Cytiva, 28995084)). After equilibration of the Biacore system in running buffer (HEPES 20mM pH 6, NaCl 300mM, p20 0.05%), DNA and RNA substrates were injected in multi-cycle kinetics over TIRR-His protein in a dose-response up to 200µM with 100s association and 100s dissociation at 30 µL/min. Binding curves were analysed using Insight Evaluation Software and fitted when possible with a 1:1 steady-state affinity model.

2.2.41 Protein purification of 1-211 and 6-211 Thrombin His-TIRR

BL21(DE3) *E.* coli were transformed with plasmid expressing 1-211 His-TIRR or 6-211 His-TIRR. Six colonies were picked and 10ml of 2XYT with 100µg/ml ampicillin was inoculated overnight with shaking at 180rpm at 37 ºC. The following day, the overnight culture was added to 2L of XYT with 100µg/ml ampicillin and grown with shaking at 37ºC until the OD reached 0.6. After reaching OD 0.6, the culture was cooled at RT for 30 minutes, and then 0.5mM Isopropyl β- d-1-thiogalactopyranoside (IPTG) was added. Cultures were incubated overnight

at 18ºC. The following day, cultures were centrifuged at 4000g for 10 minutes at 4ºC. Bacterial pellets were lysed in 1.5X pellet volume bacterial lysis buffer (NiNTA Buffer A) with DNase I and lysozyme. Bacteria were homogenised and then centrifuged at 35,000g for 45 minutes at 4ºC to separate the soluble and insoluble fractions. The supernatant was incubated with 4ml of Ni-NTA resin for 1.5 hours on a wheel at 4ºC. The Ni-NTA beads were washed with Ni-NTA high salt buffer, and then 4ml fractions were eluted using Ni-NTA high imidazole buffer. Selected fractions were pooled and dialysed overnight in SEC buffer. Dialysed samples were then concentrated using a 10kDa MWCO vivaspin and ran on a Superose 6 10/300 GL (Cytiva) SEC column. This purification process with 1-211 and 6-211 His-TIRR is shown in **Figure 2.3**.

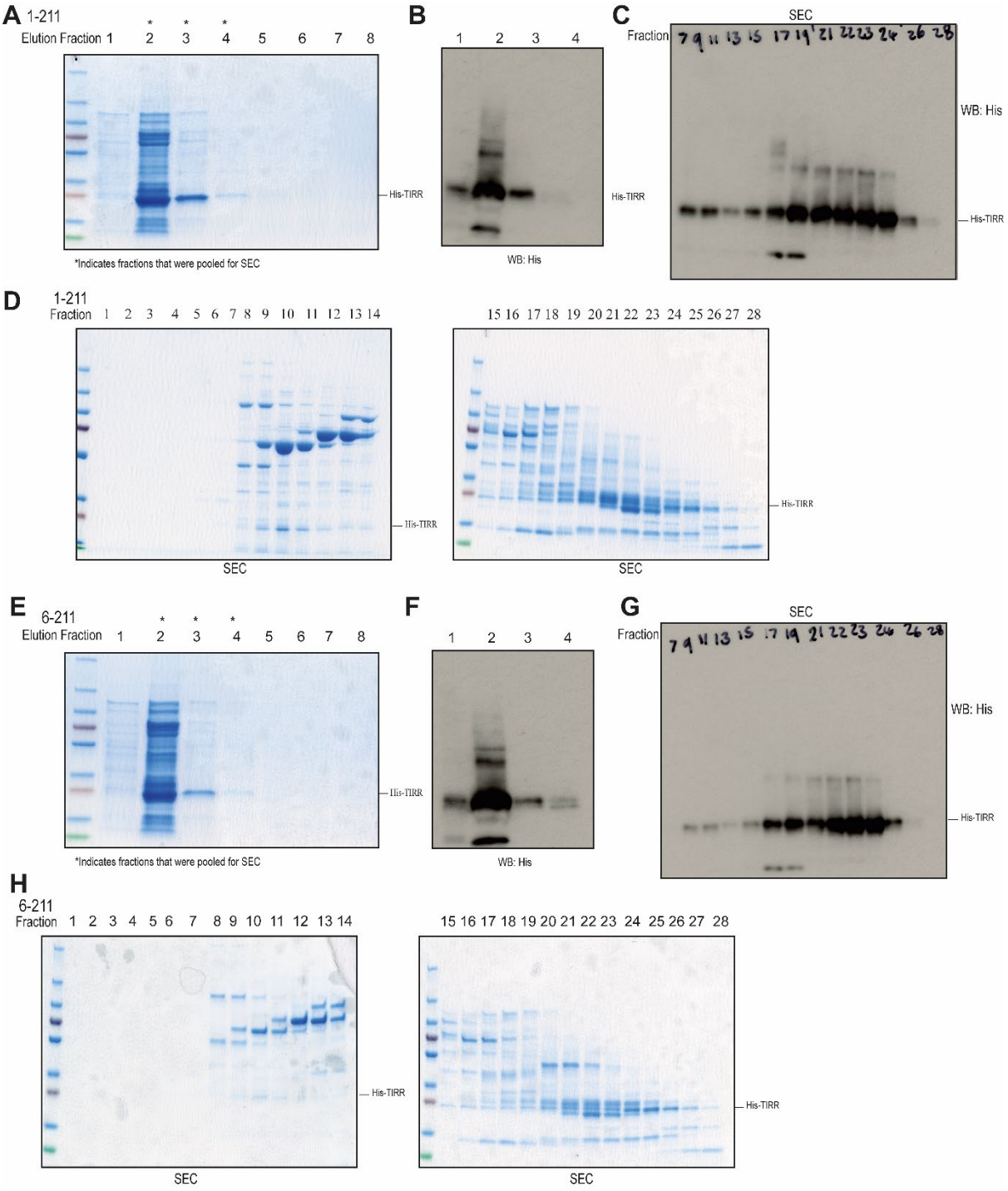


Figure 2.3: *Unsuccessful purification of 1-211 His-tagged TIRR.* ***A)*** *His-TIRR was captured on Ni-NTA resin and fractions eluted. Fractions were visualised using Coomassie Blue or* ***B)*** *western blot for His. Fractions which were pooled for size exclusion are highlighted with an asterisk.* ***C)*** *Western blot of fractions after size exclusion and* ***D)*** *Coomassie blue of SEC fractions. Fractions had high levels of contaminants.* ***E)*** *Purification was also attempted using 6-211 TIRR. Coomassie of Ni-NTA elution fractions and* ***F)*** *western blot with His antibody was performed.* ***G)*** *Pooled fractions from Ni-NTA were then subjected to size exclusion, and the fractions visualised by western blot and* ***H)*** *Coomassie blue. Similarly to 1-211, 6-211 TIRR yielded impure fractions.*

2.2.42 Protein purification 1-211 His-TIRR (final)

This final purification was done with the help of Dr Esra Balıkçı in the lab of Dr Kilian Huber at the Target Discovery Institute in Oxford using the following method. Rosetta™(DE3) *E.* coli cells from a glycerol stock were grown in TB supplemented with 8g/L glycerol, 100µg/ml kanamycin and 34µg/ml chloramphenicol at 37 ºC overnight. The overnight culture was used to inoculate three 2L bottles, each containing 1L TB supplemented with 8g/L glycerol, 50µg/ml kanamycin and approximately 200µl 204 Antifoam A6426 (Sigma). The culture was at 37 ºC until the OD600 reached ~1.0. The culture was down-tempered to 18ºC over a period of 1 hour before target expression was induced by addition of 0.5mM IPTG. Expression was allowed to continue overnight and cells were harvested the following morning by centrifugation (4,430g, 10 min, 4 ºC). The resulting cell pellet was stored at -80 ºC.

Cells were resuspended in IMAC wash1 buffer (50mM HEPES pH 7.6, 500mM NaCl, 0.5mM TCEP), supplemented with 6000 U Benzonase (Merck) and three tablets of Complete EDTA-free protease inhibitor (Roche) and lysed by sonication. The cell suspension HisTrap 5ml column was equilibrated with IMAC wash1 buffer, and the size exclusion column (HiLoad 16/60 Superdex 75 Prep Grade (GE Healthcare)) was equilibrated with GF buffer (20mM HEPES pH 7.6, 500mM NaCl, 0.5mM TCEP). Purification of the protein was performed on an AKTA prime system (GE Healthcare). The filtered lysate was loaded onto the HisTrap column and washed with IMAC wash1 buffer. Bound protein was eluted from the IMAC column with a gradient increase in the imidazole concentration. The eluted protein was injected into a size exclusion column and fractions containing the target protein were identified by SDS-PAGE. Fresh TCEP was added to a final concentration of 2mM. The protein was concentrated using a Vivaspin 20 centrifugal filter device (10,000 MWCO; Vivascience) and the identity of the

protein was confirmed by mass spectrometry. The purification of His-TIRR using this method is shown in **Figure 2.4**.

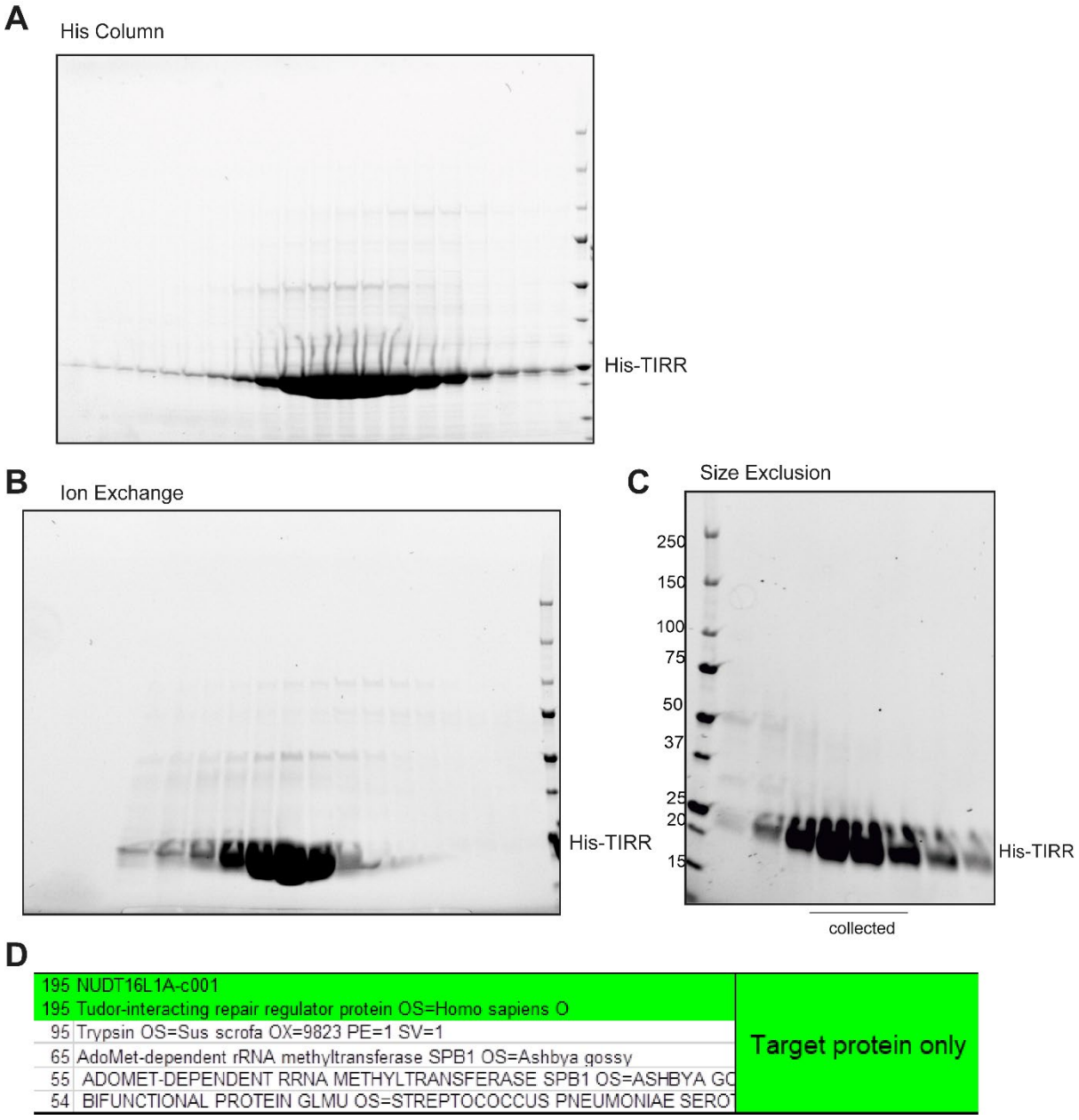


Figure 2.4: *Purification of His-tagged TIRR.* ***A)*** *His-TIRR was captured using a His Column.* ***B)*** *Ion exchange was performed on collected fractions from A.* ***C)*** *Size exclusion was performed on fractions collected from ion exchange.* ***D)*** *Mass spectrometry on collected fractions confirming only TIRR is present in the purified protein sample. Protein purification performed with the help of Dr Esra Balıkçı.*

2.2.43 HADDOCK modelling

Modelling was performed using the online software HADDOCK (High Ambiguity Driven protein-protein DOCKing) (https://wenmr.science.uu.nl/haddock2.4/), which allows us to dock/model two (or more) molecules of interest by setting 'active' residues at the interaction interface which has been previously determined using experimental data, such as NMR or crosslinking data. For modelling of TIRR with RNA, active residues on TIRR (PDB: 6D0L[7]) were set by comparison with NUDT16 bound to IMP (PDB: 3COU[8]). In PyMol[9], residues on NUDT16 within 5Å of IMP were selected as active residues and confirmed by modelling of NUDT16 and IMP in HADDOCK2.4[10] with these residues. NUDT16 and TIRR were overlaid in PyMol and the corresponding residues on NUDT16 were selected on TIRR. Residues on TIRR which did not align well with active residues on NUDT16 were excluded. HADDOCK2.4 was run for TIRR-RNA modelling, the protein-RNA method was run with 'Easy' mode default settings. The top three clusters with the lowest HADDOCK score were inspected manually in PyMol and the first model was chosen. During the inspection of the model, we increased the interaction between the monomer protein and the RNA by reducing the distance between the target residues. We then used this model as the starting structure for MD simulations of the monomer in complex with the RNA. The RNA structures were generated using RNAfold[11] and RNAComposer[12]. For the HADDOCK model of the hairpin RNA and TIRR, the following active residues were set in HADDOCK2.4; using 6D0L chain A for TIRR (27, 29, 55, 56, 57, 61, 62, 110, 166, 168, 169, 172) and RNA hairpin (active (in loop): 21, 22, 23, 24, 25, 26).

2.2.44 Molecular Dynamics Simulations

Molecular Dynamics Simulations were performed by Dr Federica Battistini as part of our collaboration according to the following protocol. The system of the hairpin RNA bound to the TIRR dimer was built using the TIRR structure (PDB:6D0L). The information on the positions

of the missing residues of the TIRR protein in the 6D0L structure were taken from the PDB structure 6CO1, and placed by overlapping the two structures using PyMol. Both systems, RNA-TIRR monomer and RNA-TIRR dimer, were placed at the centre of a truncated octahedral box of TIP3P[13] water molecules leaving 1.5nm between the protein-RNA atoms and the edges of the box, neutralised by K+ ions, and additional ions (K+ and Cl)[14] added to reach a concentration of 150mM. Each system was minimised using a multi-step procedure[15,16], thermalised to 298K (in the NVT ensemble), and then equilibrated and simulated without restraints collecting 500ns for each simulation as previously described[15,16] in the NPT ensemble (pressure=1atm, integration step=2fs), using Particle-Mesh Ewald corrections[17] and periodic boundary conditions. SHAKE was used to constrain bonds involving hydrogen[18]. We used the revised force field parmbsc0-OL3 for the RNA[19,20] and the amber14sb force field for the protein. Each simulation was extended for at least 500ns of production time using AMBER 20[21], followed by analysis with the CPPTRAJ[22] and BIGNASIM[23] suite of programs for the base-pair parameters. The systems were visualised with VMD v1.9.4[24]. The simulations are stored and available in the database BIGNASIM[23]. The electrostatic interactions between the protein residues and the RNA were determined by solving the linear Poisson–Boltzmann equation, while the van der Waals contribution was determined using standard AMBER Lennard–Jones parameters (cMIP[25]).

2.2.45 Data and Statistical Analysis

Bioinformatics Analysis

Bioinformatics analysis on RNA-Seq, RIP-Seq, and GO analysis of WCL Mass Spectrometry datasets was performed by Dr Irina Chelysheva, according to the following method. The sequencing data was aligned against the whole human (*Homo sapiens*) genome build GRCh38 (https://ccb.jhu.edu/software/hisat2/index.shtml), using STAR (version 2.7.3a). Gene features

were counted using HTSeq (version 0.11.1), using human gene annotation general transfer format version GRCh38.92 (www.ensembl.org). Genes with low counts across most libraries were removed. Ribosomal RNA (rRNA), sex chromosome genes, mitochondrial RNA and haemoglobin genes were excluded from downstream analysis. Differential gene expression was conducted using the R Bioconductor packages "edgeR" and "limma"[26–30]. RNA-sequencing data were then normalised for RNA composition using the trimmed mean of M-value (TMM) method[29]. Data were transformed using the limma "voom" function. A linear model was fitted to the data using the limma "lmFit" function using the empirical Bayes method[27]. The cut-off for statistical significance was set at false-discovery rate (FDR) <0.05. PCA analysis and heat maps were performed using the R Bioconductor package "pcaExplorer"[31] on the log transformed data; confidence interval level of 0.95 has been used. GO-terms enrichment analysis and characterisation of the gene lists compared to the whole genome were performed in ShinyGO (version 0.76)[32] using GO Biological process and GO Molecular function databases, where specified. The cut-off for statistical significance was set at false-discovery rate (FDR) <0.05, up to 20 top pathways were shown with redundant pathways removed.

Mass Spectrometry Analysis

Mass Spectrometry analysis on WCL Mass Spectrometry, TurboID, and GFP pull-down datasets was performed by Dr Marjorie Fournier, according to the following method. Tandem mass (MS/MS) spectra were searched using Sequest HT in Proteome discoverer software version 1.4 as follows: MS/MS data from whole cell lysate samples were searched against a protein sequence database containing 20,405 protein entries, including 20,122 Homo sapiens proteins (Uniprot release from 2020-04-14) and 283 common contaminants. MS/MS data from Turbo-TIRR and GFP-TIRR pulldown samples were searched against a protein sequence

database containing 20,549 protein entries, including 20,266 Homo sapiens proteins (Uniprot release from 2022-01-24) in which TIRR protein sequence (Q9BRJ7) was replaced by either V5-Turbo or GFP tagged TIRR protein sequence, and 283 common contaminants. During database searching cysteines (C) were considered to be fully carbamidomethylated (+57,0215, statically added), methionine (M) to be fully oxidised (+15,9949, dynamically added), all N-terminal residues to be acetylated (+42,0106, dynamically added). Two missed cleavages were permitted. Peptide mass tolerance was set at 50ppm on the precursor and 0.6 Da on the fragment ions. Data was filtered at FDR below 1% at PSM level. Label free quantification was performed by Normalised Spectral Abundance (NSAF) as previously described[33], as the number of spectral counts (PSM) that identify a protein, divided by the protein length (L), the PSM/L value represents the SAF, which is then divided by the sum of PSM/L for all proteins in the experiment. NSAF values were calculated after common contaminants were removed. For better visualisation of the data, NSAF values were multiplied by 100 (NSAF·100). The statistical analysis was performed on NSAF values using t-test in Perseus[34] and scatter plots were generated in GraphPad Prism 9.2.0. Proteins with a minimum fold-change of two between each condition and a p-value cut-off of 0.05 are highlighted on the plots.

Cell Profiler

PLA foci quantification was performed using Cell Profiler[5], using the speckle counter pipeline. The output generated, PLA foci ('children') per nucleus ('parent') was plotted to generate Foci per nucleus.

ColonyArea

The ImageJ plugin ColonyArea was used to quantify colony formation in colony formation assays[35].

GraphPad Prism

Data were plotted and visualised, and statistical tests performed using GraphPad Prism 9.

STRING analysis

STRING analysis of mass spectrometry datasets was performed using the online tool https://string-db.org/. STRING generates a network based on input proteins 'nodes' and connects the network using 'edges'. Edges can comprise experimentally determined and known interactions from databases, and predicted interactions based on different parameters such as text-mining and co-expression. Further information on how STRING builds a network and determines edges can be found at https://string-db.org/cgi/help?sessionId=bVjxAGwxSv7W.

Statistical Tests

Statistical analysis was performed using GraphPad Prism 9. The Kolmogorov-Smirnov normality test was performed to test for a normal distribution. If data met the requirements of a normal distribution, an unpaired t test was performed. If data did not show a normal distribution, for a comparison of two groups, a Mann-Whitney test was performed. For comparison of more than two groups, a Kruskal-Wallis with Dunn's multiple comparisons test was performed.

2.3 References

1. Chen, L. *et al.* R-ChIP Using Inactive RNase H Reveals Dynamic Coupling of R-loops with Transcriptional Pausing at Gene Promoters. *Mol. Cell* **68**, 745-757.e5 (2017).
2. Richardson, C., Moynahan, M. E. & Jasin, M. Double-strand break repair by interchromosomal recombination: suppression of chromosomal translocations. *Genes Dev.* **12**, 3831–3842 (1998).
3. Aranda, P. S., Lajoie, D. M. & Jorcyk, C. L. Bleach gel: A simple agarose gel for analyzing RNA quality. *Electrophoresis* **33**, (2012).
4. Alagia, A., Ketley, R. F. & Gullerova, M. Proximity Ligation Assay for Detection of R-Loop Complexes upon DNA Damage. in *R-Loops* (eds. Aguilera, A. & Ruzov, A.) vol. 2528 289–303 (Springer US, 2022).
5. Carpenter, A. E. *et al.* CellProfiler: image analysis software for identifying and quantifying cell phenotypes. *Genome Biol.* **7**, R100 (2006).
6. Cho, K. F. *et al.* Proximity labeling in mammalian cells with TurboID and split-TurboID. *Nat. Protoc.* **15**, 3971–3999 (2020).
7. Botuyan, M. V. *et al.* Mechanism of 53BP1 activity regulation by RNA-binding TIRR and a designer protein. *Nat. Struct. Mol. Biol.* **25**, 591–600 (2018).
8. RCSB PDB - 3COU: Crystal structure of human Nudix motif 16 (NUDT16). https://www.rcsb.org/structure/3cou.
9. Schrodinger LLC. The PyMOL Molecular Graphics System, Version 2.5. (2021).
10. van Zundert, G. C. P. & Bonvin, A. M. J. J. Modeling protein–protein complexes using the HADDOCK webserver "modeling protein complexes with HADDOCK". *Methods Mol. Biol.* **1137**, (2014).
11. Lorenz, R. *et al.* ViennaRNA Package 2.0. *Algorithms Mol. Biol.* **6**, (2011).
12. Biesiada, M., Pachulska-Wieczorek, K., Adamiak, R. W. & Purzycka, K. J. RNAComposer and RNA 3D structure prediction for nanotechnology. *Methods* **103**, (2016).
13. Jorgensen, W. L., Chandrasekhar, J., Madura, J. D., Impey, R. W. & Klein, M. L. Comparison of simple potential functions for simulating liquid water. *J. Chem. Phys.* **79**, 926–935 (1983).
14. Smith, D. E. & Dang, L. X. Computer simulations of NaCl association in polarizable water. *J. Chem. Phys.* **100**, 3757–3766 (1994).
15. Pasi, M. *et al.* μABC: a systematic microsecond molecular dynamics study of tetranucleotide sequence effects in B-DNA. *Nucleic Acids Res.* **42**, 12272–12283 (2014).
16. Ivani, I. *et al.* Parmbsc1: a refined force field for DNA simulations. *Nat. Methods* **13**, 55–58 (2016).
17. Darden, T., York, D. & Pedersen, L. Particle mesh Ewald: An $N \cdot \log(N)$ method for Ewald sums in large systems. *J. Chem. Phys.* **98**, 10089–10092 (1993).
18. Ryckaert, J.-P., Ciccotti, G. & Berendsen, H. J. C. Numerical integration of the cartesian equations of motion of a system with constraints: molecular dynamics of n-alkanes. *J. Comput. Phys.* **23**, 327–341 (1977).
19. Pérez, A. *et al.* Refinement of the AMBER Force Field for Nucleic Acids: Improving the Description of α/γ Conformers. *Biophys. J.* **92**, 3817–3829 (2007).
20. Zgarbová, M. *et al.* Refinement of the Cornell et al. Nucleic Acids Force Field Based on Reference Quantum Chemical Calculations of Glycosidic Torsion Profiles. *J. Chem. Theory Comput.* **7**, 2886–2902 (2011).
21. Case, D. A. *et al.* Amber 2021. (2021) doi:10.13140/RG.2.2.15902.66881.
22. Roe, D. R. & Cheatham, T. E. PTRAJ and CPPTRAJ: Software for Processing and Analysis of Molecular Dynamics Trajectory Data. *J. Chem. Theory Comput.* **9**, 3084–3095 (2013).
23. Hospital, A. *et al.* BIGNASim: a NoSQL database structure and analysis portal for nucleic acids simulation data. *Nucleic Acids Res.* **44**, D272–D278 (2016).
24. Humphrey, W., Dalke, A. & Schulten, K. VMD: Visual molecular dynamics. *J. Mol. Graph.* **14**, 33–38 (1996).
25. Gelpí, J. L. *et al.* Classical molecular interaction potentials: Improved setup procedure in molecular dynamics simulations of proteins: CMIP in the Setup of MD Simulations. *Proteins Struct. Funct. Bioinforma.* **45**, 428–437 (2001).
26. McCarthy, D. J., Chen, Y. & Smyth, G. K. Differential expression analysis of multifactor RNA-Seq experiments with respect to biological variation. *Nucleic Acids Res.* **40**, 4288–4297 (2012).
27. Ritchie, M. E. *et al.* limma powers differential expression analyses for RNA-sequencing and microarray studies. *Nucleic Acids Res.* **43**, e47–e47 (2015).
28. R Core Team. R: A Language and Environment for Statistical Computing. R Foundation for Statistical Computing, Vienna. (2013).
29. Robinson, M. D. & Oshlack, A. A scaling normalization method for differential expression analysis of RNA-seq data. *Genome Biol.* **11**, R25 (2010).
30. Robinson, M. D., McCarthy, D. J. & Smyth, G. K. edgeR: a Bioconductor package for differential expression analysis of digital gene expression data. *Bioinformatics* **26**, 139–140 (2010).
31. Marini, F. & Binder, H. pcaExplorer: an R/Bioconductor package for interacting with RNA-seq principal components. *BMC Bioinformatics* **20**, 331 (2019).

32. Ge, S. X., Jung, D. & Yao, R. ShinyGO: a graphical gene-set enrichment tool for animals and plants. *Bioinformatics* **36**, 2628–2629 (2020).
33. Florens, L. *et al.* Analyzing chromatin remodeling complexes using shotgun proteomics and normalized spectral abundance factors. *Methods San Diego Calif* **40**, 303–311 (2006).
34. Tyanova, S. *et al.* The Perseus computational platform for comprehensive analysis of (prote)omics data. *Nat. Methods* **13**, 731–740 (2016).
35. Guzmán, C., Bagga, M., Kaur, A., Westermarck, J. & Abankwa, D. ColonyArea: An ImageJ Plugin to Automatically Quantify Colony Formation in Clonogenic Assays. *PLoS ONE* **9**, e92444 (2014).

Chapter 3: The Role of RNA in the separation of TIRR and 53BP1 after DNA Double Strand Breaks

3.1 Summary

TIRR is an RNA binding protein and a negative regulator of the DNA repair factor 53BP1. In non-damage conditions, TIRR is bound to the Tudor domain of 53BP1 in the nucleoplasm. After DNA damage, TIRR and 53BP1 dissociate and 53BP1 binds the chromatin at the DSB through the Tudor and UDR domains to promote NHEJ-mediated repair of the DSB. However, the exact mechanistic details of this dissociation in response to DSBs are not known. The RNA-binding region on TIRR overlaps with the 53BP1 binding site, and increasing evidence has implicated RNA as a crucial factor in the DDR. In this chapter, we investigate the potential of RNA to dissociate TIRR and 53BP1 after DSBs. We show that TIRR can bind RNA with specific secondary structures, including RNA hairpins, and this RNA can separate TIRR and 53BP1 *in vitro* and *in vivo*. We also show that RNAPII, but not RNAPIII, transcription is needed for TIRR and 53BP1 separation, as well as Dicer and Drosha. Furthermore, we show that the TIRR is recruited to DSBs as part of the complex with 53BP1, in a RNAPII transcription-dependent manner, suggesting that TIRR and 53BP1 dissociate in close proximity to the break itself, rather than distally in the nucleus. Additionally, by developing a new technique, FISH-PLA, we show that both TIRR and 53BP1 are in proximity to RNA transcribed at the break, suggesting that *de novo* RNAPII transcribed transcripts may play a role in TIRR/53BP1 dissociation. Finally, we show through modelling of TIRR bound to hairpin RNA, that RNA could disrupt the 53BP1 and TIRR interaction by binding to the same residues on TIRR as 53BP1. Our results uncover a previously unknown role of DSB derived RNA in modulating a protein-protein interaction, and further our understanding of 53BP1 regulation in DSB repair.

3.2 Introduction

It is well described that TIRR and 53BP1 separate after DSB induction, with TIRR regulating 53BP1 functions in DSB repair (**Section 1.4.1**)[1–4]. The regulation of TIRR/53BP1 separation has not been well characterised, although ATM phosphorylation of 53BP1 at the ST/Q sites and RIF1 have been implicated in this mechanism[2]. TIRR is also an RNA binding protein[5]. Mapping of RNA binding sites using RNA crosslinking followed by mass spectrometry (RBR-ID)[6], where a crosslinked site results in a change in mass which can be detected by mass spectrometry, defined the RNA binding site on TIRR as within the region 91-107 (LTEADYLSSHLTEGPHR)[6] (**Figure 3.1.A**). This RNA binding site overlaps directly with the 53BP1 Tudor binding site on TIRR, in particular the important 53BP1-binding loop composed of residues 101 to 107 on TIRR[1] (**Figure 3.1.B**).

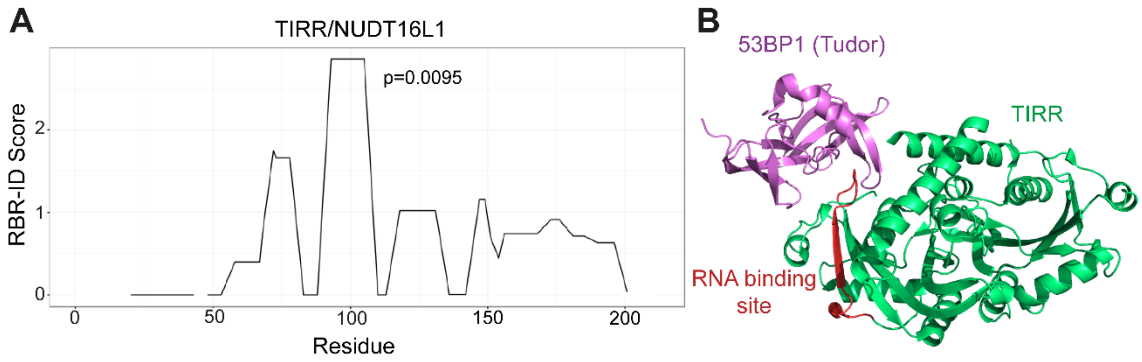


Figure 3.1: ***A)*** *The mapped RNA binding site as identified from RBR-ID[6]. The statistically significant RNA binding region is between residues 91-107 on TIRR. RBR = RNA-binding region.* ***B)*** *The crystal structure of the TIRR dimer bound to 53BP1 Tudor domain (PDB: 6CO1), with the identified RNA binding region on TIRR highlighted in red. Note the overlap between the site of 53BP1 binding and the mapped RNA binding site.*

Preliminary published data from Botuyan *et al*[1] showed that a ribonucleotide, IMP, can separate 53BP1 and NUDT16 modified with a TIRR binding loop *in vitro*, suggesting that RNA may be able to separate TIRR and 53BP1. We hypothesised that, given the known importance of

RNA in DNA damage repair, a new role for RNA in DSB repair may involve the separation of TIRR and 53BP1 after DSBs. We hypothesised that this RNA could originate either distally to the DSB site, such as a lncRNA which is upregulated after DSBs (**Section 1.5.2**), or from RNA which is *de novo* transcribed at DSBs (**Section 1.5.5**). In this Chapter, we characterise the separation of TIRR and 53BP1 after DSBs, including exploring the role of transcription, specific RNA structures, and the RNA-processing enzymes Dicer and Drosha (**Section 1.5.7**).

3.3 Results

3.3.1 TIRR and 53BP1 separate after damage

In order to study the TIRR/53BP1 interaction in cells, we perform the *in situ* Proximity Ligation Assay (PLA) technique for TIRR and 53BP1. PLA is a technique used to detect the proximity of two proteins within ~40nm of each other and visualise their location within the cell by observation of discrete fluorescent foci. The technique firstly uses specific antibodies from two different species recognising the proteins of interest. Subsequently, secondary antibodies with oligonucleotide conjugates, known as PLA probes, are then added. If these antibodies are in close proximity, i.e., the two proteins of interest are within ~40nm of one another, the connector oligonucleotides will be ligated together after the addition of a ligase. A DNA polymerase is added, and the ligated oligonucleotides can act as a primer for amplification, which can then be bound by complementary fluorescently labelled oligonucleotides[7]. The result is a distinct PLA signal which can be visualised by microscopy and quantified using various software such as Cell Profiler[8] (**Figure 3.2.A**). We performed PLA using antibodies against TIRR and 53BP1 in control WT Hela cells not exposed to any DNA damaging agents, or cells exposed to 10μM Etoposide for 2 hours, a Topoisomerase II poison which stabilises the TopoII-DNA cleavage complex, resulting in the formation of a DSB[9]. We observed PLA foci in the control cells not exposed to Etoposide, indicating that TIRR and 53BP1 are bound in non-damage conditions and we can detect this interaction using PLA (**Figure 3.2.B**). After exposure to Etoposide, we observe that these PLA foci are significantly reduced, indicating that TIRR and 53BP1 are no longer in close proximity to one another (**Figures 3.2.B and 3.2.C**). To further confirm the specificity of this technique, we use a Hela cell line with an integrated doxycycline inducible shRNA targeting TIRR, or an shGFP as a control. After performing PLA on cells treated with 1μg/ml Doxycycline for 48 hours, PLA foci were observed in shGFP cells, and the number of foci were reduced in shTIRR cells, as would be expected as less TIRR protein would result in

less TIRR/53BP1 interaction (**Figures 3.2.D and 3.2.E**). Therefore, we confirm that we can use the PLA method to study the TIRR/53BP1 interaction in DNA damage.

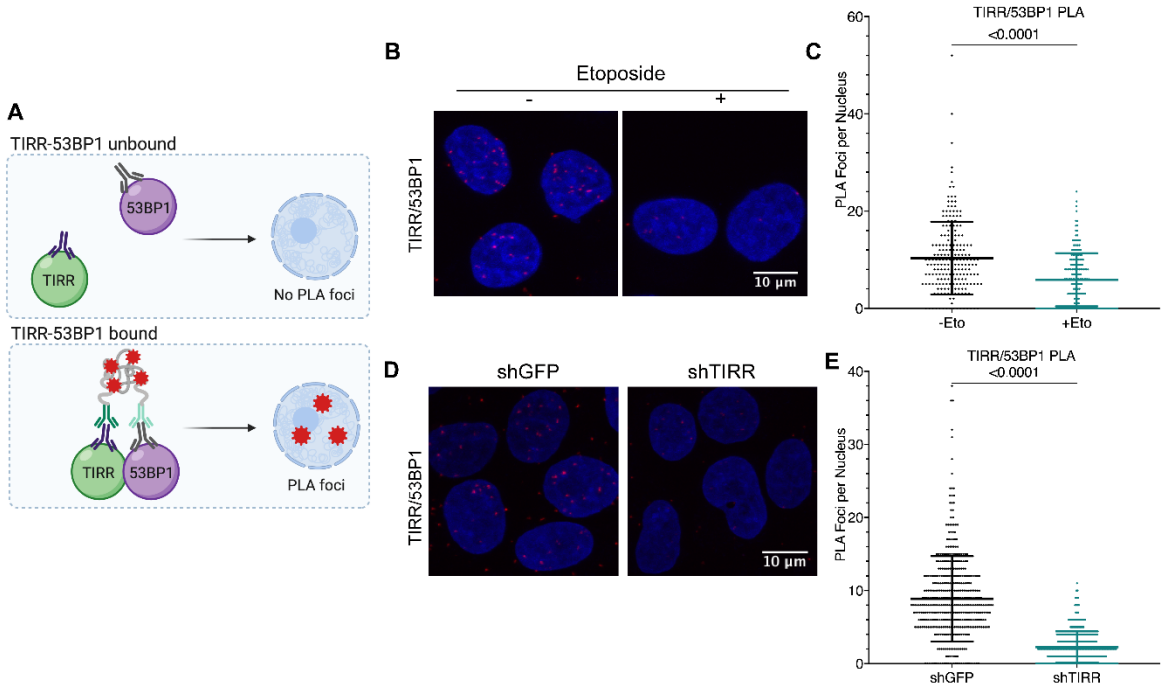


Figure 3.2: *The proximity ligation assay to study the TIRR/53BP1 complex.* ***A)*** *Depiction of TIRR and 53BP1 bound (resulting in PLA foci) and unbound (resulting in no PLA foci).* ***B)*** *PLA of TIRR and 53BP1 with Etoposide (10µM, 2 hours). n(-Eto)=206, n(+Eto)=191.* ***C)*** *Quantification of B (mean ± sd, n=2).* ***D)*** *PLA of TIRR and 53BP1 in shGFP and shTIRR inducible Flp-IN TRex Hela cells (n(shGFP)=453, n(shTIRR)=521).* ***E)*** *Quantification of D (mean ± sd, n=2).*

3.3.2 RNA Polymerase II transcription, but not RNA polymerase III, is required for TIRR and 53BP1 dissociation after damage

As RNAPII RNA transcripts are known to play a key role in DSB repair[10–14], we asked whether transcription and RNA transcripts could play a role in TIRR/53BP1 dissociation. We performed the PLA assay in the presence of an RNAPII inhibitor, α-Amanitin (2µg/ml, 6 or 24 hours)[10], which binds to the RNAPII catalytic site and prevents RNA transcription[15]. We observed that TIRR/53BP1 dissociation is impaired when RNAPII transcription is inhibited prior to the induction of DSBs by Etoposide (10µM, 2 hours) (**Figures 3.3.A and 3.3.B**) and by Ionising Radiation (IR, 10Gy, 1 hour) (**Figures 3.3.C and 3.3.D**), indicating that RNAPII transcription

inhibition prevents TIRR and 53BP1 dissociation in response to DSBs induced by Etoposide and IR. To further support this result, we also performed PLA in the presence of THZ1, an inhibitor of CDK7, which inhibits the phosphorylation of RNAPII C-terminal domain at serines 5 and 7, impairing RNAPII transcription[16]. After treatment with THZ1 (100nM, 2 hours), the interaction of TIRR and 53BP1 was not significantly reduced by Etoposide, in contrast to the DMSO treated condition, as indicated by the persistence of PLA foci after DNA damage induction in the presence of THZ1 (**Figures 3.3.E and 3.3.F**). Therefore, inhibition of RNAPII transcription by two different drugs, α-Amanitin and THZ1, prevented TIRR and 53BP1 dissociation after damage, implicating RNA transcription in the mechanism of TIRR and 53BP1 dissociation.

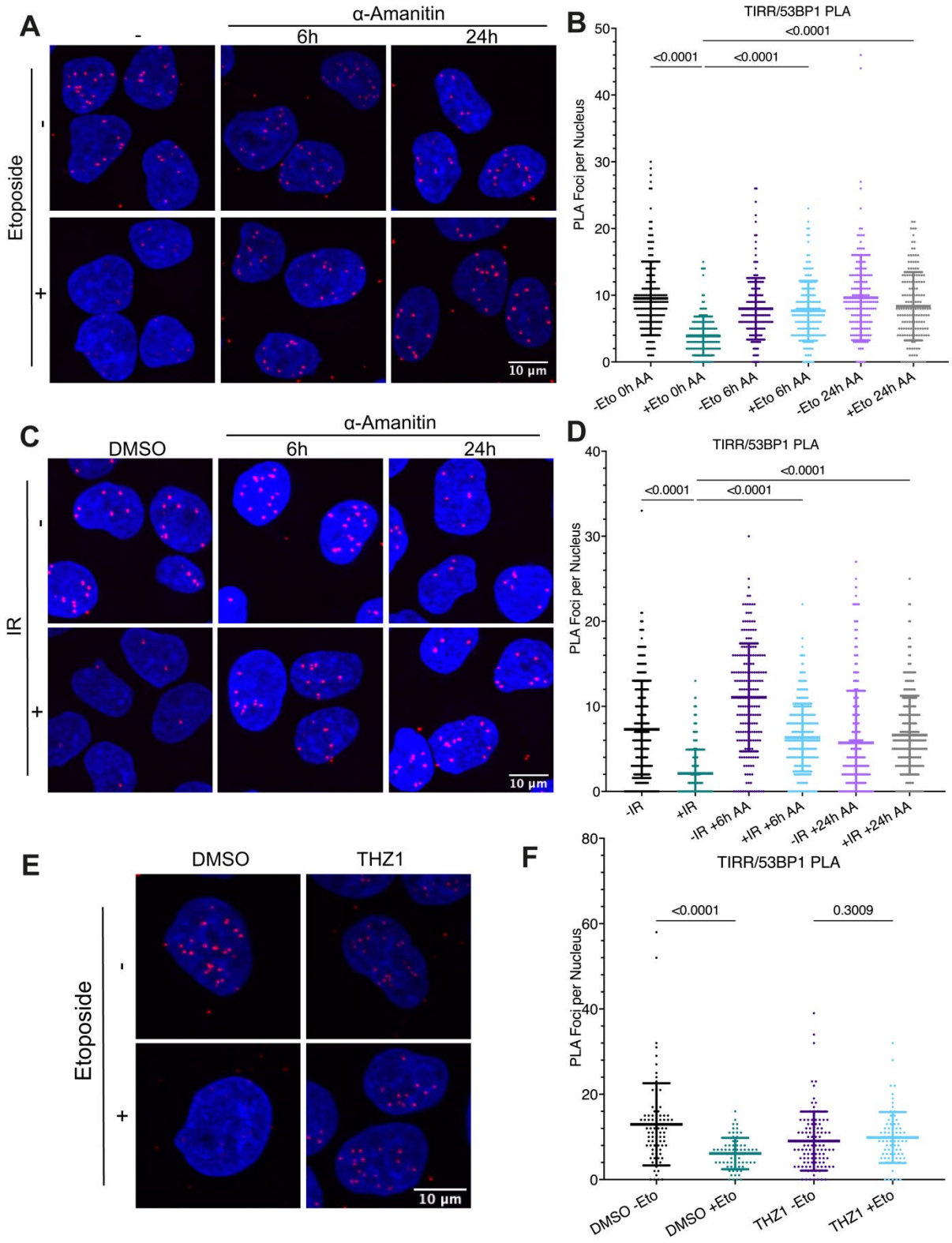


Figure 3.3: *RNA Polymerase II Transcription is required for TIRR/53BP1 dissociation.* ***A)*** *PLA of TIRR and 53BP1 with and without etoposide (10μM, 2 hours) in the presence of α-amanitin (2μg/ml, 6 or 24 hours). n(0h -Eto)=187, n(0h +Eto)=158, n(6h -Eto)=166, n(6h +Eto)=173, n(24h -Eto)=158, n(24h +Eto)=155.* ***B)*** *Quantification of A. (mean ± sd, n=2).* ***C)*** *PLA of TIRR and 53BP1 with and without IR (10Gy, 1 hour) in the presence of α-amanitin (2μg/ml, 6 or 24 hours). n(0h -IR)=350, n(0h +IR)=528, n(6h -IR)=196, n(6h +IR)=359, n(24h*

-IR)=417, n(24h +IR)=317. ***D)*** *Quantification of C (mean ± sd, n=2).* ***E)*** *PLA of TIRR and 53BP1 in the presence of THZ1 (100nM, 2 hours) with and without etoposide. n(DMSO -Eto)=84, n(DMSO +Eto)=67, n(THZ1 -Eto)=107, n(THZ1 +Eto)=76.* ***F)*** *Quantification of E. (mean ± sd, n=1).*

Although RNAPII is widely implicated in transcription at DNA break sites, RNAPIII has also been suggested to transcribe RNA at DSBs[17]. Therefore, to assess the contribution of RNAPIII transcription, we also performed PLA in the presence of an RNAPIII inhibitor (ML-60218, 30μM for 24 hours)[18]. Exposure to IR after treatment with ML-60218 did not result in impaired reduction of the number of PLA foci observed, and a significant decrease in the number of foci, even after ML-60218 treatment, was still seen. This suggests that inhibition of RNAPIII transcription did not have a measurable impact on TIRR/53BP1 dissociation after IR (**Figures 3.4.A and 3.4.B**). Collectively, this data suggests that TIRR/53BP1 dissociation after DNA damage is dependent on RNAPII, but not RNAPIII, transcription.

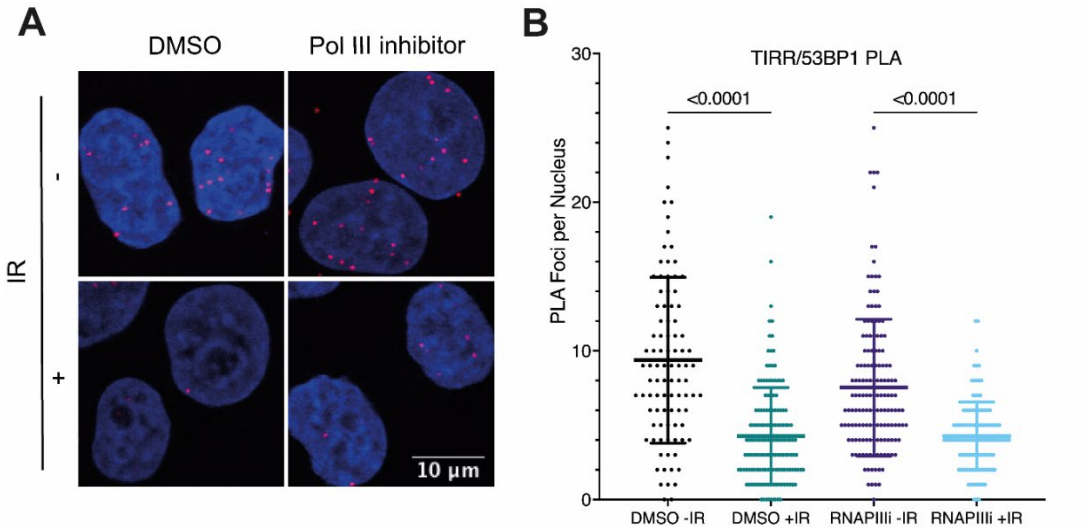
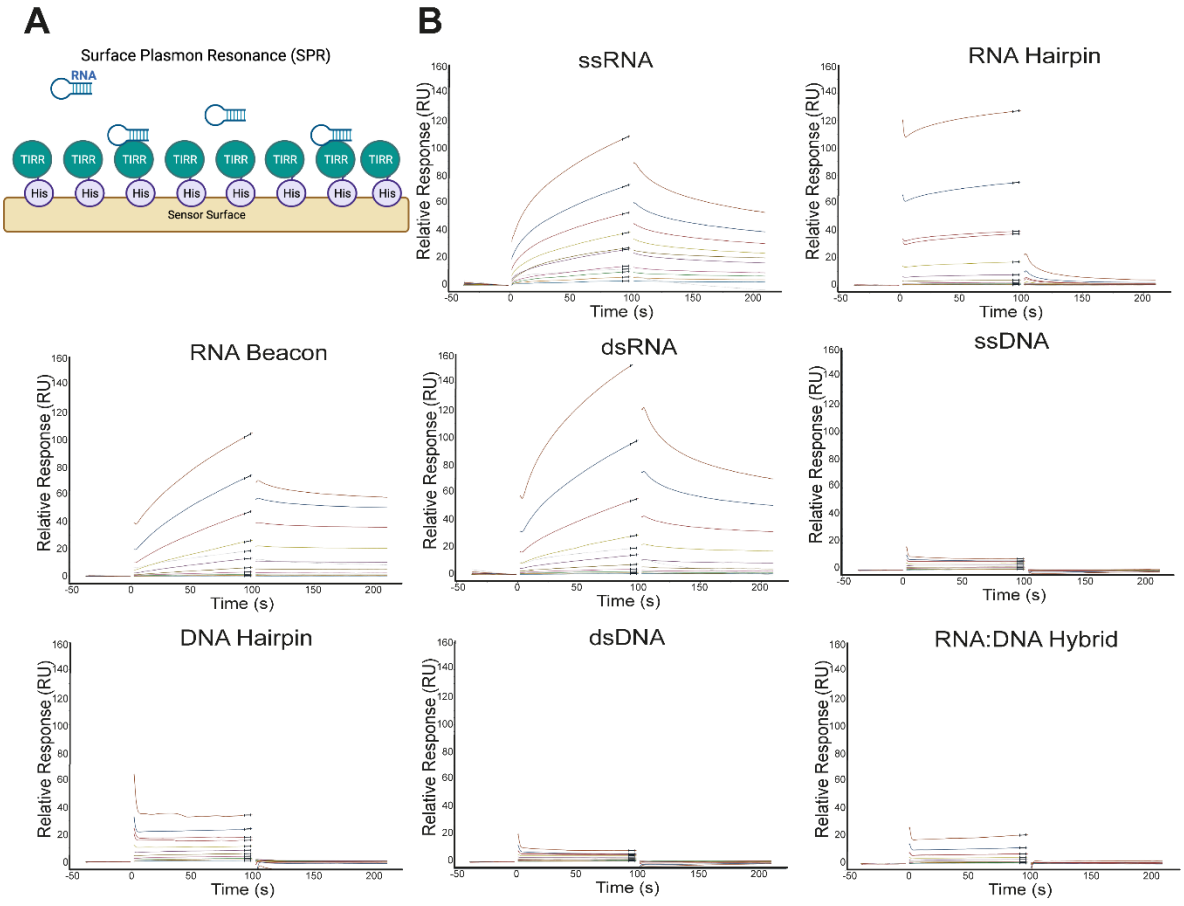


Figure 3.4: ***A)*** *PLA of TIRR and 53BP1 with and without IR (10Gy, 1 hour) in the presence of a RNAPIII inhibitor (30μM for 24 hours). n(DMSO -IR)=94, n(DMSO +IR)=148, n(RNAPIIIi -IR)=149, n(RNAPIIIi +IR)=117.* ***B)*** *Quantification of A (mean ± sd, n=2).*

3.3.3 TIRR binds preferentially to single strand and hairpin RNA

RNA can exert its functions in cells in a variety of ways, including by having a specific sequence or a specific secondary structure. RNAs of different secondary structures have been shown to play important roles in DNA DSB repair, including RNA:DNA hybrid structures and short double-stranded RNAs (dsRNA)[10,12]. Whilst TIRR is a known RNA binding protein[5], the RNA binding preferences of TIRR are mostly unknown. Therefore, we decided to test if TIRR exhibited a binding preference for RNA substrates with different secondary structures. We designed RNA substrates with a single strand structure (20nt in length, 50% GC content), a double stranded structure (20nt, the same sequence as the single strand with an annealed antisense RNA strand), an RNA:DNA hybrid (20nt, the same sequence as the single strand with an annealed antisense DNA strand), and two different RNA hairpin structures. The first hairpin structure, referred to as RNA Hairpin, is 46nt in length with a 6nt loop and a stem with the same sequence as the dsRNA; and the second, referred to as RNA Beacon, is shorter at 25nt in length and has a larger 15nt loop, but does not contain any of the sequence from the ssRNA structure. As controls, a ssDNA structure, a dsDNA structure, and a DNA Hairpin with the same sequences as their RNA counterparts were also utilised (**Methods 2.1.7**). As part of our collaboration, Dr Clémence Mondielli and Florence Iehl at the Biophysics Group, Evotec (France), performed Surface Plasmon Resonance (SPR) to assess binding of TIRR to the nucleic acid substrates. SPR is an optical technique which comprises a sensor surface in a flow cell. A ligand of interest (in this case TIRR) is immobilised on the sensor surface and analytes (our RNA and DNA substrates) are flowed over the ligand. SPR measures the refractive index of the sensor surface which changes as the analyte is flowed over the ligand and binding occurs. This is measured as response units (RU) and can be determined at different analyte concentrations to calculate a binding affinity (Kd) of the interaction between the ligand and analyte (**Figure 3.5.A**)[19].

In the SPR experiment, we observed that TIRR can bind to ssRNA and RNA hairpins with a comparable approximate affinity (Kd) of around 100μM, and to a lesser extent dsRNA with a lower approximate affinity (200μM). We did not observe any binding to RNA:DNA hybrids or any of the DNA substrates tested (**Figures 3.5.B and 3.5.C**). It is important to note that a limitation of this experimental set-up is that in our SPR experiment, the binding did not reach steady-state (the curve did not flatten) during the time period over which the SPR was conducted, so the affinity calculated (Kd) using steady-state equation fitting is an estimate. As a steady-state/saturation (Rmax) was not reached, the Kd calculated using the steady-state calculation (Response Units vs Concentration) will not be an exact estimation of the binding affinity, but instead an overestimate. The actual binding affinity is therefore likely a lower (stronger) affinity than that calculated here[20].



C

Oligonucleotide	Binding to TIRR?	Approximate Kd
ssRNA	Yes	>100μM
RNA Hairpin	Yes	>100μM
RNA Beacon	Yes	>100μM
dsRNA	Yes	>200μM
ssDNA	No	-
DNA Hairpin	No	-
dsDNA	No	-
RNA:DNA Hybrid	No	-

Figure 3.5: ***A)*** *Principles of the Surface Plasmon Resonance (SPR) assay. His-TIRR is immobilised on a sensor surface and increasing concentrations of RNA and DNA substrates are added and binding is measured.* ***B)*** *SPR with His-TIRR and (left → right) ssRNA, RNA Hairpin, RNA Beacon, dsRNA, ssDNA, DNA Hairpin, dsDNA, RNA:DNA hybrid.* ***C)*** *Summary of B. Table showing the calculated binding constant (Kd) from the SPR data. SPR and analysis performed by Dr Clémence Mondielli and Florence Iehl at the Biophysics Group, Evotec (France).*

3.3.4 TIRR binds to single strand and hairpin RNA, but 53BP1 Tudor does not

To further support the observation that TIRR is able to bind ssRNA and hairpin RNA, we wanted to validate these results using another binding technique, Electrophoretic Mobility Shift

Assay (EMSA). The EMSA technique involves incubating a protein of interest with RNA or DNA substrates, followed by electrophoresis on a non-denaturing native gel, where the migration of the nucleic acid is observed. RNA/DNA which is bound by the protein will have impaired migration through the gel, and therefore bound and free nucleic acid will separate into distinct bands (**Figure 3.6.A**). Radiolabelling of the RNA/DNA allows visualisation of bound and free nucleic acid. To perform EMSAs, we purified recombinant TIRR with the help of Dr Esra Balıkçı at the Target Discovery Institute, Oxford (**Section 2.2.42**) (purified recombinant protein is often used in EMSAs to ensure a good level of purity and homogeneity of the sample). In this assay we use increasing concentrations of the TIRR protein (0-12μM) with a constant RNA/DNA concentration (10nM) to enable an approximation of the binding affinity of TIRR for the RNA. We also include a cold competitor control, which is the addition of 1000-fold excess of the RNA/DNA substrate which is not radiolabelled. If the band corresponding to TIRR-bound RNA is specific, the addition of the cold competitor should reduce the appearance of the bound band. Despite a significant portion of TIRR precipitating at the low salt concentrations needed to foster RNA-protein interactions in this assay (as evidenced by the presence of nonspecific signals in the well (**Figure 3.6**), due to TIRR propensity to precipitate in solution unless maintained at high salt concentrations (>300mM[1])), incubating increasing concentrations of TIRR protein with 5' radiolabelled ssRNA at 37°C for 15 minutes resulted in a band appearing that corresponds to bound RNA, which increased in intensity with increasing concentrations of TIRR. This band was also able to be out-competed with the addition of a cold competitor ssRNA, indicating that TIRR can specifically bind ssRNA in our EMSA experiments (**Figure 3.6.B**). Additionally, RNA was previously shown to be necessary for 53BP1 IR-induced foci (IRIF) formation via the Tudor domain and these foci were sensitive to RNase A treatment[21]. Therefore, we included recombinant 53BP1 Tudor domain (Cayman) in our EMSAs. We did not observe any binding of 53BP1 Tudor to ssRNA in our assay

(**Figures 3.6.C and 3.6.D**), and we conclude that TIRR but not 53BP1 can bind ssRNA. The approximate estimated affinity (Kd) of TIRR for ssRNA in our assay is ~100μM, although this estimate should be treated with caution as it is likely an underestimate of the affinity. The actual affinity of TIRR for RNA is likely stronger, as we know a portion of TIRR will precipitate in the assay, therefore would be unable to bind RNA. However, it is difficult to estimate what proportion of TIRR precipitated in the EMSA experiments, so this should be taken into account when considering the binding affinity. Nevertheless, there is agreement between the SPR and EMSA data that TIRR can bind ssRNA. We also performed the EMSA using the radiolabelled RNA hairpin (beacon) and, similarly to the ssRNA, observe that TIRR, but not 53BP1 Tudor, can bind the RNA hairpin as was observed in the SPR, and this can be outcompeted by cold competitor hairpin RNA (**Figures 3.6.E and 3.6.F**). Lastly, we performed EMSA with ssDNA with TIRR and 53BP1 Tudor as a negative control, as TIRR was not observed to bind to DNA in the SPR assay. In agreement, we did not detect any binding of TIRR to the ssDNA, nor did we observe any binding of 53BP1 Tudor to DNA **(Figures 3.6.G and 3.6.H**). When quantified, we saw that TIRR binds ssRNA and RNA hairpin structures with similar affinity, as observed in the SPR **(Figure 3.6.I**). Taken together with the SPR data, we conclude that TIRR, unlike 53BP1, binds ssRNA and RNA hairpin structures, but not DNA structures.

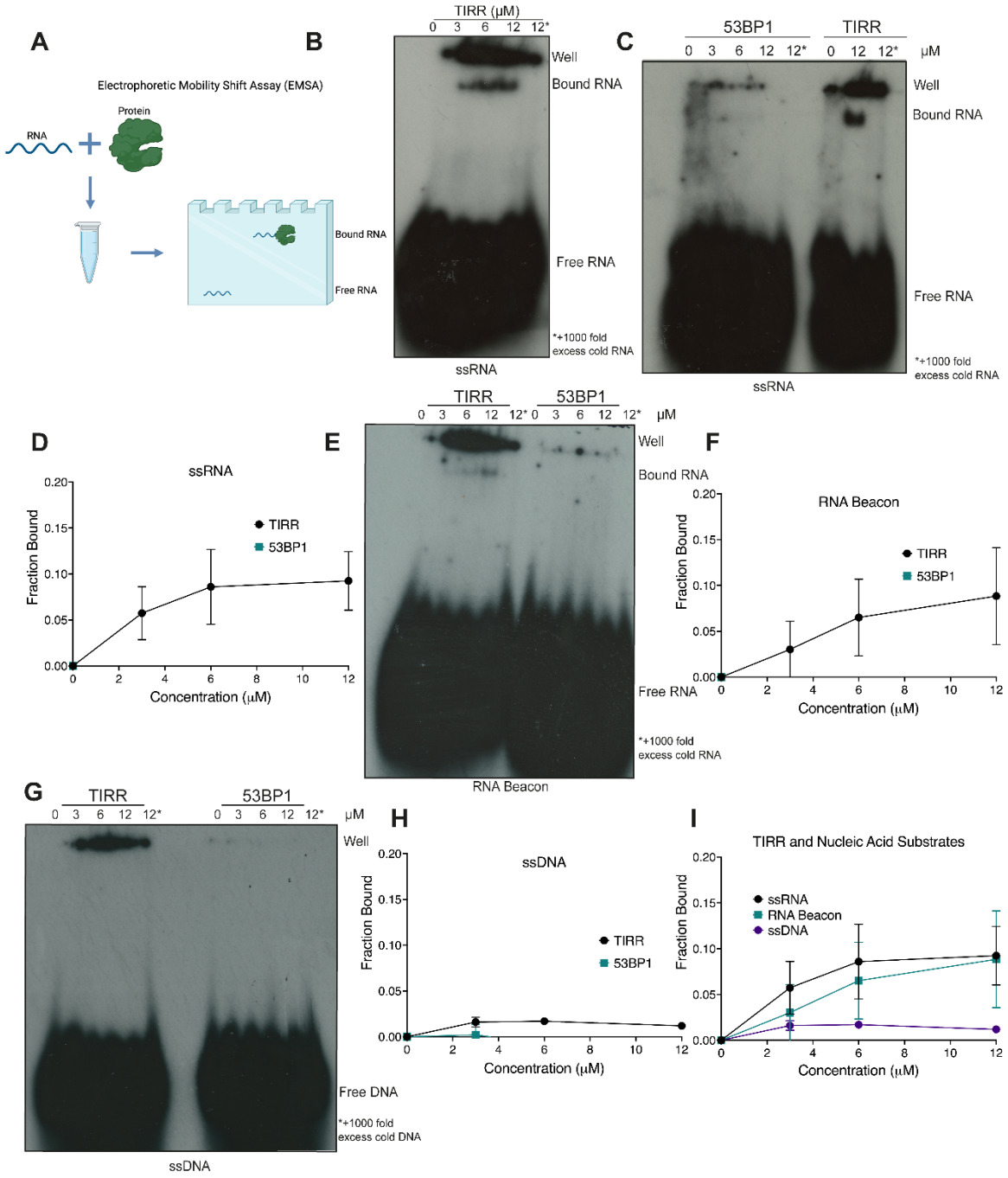


Figure 3.6: *A) Representation of the EMSA assay.* ***B)*** *EMSA with ssRNA with increasing concentration of TIRR* ***C)*** *EMSA with ssRNA with increasing concentration of 53BP1 Tudor domain. TIRR is used as a positive control for binding.* ***D)*** *Quantification of EMSAs showing comparison with ssRNA and increasing concentration of TIRR (as shown in B) (n=4) and 53BP1 Tudor (as shown in C) (n=3) (mean ± sd).* ***E)*** *EMSA with RNA beacon and increasing concentration of TIRR and 53BP1 Tudor.* ***F)*** *Quantification of EMSAs showing comparison with RNA Beacon and increasing concentration of TIRR (n=3) and 53BP1-tudor (n=3) (as shown in E) (mean ± sd).* ***G)*** *EMSA with ssDNA with increasing concentration of TIRR and 53BP1 Tudor.* ***H)*** *Quantification of EMSAs showing comparison with ssDNA and increasing concentration of TIRR (n=3) and 53BP1-tudor (n=2) (mean ± sd). (as shown in G).* ***I)*** *Quantification of EMSAs with TIRR with different nucleic acid substrates as shown in Figures B-H for comparison.*

3.3.5 RNA extracted from cells can separate the TIRR/53BP1 complex

Having observed that TIRR can bind specifically to RNA, and that transcription is important for TIRR and 53BP1 dissociation after DNA damage, we next asked the question if RNA itself is actually sufficient to disrupt TIRR and 53BP1 binding. To do this we developed an *in vitro* competition assay using purified Flag-TIRR (full length) and HA-53BP1 (Tudor domain). Briefly, the steps of the competition assay are as follows: Flag-TIRR and HA-53BP1-Tudor were pre-bound together by incubation for 1 hour at 4°C in TGEN150 buffer with Anti-FLAG M2 magnetic beads to capture the complex. Beads were then washed and incubated at room temperature for 1 hour with increasing amounts of RNA isolated from the nucleus of Hela cells (1 hour after irradiation at 10Gy). After washing, bound material from the Flag beads was eluted and binding visualised by running a western blot (**Figure 3.7.A**). By employing this assay, we observed that increasing amounts of RNA was able to reduce the binding of 53BP1 Tudor to TIRR (**Figures 3.7.B and 3.7.C**). This provides proof-of-principle that RNA is capable of dissociating TIRR and 53BP1.

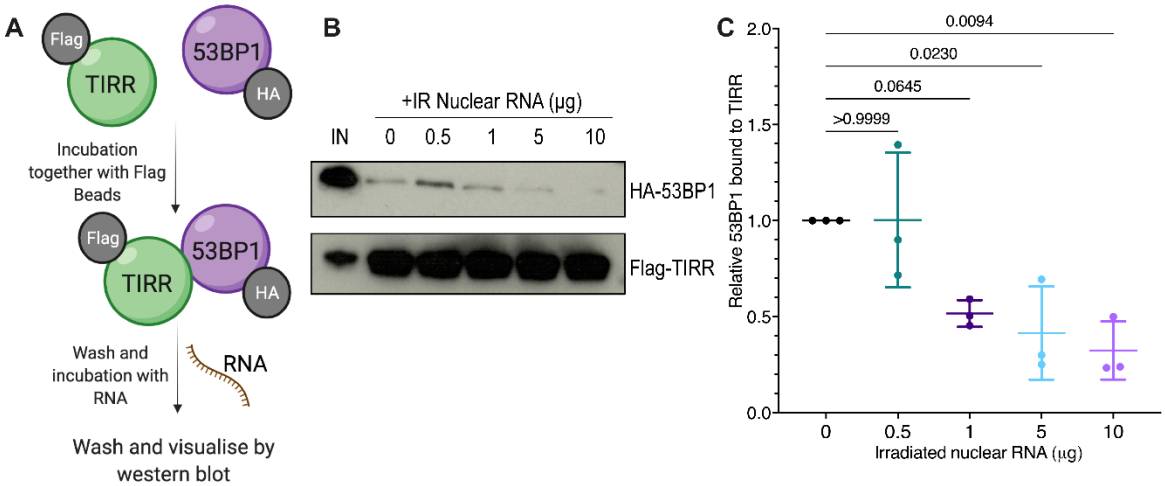


Figure 3.7: *RNA isolated from damaged cells promotes TIRR/53BP1 separation in vitro.* ***A)*** *Representation of the in vitro RNA competition assay. Flag-TIRR and HA-53BP1 are incubated together with Flag beads, after which nuclear irradiated RNA is added. The amount of 53BP1 bound to TIRR after RNA addition is visualised by western blotting.* ***B)*** *Western blot showing*

amount of HA-53BP1 bound to Flag-TIRR after Flag pull down in RNA competition experiments with increasing amounts of nuclear irradiated RNA. ***C)*** *Quantification of B (mean ± sd, n=3). Purified TIRR and 53BP1 Tudor protein used in this experiment was obtained from the Biophysics Group, Evotec (France), as part of our collaboration.*

3.3.6 Hairpin RNA can dissociate the TIRR and 53BP1 complex

Having provided proof-of-principle that RNA is capable of separating TIRR and 53BP1, and with the knowledge that TIRR has a binding preference for certain RNA structures, we wanted to narrow down what type of RNA is specific for TIRR/53BP1 dissociation. To do this, we employed the use of a more high-throughput fluorescence-based assay, Homogeneous Time Resolved Fluorescence assay (HTRF), which was performed by Dr Clémence Mondielli and Florence Iehl at the Biophysics Group, Evotec (France) as part of our collaboration. HTRF is similar to a Fluorescence Resonance Energy Transfer (FRET) assay, where the emission wavelength of a donor fluorophore can excite an acceptor fluorophore when within a certain distance, and the resulting FRET signal is then measured. Therefore, the FRET signal is a measurement of binding. HTRF uses a donor fluorophore with a longer emission time, which allows a time delay to be introduced before acceptor emission measurement, meaning background fluorescence (which is short-lived in nature) can be eliminated (**Figure 3.8.A**)[22]. Recombinant Flag-TIRR and HA-53BP1 Tudor were incubated together with donor and acceptor fluorophores recognising Flag (Donor, TB3+) and HA (Acceptor, XL665) and increasing concentrations of RNA substrates. In this assay, we used ssRNA, antisense ssRNA (ssRNA 2), dsRNA, an RNA hairpin, and RNA:DNA hybrids (using ssRNA sense for RNA:DNA hybrid 1, and antisense ssRNA for RNA:DNA hybrid 2). The extent of binding/dissociation of TIRR and 53BP1 was calculated and normalised to give a percentage dissociation based on controls of 100% binding (TIRR and 53BP1 proteins with DMSO only) and 0% binding (no proteins). Interestingly, despite being able to bind to TIRR, ssRNA did not largely impact TIRR and 53BP1 dissociation even at the highest concentrations tested

(ssRNA1: 18± 9.93%, ssRNA2: 13± 4.64%, mean± sd) (**Figure 3.8.B**). DsRNA also showed minimal dissociation activity at the highest concentration used (24± 2.35%) (**Figure 3.8.B**). However, the RNA hairpin which can bind to TIRR, was able to separate the TIRR/53BP1 complex to a much greater extent (62.4±1.14% dissociation at the highest concentration of RNA tested) and was the most active out of all the RNA substrates tested, suggesting that the structure of the RNA may influence TIRR and 53BP1 dissociation (**Figure 3.8.B**). Surprisingly, in the HTRF assay, we saw that RNA:DNA hybrids showed modest TIRR and 53BP1 dissociation activity (RNA:DNA hybrid 1: 46±1.87%, RNA:DNA hybrid 2: 52±1.87%) at the highest RNA concentrations tested, despite not being able to bind to TIRR. This was a surprising result as we expected only RNA which can bind to TIRR to possess any dissociation activity (see **Section 3.3.8** for further discussion). The results of this assay suggest that the secondary structure of RNA is of importance for TIRR/53BP1 dissociation, and hairpin RNA was most effective at separating TIRR and 53BP1 *in vitro*.

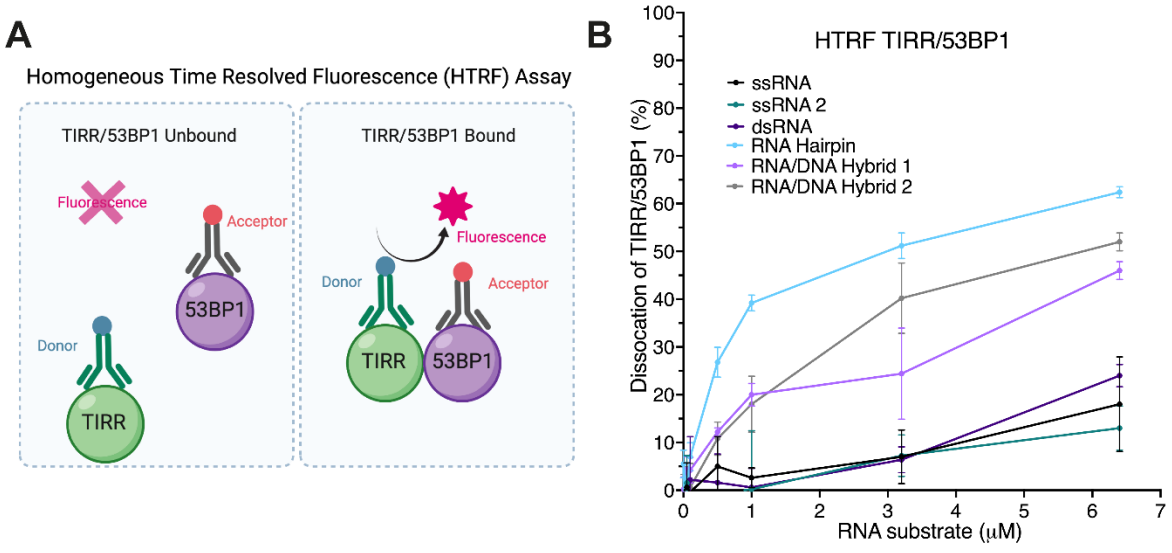


Figure 3.8: ***A)*** *Principles of the Homogeneous Time Resolved Fluorescence (HTRF) Assay with TIRR and 53BP1.* ***B)*** *Graph showing data from the HTRF assay with increasing concentrations of ssRNA 1, ssRNA 2, dsRNA, RNA hairpin, RNA/DNA hybrid 1, RNA/DNA hybrid 2 (mean ± sd, n=6). HTRF was performed by the Biophysics Group, Evotec (France), as part of our collaboration.*

3.3.7 Hairpin RNA can separate TIRR and 53BP1 *in vivo*

HTRF is an informative technique which enables us to test the dissociation of TIRR and 53BP1 in an isolated system. That is, a system which is devoid of the complexity of the cell and therefore allows the control of only one variable without any indirect effects found in *in vivo* systems. However, this also comes with the disadvantage of events which may occur *in vitro* not reflecting real biology, and may be a result of the artificial *in vitro* system. To try and determine if hairpin mediated dissociation of TIRR and 53BP1 could occur within the environment of the cell, we wanted to introduce hairpin RNA to the cell and determine if this influences TIRR and 53BP1 interaction. Firstly, we had to consider several key points associated with transfection of an RNA: identification of the correct RNA concentration and the correct time point post-transfection, confirmation of the nuclear entry of the RNA, and minimisation of any off-target effects induced by RNA transfection, such as DNA damage induction. It has been reported that hairpin shaped RNAs used for the purposes of RNA visualisation within cells (Molecular Beacons) are sequestered into the nucleus shortly after entering cells either by microinjection or transfection[23]. As the TIRR/53BP1 complex is located within the nucleus[2], we therefore decided to exploit this phenomenon and utilise a Molecular Beacon. We used a Molecular Beacon which had a similar structure to the RNA hairpins used in previous experiments (23nt, with a 15nt loop) (**Methods 2.1.7**), which had been shown previously to be sequestered into the nucleus[23], and was designed specifically not to target any RNA or DNA sequence in cells. We labelled this RNA with Cy3 at the 5' end to allow visualisation of the RNA and transfected the cell with 20nM and 100nM of annealed hairpin RNA. Cells were fixed 3 or 24 hours after transfection for visualisation of the RNA. We observed that not all the signal was localised in the nucleus, but at 3 hours, some nuclear RNA was observed at both 20nM and 100nM, although more signal was observed with 100nM. At 24 hours, most of the RNA appeared to have been exported from the nucleus and was

cytoplasmic (**Figure 3.9.A**). Therefore, 100nM was chosen as the concentration for transfection, and 3 hours or less was selected as the time point at which a portion of the hairpin RNA would be present in the nucleus. It should be noted that the signal was not homogenous and appeared to be localised in large bright foci, however the reason for the formation of these foci is not clear. We therefore assessed if transfection of the hairpin was resulting in any DNA damage, which would prohibit its use in our experiments as TIRR and 53BP1 could be dissociated by DNA damage signalling, rather than the hairpin itself directly. After transfection of 100nM hairpin, cells were fixed at 1 and 3 hours post-transfection. As previously observed, fluorescent signals were visible in the nucleus at both 1 and 3 hours (**Figures 3.9.B**). To assess if any DNA damage was occurring, we probed for ɣH2AX, a marker of DNA damage, using Etoposide as a positive control for damage induction. At both 1 hour and 3 hours post-transfection, we did not see a significant number of ɣH2AX foci above the control mock transfected condition (**Figures 3.9.B and 3.9.C**), which indicates that the transfection of the hairpin is not inducing DNA damage. Now that we determined the hairpin can reach the nucleus and does not induce DNA damage itself, we then assessed if this hairpin would have any effect on the TIRR/53BP1 complex. Performing PLA with TIRR and 53BP1 antibodies on cells fixed either 1 hour or 3 hours after hairpin transfection resulted in significantly reduced numbers of PLA foci per cell compared to the mock (**Figures 3.9.D and 3.9.E**), suggesting that hairpin transfection may be able to reduce the association of TIRR and 53BP1 *in vivo*. We anticipate that hairpin RNA would dissociate TIRR and 53BP1 through interaction with TIRR, so we also performed PLA using Cy3 and TIRR antibodies, to detect the interaction of TIRR with the hairpin RNA. We observed PLA signals indicating TIRR and RNA hairpin proximity, and interestingly these PLA signals seemed to often overlap with the Cy3 signal from the hairpin, which would be expected if the PLA signal was specific (**Figures 3.9.F and 3.9.G**). Not all PLA signals overlapped with the Cy3 signals, which could be due to either nonspecific PLA

signals, or that the hairpin present at a diffuse low level is interacting with TIRR, not just RNA found in the bright puncta. Additionally, not every Cy3 RNA molecule would be expected to generate a PLA signal as not every hairpin would be expected to interact with TIRR, and the PLA reaction itself is not 100% efficient. We also performed this assay with a second RNA hairpin labelled with Cy3 and similarly observed reduced interaction of TIRR and 53BP1, suggesting this is not specific to one hairpin sequence (**Figure 3.9.H and 3.9.I**). It is also important to note that there are several significant limitations of this assay. Firstly, we are unable to say definitively if the RNA hairpin is reaching the TIRR/53BP1 complex intact, or if the RNA is degraded after transfection. We anticipate a certain portion of the RNA would be degraded by cellular ribonucleases, but the extent to which this occurs is not known. It may be advantageous to modify this RNA to help reduce RNA degradation, such as with 2'-O-methylation[23]. Furthermore, it would be interesting to assess the behaviour of a ssRNA and its influence on TIRR/53BP1 separation. We would anticipate that transfecting ssRNA would not impact their association, although we would also anticipate that ssRNA would be significantly more unstable/vulnerable to degradation than a hairpin.

Taken together, whilst this experiment has limitations which need to be considered when interpreting the results, it appears that transfection of the RNA hairpin can separate TIRR and 53BP1 complex via the RNA interaction with TIRR. This is in agreement with the HTRF data, that an RNA hairpin can separate TIRR and 53BP1 *in vitro* (**Section 3.3.6**).

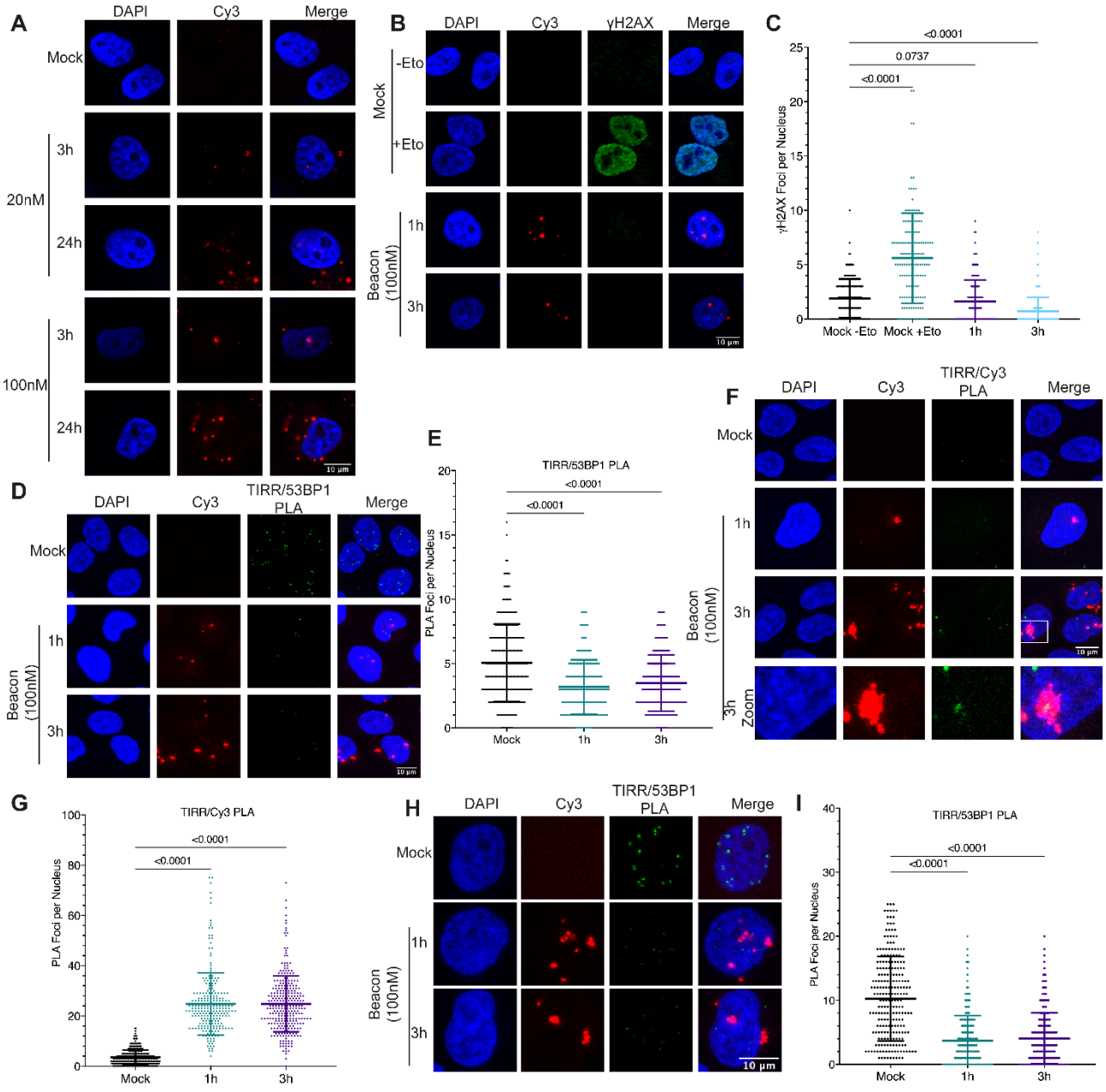


Figure 3.9: ***A)*** *Immunofluorescence microscopy of Hela cells transfected with a Cy3 labelled RNA hairpin at 20nM or 100nM, fixed 3 hours and 24 hours post-transfection.* ***B)*** *Immunofluorescence microscopy of cells transfected with Cy3 labelled RNA hairpin and probing for γH2AX. Etoposide was added as a positive control for damage induction.* ***C)*** *Quantification of B (mean ± sd, n=2).* ***D)*** *PLA of TIRR and 53BP1 1 or 3 hours after transfection of a Cy3 labelled RNA hairpin (100nM). n(Mock)=275, n(1h)=266, n(3h)=315.* ***E)*** *Quantification of D (mean ± sd, n=2).* ***F)*** *PLA of TIRR and Cy3 1 or 3 hours after transfection of a Cy3 labelled RNA hairpin (100nM). n(Mock)=313, n(1h)=241, n(3h)=291.* ***G)*** *Quantification of F (mean ± sd, n=2).* ***H)*** *PLA of TIRR and 53BP1 with a second Cy3 labelled RNA hairpin with a different sequence. (n(Mock)=230, n(1h)=249, n(3h)=262.* ***I)*** *Quantification of D (mean ± sd, n=2).*

3.3.8 RNA:DNA hybrids do not appear to play a role in TIRR/53BP1 dissociation *in vivo*

The RNA structures RNA:DNA hybrids are known to be associated with DSB repair[24–26]. Despite RNA:DNA hybrids showing no binding to TIRR in the SPR (**Section 3.3.3**), we observed moderate dissociation of TIRR and 53BP1 in the HTRF assay with increasing concentrations of RNA:DNA hybrid (**Section 3.3.6**). To clarify if RNA:DNA hybrids play a role in TIRR/53BP1 dissociation, or if this may be an *in vitro* artefact, we expressed RNaseH1 WT, which will degrade RNA:DNA hybrids in the cell, and an RNaseH1 WKKD mutant, which is a binding and catalytic mutant RNaseH1[27] as a control. We checked that the RNaseH1 proteins were expressing to similar levels (**Figure 3.10.A**), and that we were able to induce damage using IR to comparable levels in Mock transfected and WT or WKKD RNaseH1 transfected cells, as measured by ɣH2AX levels. Although expression of WT and WKKD RNaseH1 induced some ɣH2AX themselves, we were able to induce damage to comparable levels after IR treatment as assessed by western blot (**Figure 3.10.A**) and immunofluorescence microscopy (**Figure 3.10.B**). We also observed the nuclear localisation of WT and WKKD RNaseH1 by IF for V5, a tag present on the expressed RNaseH1 (**Figure 3.10.B**), which is important for degradation of RNA:DNA hybrids in the nucleus. Performing PLA using TIRR and 53BP1 antibodies in mock, RNaseH1 WT, or RNaseH1 WKKD expressing conditions revealed that after IR, the PLA foci observed were reduced significantly, suggesting that TIRR and 53BP1 were still able to dissociate after IR, even when RNA:DNA hybrids are depleted (**Figures 3.10.C and 3.10.D**). This suggests that RNA:DNA hybrids do not influence TIRR and 53BP1 dissociation. It is not clear why RNA:DNA hybrid structures were able to dissociate TIRR and 53BP1 in HTRF, but not *in vivo*, although there are several possible explanations. Firstly, this could be due to differences *in vivo*, for example, RNA:DNA hybrids may not be accessible for TIRR and 53BP1 separation in the same way as *in vitro*, such as due to binding of other proteins to RNA:DNA hybrids. Alternatively, this could potentially be due to a

technical issue of RNA:DNA hybrids not being fully removed after RNaseH1 overexpression. Therefore, we tested if RNaseH1 expression in cells was able to actually digest RNA:DNA hybrids by performing immunofluorescence with the S9.6 antibody, which specifically recognises RNA:DNA hybrids. We observed that the S9.6 signal was reduced after RNaseH1 WT expression, indicating that RNA:DNA hybrids were being digested (**Figures 3.10.E and 3.10.F)**. However, a small amount of S9.6 signal remained after RNaseH1 WT expression (**Figure 3.10.E)**. We therefore can't completely rule out the possibility that the remaining RNA:DNA hybrids may influence TIRR and 53BP1 separation. Nevertheless, it doesn't seem to be the case that TIRR and 53BP1 separation after IR is influenced by RNA:DNA hybrids *in vivo*, and therefore we conclude that RNA:DNA hybrids are unlikely to play a role in RNA-mediated TIRR/53BP1 dissociation after IR.

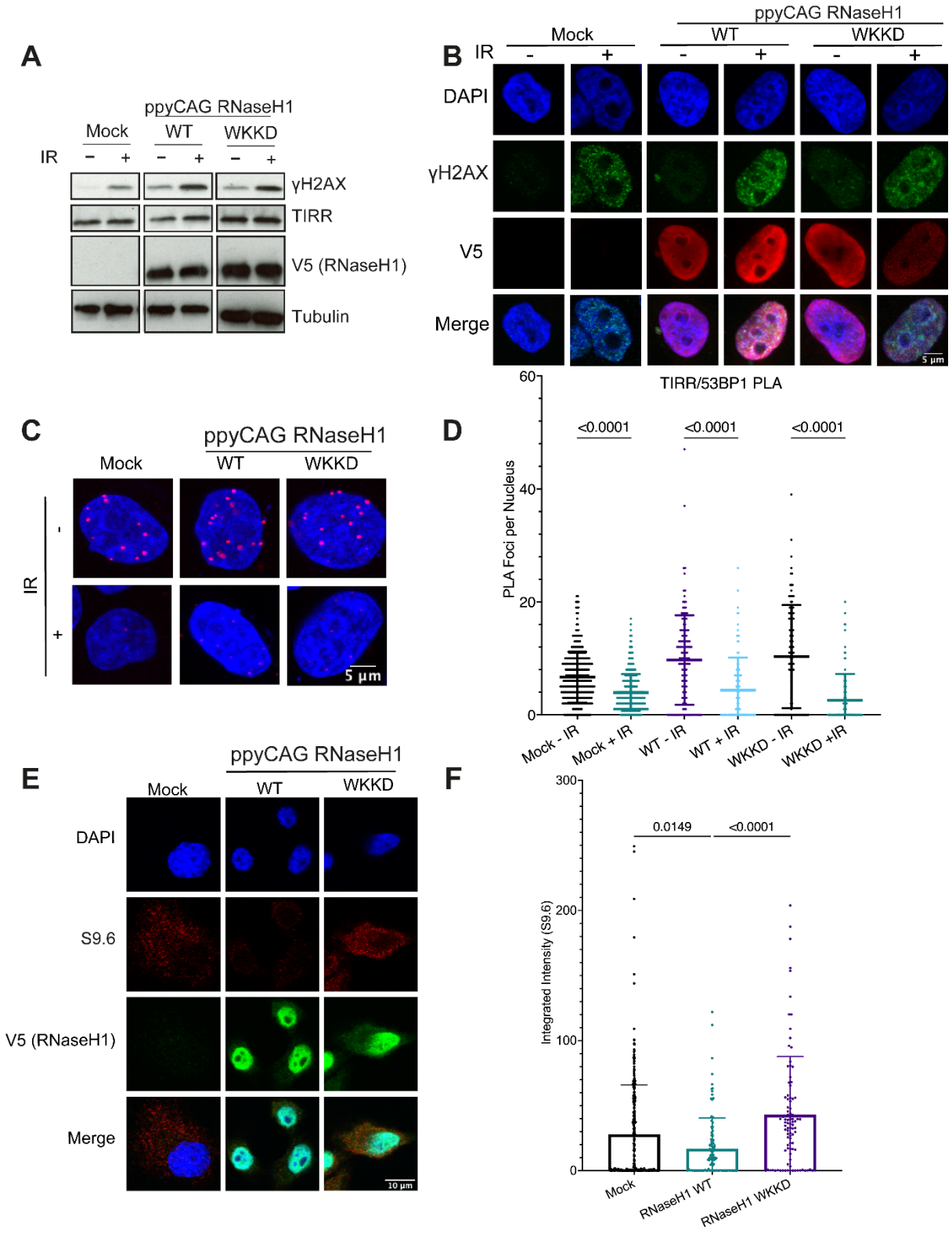


Figure 3.10: ***A)*** *Western blot showing induction of γH2AX after IR and expression of RNaseH1 WT and WKKD mutant.* ***B)*** *Immunofluorescence microscopy showing induction of γH2AX after IR and nuclear localisation of RNaseH1.* ***C)*** *PLA of TIRR and 53BP1 with and without IR (10Gy, 1 hour) with transfection prior to damage of either mock, WT RNasH1, or WKKD mutant RNaseH1. n(mock -IR)=329, n(mock +IR)=487, n(WT -IR)=135, n(WT +IR)=98, n(WKKD -IR)=102, n(WKKD +IR)=89.* ***D)*** *Quantification of C (mean ± sd, n=2).*

E) *Immunofluorescence of S9.6 in Mock, RNaseH1 WT, or RNaseH1 WKKD transfected cells to assess digestion of RNA:DNA hybrids. (n(Mock)=328, n(WT)=111, n(WKKD)=94. S9.6 IF experiment performed by Dr Adele Alagia.* ***F)*** *Quantification of E (mean ± sd, n=1).*

3.3.9 Dicer and Drosha, but not DGCR8, are required for TIRR/53BP1 dissociation

Dicer and Drosha are key components of the miRNA processing pathway which have also been shown to be important in the RNA dependent DDR[10,28,29]. Hairpin structures are also known Dicer and Drosha substrates, such as pri-microRNA and pre-microRNA. Therefore, we wanted to assess if Dicer and Drosha activity is required for TIRR/53BP1 dissociation. To this end, we knocked down Dicer and Drosha using siRNA. We first assessed the knockdown of Dicer and Drosha by western blot, observing a good level of knockdown at the protein level (**Figure 3.11.A**). Additionally, we were still able to induce DNA damage by IR to comparable levels in Dicer and Drosha knockdown conditions as assessed by western blot probing for ɣH2AX (**Figure 3.11.A**). By performing PLA with TIRR and 53BP1 antibodies in control Negative siRNA, Dicer siRNA, and Drosha siRNA conditions, we found that the complex did not separate after IR in Dicer and Drosha knockdown conditions, as we still observed comparable numbers of PLA foci in both siDicer and siDrosha conditions before and after IR, whereas there was a significant reduction in siNeg conditions after IR (**Figures 3.11.B and 3.11.C**). Therefore, both Dicer and Drosha are required for TIRR and 53BP1 dissociation after IR. We reasoned that Dicer and Drosha could be involved in two separate pathways, firstly through their canonical roles in microRNA processing, or via their non-canonical roles in the biogenesis of RNA from the sites of DSBs, as both Dicer and Drosha are active in the microRNA pathway as well as in the RNA dependent DDR (**Section 1.5.7**). To dissect which pathway may be influencing TIRR and 53BP1 separation, we knocked down DGCR8, a Drosha cofactor involved in miRNA processing. Whilst DGCR8 has been shown to participate in DSB repair through recruitment of RNF168 to DSBs[30], this role is independent of Drosha binding and importantly, DGCR8 has no known role in the biogenesis or processing of RNA generated at

DSBs (**Figure 3.11.D**). Knockdown of DGCR8 was confirmed by western blot (**Figure 3.11.E**), and we performed TIRR and 53BP1 PLA as before. After induction of DNA damage by IR, we observed a reduction of PLA foci in both the siNeg and siDGCR8 conditions, suggesting that DGCR8 is not involved in TIRR and 53BP1 separation after IR (**Figures 3.11.F and 3.11.G**). This suggests that the role of Dicer and Drosha in TIRR and 53BP1 separation is likely not in the microRNA processing pathway, and is instead is more likely in the biogenesis of RNA from the break. Whilst we cannot completely exclude the possibility of Dicer and Drosha playing another role in TIRR/53BP1 dissociation such as via protein-protein interactions, or an as yet unknown role in RNA processing independent of break sites, this data suggests that Dicer and Drosha are needed for TIRR/53BP1 dissociation after IR independently of the microRNA pathway.

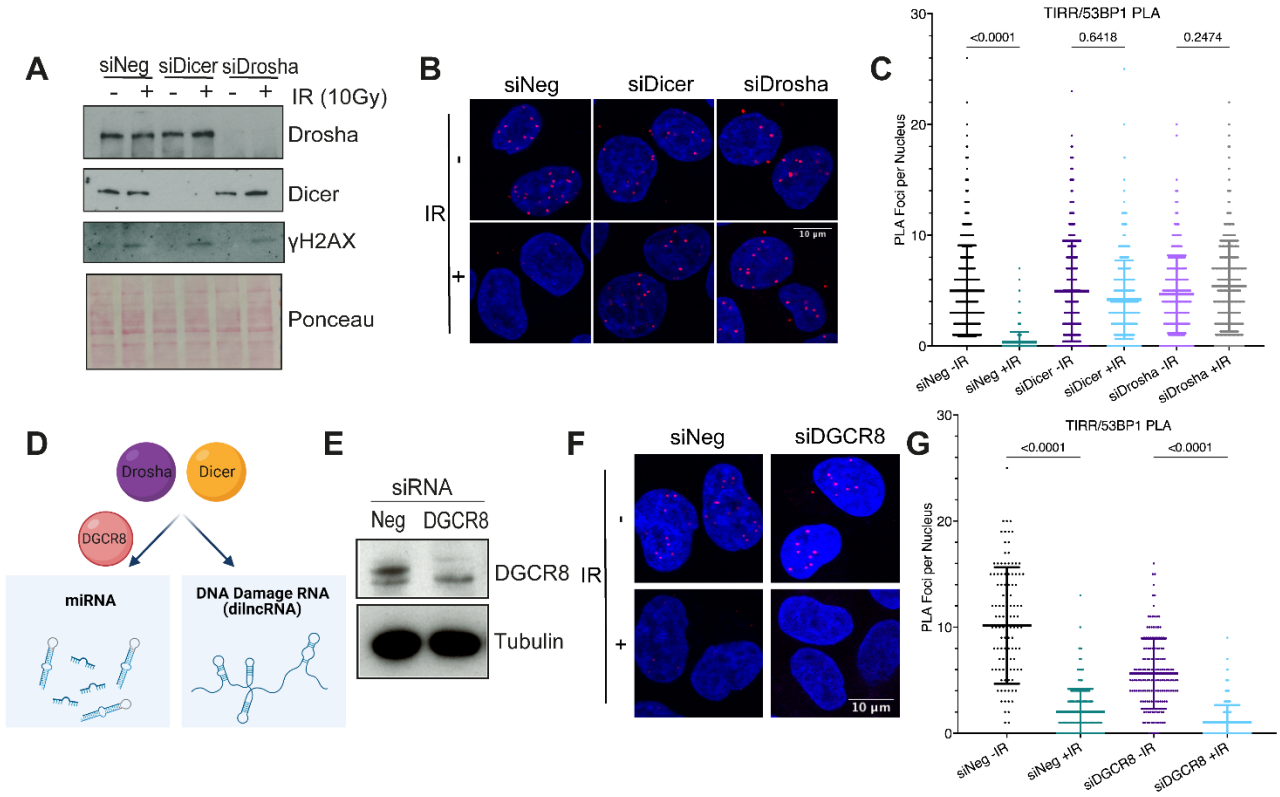


Figure 3.11: ***A)*** *Western blot showing knockdown of Dicer and Drosha and induction of γH2AX after IR.* ***B)*** *PLA of TIRR and 53BP1 with and without IR (10Gy, 1 hour) with knockdown of Dicer or Drosha prior to damage induction. n(siNeg -IR)=551, n(siNeg*

+IR)=428, n(siDicer -IR)=459, n(siDicer +IR)=391, n(siDrosha -IR)=336, n(siDrosha +IR)=271. ***C)*** *Quantification of B (mean ± sd, n=2).* ***D)*** *Scheme depicting the involvement of Dicer and Drosha in the RNA dependent DNA damage response and miRNA pathways, and DGCR8 involvement in miRNA processing.* ***E)*** *Western Blot of DGCR8 knockdown.* ***F)*** *PLA of TIRR and 53BP1 with and without IR (10Gy, 1 hour) with knockdown of DGCR8 prior to damage induction. n(siNeg -IR)=114, n(siNeg +IR)=178, n(siDGCR8 -IR)=155, n(siDGCR8 +IR)=251.* ***G)*** *Quantification of F (mean ± sd, n=2).*

3.3.10 TIRR is recruited to the sites of DNA damage

Given the involvement of Dicer and Drosha in TIRR/53BP1 dissociation, we hypothesised that RNA from the break may influence TIRR and 53BP1 dissociation. We envisaged two different models for how TIRR/53BP1 may be influenced by RNA originating from the break. Firstly, RNA may dissociate TIRR and 53BP1 distally to the break, i.e., RNA somehow finds the TIRR and 53BP1 in the nucleoplasm where the complex resides, dissociating the complex, then allowing 53BP1 recruitment. Alternatively, TIRR and 53BP1 could be bound as a complex and recruited together in proximity to the DSB, where they are then dissociated. To begin to examine this, we sought to assess if TIRR itself may be in proximity to the break after damage. 53BP1 is well known to be recruited to DSB sites to bind chromatin via H4K20me2 and H2AK15Ub[31], however little is known about TIRR recruitment and where in the cell the TIRR/53BP1 complex dissociates. PLA with antibodies targeting a protein of interest and ɣH2AX has been reported to detect proteins which can localise to sites of DNA damage[32]. Therefore, we first performed PLA using antibodies against TIRR and ɣH2AX with and without IR. Fixing cells 1 hour after IR, we observed an increase in PLA foci after IR, suggesting that TIRR and ɣH2AX are in close proximity after DSBs have been induced (**Figures 3.12.A and 3.12.B**). As an additional control, we performed PLA with antibodies for 53BP1 and ɣH2AX, and after inducing damage with IR, we observed an increase in PLA foci, in agreement with previous observations (**Figures 3.12.A and 3.12.B**)[32]. We also used ɣH2AX antibody only to control for the increase in ɣH2AX after DNA damage and possible nonspecific signals. We did not observe any significant increase in PLA foci after damage, suggesting that

the TIRR/γH2AX and 53BP1/γH2AX PLA foci observed after IR are due to an increased proximity with γH2AX, not due to the presence of more γH2AX itself (**Figures 3.12.A and 3.12.B**). This suggests that TIRR is recruited to damage after IR, similarly to 53BP1.

To further validate the observation that TIRR is in proximity to γH2AX after DSBs, we performed Co-Immunoprecipitation (Co-IP) using a doxycycline inducible Hela cell line expressing TIRR-GFP, or a control cell line expressing GFP only. GFP immunoprecipitation after damage revealed an increased Co-IP efficiency of γH2AX with TIRR-GFP after IR (10Gy, 1 hour), which was not observed in the GFP control. As an additional control, we also probed for 53BP1 and saw a reduced association of 53BP1 with TIRR after damage (**Figures 3.12.C, 3.12.D, and 3.12.E**).

Lastly, we performed laser microirradiation on cells pre-sensitised with Hoechst 33242[33]. DNA which is treated with pre-sensitisation agents, such as Hoechst 33242 or Brdu, is sensitive to damage with UV light[33]. Thus, laser striping of a specific area of the nucleus can induce localised damage. Laser stripping with a 405nm laser can lead to the production of DSBs[34–36], although it is important to note other types of DNA damage may also be induced, such as cyclobutane pyrimidine dimers (CPDs), which are repaired by nucleotide excision repair (NER)[34]. After laser striping Hela cells expressing doxycycline inducible TIRR-GFP, we saw a faint, but detectable above background, recruitment to the damage site, which reached a plateau quickly after initial appearance. When laser striping was performed on U2OS cells stably expressing 53BP1-GFP, we observed robust recruitment of 53BP1 to the damage stripe, which appeared to be stable and increasing over time until the final time point recorded (240s) (**Figures 3.12.F and 3.12.G**). We also performed a control experiment using doxycycline inducible GFP expressing Hela cells, and did not observe any recruitment to the site of laser-

induced damage (**Appendix Figure 1**), which suggests the recruitment observed is specific to TIRR and 53BP1, and not a nonspecific accumulation of protein/GFP. Whilst recruitment to the laser stripe does not suggest direct binding, but rather a site-specific increase in the amount of protein, taken together with PLA and Co-IP data, this suggests that TIRR is in proximity to DSB sites. This raises an interesting possibility that TIRR and 53BP1 are recruited to the break together for dissociation, although we cannot say if the population of TIRR which is recruited to damage is bound to 53BP1, or if this is a population which is not bound to 53BP1 at the point of damage, or dissociates from 53BP1 and is recruited independently.

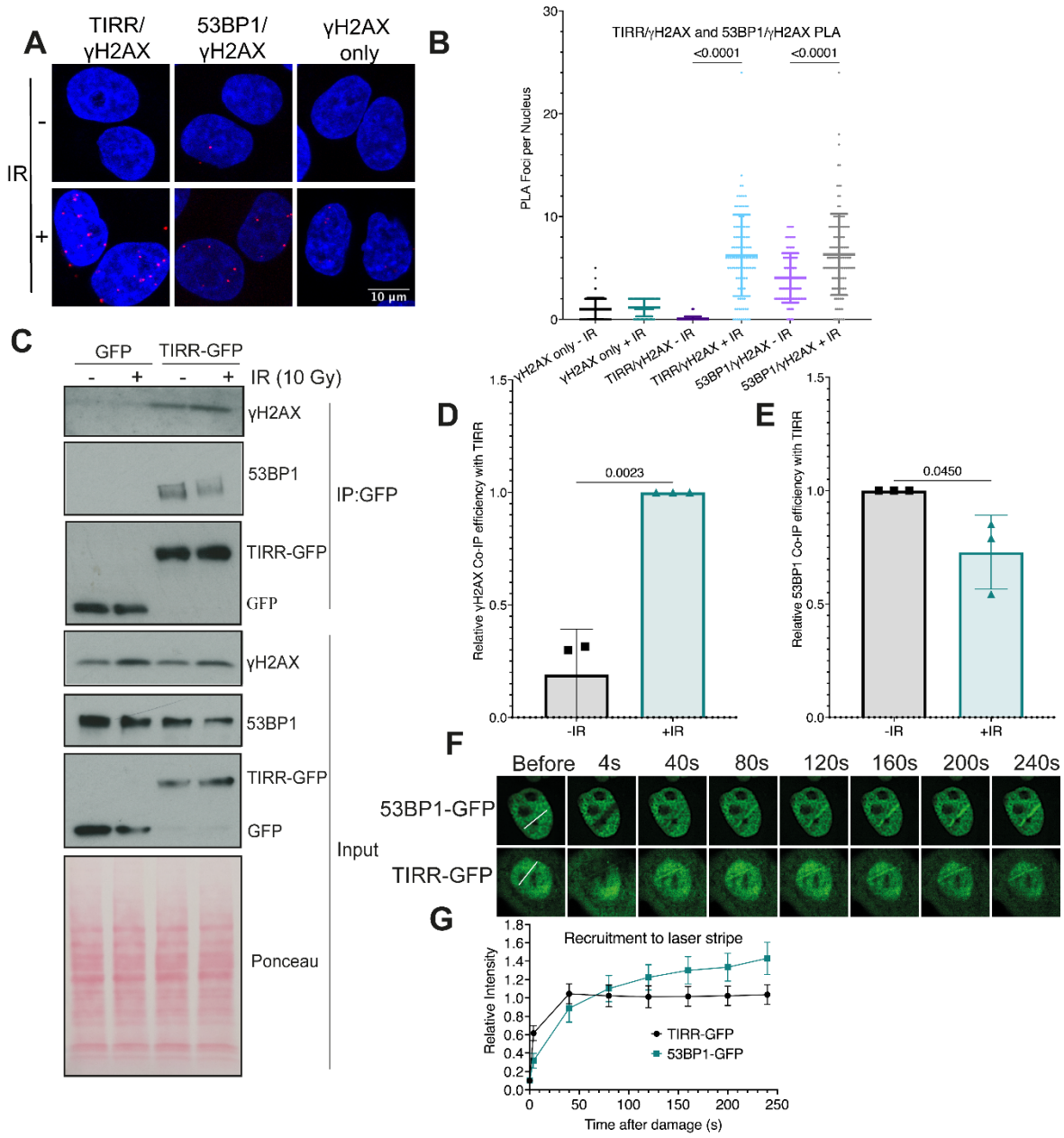


Figure 3.12: ***A)*** *PLA of TIRR and γH2AX, 53BP1 and γH2AX, or γH2AX alone with and without IR (10Gy, 1 hour) (n(γH2AX -IR)=65, n(γH2AX +IR)=75, n(γH2AX + TIRR -IR)=73, n(γH2AX + TIRR +IR)=105, n(γH2AX + 53BP1 -IR)=123, n(γH2AX + 53BP1 +IR)=122).* ***B)*** *Quantification of A (mean ± sd, n=2).* ***C)*** *Co-immunoprecipitation of TIRR-GFP or GFP with and without IR (10Gy, 1 hour). Ponceau is used as a loading control.* ***D)*** *Quantification of C, γH2AX bound to TIRR-GFP +/- IR. (mean ± sd, n=3)* ***E)*** *Quantification of C, 53BP1 bound to TIRR-GFP +/- IR. (mean ± sd, n=3)* ***F)*** *Laser stripping of 53BP1-GFP U2OS cells and TIRR-GFP Hela cells. The white line depicts the location of the laser stripe. Laser microirradiation and analysis was performed by Dr Monika Gullerova.* ***G)*** *Quantification of F (mean ± sd of 10 cells, n=1).*

3.3.11 The interaction of 53BP1 with TIRR is required for the recruitment of TIRR to damage sites

To address the question of whether TIRR and 53BP1 are recruited together as a complex, or the population of TIRR we observe being recruited to damage is not bound to 53BP1, we generated a mutant of TIRR which is defective for 53BP1 binding. The K10 residue on TIRR, when mutated to Glutamic acid, has been reported in multiple studies to abolish the binding of TIRR to 53BP1[2,3,37]. We generated a construct expressing TIRR either WT or K10E, fused to Neongreen for visualisation. We confirmed this construct was successfully mutated K→E at position 10 by Sanger Sequencing (**Figures 2.1.A, 2.1.B, and 2.1.C**), and transfected WT and K10E TIRR in Hela cells to check their expression. Both K10E and WT TIRR expressed to comparable levels when transiently transfected into cells, as detected by western blot with a TIRR antibody (**Figure 3.13.A**). We then performed the same laser stripe experiment in Hela cells transiently expressing WT or K10E TIRR. We interestingly observed impaired recruitment of K10E TIRR to damage when compared to the WT TIRR, suggesting that the 53BP1 binding mutant TIRR was not recruited to damage with the same efficiency as the WT TIRR (**Figures 3.13.B and 3.13.C**).

To further confirm this observation, we performed PLA using antibodies against ɣH2AX and Neongreen in cells transiently transfected with either WT or K10E TIRR. After exposure to IR, we observed an increase in PLA foci in cells expressing WT TIRR, indicating that TIRR is in close proximity to ɣH2AX after damage, as previously observed (**Figures 3.13.D and 3.13.E**). However after IR, in cells expressing K10E TIRR, we saw significantly fewer PLA foci with ɣH2AX and Neongreen when compared to WT, indicating that K10E recruitment to ɣH2AX was impaired compared to WT TIRR, in agreement with laser striping data (**Figures 3.13.D and 3.13.E**). This again suggests that TIRR which is unable to bind 53BP1 is not recruited as efficiently to damage sites. Finally, as a control, we also performed this same PLA

using antibodies against γH2AX and TIRR. We observed a very similar result, and although there was a significant increase in PLA foci in the K10E sample after IR when compared to undamaged cells (likely confounded by the detection of endogenous WT TIRR), this was nevertheless significantly less than in the WT sample (**Figures 3.13.F and 3.13.G**). Taken together, this data suggests that binding-null mutant TIRR, which cannot interact with 53BP1, is impaired in recruitment to DSB sites.

Although we cannot rule out the possibility that the K10 residue may mediate other protein-protein interactions which may influence TIRR recruitment to DSBs, it appears plausible that TIRR which is bound to 53BP1 is the population of TIRR recruited to damage. Our interpretation of this data is that TIRR and 53BP1 are therefore likely recruited to damage sites as a complex for dissociation, rather than dissociation occurring in the nucleoplasm away from the break.

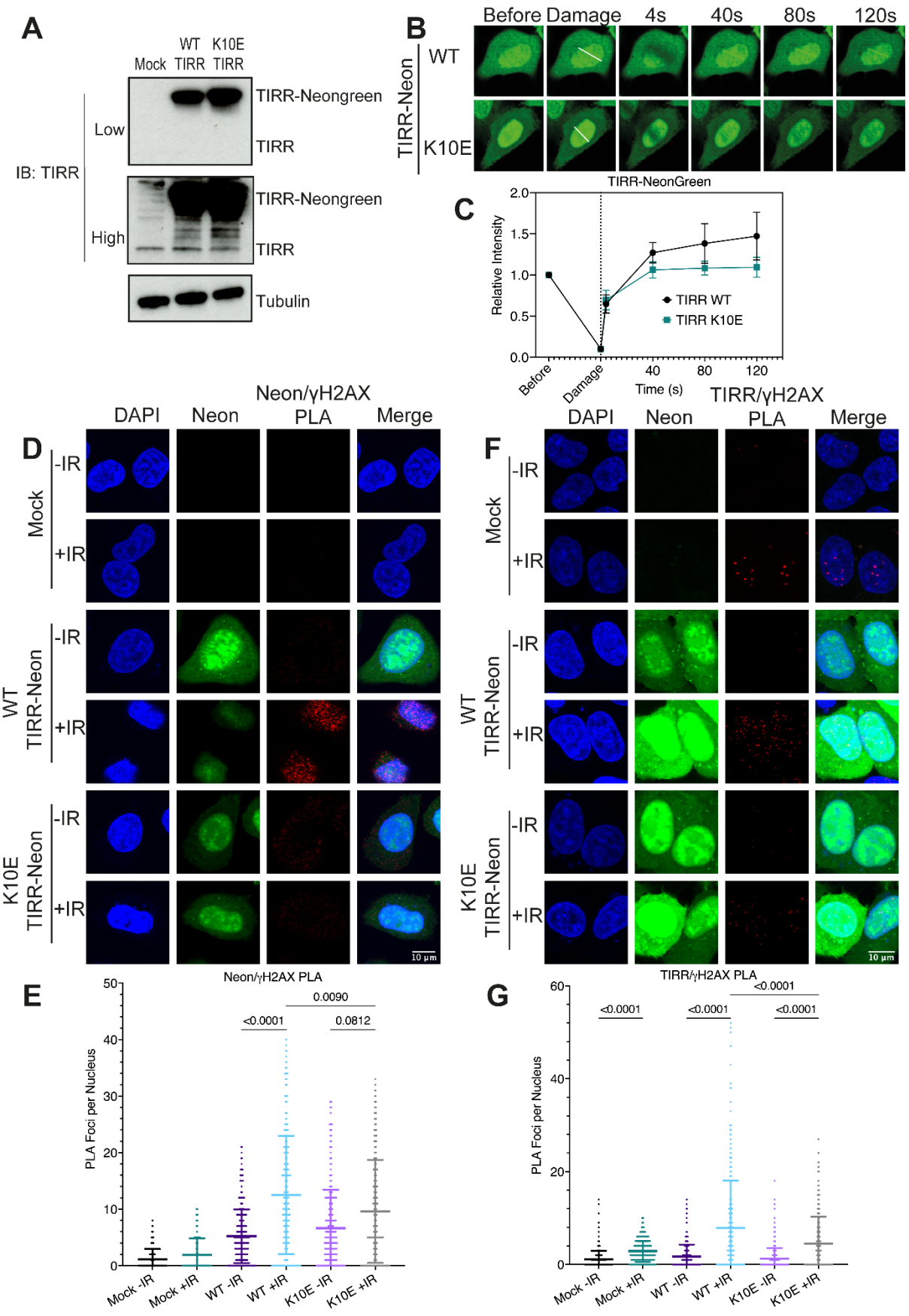


Figure 3.13: *A) Western blot to confirm expression of WT Neongreen-TIRR and K10E Neongreen-TIRR after transfection.* ***B)*** *Laser stripping of Hela cells with transfection prior to*

damage of either mock, WT Neongreen-TIRR, or K10E Neongreen-TIRR. The white line depicts the location of the laser stripe. ***C)*** *Quantification of B (mean ± sd of 10 cells, n=1). Laser microirradiation performed by Dr Monika Gullerova.* ***D)*** *PLA of Neongreen and ɣH2AX with and without IR (10Gy, 1 hour) with transfection prior to damage of either mock, WT Neongreen-TIRR, or K10E Neongreen-TIRR. n(mock -IR)=315, n(mock +IR)=309, n(WT -IR)=343, n(WT +IR)=289, n(K10E -IR)=324, n(K10E +IR)=258.* ***E)*** *Quantification of D (mean ± sd, n=2).* ***F)*** *PLA of TIRR and ɣH2AX with and without IR (10Gy, 1 hour) with transfection prior to damage of either mock, WT Neongreen-TIRR, or K10E Neongreen-TIRR. n(mock -IR)=347, n(mock +IR)=402, n(WT -IR)=329, n(WT +IR)=339, n(K10E -IR)=432, n(K10E +IR)=338.* ***G)*** *Quantification of F (mean ± sd, n=2).*

3.3.12 TIRR recruitment to damage sites is dependent on RNA Polymerase II transcription

Given that transcription was required for TIRR and 53BP1 separation, we then decided to explore if transcription was also required for the recruitment of TIRR, and therefore the TIRR/53BP1 complex, to damage. To this end, we first performed TIRR and ɣH2AX PLA in the presence of α-amanitin, DRB (a CDK9 inhibitor which prevents RNAPII transcription elongation[38]), and DMSO as a control. We observed a significant increase in TIRR and ɣH2AX PLA foci after IR, however this was significantly impaired in the presence of either α-amanitin or DRB (**Figures 3.14.A and 3.14.B**), suggesting that TIRR recruitment to DSBs, and by extension TIRR and 53BP1 complex recruitment, requires RNAPII transcription.

To assess if both TIRR and 53BP1 recruitment to damage was impaired by transcription inhibition, we performed laser striping in cells expressing either 53BP1-GFP or TIRR-GFP, in the presence or absence of DRB to inhibit transcription. We observed that the recruitment of 53BP1 was impaired in the presence of DRB (**Figures 3.14.C and 3.14.D**), in agreement with previously published data[39]. Furthermore, we also observed impaired recruitment of TIRR-GFP in the presence of DRB (**Figures 3.14.E and 3.14.F**), consistent with our previous observations using PLA (**Figures 3.14.A and 3.14.B**).

Lastly, to evaluate the contribution of RNAPII directly in a protein-protein interaction for TIRR recruitment, compared with RNA transcribed by RNAPII, we performed a Co-IP on TIRR-GFP and assessed for RNAPII binding. We were unable to observe any binding of RNAPII to TIRR in this assay (**Figure 3.13.G**), suggesting the recruitment of TIRR to DSBs is more likely dependent on RNAPII transcription rather than RNAPII binding.

Combined with our previous observations that transcription is required for TIRR/53BP1 complex separation, and that TIRR and 53BP1 are likely recruited to the DSB together before separation, this data suggesting that RNAPII transcription is required for both 53BP1 and TIRR recruitment to DSBs implies that RNA transcription at the DSB is important not only for TIRR and 53BP1 complex separation, but also TIRR and 53BP1 recruitment to damage.

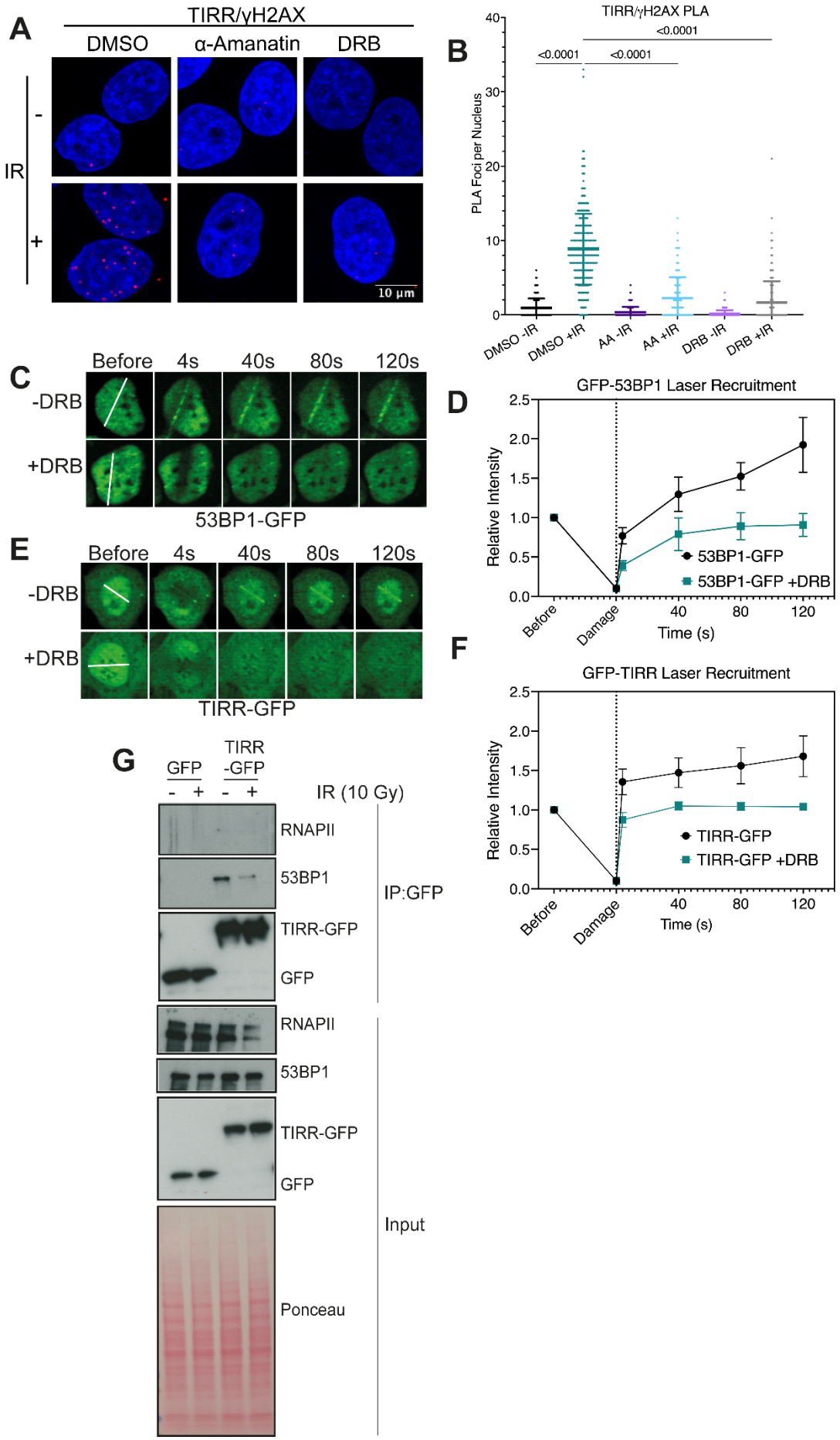

A
TIRR/γH2AX
DMSO
α-Amanatin
DRB
IR
-
+
10 μm
B
TIRR/γH2AX PLA
<0.0001
<0.0001
<0.0001
PLA Foci per Nucleus
DMSO -IR
DMSO +IR
AA -IR
AA +IR
DRB -IR
DRB +IR
C
Before
4s
40s
80s
120s
-DRB
+DRB
53BP1-GFP
D
GFP-53BP1 Laser Recruitment
Relative Intensity
53BP1-GFP
53BP1-GFP +DRB
Before
Damage
Time (s)
E
Before
4s
40s
80s
120s
-DRB
+DRB
TIRR-GFP
F
GFP-TIRR Laser Recruitment
Relative Intensity
TIRR-GFP
TIRR-GFP +DRB
Before
Damage
Time (s)
G
GFP
TIRR -GFP
IR (10 Gy)
RNAPII
53BP1
TIRR-GFP
GFP
IP:GFP
RNAPII
53BP1
TIRR-GFP
GFP
Input
Ponceau

Figure 3.14: ***A)*** *PLA of TIRR and γH2AX with and without IR (10Gy, 1 hour) in the presence of α-amanitin (2μg/ml, 24 hours) or DRB (100μM, 1 hour). n(DMSO -IR)=240, n(DMSO +IR)=275, n(AA -IR)=241, n(AA +IR)=258, n(DRB -IR)=281, n(DRB +IR)=326.* ***B)*** *Quantification of A (mean ± sd, n=2).* ***C)*** *Laser stripping of 53BP1-GFP U2OS cells with and without DRB (100μM, 1 hour) prior to damage. The white line depicts the location of the laser stripe.* ***D)*** *Quantification of C (mean ± sd of 10 cells, n=1).* ***E)*** *Laser striping of TIRR-GFP Hela cells with and without DRB (100μM, 1 hour) prior to damage. The white line depicts the location of the laser stripe. Laser microirradiation and analysis performed by Dr Monika Gullerova.* ***F)*** *Quantification of E (mean ± sd, n=1).* ***G)*** *Co-IP of GFP or TIRR-GFP in non-damage or irradiated cells.*

3.3.13 Coordination with ATM signalling

Other proteins or post-translational modifications may contribute to the process of TIRR and 53BP1 dissociation, such as ATM phosphorylation of 53BP1[1,2]. It has also been suggested that RNAPII inhibition or Dicer and Drosha knockdown may influence phosphorylation of ATM (pATM)[29,39], although not unequivocally[40]. We found that ATM inhibition impaired the dissociation of TIRR and 53BP1 after IR (**Figures 3.15.A, 3.15.B, 3.15.C**), however RNAPII inhibition using either α-Amanitin or DRB, and Dicer and Drosha knockdown, did not influence pATM (S1981) after IR (**Figure 3.15.D**). This suggests that the RNA-dependent DDR may contribute to TIRR/53BP1 dissociation in concert with other pathways, such as ATM phosphorylation of 53BP1.

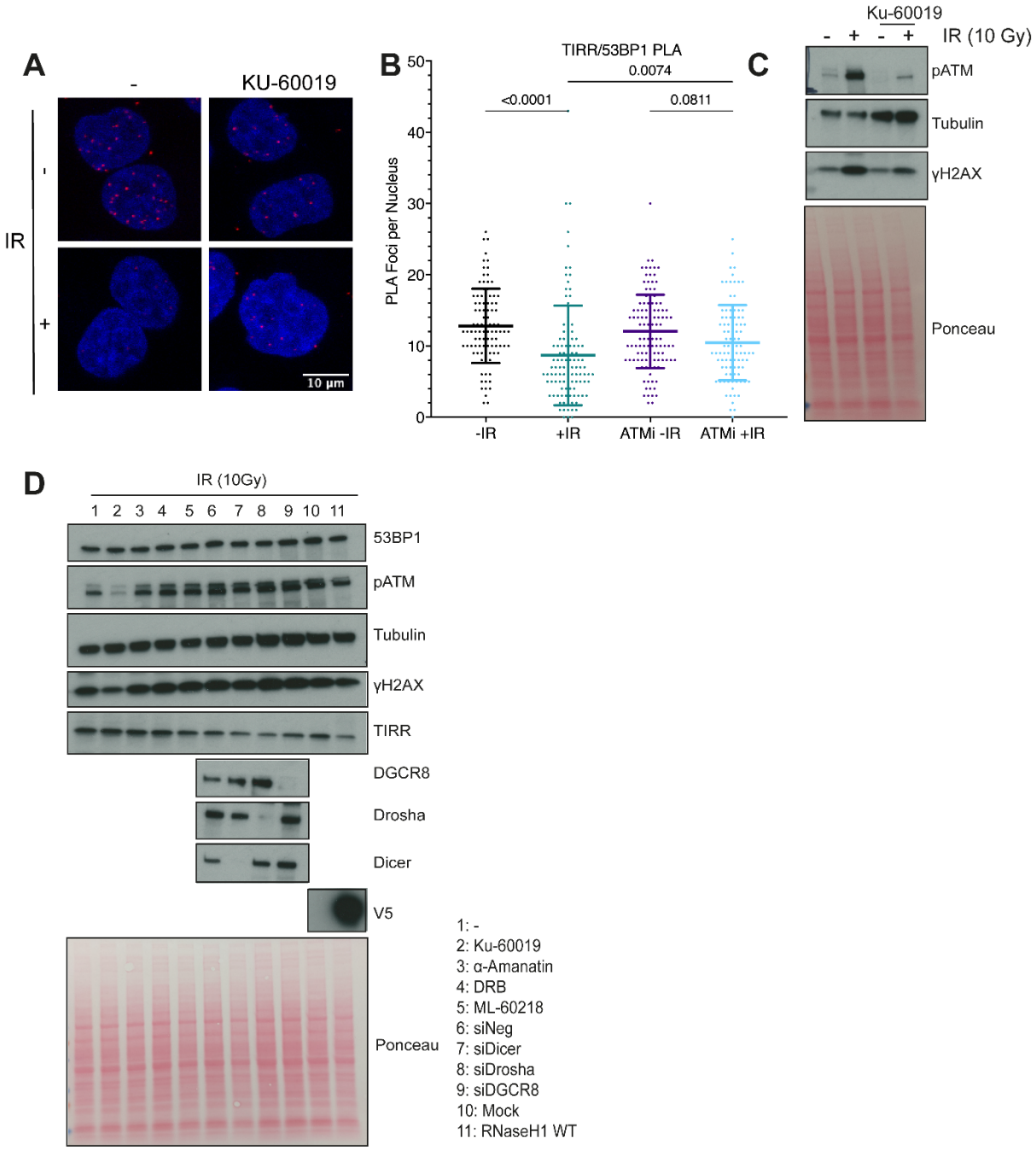


Figure 3.15: ***A)*** *PLA of TIRR and 53BP1 with ATMi (KU-60019, 10µM, 1 hour). n(-IR)=96, n(+109)=255, n(ATMi -IR)=119, n(ATMi +IR)=93.* ***B)*** *Quantification of A (mean ± sd, n=1).* ***C)*** *Western blot to assess for phosphorylated ATM* (S1981) *levels after ATM inhibition with KU-60019.* ***D)*** *Western blot to assess for phosphorylated ATM levels after RNAPII inhibition, siRNA knockdown of Dicer, Drosha, and DGCR8, or transfection of RNaseH1 WT.*

3.3.14 TIRR is in proximity to DSB-derived RNA

Given that the recruitment of TIRR and 53BP1 as a complex depends on transcription, coupled with earlier observations regarding the requirement of RNAPII and Dicer and Drosha for

separation, we hypothesised that RNA transcribed at the break may contribute to TIRR and 53BP1 separation. To understand if RNA transcribed from the break could play a role in TIRR and 53BP1 separation, we developed a new cellular assay: Fluorescence *in situ* hybridisation PLA (FISH-PLA). We employed the use of a cellular system which would enable the induction of DNA DSBs in a sequence specific manner, as IR induces breaks randomly into the genome and would not allow the measurement of the interaction between TIRR/53BP1 and RNA produced specifically at the break. We instead use the U20S-A*si*SI-ER cell line, where the A*si*SI restriction enzyme is joined with a modified ligand binding domain of the oestrogen receptor (ER), which translocates to the nucleus after addition of 4-Hydroxytamoxifen (4-OHT), where *Asi*SI cuts in a sequence-dependent manner to induce site specific DSBs [41]. As A*si*SI cuts in a sequence specific manner, we know the sequence of the RNA which would be transcribed by RNAPII at the break. Therefore, we can design DNA probes (termed FISH-probes) to target this RNA sequence. We can modify the PLA assay to detect the interaction of a protein with this RNA sequence by replacing one of the PLA secondary probes, which would usually bind to one of two antibodies for the detection of two proteins, with a FISH-probe. The FISH-probe contained added nucleotides which would usually be found on one of the secondary probes (plus probe), with a linker sequence between the target region and the PLA region of the probe. Addition of a primary antibody targeting the protein of interest is followed by incubation with the secondary minus probe. If the protein of interest is in close proximity to the FISH probe, the minus probe and the FISH-probe will be ligated together and act as a substrate for the polymerase in PLA, as would be the case if two proteins are in proximity (**Figure 3.16.A**).

We selected two different A*si*SI cut sites on which to perform FISH-PLA. *Asi*SI cuts at the sequence GCGAT/CGC, which would yield ~1000-1200 potential cut sites in the human

genome[42,43]. However, not all potential *Asi*SI cut sites in the genome are actually cleaved, meaning only around ~150-200 DSBs are actually generated after addition of 4-OHT[42,43]. Therefore, we selected two *Asi*SI sites in the genome which are validated to be cut[10,43]: hg19, chr1:89,458,643 (referred to as DS1), and hg19, chr19:30,019,487 (referred to as DS2). DS1 and DS2 are also located in two different regions of the genome. DS1 is located in the promoter-associated region of RBMXL1 (**Figure 3.16.B**), and DS2 is located in an intron of VSTM2B (**Figure 3.16.C**).

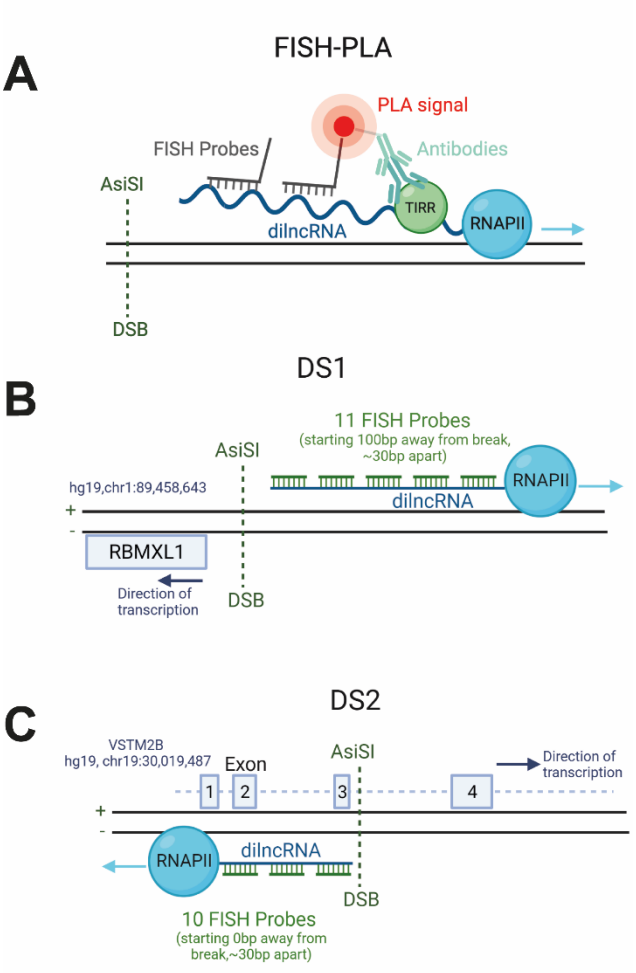


Figure 3.16: *Diagram showing the location of DS1 and DS2, and the design of FISH PLA.* ***A)*** *Representation of the FISH-PLA assay. The FISH-PLA assay was developed with the help of Dr Adele Alagia.* ***B)*** *DS1 location and FISH probe target sites.* ***C)*** *DS2 location and FISH probe target sites.*

We first performed immunofluorescence microscopy on *Asi*SI cells in the presence of 4-OHT, to detect the induction of DSBs as assessed by γH2AX foci, and in the presence of the transcriptional inhibitor α-Amanitin, which will be used as a control in our experiments. After incubation with 500nM 4-OHT for 4 hours, we can clearly observe a significant increase in γH2AX foci, indicative of induction of sequence-specific DSBs by the *Asi*SI enzyme (**Figures 3.17.A and 3.17.B**). Furthermore, the number of γH2AX foci was also not significantly altered by the addition of α-Amanitin prior to 4-OHT addition (**Figures 3.17.A and 3.17.B**). We then performed FISH-PLA using an antibody targeting either TIRR or 53BP1, with the FISH-PLA probes, in the presence or absence of 4-OHT, and with α-Amanitin. By performing FISH-PLA with TIRR and the probes for RNA from cut site DS1, we observed minimal PLA foci in the absence of 4-OHT. After 4 hours of 4-OHT incubation, we saw a significantly increased PLA signal, which was diminished with α-Amanitin treatment (**Figures 3.17.C and 3.17.D**). We also saw a very similar result when we performed FISH-PLA for DS1 with an antibody targeting 53BP1 (**Figures 3.17.E and 3.17.F**). Performing FISH-PLA at DS2 yielded a very similar result for both TIRR (**Figures 3.17.G and 3.17.H**) and 53BP1 (**Figures 3.17.I and 3.17.J**). The presence of PLA foci for both TIRR and 53BP1 at DS1 and DS2 after 4-OHT incubation, which are reduced after RNAPII inhibition, suggests that both TIRR and 53BP1 are in close proximity with RNA transcribed by RNAPII originating from the break itself. Whilst we cannot confirm whether or not this RNA separates TIRR and 53BP1 at the break, this result implicates RNA-derived from the DSB in TIRR/53BP1 separation.

It should be noted that since the DS1 and DS2 FISH-PLA probes are designed to target a single specific genomic locus which would be cut by *Asi*SI after 4-OHT incubation, we would expect to see only one or two FISH-PLA foci after 4-OHT addition. However, we see an average of 5 PLA foci for 53BP1 after +4-OHT (**Figure 3.17.E and 3.17.F**), and an average of 6 PLA foci

for TIRR at DS1 with some cells containing as many as 10 foci or more (**Figure 3.17.C and 3.17.D**). There are several possible explanations for this. Firstly, there could be some nonspecific PLA signals generated in FISH-PLA. Whilst there are some PLA foci detected in the -4-OHT samples, which can be accounted for by a certain degree of background/non-specific signal, the PLA foci are significantly increased after 4-OHT incubation, which would not be expected if the majority of the signals were originating from nonspecific amplification. Furthermore, the PLA foci observed in the +4-OHT samples were sensitive to RNAPII inhibition, which returns the PLA foci number to that in the -4-OHT samples, which we class as background levels. Therefore, the PLA foci observed in the +4-OHT samples appear to be specific. Alternatively, this could suggest a potential interaction with DSB-derived RNA processed from a long non-coding RNA transcript produced at the break, for example DDRNA[12], as the 10-11 individual FISH probes span a region up to ~1.2kb away from the cut site. It is also possible that more than one individual lncRNA could be produced at the break before it is resolved (e.g. more than a single RNAPII transcribing lncRNA from the break). Finally, after 4-OHT addition A*si*SI can cleave the same sites over again if they have been accurately repaired, so it is possible that additional transcripts could be generated by the repeated breakage of the site[44].

Taken together, FISH-PLA suggests that TIRR and 53BP1 are in proximity to RNA produced at the break, which could potentially indicate that this RNA may influence TIRR and 53BP1 separation after DNA damage.

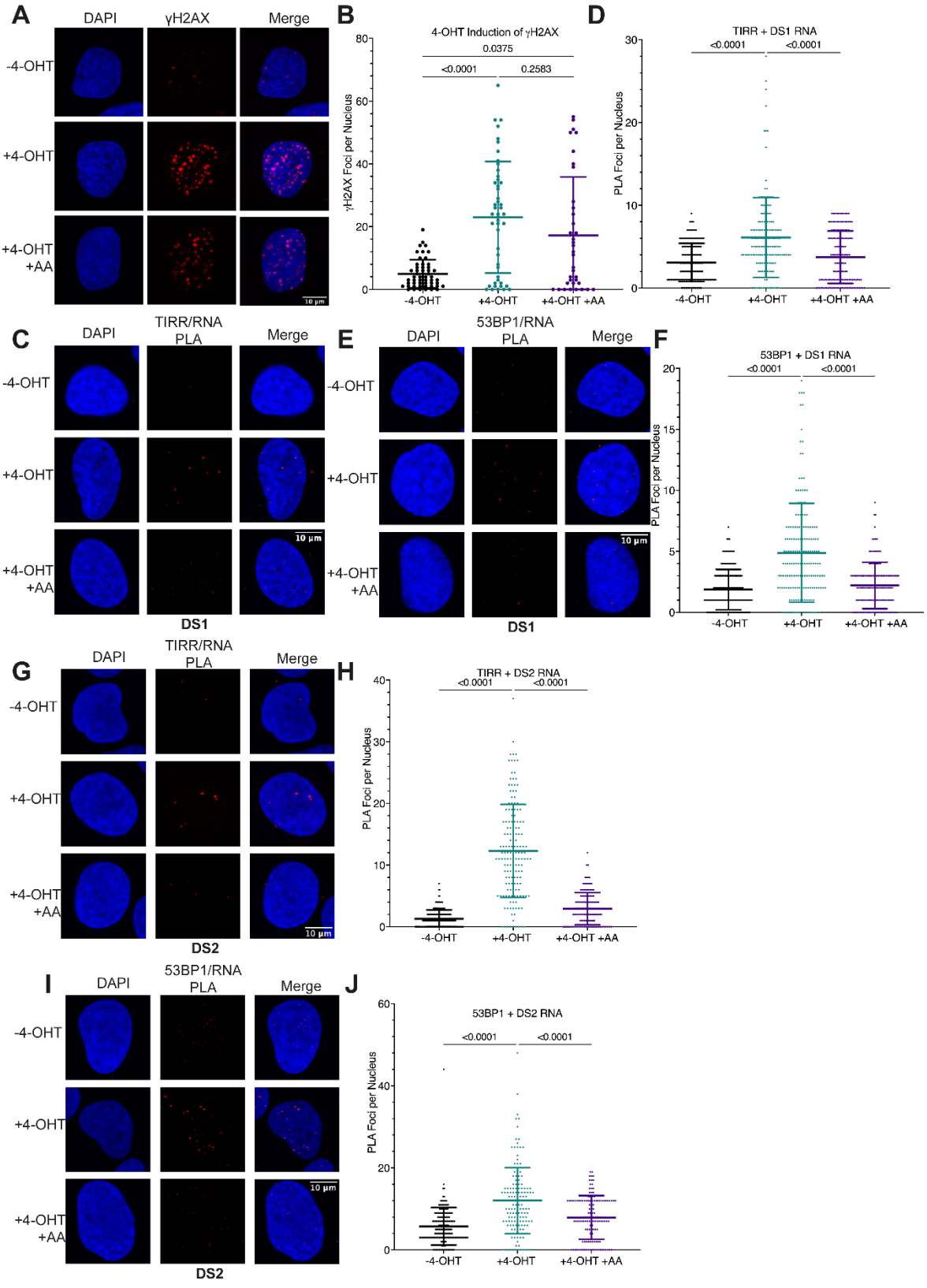


Figure 3.17: ***A)*** *Induction of DSBs as measured by γH2AX foci after the addition of 4-OHT, with the addition of α-amanitin. n(-4-OHT)=53, n(+4-OHT)=48, n(-4-OHT +AA)=36.* ***B)*** *Quantification of A (mean ± sd, n=1).* ***C)*** *FISH-PLA of TIRR and DS1 probes, with and without 4-OHT (500nM, 4 hours), or α-amanitin (2μg/ml, 24 hours). n(-4-OHT)=179, n(+4-OHT)=154, n(-4-OHT +AA)=143.* ***D)*** *Quantification of C (mean ± sd, n=2).* ***E)*** *FISH-PLA of*

53BP1 and DS1 probes, with and without 4-OHT (500nM, 4 hours), or α-amanitin (2μg/ml, 24 hours). n(-4-OHT)=169, n(+4-OHT)=171, n(-4-OHT +AA)=135. ***F)*** *Quantification of E (mean ± sd, n=2).* ***G)*** *FISH-PLA of TIRR and DS2 probes, with and without 4-OHT (500nM, 4 hours), or α-amanitin (2μg/ml, 24 hours). n(-4-OHT)=177, n(+4-OHT)=155, n(-4-OHT +AA)=136.* ***H)*** *Quantification of G (mean ± sd, n=2).* ***I)*** *FISH-PLA of 53BP1 and DS2 probes, with and without 4-OHT (500nM, 4 hours), or α-amanitin (2μg/ml, 24 hours). n(-4-OHT)=187, n(+4-OHT)=161, n(-4-OHT +AA)=129.* ***J)*** *Quantification of I (mean ± sd, n=2).*

3.3.15 HADDOCK modelling of TIRR with RNA

To understand how RNA would influence TIRR and 53BP1 interaction, we wanted to model the structure of RNA bound to TIRR. For this purpose, we used the modelling software HADDOCK2.4[45], which allows us to model RNA-protein interactions (refer to **Section 2.2.43** for further details on the HADDOCK software and parameters). To use HADDOCK, residues which are directly involved in the interaction must be set (active residues). As a benchmarking exercise, we first performed HADDOCK modelling using TIRR and 53BP1, setting the active residues from the published crystal structure of TIRR and 53BP1 (PDB: 6CO1)[1]; (TIRR (from 6D0L): 105, 106, 107, 24, 101, 10, 20, 362, and 53BP1 Tudor (from 1XNI): 1549, 1551, 1553, 1500, 1584, 1502, 1521, 1495, 1523), generating thirteen clusters. HADDOCK outputs solutions grouped into clusters, which are highly similar solutions, with Cluster 1 containing the largest number of possible solutions. Clusters are given a HADDOCK score based on various parameters which may influence how favourable a structure is, such as electrostatic energy. Manual inspection of Cluster 1, which gave the lowest (best) HADDOCK score, revealed that the model generated had a RMSD from the crystal structure of 1.98, indicating that the model generated was highly similar to the actual structure (**Figure 3.18.A**).

Satisfied that we were able to use HADDOCK to model TIRR and 53BP1, we then turned our attention to modelling TIRR with hairpin RNA. Setting active residues for this TIRR-RNA model was not trivial, as it is not known exactly which residues on TIRR are involved in the RNA interaction. To try to define these active residues, we first looked at published RNA

crosslinking mass spectrometry data[6] that approximates the RNA binding site on TIRR to span residues 91-107 (LTEADYLSSHLTEGPHR). Furthermore, the TIRR paralogue NUDT16 shares a high degree of sequence and structural complementarity with TIRR (**Figure 3.18.B**). Although we do not have a structure of TIRR bound to any nucleic acid substrates, a crystal structure of NUDT16 bound to IMP has been published (PDB: 2XSQ)[46]. The region on NUDT16 which interacts with IMP is in the vicinity of the 91-107 region on TIRR, suggesting that the nucleic acid binding region on NUDT16 is located in the same or a similar region on TIRR, enabling us to use information about how NUDT16 interacts with IMP to inform setting potential RNA-interacting residues on TIRR. To do this, we overlaid the structures of TIRR (PDB: 6D0L) and NUDT16 bound to IMP, and set active residues on TIRR which overlaid with residues on NUDT16 interacting with IMP (defined as residues on NUDT16 within 5Å of IMP) (**Figure 3.18.C**), which gave us residues 27, 29, 55-57, 61, 62, 110, 166, 168, 169, and 172. Having obtained residues which we now define as 'active' on TIRR for RNA binding, we performed modelling firstly on NUDT16 (PDB:3COU) with IMP, to assess if HADDOCK was able to successfully model a protein-ligand interaction. HADDOCK generated a single cluster solution, and we obtained a model which closely overlapped with the crystal structure of IMP and NUDT16 (PDB: 2XSQ) (**Figure 3.18.D**), suggesting that HADDOCK can model this interaction accurately. We then modelled the interaction with TIRR and IMP in HADDOCK using our defined active residues. Despite the fact that there is no evidence to suggest that TIRR actually binds IMP, we wanted to see if setting our active residues would be sufficient to model IMP correctly onto TIRR (as assessed by similarity to the NUDT16:IMP bound structure). HADDOCK generated three clusters for TIRR and IMP, and manual inspection of the top three clusters revealed that Cluster 1 yielded a structure which was highly similar to NUDT16 and IMP (**Figure 3.18.E**). We can therefore assume that these residues on TIRR would be sufficient to model TIRR binding to nucleic acid substrates, including RNA.

We then generated a structure of the RNA hairpin, using RNAfold[47] and RNAComposer[48]. For the HADDOCK model of the hairpin RNA and TIRR, we set active residues on the RNA which were found in the loop region of the hairpin (21, 22, 23, 24, 25, 26). We do not know exactly where on the RNA hairpin TIRR binds, however given that the affinity the RNA hairpin is similar to the ssRNA, and dsRNA binding to TIRR is weaker than ssRNA (**Figure 3.5.C**), we make the assumption that TIRR would bind to the single-stranded region of the hairpin in the loop. Modelling TIRR and the RNA hairpin yielded nine clusters and, after manual inspection of the top three clusters, we found that Cluster 1 gave a solution where the mode of engagement of the hairpin loop was similar to IMP (data not shown), which we selected as the most likely solution. All modelling performed by HADDOCK is summarised in **Table 3.1.**

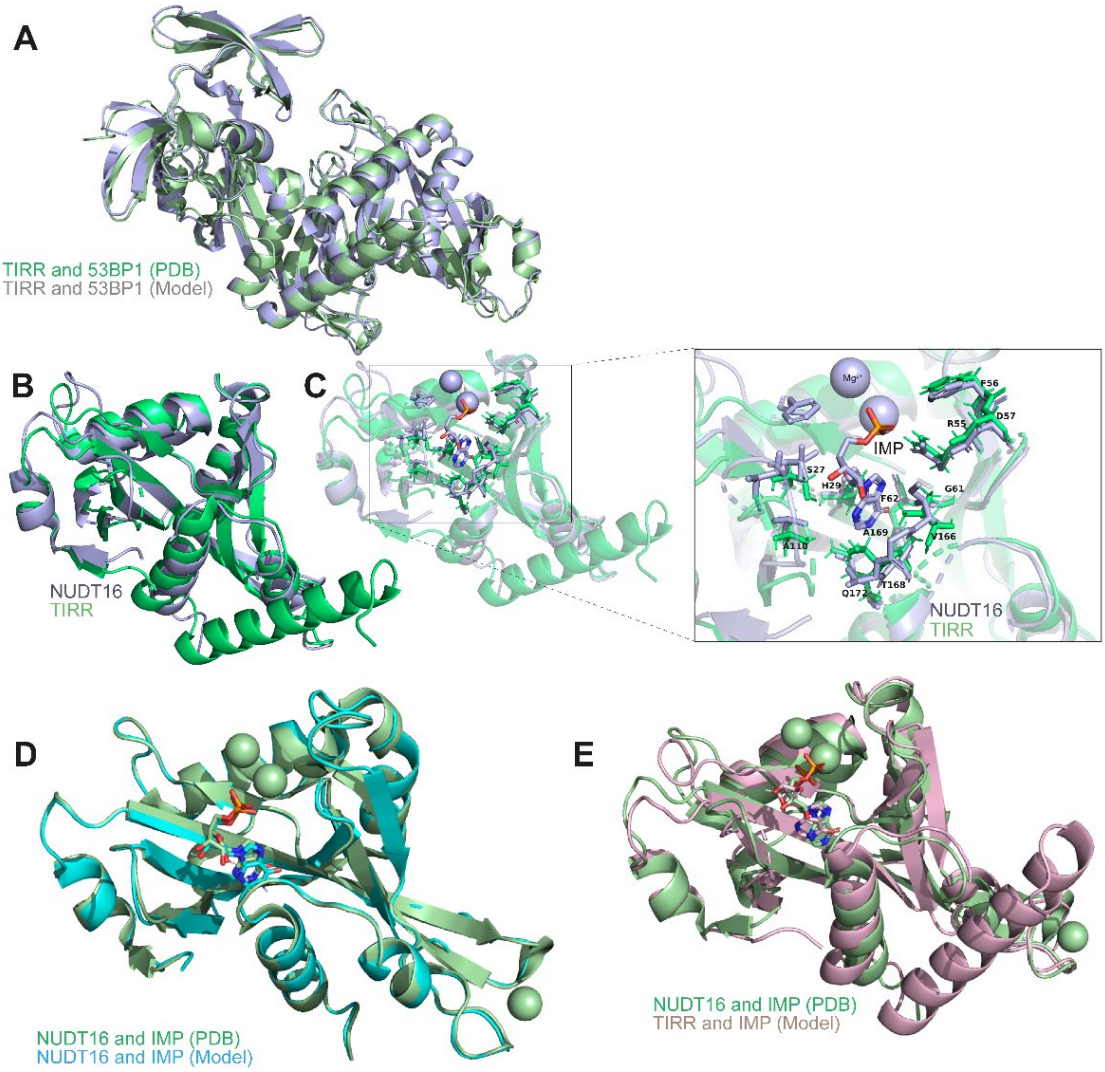


Figure 3.18: ***A)*** *Overlay of the modelled TIRR/53BP1 complex with the crystal structure of TIRR and 53BP1 (PDB: 6CO1).* ***B)*** *Overlay of NUDT16 (PDB: 3COU) and TIRR (PDB: 6D0L).* ***C)*** *The residues on NUDT16 within 5Å of IMP (PDB: 2XSQ) and the corresponding residues on TIRR (PDB: 6D0L) are highlighted.* ***D)*** *Overlay of the modelled NUDT16/IMP complex with the crystal structure of NUDT16 and IMP (PDB: 2XSQ).* ***E)*** *Overlay of the modelled TIRR/IMP complex with the crystal structure of NUDT16 and IMP (PDB: 2XSQ).*

Model	Input 1	Input 1 Active Residues	Input 2	Input 2 Active residues	Settings	Clusters Generated	Solution selected
TIRR/53BP1	TIRR PDB: 6D0L	105, 106, 107, 24, 101, 10, 20, 362	53BP1 PDB: 1XNI	1549, 1551, 1553, 1500, 1584, 1502, 1521, 1495, 1523	Protein-Protein	13	Cluster 1 (Top Ranked Z-Score)
NUDT16/IMP	NUDT16 PDB: 3COU	22, 24, 50, 51, 52, 56, 57, 61, 106, 108, 164, 165, 166, 167, 170	IMP Ligand	N/A	Protein-Ligand	1	Cluster 1 (Top Ranked Z-Score)
TIRR/IMP	TIRR PDB: 6D0L	27, 29, 55, 56, 57, 61, 62, 110, 166, 168, 169, 172	IMP Ligand	N/A	Protein-Ligand	3	Cluster 1 (Top Ranked Z-Score)
TIRR/Hairpin RNA	TIRR PDB: 6D0L	27, 29, 55, 56, 57, 61, 62, 110, 166, 168, 169, 172	RNA Hairpin	21, 22, 23, 24, 25, 26	Protein-Nucleic acid	9	Cluster 1 (Third Ranked Z-Score)

Table 3.1: *HADDOCK modelling parameters and inputs. All HADDOCK programs were run on default 'Easy' settings.*

3.3.16 Molecular Dynamics simulations of TIRR with hairpin RNA

HADDOCK generated a static model, however we are unable to say if this model is possible *in vivo* as we do not have any information about how this protein:RNA complex would behave and how stable this interaction would be. Therefore, to try and validate if this model is physiologically reasonable, we performed molecular dynamics simulations of the HADDOCK model generated. The HADDOCK model was used as the starting structure, and we slightly reduced the distance between TIRR and the RNA by manual positioning. This structure was then simulated using AMBER 20[49] performed by Dr Federica Battistini as part of our collaboration (**Sections 2.2.43 and 2.2.44** contain full details of the simulations). During the course of the 500ns simulation, we saw that the RNA 'adapts' to better interact with the TIRR protein cavity, improving the interaction with TIRR (**Figures 3.19.A and 3.19.B**).

To see how this RNA binding would influence 53BP1 binding to TIRR, we overlaid the structure of TIRR and RNA after 500ns of simulation with the structure of TIRR bound to 53BP1 (**Figure 3.19.C**). Overlaying the two structures reveals that the RNA and 53BP1 occupy almost the same site on TIRR. Comparing the interaction profiles of TIRR with 53BP1 and TIRR with RNA shows that many of the residues involved in the interaction of TIRR with 53BP1, in particular residues in the 53BP1-binding loop of TIRR (P105, H106, and R107), are also involved in the interaction with RNA (in red in **Figure 3.19.D**). During the course of the simulation, other residues also improved and stabilised the interaction between the RNA and TIRR dimer (residues closest to the RNA at the end of the simulation highlighted in blue in **Figure 3.19.D**). We also observed an improvement in the interaction energy from the contacts between the second protein of the TIRR dimer and the RNA hairpin (mainly lysine and arginine, in purple in **Figure 3.19.D**).

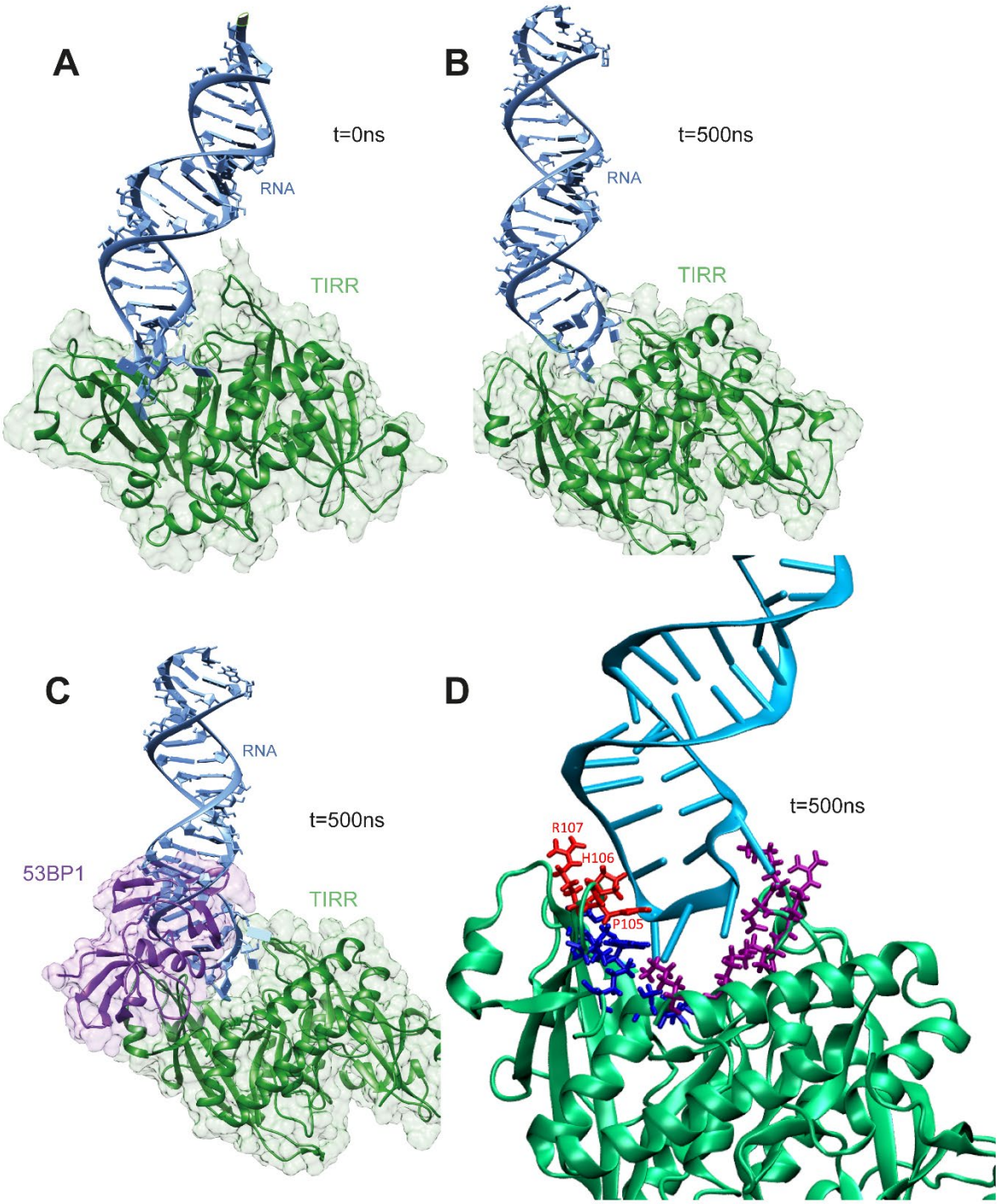


Figure 3.19: ***A)*** *Complex of the TIRR dimer (green) with the RNA hairpin (light blue) at the start (after equilibration, t=0ns) of the simulation.* ***B)*** *TIRR dimer and RNA at the end (after 500ns) of the simulation.* ***C)*** *Complex of the TIRR protein (green) with the RNA hairpin (light blue) after 500ns of MD simulation overlapped with the TIRR/53BP1 complex (purple).* ***D)*** *Complex of TIRR (green) with the RNA hairpin (light blue) with highlighted residues (shown in liquorice on the structure) on TIRR which are interacting with the RNA. In red are the residues known to interact and recognise 53BP1, in dark blue are additional residues of TIRR interacting with the RNA, and in purple are residues of the second TIRR monomer (as part of the TIRR dimer) interacting with the RNA. Molecular Dynamics simulations were performed by Dr Federica Battistini.*

We also performed the simulations with TIRR monomer and hairpin RNA and, as the monomer lacks interactions with the RNA within the second monomer of the TIRR dimer, the RNA has a bigger displacement during the course of the 500ns simulation (**Figures 3.20.A and 3.20.B**). However, we also observe that the RNA occupies the same site of binding as the 53BP1 at the end of the simulation (**Figures 3.20.C and 3.20.D**), and that the key residues on TIRR involved in the interaction with 53BP1 are also involved in the interaction with the hairpin (in red in **Figure 3.20.E**).

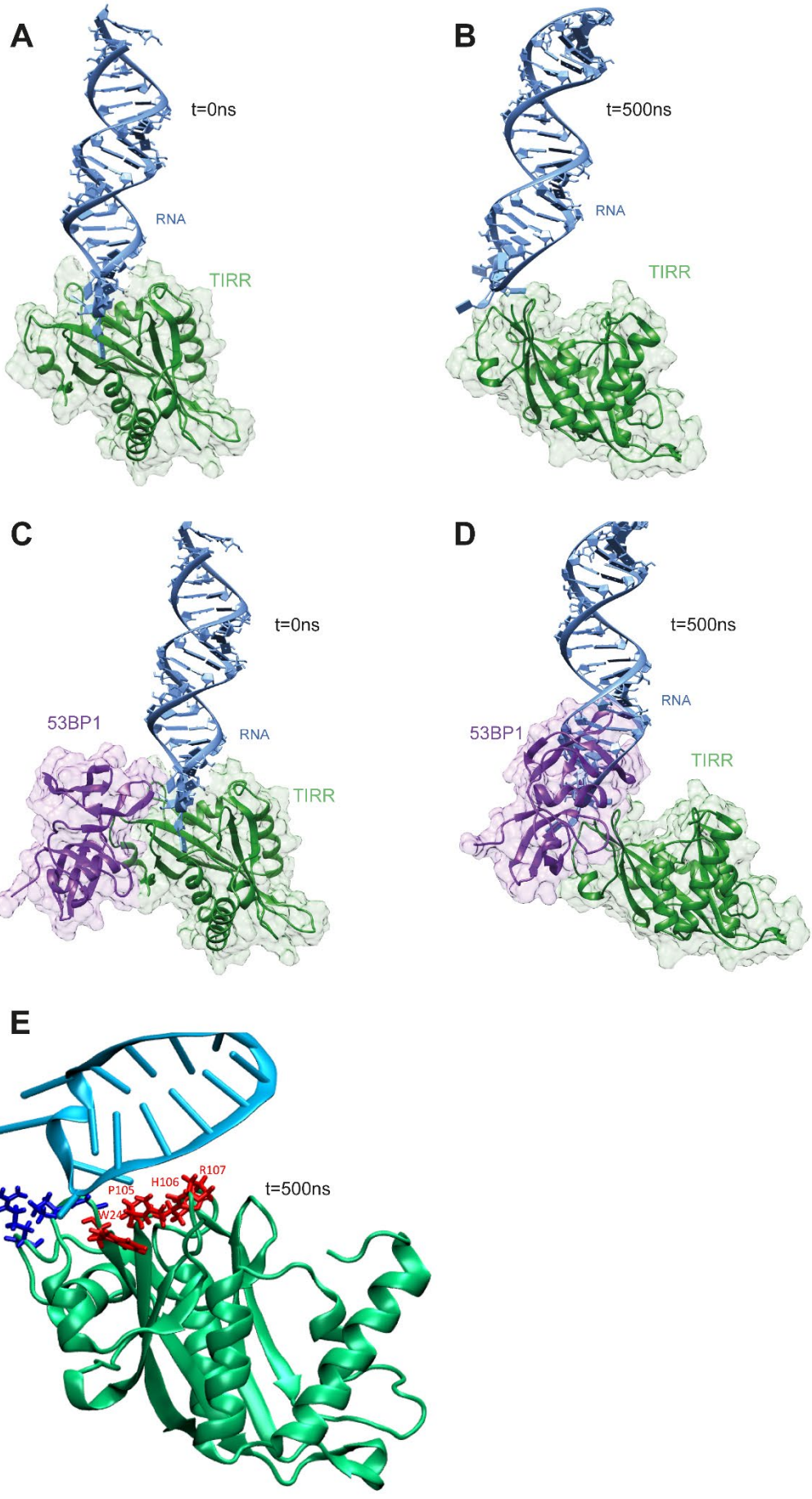

A
t=0ns
RNA
TIRR
B
t=500ns
RNA
TIRR
C
t=0ns
53BP1
RNA
TIRR
D
t=500ns
RNA
53BP1
TIRR
E
R107
H106
P105
W24
t=500ns

Figure 3.20: *Complex of the TIRR monomer protein (green) with the RNA hairpin (light blue)* ***A)*** *at the start of the MD simulation (after equilibration) and* ***B)*** *after 500ns of MD simulation.* ***C)*** *Complex of TIRR (green) with the RNA hairpin (light blue) overlapped with the complex of TIRR/53BP1 (purple), at the start of the MD simulation.* ***D)*** *as in C, at the end of the simulation.* ***E)*** *Zoomed complex of TIRR (green) with the RNA hairpin (light blue). Residues highlighted (liquorice) in TIRR which interact with the RNA. In red are the residues known to interact and recognise 53BP1, and in blue are additional residues of the TIRR monomer binding the RNA. Molecular Dynamics simulations were performed by Dr Federica Battistini.*

The simulated model of TIRR and RNA highlights that the binding of RNA to TIRR is incompatible with 53BP1 binding to TIRR, and suggests that hairpin RNA may compete with and displace 53BP1 from TIRR through occupation of the 53BP1 binding site. To fully confirm this model, it would be necessary to obtain the crystal structure of TIRR bound to RNA, however preliminary attempts to crystallise TIRR with RNA by our collaborators were unsuccessful. Nevertheless, this modelling provides a basis for understanding how RNA binding influences the TIRR/53BP1 interaction.

3.3.17 TIRR knockdown impairs HR

Finally, to assess the impact of TIRR knockdown on repair pathway choice between HR and NHEJ, we utilised the NHEJ and HR reporters E5J-GFP and DR-GFP[50]. TIRR has been shown to influence RPA and RAD51 foci formation, with TIRR knockdown reported to reduce RPA and RAD51 foci formation due to increased 53BP1 activity (**Table 1.1**). Therefore, we anticipated that TIRR knockdown may reduce HR efficiency. To examine this, we first used the E5J-GFP reporter to measure NHEJ after TIRR knockdown, or 53BP1 knockdown as a control. As expected, we can see that 53BP1 knockdown reduces NHEJ efficiency (**Figure 3.21.A**). After TIRR knockdown, we did not observe any significant impact on NHEJ efficiency (**Figure 3.21.A**). As a control, we also performed this assay in the presence of wortmannin, a PI3K inhibitor primarily acting on DNA-PK[51]. We observed that NHEJ efficiency was significantly reduced in the presence of wortmannin (**Figure 3.21.B**). We then assessed the impact of TIRR knockdown on HR efficiency. We knocked down BRCA1 as a

control and observed that HR efficiency was significantly reduced (**Figure 3.21.C**). After TIRR knockdown, we also saw a significant decrease in HR efficiency compared to the siNeg control (**Figure 3.21.C**). Whilst this decrease in HR efficiency was not as prominent as in the BRCA1 knockdown condition, it nevertheless suggests that TIRR knockdown impairs HR.

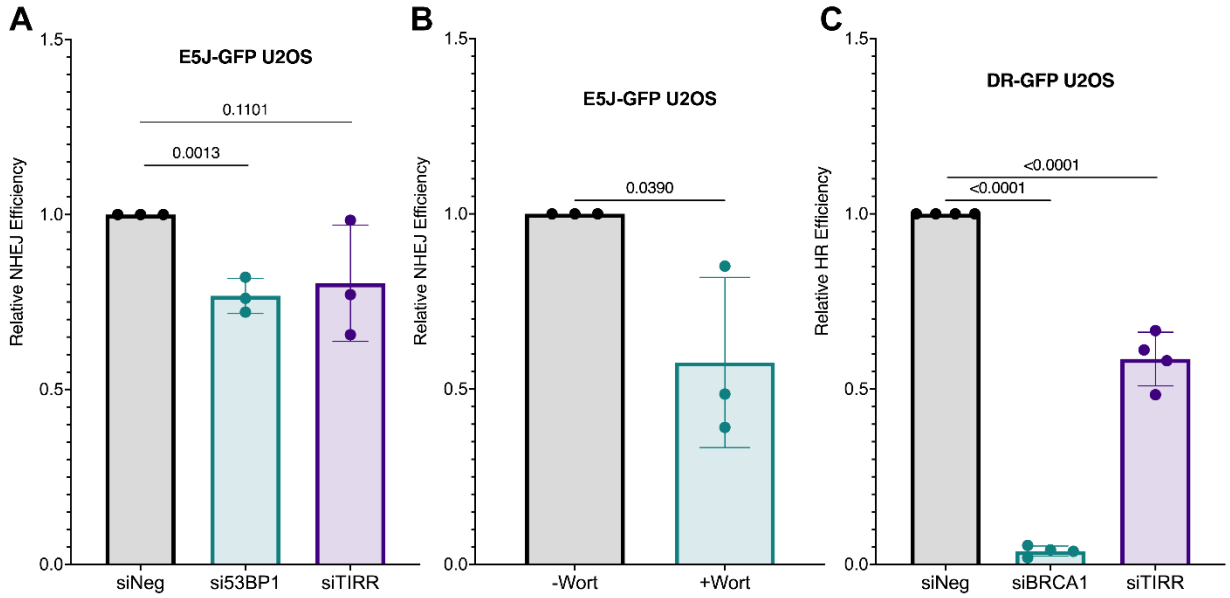


Figure 3.21: *Influence of TIRR knockdown on NHEJ and HR as assessed by E5J-GFP and DR-GFP reporters respectively.* ***A)*** *E5J-GFP reporter with siNeg, si53BP1, and siTIRR (mean ± sd, n=3).* ***B)*** *E5J-GFP reporter with wortmannin (Wort) treatment (mean ± sd, n=3).* ***C)*** *DR-GFP reporter with siBRCA1 and siTIRR (mean ± sd, n=4).*

3.4 Discussion

3.4.1 RNA can play a role in the dissociation of TIRR and 53BP1

TIRR and 53BP1 are known to separate after the induction of DSBs, although what contributes to this mechanism was unclear. ATM phosphorylation of 53BP1 was suggested to influence complex dissociation[2]. However, the observed RNA-binding ability of TIRR[1,6] and competition experiments with IMP[1], coupled with the increasing body of evidence which suggests a role for RNA in the DNA damage response, in particular in DSB repair, led us to hypothesise that RNA may play a role in TIRR/53BP1 dissociation.

In this chapter, I have described a mechanism of RNA-mediated dissociation of TIRR and 53BP1. We observe a contribution of RNAPII transcription, but not RNAPIII transcription, for TIRR and 53BP1 dissociation after IR (**Figures 3.3 and 3.4**). Additionally, we find that TIRR can be recruited to DSB sites, also dependent on RNAPII transcription, and this recruitment appears to be as a complex with 53BP1 (**Figures 3.13 and 3.14**). It was previously unknown if TIRR and 53BP1 dissociate in proximity to the DSB site or if this occurred distally to the break in the nucleoplasm, where the complex resides in non-damage conditions. Here we suggest that TIRR and 53BP1 are recruited as a complex, as 53BP1-binding null TIRR recruitment to damage was reduced compared to WT TIRR (**Figure 3.13**). Additionally, we find that Dicer and Drosha, but not DGCR8, are needed for TIRR and 53BP1 separation after damage, suggesting a non-canonical role of Dicer and Drosha (**Figure 3.11**).

We find that TIRR binds preferentially to ssRNA and RNA hairpins, and to a lesser extent dsRNA (**Figures 3.5 and 3.6**). Of these RNA substrates, a RNA hairpin was most effective in separating TIRR and 53BP1, implying that the structure of the RNA can influence complex dissociation, and this is seemingly independent of the sequence of the hairpin. Whilst we did

observe some activity of an RNA:DNA hybrid *in vitro*, we did not observe any effect of RNaseH1 WT overexpression on TIRR and 53BP1 dissociation (**Figure 3.10**). However, we cannot completely rule out a role of RNA:DNA hybrids due to several technical considerations (**Section 3.3.8**).

Additionally, through modelling and molecular dynamics simulations, we show how RNA would prevent the binding of 53BP1 to TIRR, as RNA and 53BP1 occupy the same binding site on TIRR (**Figures 3.18, 3.19, and 3.20**). Throughout the course of the MD simulations, residues found in the 53BP1-binding loop region of TIRR, such as Arg107, showed enhanced interaction with RNA. This overlap of residues involved in both 53BP1 and RNA binding further adds weight to the notion that TIRR binding to RNA would prevent 53BP1 binding.

Finally, we find that TIRR knockdown impairs the efficiency of repair by HR, consistent with the role of TIRR as a negative regulator of 53BP1 (**Figure 3.21**).

3.4.2 How does RNA outcompete 53BP1 binding to TIRR?

There are several outstanding questions which should be considered. The data from HTRF experiments (**Figure 3.8)** implies a direct competition of RNA with 53BP1 for TIRR binding, and one hypothesis is that RNA would be produced at DSBs, which then directly separates TIRR and 53BP1. Alternatively, if TIRR and 53BP1 have a high 'on/off' rate, meaning TIRR and 53BP1 may associate and separate dynamically, one could imagine a scenario where TIRR may bind RNA, which then precludes the binding of 53BP1. This seems like the more unlikely scenario, as we observe reduced recruitment of 53BP1-binding null TIRR to DSBs (**Figure 3.13**), implying TIRR and 53BP1 are recruited as a complex, which then separates.

For both these scenarios to be true, this suggests that TIRR would preferentially interact with

the RNA over 53BP1. TIRR showed a binding preference for ssRNA and hairpin RNA in SPR and EMSA assays, with a weak affinity (Kd) of ~100μM (**Figures 3.5 and 3.6**). The binding affinity of 53BP1 to TIRR has been shown to be around 1μM[52], so a direct competition of the hairpin RNA alone with 53BP1 for TIRR binding would likely be inefficient *in vivo* according to these experiments. This raises the question, how does RNA with a lower affinity for TIRR outcompete 53BP1? One explanation is that TIRR itself precipitates significantly *in vitro* at low salt concentrations needed to foster RNA-protein interactions. It is therefore possible that the binding affinity for TIRR with the RNA is underestimated as a result, as less functional TIRR would be available for RNA binding than actually calculated. Additionally, the Kd calculated by SPR is likely an underestimate as steady state was not reached, and therefore TIRR binding to RNA in our assays is likely stronger than we present here. Moreover, our data provide proof of principle for RNA-mediated dissociation, however it is highly probable that RNA actually produced at breaks in cells has a slightly different structure to that designed here (**Section 3.4.4**). Our RNA substrates were designed simply to adopt different commonly found RNA secondary structures, and were not based on any pre-existing knowledge of TIRR RNA binding preferences. Therefore, it is possible that RNA which is actually capable of TIRR and 53BP1 dissociation within cells may be better suited to TIRR binding and display a lower Kd and stronger binding affinity, and enabling it to out-compete TIRR and 53BP1 binding.

3.4.3 Would breaks produced in any genomic location result in RNA-mediated separation of TIRR and 53BP1?

Currently, it is not clear if DSBs occurring in different regions of the genome, such as transcribed or intergenic regions, would result in a different mechanism for the separation of TIRR and 53BP1. This raises the question, do all DSBs result in RNA-mediated separation of TIRR and 53BP1? *De novo* transcription at DSBs has been observed at DSBs occurring at different regions of the genome, including genic and intergenic regions[12,53], although not

unequivocally[10,54,55]. Therefore, it is possible that TIRR/53BP1 separation may be regulated differently depending on where in the genome DSBs occur. The resolution of PLA (or Co-IP) does not allow us to look at the separation of TIRR/53BP1 when DSBs are induced at a single site, which would allow the assessment of TIRR/53BP1 separation when DSBs are induced at different regions of the genome, however this would be an interesting focus of future studies.

Furthermore, FISH-PLA probes were designed to target RNA produced in the antisense direction to two cut A*si*SI sites, which we term DS1 and DS2 (**Figure 3.16**), which have been described to produce dilncRNA in previous studies[10,11]. Targeting the antisense transcript would allow the detection of *de novo* transcripts, and avoid the detection of ongoing transcription. Both DS1 and DS2 used in FISH-PLA are found within regions which have high transcriptional activity (promoter proximal and intragenic). Therefore, this assay could therefore be expanded to look at DSBs in other regions of the genome, such as those in intergenic and transcriptionally inactive regions.

3.4.4 What exactly RNA produced at breaks looks like remains enigmatic

We find that a hairpin structure appears to be significant in the separation of TIRR and 53BP1, with other structures tested (aside from RNA:DNA hybrids) having minimal effects on complex separation (**Figures 3.8 and 3.9**). Interestingly, it is not yet known exactly what structure (or structures) RNA transcribed at DSBs forms, although RNA:DNA hybrids as well as dsRNA have been described, likely aided by the availability of experimental tools such as antibodies recognising these structures (S9.6 and J2)[10]. However, we do know that transcription at DSBs can extend up to 1-3kb away from the break end[10–12]. We hypothesise that given the length of these single-stranded transcripts produced at DSBs, the dilncRNA are likely able to form RNA secondary structures, such as RNA hairpin-like structures, which could influence TIRR and 53BP1 separation. Whilst our findings suggest that a RNA hairpin secondary

structure has the capacity to separate TIRR and 53BP1 *in vitro* and *in vivo*, it is certainly possible that the actual RNA structure produced at breaks may differ slightly from this.

To support our *in vivo* data which showed RNA hairpins can dissociate TIRR and 53BP1 (**Figure 3.9**), other methods of introducing hairpins into cells were considered. One such example is expressing the hairpin RNA on a plasmid, such as in the MS2 system, where a plasmid expressing MS2 RNA hairpins (usually fused to an RNA of interest) is co-expressed with fluorescently labelled MS2-binding proteins which allow visualisation of the hairpins (and the RNA of interest)[56]. Whilst this would be advantageous in terms of increased half-life of the RNA hairpin expression, it was decided not to use the MS2 system as binding of the MS2-binding proteins to the hairpins may occlude access to the TIRR and 53BP1 complex. Additionally, without the fluorescently labelled MS2-binding protein, it would not be possible to visualise expression and location of the hairpins in the cell. Nevertheless, the MS2 system could potentially be used to confirm these results, without the positional information.

Additionally, increasing evidence has suggested that specific lncRNAs, such as LINP1, scaRNA2, and HITT, are recruited to DSBs and participate in DSB repair, such as through interactions with DNA repair proteins including DNA-PKc, ATM, and Ku70/Ku80 (**Section 1.5.2**)[57–60]. Some of these lncRNA, such as LINP1 and PRLH1, have been found to be upregulated after DSB induction[59,61]. Although the proximity to DSB-derived RNA of TIRR and 53BP1, and the involvement of Dicer and Drosha in separation, seem to suggest that DSB transcribed RNA is responsible for complex separation, it is possible that a lncRNA present at the break could influence TIRR and 53BP1 separation. LncRNA can also form structures including stem-loop hairpin-like structures[59]. This is a particularly interesting hypothesis, as it would account for the presence of RNA at breaks across the genome, as opposed to only in

certain regions of the genome, such as those with pre-existing transcriptional activity (**Section 3.4.3**).

3.4.5 What role do Dicer and Drosha play in TIRR/53BP1 dissociation?

In the canonical miRNA processing pathway, it is Dicer and Drosha cleavage activity which is important for their functions, with hairpin-shaped pri-miRNA processed by Drosha and DGCR8 in the nucleus into pre-miRNA, which is then exported to the cytoplasm where Dicer and TRBP cleave pre-miRNA into mature double stranded miRNA (**Section 1.5.1**). In our experiments, we find that the roles of Dicer and Drosha are independent of their canonical miRNA processing roles, as DGCR8 knockdown did not influence TIRR and 53BP1 separation (**Figure 3.11**), suggesting that this is related to the break-derived RNA-dependent DNA damage response. However, canonical cleavage by Dicer and Drosha would not result in a hairpin-shaped RNA, but instead a short dsRNA. Therefore, an unanswered question arises surrounding what role Dicer and Drosha play in RNA processing in relation to TIRR and 53BP1 separation?

The role of Dicer and Drosha in the RNA dependent DDR have been demonstrated in multiple publications, however the exact role which Dicer and Drosha carry out has been controversial in the literature. In the RNA-dependent DDR response, Dicer and Drosha cleavage and processing activities have been reported to be important in the biogenesis of DDRNA from longer dilncRNA, which can then act as signalling molecules[12]. DDRNA have been suggested to be single stranded, as they can hybridise to dilncRNA, or to other DDRNA[12]. The importance of Dicer catalytic activity in the processing of break-derived RNA has also been demonstrated[29], and Dicer has also been found to process dsRNA at DSBs[10]. However, one study found a role for Dicer, but not Drosha, in processing only a subset of dilncRNA into DDRNA[11]. Additionally, Dicer and Drosha have been shown to exert other roles outside of

miRNA biogenesis. Drosha can associate with RNAPII, binding to promoter-proximal regions of genes and promoting transcription, independently of Drosha cleavage activity[62]. Drosha is also recruited to DSBs by the MRN complex independently of the transcriptional status of the locus to promote NHEJ[63]. Dicer has also been shown to promote transcription termination at sites of transcription-replication conflict in S. *pombe*, promoting release of RNAPII at 3' ends of genes which are highly transcribed to maintain genome stability[64]. At 3' ends, Dicer is suggested to act on RNA hairpins formed by transcribed single-stranded RNA to promote transcription termination. Termination does not rely on Dicer catalytic activity, suggesting Dicer may bind to the RNA for recruitment of other proteins involved in RNAPII release[64]. Dicer depletion was also reported to actually make cells more resistant to DSB inducing agent Camptothecin by reducing Dicer-dependent let-7 biogenesis, resulting in upregulation of p21 and accumulation in G1, promoting NHEJ and decreasing HR[65]. Therefore, Dicer can promote HR independently of DDRNA production[65]. Interestingly, many Dicer binding sites have been identified in mRNA and lncRNA which are not processed by Dicer into smaller RNAs, and instead are hairpin structures to which Dicer binds near the loop region and stabilises the RNA[66]. Therefore, Drosha cleavage of a substrate could in theory result in pre-miRNA shaped RNA which bound to, but not further cleaved by Dicer, which is then loaded onto TIRR. Drosha, and to an extent Dicer, have also been shown to participate in RNA:DNA hybrid formation at DSBs, resulting in the recruitment of RNaseH1[40].

Dicer and Drosha could be involved independently of their dilncRNA processing roles in TIRR/53BP1 dissociation, such as in binding and stabilising RNA structures, or via modulating other signalling pathways through recruitment of other repair proteins or ATM signalling. However, we do not find any influence of Dicer and Drosha on ATM phosphorylation, ɣH2AX induction, nor on TIRR and 53BP1 total protein levels (**Figure 3.15**). We also have not found

any evidence, either in published literature or in our own pull-down mass spectrometry experiments (**Chapter 5**) to suggest that TIRR actually interacts with Dicer and Drosha, suggesting this is not protein-protein interaction mediated. Additional work, such as rescue experiments with catalytic mutants of Dicer and Drosha as part of future studies would further shed light on the mechanism of Dicer and Drosha involvement in TIRR/53BP1 dissociation.

3.4.6 Dissociation of the TIRR/53BP1 complex likely happens in proximity to the break, but what signalling pathways are involved in their recruitment?

Our data using 53BP1-binding null TIRR suggest that TIRR and 53BP1 are recruited as a complex for dissociation to the break (**Figure 3.13**). However, it can't be completely ruled out that the K10E mutation on TIRR may somehow influence TIRR interaction with other proteins or RNA, and therefore result in reduced TIRR recruitment to breaks independently of 53BP1 binding. Nevertheless, it appears that the TIRR is recruited to breaks mainly through 53BP1 binding. However, TIRR has been found on the chromatin[1] (and our observations, data not shown), so a pre-existing pool of chromatin bound TIRR may be present which is associated with γH2AX, with any additional TIRR recruited bound to 53BP1.

Additionally, while it seems the recruitment of TIRR and 53BP1 together to DSBs is dependent on RNAPII transcription (**Figure 3.14**), this raises an interesting question of what the signal for recruitment actually is. Does RNA act as a signalling molecule itself, or potentially lead to the recruitment of other proteins in a signalling cascade? We were not able to detect an interaction of TIRR with RNAPII (**Figure 3.14.G**), suggesting this is not a direct recruitment via interaction with the polymerase. It is also possible that the RNA dependent DDR and other damage signalling pathways can act together in the recruitment of TIRR and 53BP1 to breaks. For example, other proteins or post-translational modifications may contribute to this process of dissociation, such as ATM phosphorylation of 53BP1[1,2]. In agreement with this

literature, we found that ATM inhibition impaired the dissociation of TIRR and 53BP1 after IR, however RNAPII inhibition using either α-Amanitin or DRB, and Dicer and Drosha knockdown, did not influence pATM (S1981) after IR (**Figure 3.15**). This suggests that the RNA-dependent DDR may contribute to TIRR/53BP1 dissociation in concert with other pathways, such as ATM phosphorylation of 53BP1. It is also possible that ATM may regulate the RNA-dependent DNA damage response itself, such as by regulating phosphorylation of RNAPII at breaks. Indeed, ATM inhibition reduces RNAPII Y1P foci after IR[10].

3.4.7 How does other RNA in the cell not influence TIRR and 53BP1 binding: A possible role for RNA modifications?

We saw that RNA structure appears to influence TIRR and 53BP1 separation, with an RNA hairpin structure displaying the highest dissociation activity in HTRF assays (**Figure 3.8**), and we also observed that a transfected RNA hairpin has the ability to dissociate TIRR and 53BP1 (**Figure 3.9**). This raises interesting questions surrounding other hairpin structures in cells; mainly, if a hairpin can separate TIRR and 53BP1, how does the complex select for specific hairpins when RNA hairpins are not uncommon in cells (pre-microRNA or lncRNA for example), and how is the separation triggered only after DSBs have occurred? It is possible that the RNA produced at the breaks likely looks different to the RNA used in our assays to an extent (**Sections 3.4.2 and 3.4.4**), meaning that this RNA may have a somewhat 'unique' structure within the cell, which would then induce separation only after it is produced at DSBs. Furthermore, RNA modifications[67], such as m^6A[68] and m^5C[69], play important roles in DSB repair, and it is possible that the RNA responsible for TIRR/53BP1 dissociation could be modified. M^6A RNA modification has previously been shown to influence RNA structures, acting as a 'switch' for RNA-protein interaction through the regulation of binding motif accessibility on RNA, modulating binding to RNA binding proteins[70,71]. For example, RBMX/HNRNPG preferentially binds to a m^6A modified hairpin in the lncRNA MALAT1, as

m^{6}A modification of MALAT1 alters the RNA structure to enhance access of HNRNPG to a specific binding motif[71].

3.4.8 The significance of understanding TIRR/53BP1 separation: TIRR is amplified in breast cancers

Understanding the dissociation of TIRR and 53BP1 is clinically relevant. 53BP1 is involved in the development of resistance to PARPi (**Section 1.3.4**), and the amplification of TIRR, and subsequent proposed increase in 53BP1 binding and negative regulation, has been suggested as a mechanism of PARPi resistance development[1,2]. TIRR itself, found in the chromosomal region 16p13.3, is frequently amplified in cancer, in particular breast cancers[2] (**Figure 3.22.A**). It is interesting to note that when comparing patient and tumour samples with TIRR amplification to any amplifications of genes in the 16p13.3 region using patient data from TCGA PanCancer Atlas Studies accessed using cBioportal, TIRR is always amplified as part of a larger 16p13.3 region (**Figure 3.22.B and 3.22.C**). Interestingly, TIRR amplification is also associated with increased TIRR RNA expression (**Figure 3.22.D**). Increased TIRR expression is associated with deregulation of 53BP1 function (**Table 1.1**)[1,2,37] and has been suggested as a potential mechanism of PARP inhibitor resistance development. Therefore, understanding how the TIRR and 53BP1 complex is regulated, including by RNA, could help us target this complex and enhance the sensitivity of HR deficient cancer cells to PARP inhibitors.

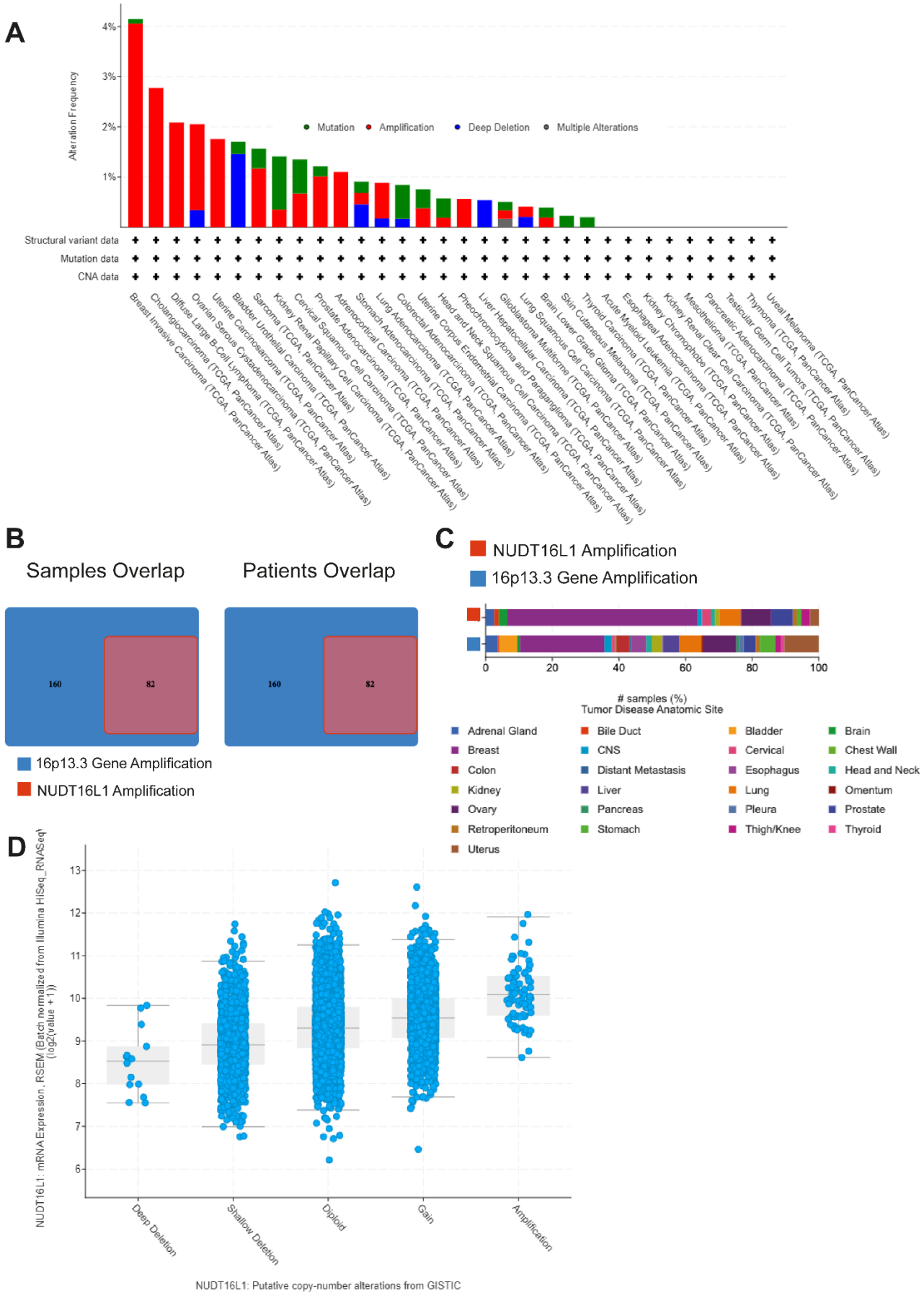

A
Alteration Frequency
4%
3%
2%
1%
Mutation
Amplification
Deep Deletion
Multiple Alterations
Structural variant data
Mutation data
CNA data
Breast Invasive Carcinoma (TCGA, PanCancer Atlas)
Cholangiocarcinoma (TCGA, PanCancer Atlas)
Diffuse Large B-Cell Lymphoma (TCGA, PanCancer Atlas)
Ovarian Serous Cystadenocarcinoma (TCGA, PanCancer Atlas)
Uterine Carcinosarcoma (TCGA, PanCancer Atlas)
Bladder Urothelial Carcinoma (TCGA, PanCancer Atlas)
Sarcoma (TCGA, PanCancer Atlas)
Kidney Renal Papillary Cell Carcinoma (TCGA, PanCancer Atlas)
Cervical Squamous Cell Carcinoma (TCGA, PanCancer Atlas)
Prostate Adenocarcinoma (TCGA, PanCancer Atlas)
Adrenocortical Carcinoma (TCGA, PanCancer Atlas)
Stomach Adenocarcinoma (TCGA, PanCancer Atlas)
Lung Adenocarcinoma (TCGA, PanCancer Atlas)
Colorectal Adenocarcinoma (TCGA, PanCancer Atlas)
Uterine Corpus Endometrial Carcinoma (TCGA, PanCancer Atlas)
Head and Neck Squamous Cell Carcinoma (TCGA, PanCancer Atlas)
Pheochromocytoma and Paraganglioma (TCGA, PanCancer Atlas)
Liver Hepatocellular Carcinoma (TCGA, PanCancer Atlas)
Glioblastoma Multiforme (TCGA, PanCancer Atlas)
Lung Squamous Cell Carcinoma (TCGA, PanCancer Atlas)
Brain Lower Grade Glioma (TCGA, PanCancer Atlas)
Skin Cutaneous Melanoma (TCGA, PanCancer Atlas)
Thyroid Carcinoma (TCGA, PanCancer Atlas)
Acute Myeloid Leukemia (TCGA, PanCancer Atlas)
Esophageal Adenocarcinoma (TCGA, PanCancer Atlas)
Kidney Chromophobe (TCGA, PanCancer Atlas)
Kidney Renal Clear Cell Carcinoma (TCGA, PanCancer Atlas)
Mesothelioma (TCGA, PanCancer Atlas)
Pancreatic Adenocarcinoma (TCGA, PanCancer Atlas)
Testicular Germ Cell Tumors (TCGA, PanCancer Atlas)
Thymoma (TCGA, PanCancer Atlas)
Uveal Melanoma (TCGA, PanCancer Atlas)
B
Samples Overlap
Patients Overlap
160
82
160
82
16p13.3 Gene Amplification
NUDT16L1 Amplification
C
NUDT16L1 Amplification
16p13.3 Gene Amplification
0
20
40
60
80
100
samples (%)
Tumor Disease Anatomic Site
Adrenal Gland
Bile Duct
Bladder
Brain
Breast
CNS
Cervical
Chest Wall
Colon
Distant Metastasis
Esophagus
Head and Neck
Kidney
Liver
Lung
Omentum
Ovary
Pancreas
Pleura
Prostate
Retroperitoneum
Stomach
Thigh/Knee
Thyroid
Uterus
D
NUDT16L1: mRNA Expression, RSEM (Batch normalized from Illumina HiSeq_RNASeq) (log2(value + 1))
13
12
11
10
9
8
7
6
Deep Deletion
Shallow Deletion
Diploid
Gain
Amplification
NUDT16L1: Putative copy-number alterations from GISTIC

Figure 3.22: ***A)*** *Amplification of TIRR across different cancer samples from the TCGA pan cancer atlas.* ***B)*** *Overlap of samples and patients with NUDT16L1/TIRR amplification and amplification of any gene which falls within the 16p13.3 region (the region where TIRR is found), without TIRR.* ***C)*** *Breakdown of tumour types with NUDT16L1/TIRR amplification and amplification of any gene which falls within the 16p13.3 region (the region where TIRR is found), without TIRR. Displayed as a percentage of the total number of samples.* ***D)*** *RNA expression of TIRR correlates with deletion or amplification of the TIRR gene.*

3.4.9 Outstanding questions and limitations of the study

Key questions remaining, alluded to in the above discussion, which should be answered in future studies include; How does a cell ensure RNA of a particular shape is produced at DSBs for separation? What does the RNA look like which can separate TIRR and 53BP1 and is this RNA modified? What signals or signalling pathways contribute to TIRR and 53BP1 complex recruitment to breaks? How do Drosha and Dicer act, potentially in RNA binding/processing, to promote TIRR/53BP1 dissociation?

Additional questions of interest include the fate of TIRR after 53BP1 dissociation. We suggest that TIRR may be only transiently recruited to DSBs, however it is not clear where TIRR goes within the cell after dissociating from 53BP1. Furthermore, more general questions about the role of RNA in DNA repair arise from these findings. Primarily, could RNA also play a role in regulating other protein-protein interactions outside of TIRR and 53BP1? RNA has previously been identified as a competitor of a protein-protein interaction with the RNAPII CTD for Pcf11 (cleavage and polyadenylation factor) in *S. cerevisiae*[72]. It is therefore possible that many more protein complexes could be regulated by RNA. TIRR has also been shown to influence p53 functions via 53BP1 binding[3], thus by extension, RNA may regulate other cellular processes by regulating protein-protein interactions. Furthermore, 53BP1 is also bound by other repair factors, such as NUMA1, and it is interesting to speculate that more 53BP1 binding interactions may be regulated by RNA. Interestingly, NUMA1 is also bound to 53BP1 in non-damage

conditions, and this binding is reduced after DNA damage[73], and NUMA1 was also identified as an RNA binding protein in the RBR-ID[6].

It is also important to be mindful of the limitations of the methods and experimental designs employed in a study. Here we show that RNAPII transcription is important for TIRR/53BP1 separation, which we interpret as a requirement of *de novo* transcription after DSBs have occurred. However, it is important to note that we can't exclude a requirement of pre-existing transcription for separation, as opposed to *de novo* break induced transcription. Furthermore, we can't exclude a role for RNA:DNA hybrids in our assays, as RNaseH1 overexpression is not 100% efficient at digesting all RNA:DNA hybrids. Additionally, whilst we interpret the PLA signal between RNA and TIRR/53BP1 observed in the FISH-PLA assay as RNA produced at the breaks being directly involved in TIRR/53BP1 separation, the maximum distance which can be measured in the assay is approximately 40nm. This is based on the length of an antibody being 10nm (primary + secondary with probe totalling 20nm), and the length of the FISH probe being approximately 20nm, giving a total maximum measurable distance of 40nm (approximately 117nt, based on the length of one nucleotide being around 0.34nm). This means that TIRR and 53BP1 could in theory be up to 40nm away from RNA produced at the breaks and still generate a PLA signal, meaning we can't say with certainty that the signal observed is due to a direct interaction/proximity. Additionally, solving the structure of TIRR bound to RNA would aid in designing a mutant TIRR which can bind 53BP1 but not RNA, to further explore the contribution of RNA to TIRR/53BP1 separation.

Nevertheless, taken together the evidence presented in this chapter suggests that RNA in proximity to DSBs could contribute to TIRR and 53BP1 complex separation (**Figure 3.23**),

highlighting an additional level of regulation of 53BP1 in DSB repair, as well as a new function of DSB-derived RNA in repair.

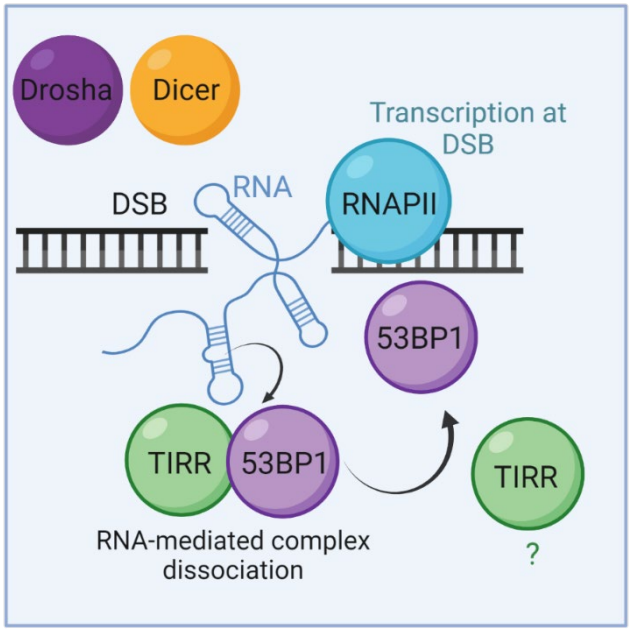


Figure 3.23: *Model of RNA-mediated TIRR/53BP1 dissociation.*

3.5 References

1. Botuyan, M. V. *et al.* Mechanism of 53BP1 activity regulation by RNA-binding TIRR and a designer protein. *Nat. Struct. Mol. Biol.* **25**, 591–600 (2018).
2. Drané, P. *et al.* TIRR regulates 53BP1 by masking its histone methyl-lysine binding function. *Nature* **543**, 211–216 (2017).
3. Parnandi, N. *et al.* TIRR inhibits the 53BP1-p53 complex to alter cell-fate programs. *Mol. Cell* **81**, (2021).
4. Zhang, A., Peng, B., Huang, P., Chen, J. & Gong, Z. The p53-binding protein 1-Tudor-interacting repair regulator complex participates in the DNA damage response. *J. Biol. Chem.* **292**, 6461–6467 (2017).
5. Avolio, R. *et al.* Protein Syndesmos is a novel RNA-binding protein that regulates primary cilia formation. *Nucleic Acids Res.* (2018) doi:10.1093/nar/gky873.
6. He, C. *et al.* High-Resolution Mapping of RNA-Binding Regions in the Nuclear Proteome of Embryonic Stem Cells. *Mol. Cell* **64**, (2016).
7. Alagia, A., Ketley, R. F. & Gullerova, M. Proximity Ligation Assay for Detection of R-Loop Complexes upon DNA Damage. in *R-Loops* (eds. Aguilera, A. & Ruzov, A.) vol. 2528 289–303 (Springer US, 2022).
8. Carpenter, A. E. *et al.* CellProfiler: image analysis software for identifying and quantifying cell phenotypes. *Genome Biol.* **7**, R100 (2006).
9. Quennet, V., Beucher, A., Barton, O., Takeda, S. & Löbrich, M. CtIP and MRN promote non-homologous end-joining of etoposide-induced DNA double-strand breaks in G1. *Nucleic Acids Res.* **39**, 2144–2152 (2011).
10. Burger, K., Schlackow, M. & Gullerova, M. Tyrosine kinase c-Abl couples RNA polymerase II transcription to DNA double-strand breaks. *Nucleic Acids Res.* (2019) doi:10.1093/nar/gkz024.
11. Bonath, F., Domingo-Prim, J., Tarbier, M., Friedländer, M. R. & Visa, N. Next-generation sequencing reveals two populations of damage-induced small RNAs at endogenous DNA double-strand breaks. *Nucleic Acids Res.* **46**, (2018).
12. Michelini, F. *et al.* Damage-induced lncRNAs control the DNA damage response through interaction with DDRNAs at individual double-strand breaks. *Nat. Cell Biol.* **19**, 1400–1411 (2017).
13. Wei, W. *et al.* A Role for Small RNAs in DNA Double-Strand Break Repair. *Cell* **149**, 101–112 (2012).
14. Michalik, K. M., Böttcher, R. & Förstemann, K. A small RNA response at DNA ends in Drosophila. *Nucleic Acids Res.* **40**, 9596–9603 (2012).
15. Tufegdzic Vidakovic, A. *et al.* Analysis of RNA polymerase II ubiquitylation and proteasomal degradation. *Methods* **159–160**, 146–156 (2019).
16. Kwiatkowski, N. *et al.* Targeting transcription regulation in cancer with a covalent CDK7 inhibitor. *Nature* **511**, 616–620 (2014).
17. Liu, S. *et al.* RNA polymerase III is required for the repair of DNA double-strand breaks by homologous recombination. *Cell* **184**, 1314-1329.e10 (2021).
18. Wu, L. *et al.* Novel Small-Molecule Inhibitors of RNA Polymerase III. *Eukaryot. Cell* **2**, 256–264 (2003).
19. van der Merwe, P. A. Surface Plasmon Resonance. in (2001). doi:10.1007/SpringerReference_33963.
20. Cytiva. Steady-state affinity analysis using Biacore systems.
21. Pryde, F. *et al.* 53BP1 exchanges slowly at the sites of DNA damage and appears to require RNA for its association with chromatin. *J. Cell Sci.* **118**, 2043–2055 (2005).
22. Degorce, F. *et al.* HTRF: A technology tailored for drug discovery - A review of theoretical aspects and recent applications. *Curr. Chem. Genomics* **3**, (2009).
23. Mhlanga, M. M., Vargas, D. Y., Fung, C. W., Kramer, F. R. & Tyagi, S. tRNA-linked molecular beacons for imaging mRNAs in the cytoplasm of living cells. *Nucleic Acids Res.* **33**, (2005).
24. Marnef, A. & Legube, G. R-loops as Janus-faced modulators of DNA repair. *Nat. Cell Biol.* **23**, (2021).
25. Bader, A. S. & Bushell, M. DNA:RNA hybrids form at DNA double-strand breaks in transcriptionally active loci. *Cell Death Dis.* **11**, (2020).
26. Domingo-Prim, J., Bonath, F. & Visa, N. RNA at DNA Double-Strand Breaks: The Challenge of Dealing with DNA:RNA Hybrids. *BioEssays* 1900225 (2020) doi:10.1002/bies.201900225.
27. Chen, L. *et al.* R-ChIP Using Inactive RNase H Reveals Dynamic Coupling of R-loops with Transcriptional Pausing at Gene Promoters. *Mol. Cell* **68**, 745 (2017).
28. Burger, K. *et al.* Nuclear phosphorylated Dicer processes double-stranded RNA in response to DNA damage. *J. Cell Biol.* **216**, 2373–2389 (2017).
29. Francia, S. *et al.* Site-specific DICER and DROSHA RNA products control the DNA-damage response. *Nature* **488**, 231–5 (2012).
30. Hang, Q. *et al.* Non-canonical function of DGCR8 in DNA double-strand break repair signaling and tumor radioresistance. *Nat. Commun.* **12**, (2021).
31. Panier, S. & Boulton, S. J. Double-strand break repair: 53BP1 comes into focus. *Nat. Rev. Mol. Cell Biol.* **15**, 7–18 (2014).

32. Rassoolzadeh, H., Coucoravas, C. & Farnebo, M. The proximity ligation assay reveals that at DNA double-strand breaks WRAP53β associates with γH2AX and controls interactions between RNF8 and MDC1. *Nucleus* **6**, (2015).
33. Lukas, C., Bartek, J. & Lukas, J. Imaging of protein movement induced by chromosomal breakage: tiny 'local' lesions pose great 'global' challenges. *Chromosoma* **114**, 146–154 (2005).
34. Lee, D. *et al.* ZMYM2 restricts 53BP1 at DNA double-strand breaks to favor BRCA1 loading and homologous recombination. *Nucleic Acids Res.* **50**, 3922–3943 (2022).
35. Rother, M. B. *et al.* CHD7 and 53BP1 regulate distinct pathways for the re-ligation of DNA double-strand breaks. *Nat. Commun.* **11**, 5775 (2020).
36. Wang, W.-Y. *et al.* Interaction of FUS and HDAC1 regulates DNA damage response and repair in neurons. *Nat. Neurosci.* **16**, 1383–1391 (2013).
37. Wang, J. *et al.* Molecular basis for the inhibition of the methyl-lysine binding function of 53BP1 by TIRR. *Nat. Commun.* **9**, (2018).
38. Bensaude, O. Inhibiting eukaryotic transcription. Which compound to choose? How to evaluate its activity?: Which compound to choose? How to evaluate its activity? *Transcription* **2**, 103–108 (2011).
39. Pessina, F. *et al.* Functional transcription promoters at DNA double-strand breaks mediate RNA-driven phase separation of damage-response factors. *Nat. Cell Biol.* **21**, 1286–1299 (2019).
40. Lu, W.-T. *et al.* Drosha drives the formation of DNA:RNA hybrids around DNA break sites to facilitate DNA repair. *Nat. Commun. 2018 91* **9**, 1–13 (2018).
41. Massip, L., Caron, P., Iacovoni, J. S., Trouche, D. & Legube, G. Deciphering the chromatin landscape induced around DNA double strand breaks. *Cell Cycle* **9**, 3035–3044 (2010).
42. Iacovoni, J. S. *et al.* High-resolution profiling of γH2AX around DNA double strand breaks in the mammalian genome. *EMBO J.* **29**, 1446–1457 (2010).
43. Iannelli, F. *et al.* A damaged genome's transcriptional landscape through multilayered expression profiling around in situ-mapped DNA double-strand breaks. *Nat. Commun.* **8**, (2017).
44. Aymard, F. *et al.* Transcriptionally active chromatin recruits homologous recombination at DNA double-strand breaks. *Nat. Struct. Mol. Biol.* **21**, 366–374 (2014).
45. van Zundert, G. C. P. & Bonvin, A. M. J. J. Modeling protein–protein complexes using the HADDOCK webserver "modeling protein complexes with HADDOCK". *Methods Mol. Biol.* **1137**, (2014).
46. Trésaugues, L. *et al.* Structural Basis for the Specificity of Human NUDT16 and Its Regulation by Inosine Monophosphate. *PLOS ONE* **10**, e0131507 (2015).
47. Lorenz, R. *et al.* ViennaRNA Package 2.0. *Algorithms Mol. Biol.* **6**, (2011).
48. Biesiada, M., Pachulska-Wieczorek, K., Adamiak, R. W. & Purzycka, K. J. RNAComposer and RNA 3D structure prediction for nanotechnology. *Methods* **103**, (2016).
49. Case, D. A. *et al.* Amber 2021. (2021) doi:10.13140/RG.2.2.15902.66881.
50. Bennardo, N., Cheng, A., Huang, N. & Stark, J. M. Alternative-NHEJ Is a Mechanistically Distinct Pathway of Mammalian Chromosome Break Repair. *PLoS Genet.* **4**, e1000110 (2008).
51. Hashimoto, M. *et al.* DNA-PK: the Major Target for Wortmannin-mediated Radiosensitization by the Inhibition of DSB Repair via NHEJ Pathway. *J. Radiat. Res. (Tokyo)* **44**, 151–159 (2003).
52. Dai, Y., Zhang, A., Shan, S., Gong, Z. & Zhou, Z. Structural basis for recognition of 53BP1 tandem Tudor domain by TIRR. *Nat. Commun.* **9**, (2018).
53. D'Alessandro, G. *et al.* BRCA2 controls DNA:RNA hybrid level at DSBs by mediating RNase H2 recruitment. *Nat. Commun. 2018 91* **9**, 1–17 (2018).
54. Domingo-Prim, J. *et al.* EXOSC10 is required for RPA assembly and controlled DNA end resection at DNA double-strand breaks. *Nat. Commun.* **10**, 1–13 (2019).
55. Vítor, A. C. *et al.* Single-molecule imaging of transcription at damaged chromatin. *Sci. Adv.* **5**, eaau1249 (2019).
56. George, L., Indig, F. E., Abdelmohsen, K. & Gorospe, M. Intracellular RNA-tracking methods. *Open Biol.* **8**, 180104 (2018).
57. Zhao, K., Wang, X., Xue, X., Li, L. & Hu, Y. A long noncoding RNA sensitizes genotoxic treatment by attenuating ATM activation and homologous recombination repair in cancers. *PLOS Biol.* **18**, e3000666 (2020).
58. Zhang, Y. *et al.* Long noncoding RNA LINP1 regulates repair of DNA double-strand breaks in triple-negative breast cancer. *Nat. Struct. Mol. Biol.* **23**, 522–530 (2016).
59. Thapar, R. *et al.* Mechanism of efficient double-strand break repair by a long non-coding RNA. *Nucleic Acids Res.* **48**, (2020).
60. Bergstrand, S. *et al.* Small Cajal body-associated RNA 2 (scaRNA2) regulates DNA repair pathway choice by inhibiting DNA-PK. *Nat. Commun.* **13**, 1015 (2022).
61. Deng, B. *et al.* An LTR retrotransposon-derived lnc RNA interacts with RNF 169 to promote homologous recombination. *EMBO Rep.* **20**, (2019).
62. Gromak, N. *et al.* Drosha Regulates Gene Expression Independently of RNA Cleavage Function. *Cell Rep.* **5**, 1499–1510 (2013).

63. Cabrini, M. *et al.* DROSHA is recruited to DNA damage sites by the MRN complex to promote non-homologous end joining. *J. Cell Sci.* **134**, jcs249706 (2021).
64. Castel, S. E. *et al.* Dicer Promotes Transcription Termination at Sites of Replication Stress to Maintain Genome Stability. *Cell* **159**, 572–583 (2014).
65. Liu, B. *et al.* DICER-dependent biogenesis of let-7 miRNAs affects human cell response to DNA damage via targeting p21/p27. *Nucleic Acids Res.* **43**, (2015).
66. Rybak-Wolf, A. *et al.* A variety of dicer substrates in human and C. elegans. *Cell* **159**, (2014).
67. Jimeno, S., Balestra, F. R. & Huertas, P. The Emerging Role of RNA Modifications in DNA Double-Strand Break Repair. *Front. Mol. Biosci.* **8**, (2021).
68. Zhang, C. *et al.* METTL3 and N6-Methyladenosine Promote Homologous Recombination-Mediated Repair of DSBs by Modulating DNA-RNA Hybrid Accumulation. *Mol. Cell* **79**, 425-442.e7 (2020).
69. Chen, H. *et al.* m5C modification of mRNA serves a DNA damage code to promote homologous recombination. *Nat. Commun.* **11**, 2834 (2020).
70. Liu, N. *et al.* N(6)-methyladenosine-dependent RNA structural switches regulate RNA-protein interactions. *Nature* **518**, 560–564 (2015).
71. Liu, N. *et al.* N6-methyladenosine alters RNA structure to regulate binding of a low-complexity protein. *Nucleic Acids Res.* **45**, 6051–6063 (2017).
72. Hollingworth, D., Noble, C. G., Taylor, I. A. & Ramos, A. RNA polymerase II CTD phosphopeptides compete with RNA for the interaction with Pcf11. *RNA* **12**, (2006).
73. Moreno, N. S. *et al.* The nuclear structural protein NuMA is a negative regulator of 53BP1 in DNA double-strand break repair. *Nucleic Acids Res.* **47**, 10475–10475 (2019).
74. Rocha, C. R. R., Silva, M. M., Quinet, A., Cabral-Neto, J. B. & Menck, C. F. M. DNA repair pathways and cisplatin resistance: an intimate relationship. *Clinics* **73**, e478s (2018).
75. Dziadkowiec, K. N., Gąsiorowska, E., Nowak-Markwitz, E. & Jankowska, A. PARP inhibitors: review of mechanisms of action and BRCA1/2 mutation targeting. *Menopausal Rev.* **4**, 215–219 (2016).

Chapter 4: The wider influence of TIRR on DNA damage and Repair

4.1 Summary

TIRR is an RNA binding protein with poorly understood function. TIRR can bind many different RNA species, and very preliminary evidence suggests that this could be dependent on cell stress[1,2]. TIRR also plays an important role in the DNA damage response through 53BP1 regulation (**Chapter 3**)[3,4]. Here, we investigate if TIRR RNA binding may play additional roles in the response to DNA damage and cell stress. Using a combination of RIP-Seq, RNA-Seq, Mass Spectrometry on whole cell lysates (WCL), and *in vivo* experiments, we find that TIRR can bind to different RNAs involved in RNA metabolism and transcription, and suggest that TIRR may augment the DDR through RNA binding and regulation. We further show that TIRR can localise to RNA-containing membrane-less cytoplasmic compartments known as stress granules and processing bodies, and find that TIRR may regulate the formation of these compartments in response to stress. We also identify a Nuclear Export Sequence motif in TIRR and show that TIRR interacts with Exportin-1 after DNA damage, likely through this motif, suggesting TIRR export into the cytoplasm may be important for TIRR function after damage. In addition, during the course of our investigation on TIRR, we found that multiple different siRNAs used for knockdown of TIRR elicit off-target effects resulting in cell death. We summarise these knockdown experiments to illustrate the importance of choosing an appropriate knockdown method when studying TIRR. Taken together, this preliminary characterisation of TIRR RNA binding function after DNA damage suggests that in addition to 53BP1 binding, TIRR may also influence the DNA damage response through the regulation of RNA processing.

4.2 Introduction

Whilst the role of TIRR in 53BP1 binding and regulation in the DSB repair response has received a lot of attention since the initial characterisation of TIRR as a 53BP1 binding partner in late 2017/early 2018[3,5,6], the wider role of TIRR outside of 53BP1 binding has not been extensively explored, especially in the context of DNA damage. As detailed in Chapter 3, the RNA binding function of TIRR is mutually exclusive with 53BP1 binding, and therefore the RNA binding role of TIRR is likely distinct from 53BP1 binding.

TIRR has been characterised as an RNA binding protein[1,7] (and **Chapter 3**), binding a wide range of RNA, particularly mRNA[1]. Initial characterisation of the role of TIRR via RNA binding suggest that TIRR can act as a translational repressor, with TIRR overexpression resulting in reduced translation. TIRR knockdown conversely results in increased translation, as assessed by [^{35}S]-Met/Cys labelling[1]. Furthermore, the majority of differentially translated mRNA in ribosome profiling experiments upon TIRR overexpression were downregulated (1368/2058, 66.5%). A total of 399 mRNA of the 2058 differentially translated mRNA are direct binding targets of TIRR as identified by iCLIP-Seq in non-damage conditions[1]. This suggests that TIRR may, at least in part, regulate RNA translation through direct association with specific mRNA[1]. Interestingly, as well as mRNA, TIRR was also identified as a pre-miRNA binding protein in *in vitro* capture and mass spectrometry experiments. TIRR binds multiple different pre-miRNA[8], although it has not yet been investigated if this plays a role in miRNA maturation or miRNA-mediated silencing. Preliminary data also showed TIRR can to localise to stress granules and colocalise with RNA poly(A) signals after oxidative stress[2]. Therefore, TIRR binds a broad spectrum of RNA in non-damage cells, with poorly characterised functionality, but may exhibit some regulation in these RNA binding properties after cell stress.

Stress granules (SGs) and Processing bodies (P-bodies or PBs) are the two main types of cytoplasmic RNA granules in cells[9]. SGs and PBs are cytoplasmic membrane-less compartments which contain RNAs and various RNA-binding proteins (RBPs). In general, PBs and SGs are considered to be sites of non-translating mRNA, and their formation depends on the repression of translation and polysome (mRNA with a cap and poly(A) tail, with multiple ribosomes bound) disassembly[10]. In agreement with this, the number of SGs and PBs increases after cell stress, reflecting a general repression of translation. PBs are also present in unstressed conditions, with an estimated ~10-20% of RNAs existing in RNA granules in unstressed cells[9,11], but can be further induced in number after cell stress. PBs contain components of the mRNA degradation machinery, such as DCP1/2, XRN1, and the CCR4-NOT complex, which are involved in mRNA decapping and deadenylation, as well as components of the miRNA pathway, such as GW182 and miRNAs[12]. SGs on the other hand are not usually present in unstressed cells, and are induced after cell stress, such as oxidative damage induced by Sodium Arsenite (SA) treatment. Stress granules are comprised of RNAs which are stalled at the point of translation initiation, and therefore contain translation initiation factors, such as poly(A) binding protein (PABP), 40S ribosomal subunits, and EIF4B and EIF4G, in contrast to PBs which mostly do not contain translation initiation factors aside from EIF4E[13,14]. In addition to proteins involved in the regulation of translation, SGs and PBs contain a wide variety of proteins involved in RNA processing, for example, identified PB proteins include those involved in splicing, mRNA transport, and transcription[15]. However, some RBPs and RNAs can localise in both compartments, such as eIF4E and XRN1, which associate with PBs in unstressed conditions, but then relocalise to SGs after stress[16]. Moreover, SGs and PBs are known to be highly dynamic, and can often associate and are juxtaposed to one another[16]. Both PBs and SGs can associate with polysomes[17] and mRNAs can move between polysomes where

they are translated, and SGs and PBs, where they can be either stored and re-enter translation or are degraded, in a model known as the mRNA cycle[11,13,17]. Factors influencing PB and SG assembly include RNA length, with longer RNAs preferentially sequestered into RNA granules, potentially due to an increase in RNA:RNA interactions[18], increased RBP binding or RNA secondary structure[9], or a reduced translation efficiency[19]. Additionally, RNAs in PBs tend to be AU-rich[19], and RNAs sequestered in SGs can also contain AU-rich elements[9]. Furthermore, PTMs of PB and SG proteins as well as RNA modification may also influence granule formation[14]. For example, m^6A and m^1A modified RNAs were found to be enriched in SGs[18].

Functionally, SGs are thought to promote cell survival after stress by sequestering mRNAs which stall at translation initiation, triggered by phosphorylation of EIF2A, resulting in the run off of actively translating ribosomes and disassembly of polysomes[16,18]. SGs are considered storage sites for RNA, preventing unnecessary translation and energy expenditure during stress conditions[9,13], and these RNA can either re-enter translation or are degraded[13]. Initially, SGs were proposed to generally sequester RNA after stress, however the process of sequestration appears to be much more regulated, with specific RNA transcripts localised to SGs in different stress conditions[9]. Additionally, not all RNAs which are translationally repressed after stress are universally targeted to SGs, and RNAs which do not have translational capacity can be recruited to SGs, such as the lncRNA NORAD after ER stress[9].

PBs were considered to be the key sites of mRNA decay, although it is now apparent that PBs can also facilitate the storage of RNA, preventing decay and stabilising specific RNAs[10,17,19]. RNAs targeted to PBs appear to be related to dynamic regulatory processes, for example RNAPII transcription. This suggests PBs may contribute to the regulation of RNA fate

(translation and/or storage/decay) under different conditions, allowing PBs to dynamically influence the cellular response to specific stimuli[11]. In agreement with this, PBs have been shown to promote either stability or decay of specific RNAs after different stressors, in order to promote cell survival[17]. In yeast, RNA binding protein Puf5p was able to exhibit dual functionality on different RNAs, both to promote RNA decay in PBs (likely through interaction with the CCR4-NOT complex) and stability (by localising an mRNA into P-bodies), depending on the individual RNA[17]. Therefore, the fate of each RNA within PBs may depend on the specific RNA, the RNA binding protein to which it binds, and the cellular context[17]. PBs have also been suggested to be involved in feedback loops, as RNAs encoding PB proteins were found to be enriched in PBs, suggesting a potential mechanism of 'self-regulation' of PB formation[11].

Aside from cell stressors such as oxidative stress induced by SA, the formation of SGs and PBs also appears to occur when DNA is damaged. In response to UV damage, translation is downregulated and SGs can form 1h post-exposure. Unlike SA induced SG formation, UV-induced SG formation can occur independently of EIF2A phosphorylation-dependent translation arrest, indicating that distinct mechanisms regulate SG formation dependent on the type of stress/damage[20,21]. Furthermore, after replication stress, the PB component Lsm1 can bind a subset of RNAs which are needed for cell survival. Lsm1 binds to the YOX1 mRNA and promotes its degradation in PBs, preventing YOX1 accumulation and promoting the expression of genes needed for the replication stress response and survival[22]. Additionally, P-body formation was influenced by Mec1 and Tel1 in yeast (ATR and ATM in humans), highlighting a link between PB formation and the DDR[23].

I describe above the role of TIRR in DSB repair, showing its differential binding to 53BP1 in

damage and non-damage conditions, regulated by RNA (**Chapter 3**). Since DNA damage is known to generally impact RNA metabolism/functions, we wanted to assess if TIRR may regulate RNA metabolism in response to DSBs. Given that so little is known about the function of TIRR RNA-binding, TIRR could in theory participate at any stage of RNA metabolism, such as transcription, splicing and export from the nucleus, translation into proteins, and RNA decay[9]. To this end, we first optimise our knockdown of TIRR. We then performed RNA immunoprecipitation experiments to identify RNA bound to TIRR after DNA damage. We performed RNA sequencing and WCL mass spectrometry, to assess if TIRR knockdown would subsequently impact steady-state RNA or protein levels respectively. Notably, TIRR binds to RNAs involved in RNA metabolism and RNAPII transcription, and can also interact with nuclear export machinery after DNA damage. We further show that TIRR can localise to both PBs and SGs, and may participate in the regulation RNA granule formation. These experiments begin to characterise the role of TIRR in RNA binding and in the regulation of the DNA damage response.

4.3 Results

4.3.1 Optimising the knockdown of TIRR

In order to study a protein's function, the ability to significantly reduce the level of a protein of interest specifically without inducing off-target effects is critical for the interpretation of the phenotype under study. Knockdown using siRNA is a widely used method to study the biological function of a protein of interest due to its ease of use, relatively low cost, and the ability to achieve high levels of knockdown (upwards of ~90%) in only 24-48 hours after transfection. To study the function of TIRR in the wider DNA damage response, siRNA knockdown of TIRR was performed. Initial knockdown experiments using an individual predesigned siRNA from Sigma (SASI_Hs01_00138264, referred to as Sigma siRNA) against TIRR in Hela cells resulted in a high level of knockdown of TIRR at the protein level as assessed by western blot (**Figure 4.1.A**). Unexpectedly, knockdown of TIRR using this siRNA in Hela cells resulted in a reproducibly high level of cell death (**Figures 4.1.B and 4.1.C**). The loss of viability after TIRR knockdown was consistently observed across the three different cell lines tested; Hela, MDA-MB-436 (**Figures 4.1.D, 4.1.E, and 4.1.F**), and HCC1937 (**Figure 4.1.G, 4.1H, and 4.1.I**), indicating that cell death upon TIRR knockdown using the Sigma siRNA was not variable between cell lines. Given that TIRR knockdown has not been previously reported to negatively impact cell survival, we wanted to explore this effect further and assess if TIRR knockdown impacted cell survival due to an essential cellular role of TIRR, or due to an unspecific effect of the siRNA knockdown itself.

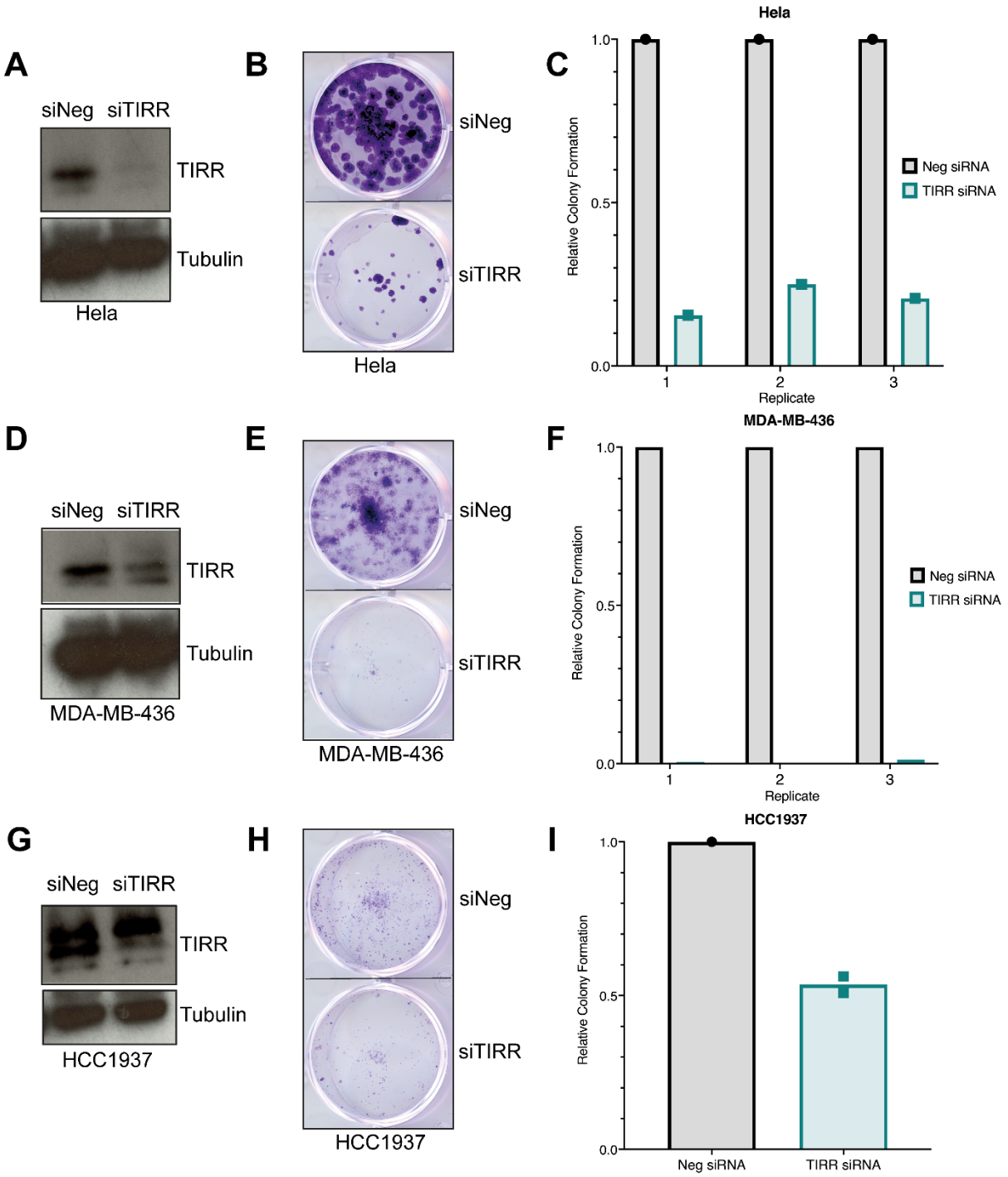


Figure 4.1: *Knockdown of TIRR using Sigma Predesigned siRNA (SASI_Hs01_00138264) in different cell lines.* ***A)*** *Western blot confirming knockdown of TIRR in Hela cells.* ***B)*** *Colony formation of Hela cells treated with a non-targeting negative control siRNA or TIRR siRNA for 24 hours, before replating into 12-well plates and being allowed to form colonies for ~10 days.* ***C)*** *Quantification of the colony formation from B of Hela cells treated with TIRR siRNA compared to the negative control siRNA (n=3).* ***D)*** *Western blot confirming knockdown of TIRR in MDA-MB-436 cells.* ***E)*** *As in B, in MDA-MB-436 cells.* ***F)*** *Quantification of E (n=3).* ***G)*** *Western blot confirming knockdown of TIRR in HCC1937 cells.* ***H)*** *As in B, in HCC1937 cells.* ***I)*** *Quantification of H (n(siNeg)=1, n(siTIRR)=2). SiNeg is a non-targeting siRNA control (***Table 2.6).**

To further explore the effect of TIRR knockdown on cell viability, we selected additional siRNAs targeting TIRR. Firstly, an individual siRNA targeting TIRR available from Thermo Fisher (Assay ID HSS189023, Stealth siRNA, referred to as Thermo siRNA) was selected[3]. This siRNA effectively reduced the protein level of TIRR, and also induced significant cell death as assessed by the colony formation potential in both Hela and MDA-MB-436 cells (**Figures 4.2.A, 4.2B, 4.2.C, and 4.2.D**). We also observed a significant reduction in S phase cells and an accumulation in G1 when cells were treated with either Sigma or Thermo siRNAs, as assessed by Edu incorporation and DAPI staining in both Hela and MCF7 cells (**Figures 4.2E, 4.2.F, and 4.2.G**). We also confirmed this was not due to the specific batch of siRNA, as knockdown of TIRR using a second vial of Thermo siRNA also resulted in comparable cell death (data not shown).

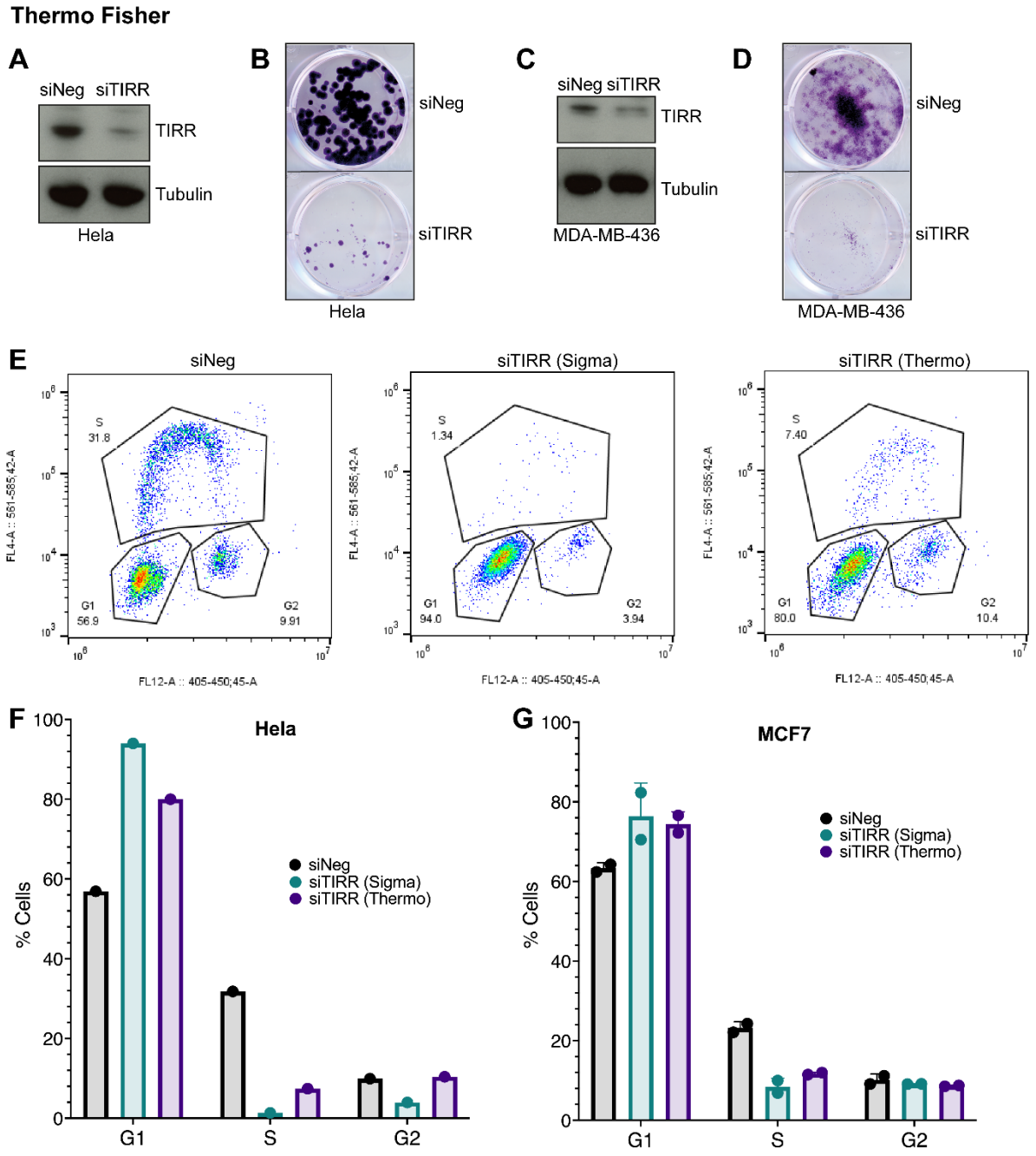


Figure 4.2*: A) Western blot confirming knockdown of TIRR using Thermo Fisher Stealth siRNA (Assay ID HSS189023) in Hela cells.* ***B)*** *Colony formation of Hela cells treated with a non-targeting negative control siRNA or Thermo TIRR siRNA for 24 hours, before re-plating into 12-well plates and being allowed to form colonies for ~10 days (n=3).* ***C)*** *Western blot confirming knockdown of TIRR in MDA-MB-436 cells.* ***D)*** *As in B, in MDA-MB-436 cells (n=1).* ***E)*** *Cell cycle profile of Hela cells treated with negative control siRNA (left panel), siTIRR (Sigma) (middle panel), or siTIRR (Thermo) (right panel) (n=1). The x-axis measures DAPI intensity, and the y-axis measures Alexa Fluor 555 intensity as a readout of cellular Edu content.* ***F)*** *Graphical representation of E.* ***G)*** *Quantification of the cell cycle profile as in E, in MCF7 cells (n=2). SiNeg is a non-targeting siRNA control (***Table 2.6).**

Furthermore, using a pool of 30 siRNAs designed to reduce off-target effects from siTools[24] (hsNUDT16L1, 84309) resulted in a comparable knockdown of TIRR and reduced cell viability (**Figures 4.3.A and 4.3.B**). Taken together, it seemed relatively convincing that the knockdown of TIRR was eliciting the observed phenotypes given that three different TIRR siRNA knockdown strategies resulted in a loss of cell viability, and both Sigma and Thermo siRNAs resulted in comparable cell cycle defects, suggesting that TIRR was required for cell fitness and survival. However, several pieces of information made us question these observations. Firstly, TIRR has an overall slightly negative Gene Effect score on DepMap (distribution peak of around -0.3 on a scale of 0 to -1, with a more negative the score indicating a greater dependency of a cell line on a given protein, with -1 being the median of all common essential genes). However, only 114/1086 cell lines have a score of less than -0.5 (CRISPR (DepMap 22Q2 Public+Score, Chronos)) which would indicate a dependency on TIRR for survival (https://depmap.org/portal/gene/NUDT16L1?tab=overview). Secondly, in the BioGRID Open Repository of CRISPR screens (ORCS), TIRR was a hit in only a small number of screens measuring cell proliferation (65 hits in 1111 screens, https://orcs.thebiogrid.org/Gene/84309). Lastly, stable TIRR knockout cell lines have been generated in Hela, RPE-1, and U2OS[3,25] cell lines with no reported significant effect on proliferation or survival in steady state conditions. Given this information, we utilised additional knockdown methods; a previously published stable doxycycline inducible shRNA Hela cell line[1], an individual Dharmacon siRNA targeting the 3' UTR region of TIRR, and a pool of 4 siRNAs from Dharmacon. Interestingly, the inducible shRNA (**Figures 4.3.C and 4.3.D**), the individual 3'UTR targeting siRNA (**Figures 4.3.E and 4.3.F**), and the pool of 4 siRNAs (data not shown), did not lead to a loss of viability compared to the negative controls despite reducing the level of TIRR to comparable levels as the Sigma, Thermo, and siTools siRNAs as assessed by western blot. We also did not observe any cell cycle alterations when

knocking down TIRR using the Dharmacon 3'UTR siRNA (**Figures 4.3.G and 4.3.H**). Taken together, this indicated that the effects on cell viability and the cell cycle, which are seemingly very similar between three different siRNAs; the Sigma (individual), Thermo (individual), and siTools (pool) siRNAs, which would usually be considered adequate evidence of specificity, are not reproducible when additional siRNAs and a shRNA are utilised. This led us to suspect that the Sigma, Thermo, and siTools siRNAs were eliciting off-target effects and the observed phenotypes were unspecific.

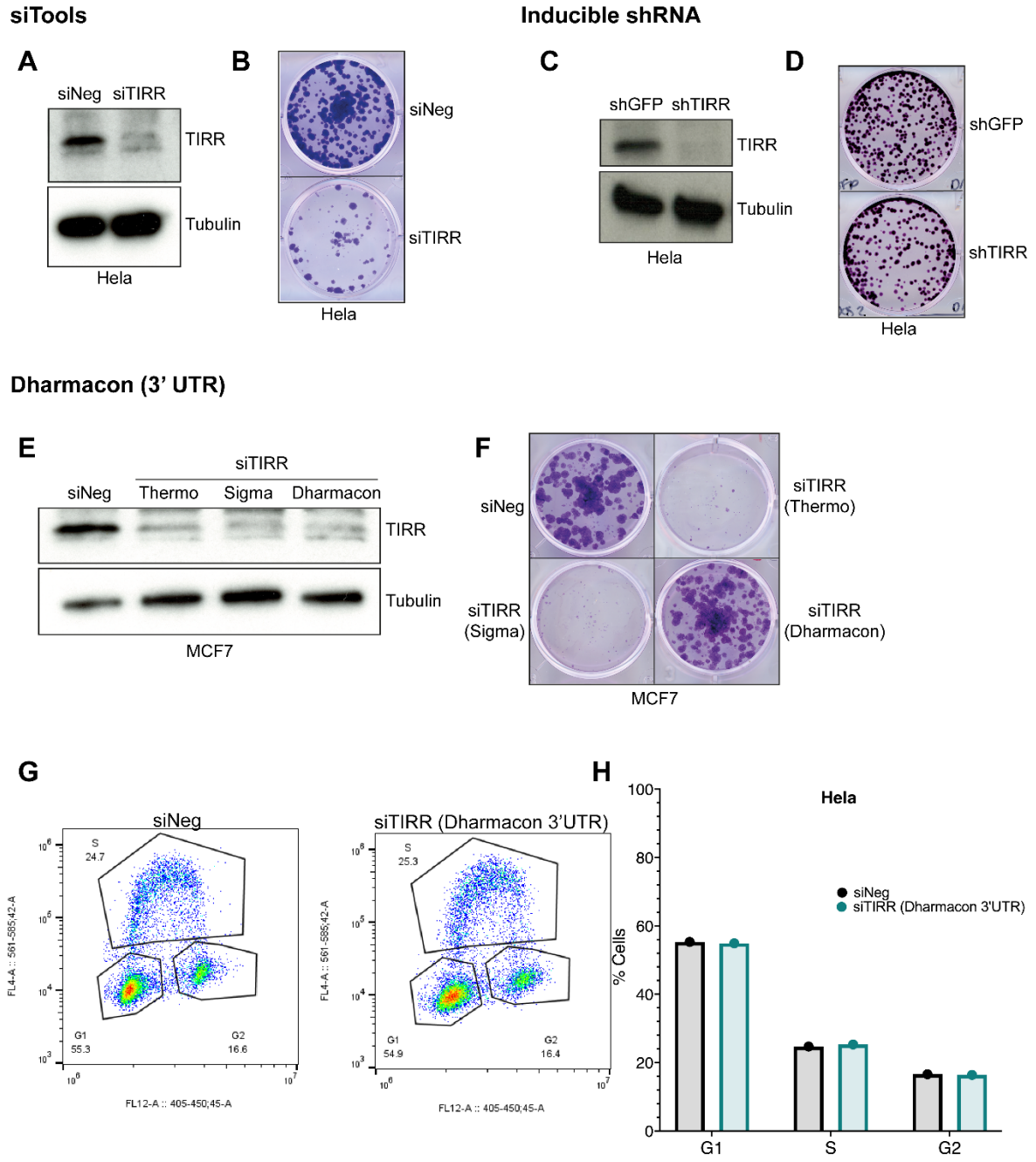


Figure 4.3: *A) Western blot confirming knockdown of TIRR using siTools siPool (hsNUDT16L1, 84309). **B)** Colony formation of Hela cells treated with siPool or negative control siRNA. **C)** Western blot of TIRR knockdown using an inducible shRNA targeting TIRR or GFP as a negative control. **D)** Colony formation of cells induced with doxycycline expressing either shGFP or shTIRR. **E)** Western blot of MCF7 cells transfected with Thermo, Sigma, or Dharmacon (3' UTR) siRNAs targeting TIRR or a non-targeting siRNA as a negative control. **F)** Colony formation of cells transfected with either Sigma, Thermo, or Dharmacon (3' UTR) siRNAs. **G)** Cell cycle profile of Hela cells treated with negative control siRNA (left panel), or siTIRR (Dharmacon 3' UTR) (right panel) (n=1). **H)** Graphical representation of G. SiNeg is a non-targeting siRNA control (***Table 2.6).***

Given that three different siRNAs showed a reduction in cell viability, to fully confirm the nonspecific nature of this phenotype, we performed a rescue experiment by designing a plasmid expressing TIRR which would be resistant to knockdown induced by the Thermo siRNA. TIRR was cloned with modifications to the RNA sequence which would render the TIRR RNA resistant to the Thermo siRNA but would not influence the amino acid sequence and therefore the functionality of the TIRR protein (**Figures 2.1.G and 2.1.H**). Expression of exogenous TIRR and resistance to siRNA transfection in Hela cells was confirmed (**Figure 4.4.A**), however when colony formation assays were performed after transient expression of siRNA resistant TIRR, cells expressing exogenous TIRR failed to rescue cell death after siRNA transfection (**Figures 4.4.B, 4.4.C, 4.4.D, and 4.4.E**). To exclude that this lack of rescue could be due to the transient nature of the TIRR expression, a stable cell line was generated which constitutively expressed the siRNA resistant TIRR by culturing cells with hygromycin after plasmid transfection. Constitutive expression of TIRR and resistance to the Thermo TIRR siRNA was confirmed by western blot (**Figure 4.4.F**). However, once again cells expressing siRNA resistant TIRR failed to rescue the observed cell death in colony formation assays (**Figures 4.4.G and 4.4.H**). Expression of TIRR also failed to rescue the accumulation of cells in G1 after TIRR knockdown (**Figure 4.4.I**). Sequencing of Hela cells transfected with Thermo siRNA (**Appendix Figure 2.A**) also revealed widespread remodelling of the transcriptome as assessed by differential gene expression analysis of RNA sequenced from negative control cells compared to TIRR siRNA (**Appendix Figure 2.B**). Multiple pathways involved in cell survival were differentially regulated in response to TIRR knockdown, with a down regulation of pathways needed for cell survival, including cell cycle progression and DNA repair (**Appendix Figure 3**) and an upregulation of pro-apoptotic pathways (**Appendix Figure 4**). Collectively, this data confirms that the phenotypes observed with the Sigma, Thermo, and siTools siRNAs are not specific to loss of TIRR, and are instead an off-target effect associated with the siRNA

itself. Therefore, the inducible shRNA, and Dharmacon individual 3'UTR and pool siRNAs were selected for the rest of this chapter to study phenotypes associated with knockdown of TIRR.

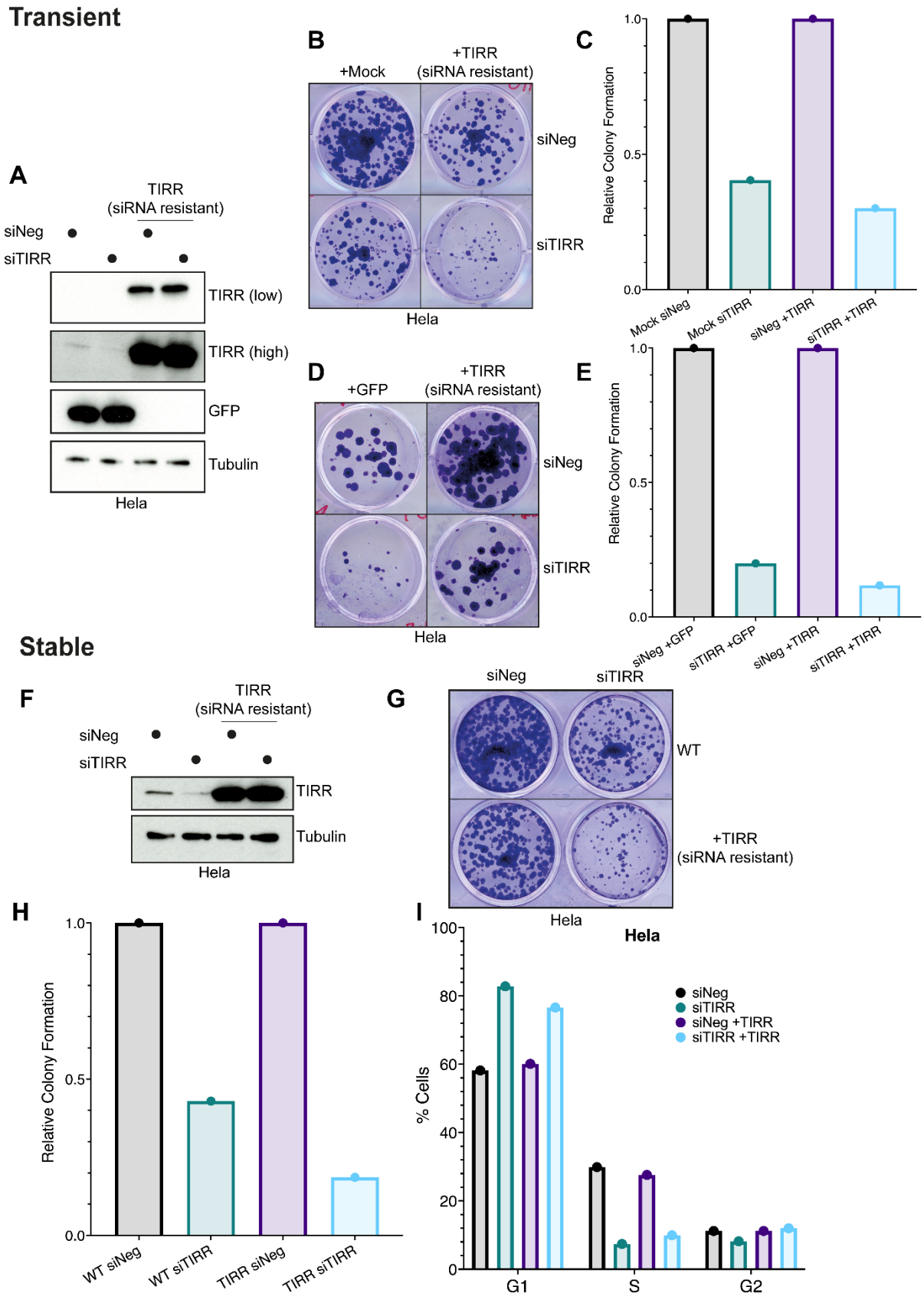


Figure 4.4: *Rescue of cell death and cell cycle phenotypes using plasmid expressing an siRNA resistant version of TIRR in Hela cells both transiently and stably.* ***A)*** *Western blot confirming knockdown of TIRR using the Thermo siRNA in Hela cells and the expression of the siRNA*

resistant TIRR when cells are treated with both the negative control siRNA and the Thermo TIRR siRNA. ***B)*** *Colony formation assay with Hela cells treated with Thermo siRNA or non-targeting siRNA expressing siRNA resistant TIRR or mock-treated.* ***C)*** *As in B, using a plasmid expressing GFP instead of a mock transfection as a control.* ***D)*** *Quantification of B.* ***E)*** *Quantification of C.* ***F)*** *Hela cells stably expressing siRNA resistant TIRR transfected with non-targeting siRNA or TIRR siRNA.* ***G)*** *Colony formation assay of WT Hela or Hela cells stably expressing siRNA resistant TIRR transfected with either non-targeting siRNA or Thermo TIRR siRNA.* ***H)*** *Quantification of G.* ***I)*** *Quantification of the cell cycle profile of WT or siRNA resistant Hela cells treated with siNeg or siTIRR (Thermo). SiNeg is a non-targeting siRNA control (***Table 2.6).

4.3.2 TIRR binds RNA involved in RNA metabolism and RNAPII transcription

We then turned our attention to characterising TIRR RNA binding activity. To identify RNA targets of TIRR in damage conditions, we performed RNA Immunoprecipitation and Sequencing (RIP-Seq) with cross linking with UV[26–28]. UV light at 254nm allows the direct crosslinking of RNA and protein, but not protein-protein, meaning stringent wash conditions can be used in the immunoprecipitation to remove any nonspecific RNA or RNA associated with TIRR binding proteins. Crosslinking and stringent purification also prevents the re-association of RNA and proteins in cell lysates, although disadvantageously, crosslinking efficiency is estimated to be very low[29]. We use a doxycycline inducible TIRR-GFP, as well as GFP only as a control for background, and induce expression of TIRR-GFP for 16 hours (**Figure 4.5.A**). We then induce DSBs using Etoposide for 2 hours after TIRR or GFP induction (**Figure 4.5.B**), and perform RIP-Seq (**Figure 4.5.C**). In total, we identified 729 RNAs bound to TIRR in non-damage conditions (**Figure 4.5.D**), and 1207 RNAs bound to TIRR after damage (**Figure 4.5.E**). Intersection of these RNAs revealed an overlap of 572 RNAs (**Figure 4.6.A**).

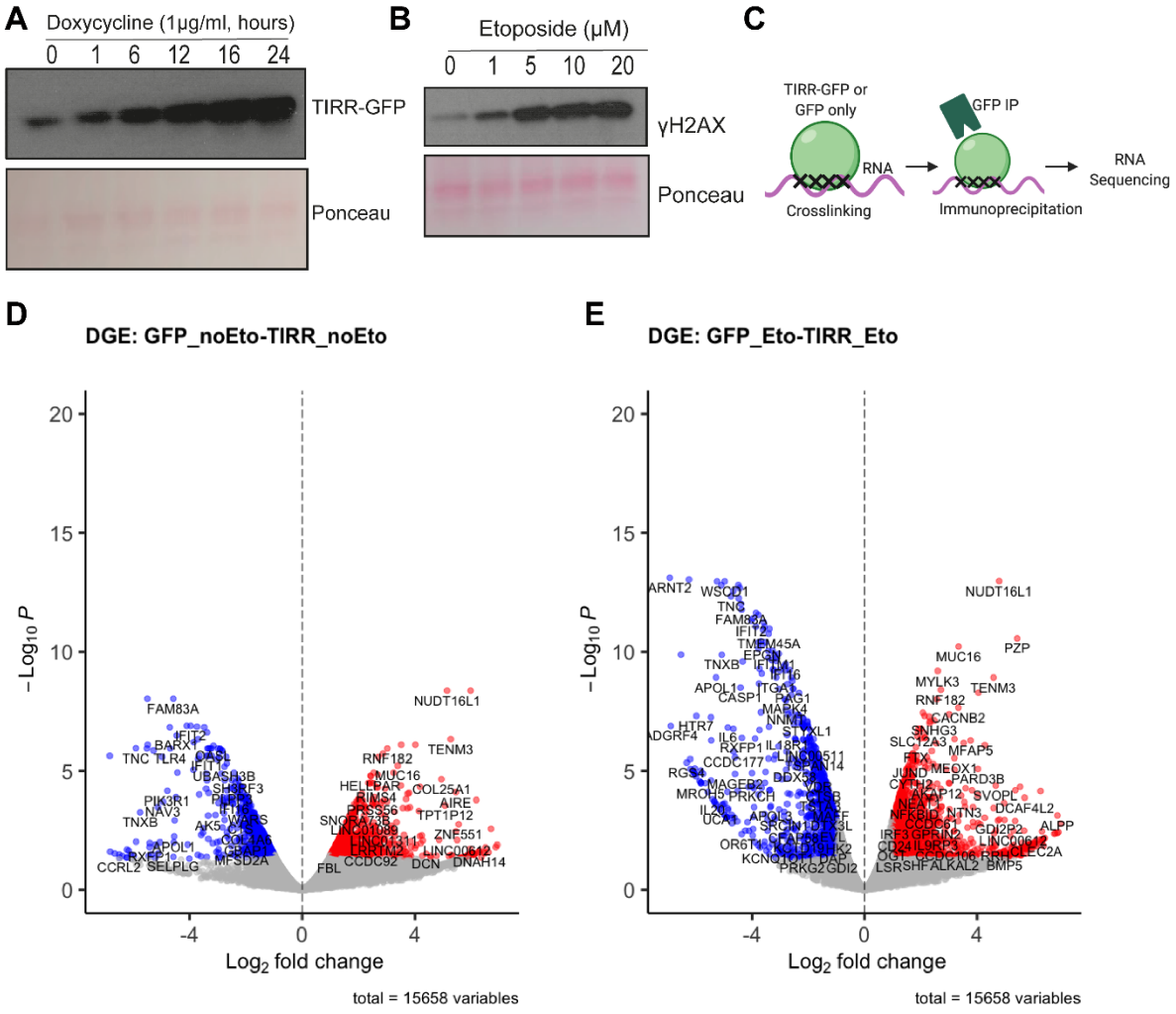


Figure 4.5: ***A)*** *TIRR-GFP Flp-IN Trex cells were induced to express TIRR-GFP using Doxycycline at different time points up to 24 hours. A time point of 16 hours was used for RIP-Seq.* ***B)*** *Etoposide was used to induce DSBs in TIRR-GFP expressing cells using different concentrations up to 20µM. 5µM was used for RIP-Seq.* ***C)*** *Overview of UV RIP-Seq protocol.* ***D)*** *Volcano plot showing differentially enriched RNAs in TIRR-GFP IP over GFP only IP in non-damaged conditions. TIRR-GFP IP (n=2), GFP IP (n=1).* ***E)*** *As in D, in damage conditions. Bioinformatics analysis performed by Dr Irina Chelysheva.*

Comparison of RNAs identified bound to TIRR in non-damage conditions in this thesis with those identified in published iCLIP-Seq[1], also in non-damage conditions, showed that a portion of the RNAs identified by us were also present in data generated from iCLIP-Seq[1] (**Figure 4.6.B**). This suggests we can identify specific RNAs bound to TIRR. GO analysis of RNAs found both in damage and non-damage conditions showed an enrichment in biological processes including mRNA processing and mRNA splicing, suggesting a role for TIRR in RNA

metabolism (**Figure 4.6.C**), and a potentially as yet uncharacterised role of TIRR in RNA splicing. Indeed, a role of TIRR in RNA splicing has been suggested previously, due to HNRNPH3, a protein involved in splicing, being identified in TIRR pull down mass spectrometry[1] (discussed further in **Section 4.3.6**). GO analysis of RNAs which were bound to TIRR specifically after damage (635 RNAs) showed an enrichment for pathways involved in the regulation of RNAPII transcription, including; DNA-binding transcription factor activity, sequence specific DNA binding, and RNAPII transcription regulatory region sequence specific binding (**Figures 4.6.D and 4.7.A**). This suggests that TIRR binds to RNA transcripts of genes involved in transcription regulation after DNA damage.



Figure 4.6: ***A)*** *Overlap between RNA transcripts identified to TIRR in non-damage conditions and damage conditions.* ***B)*** *Comparison of RNAs bound to TIRR in non-damage identified in this thesis and those identified using iCLIP-Seq*[1]*.* ***C)*** *GO analysis of RNAs found to be bound to TIRR in both damage and non-damage conditions.* ***D)*** *GO analysis of RNAs bound to TIRR in damage conditions. Bioinformatics analysis performed by Dr Irina Chelysheva.*

Further analysis of RNAs bound to TIRR uniquely after damage showed no significant difference in 5'UTR length (**Figure 4.7.B**), transcript length (**Figure 4.7.C**), or 3'UTR length

(**Figure 4.7.D**) relative to the rest of the genome. However, analysis of the GC content of RNAs bound to TIRR revealed a significant enrichment of RNAs with lower GC content (**Figure 4.7.E**). A higher AU-content in RNAs has been linked with reduced translation efficiency and lower protein yield, as well as preferential localisation to RNA granules, in particular P-bodies[19], or stress granules after ER stress[9], and may also influence RNA stability[19]. GC content may also influence the nuclear export of RNAs[30].

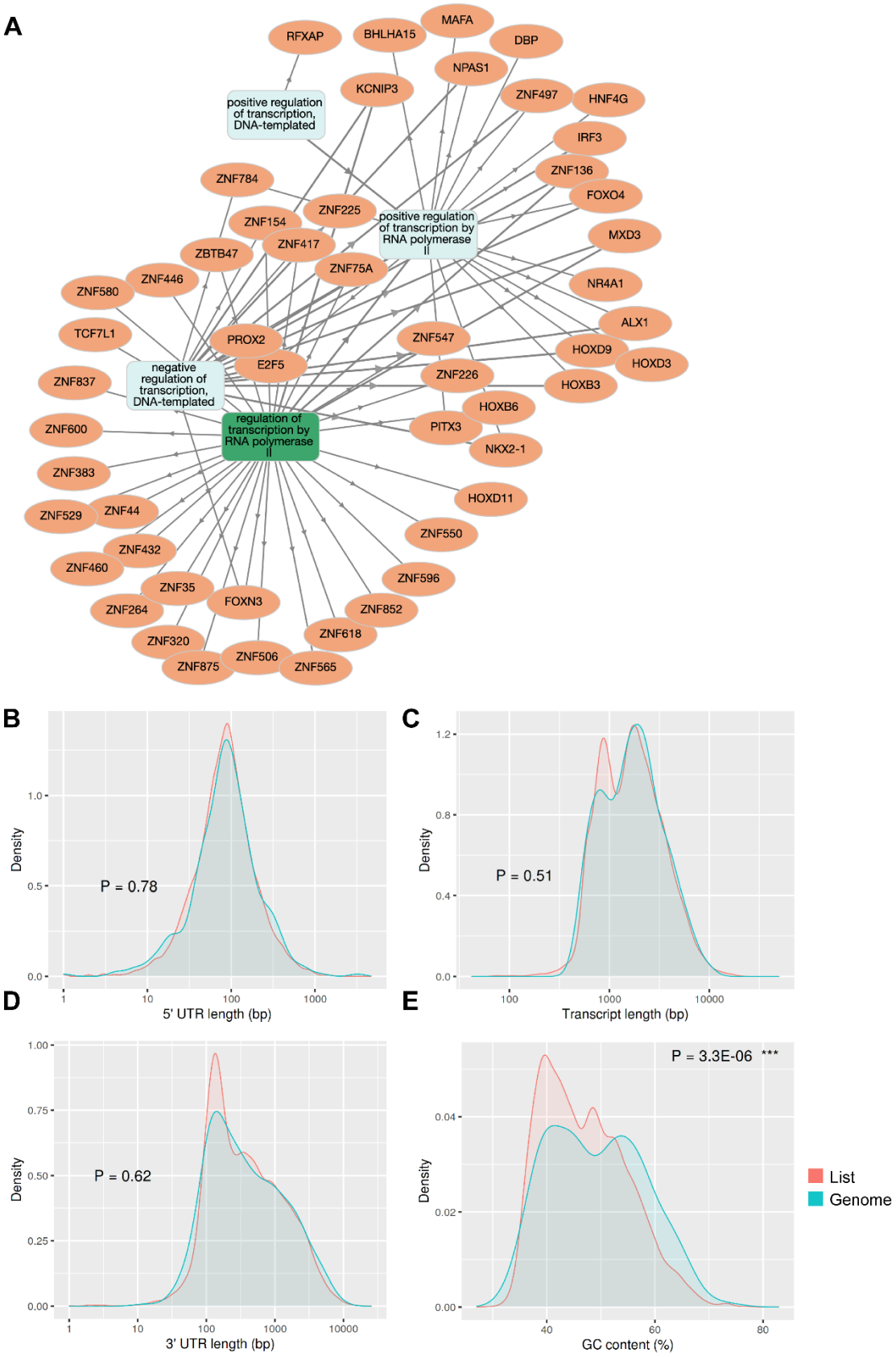


Figure 4.7: ***A)*** *Network presentation of RNAs bound to TIRR in damage conditions, which were identified through GO analysis as significantly enriched in RNAPII transcription*

regulation. ***B-E)*** *Comparison of features of RNAs bound to TIRR in damage conditions vs the reference genome.* ***B)*** *5'UTR length comparison.* ***C)*** *Transcript length.* ***D)*** *3' UTR length.* ***E)*** *GC content. Bioinformatics analysis performed by Dr Irina Chelysheva.*

4.3.3 TIRR does not broadly influence steady state RNA levels in damage and non-damage conditions

To assess if TIRR RNA binding may regulate steady state RNA levels in non-damage and damage conditions, we performed total RNA-Seq in inducible shRNA cells, expressing shRNA for TIRR or GFP as a control. TIRR knockdown was induced using doxycycline for 48 hours, before inducing damage using IR (10Gy) (**Figure 4.8.A**). RNA was collected 6 hours after IR and subjected to paired end total RNA sequencing. As a control, we can see that TIRR RNA was depleted in our sequencing experiments, due to a decrease in the relative expression of TIRR/NUDT16L1 RNA after TIRR KD (**Figure 4.8.B**). Globally, TIRR knockdown did not result in many large changes in total RNA levels (very few RNAs showed a log_2FC greater than 1 or less than -1), suggesting TIRR does not have a large influence on steady-state RNA levels. Differential expression analysis of transcripts in TIRR knockdown compared to the GFP control showed 43 RNAs were significantly (padj<0.05) upregulated after TIRR knockdown with a $log_2FC>1$, and 22 RNAs were downregulated after TIRR knockdown with a $log_2FC<-1$ (**Figure 4.8.C**). Many of the same RNAs were also differentially expressed in TIRR knockdown compared to the control in damage conditions, with 25 RNAs upregulated and 17 downregulated in TIRR knockdown after IR (**Figure 4.8.D**). In agreement with this broadly similar steady state RNA transcriptome in TIRR knockdown both in non-damage and damage conditions, principal component analysis (PCA) showed only 15.16% variance representing the difference between shGFP and shTIRR samples (PC2), compared to 79.06% variance explained by PC1, which shows a distinction between -IR and +IR samples (**Figure 4.8.E**). In TIRR KD, COL3A1, which encodes collagen type III, BOD1L1, which is involved in replication fork protection[31], and PIK3R1, involved in PI3K/Akt signalling and cell

migration[32], are amongst the most downregulated RNAs, while DCAF4L2, which promotes cancer cell migration[33], was amongst the most upregulated after TIRR knockdown (**Figure 4.8.F**).

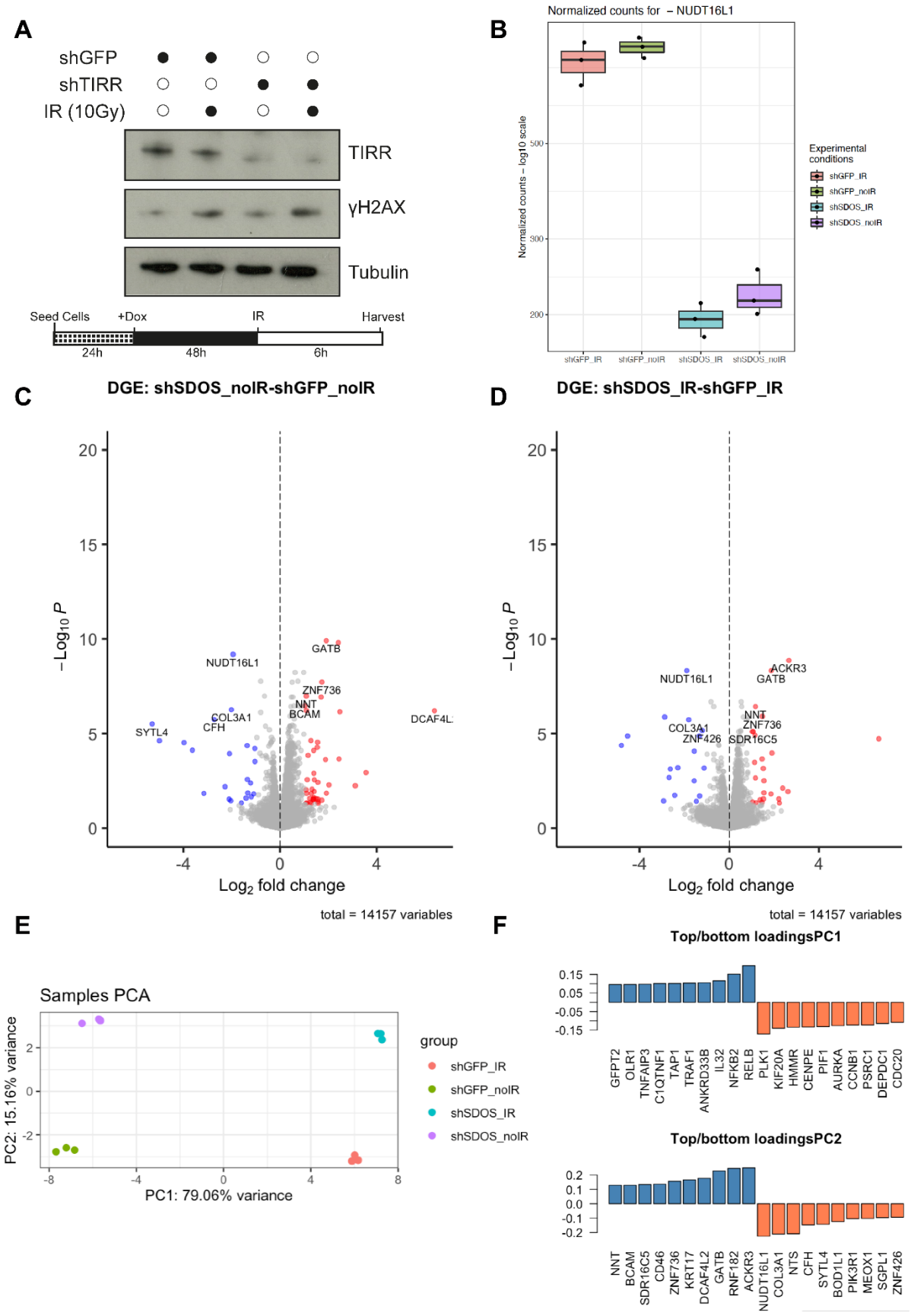


Figure 4.8: ***A)*** *Western blot confirming TIRR knockdown and doxycycline incubation for 48 hours. DNA damage was induced using IR and cells were harvested 6 hours post-IR.* ***B)***

Relative RNA expression of TIRR (NUDT16L1) in shGFP control and shTIRR samples -IR and +IR. TIRR knockdown can be seen by the relative decrease in RNA expression after shTIRR. ***C)*** *Volcano plot showing differentially expressed RNA in TIRR knockdown samples in -IR conditions and* ***D)*** *6h post-IR conditions (padj<0.05, $log_2FC<-1$ and $log_2FC>1$).* ***E)*** *PCA plot showing variance between shTIRR and shGFP total RNA samples in -IR and +IR conditions. PC1 is driven by changes due to IR, and PC2 is driven by changes due to TIRR KD. Replicates (n=3 per condition) cluster together.* ***F)*** *Bar graphs showing RNAs principally responsible for driving variance across samples for PC1 and PC2. Bioinformatics analysis performed by Dr Irina Chelysheva. TIRR = SDOS/NUDT16L1.*

GO analysis of downregulated RNAs did not yield any significant biological processes or molecular functions. However, GO analysis of upregulated differentially expressed RNAs in TIRR vs GFP knockdown conditions without damage showed an enrichment for processes including cell adhesion, cell migration, and cell motility (**Figure 4.9.A**). In damage conditions, many of the same biological pathways were observed, primarily involving cell migration and adhesion (**Figure 4.9.B**). This suggests that TIRR may influence the steady-state levels of RNAs involved in cell migration and adhesion. Interestingly, TIRR has previously been shown to influence cell migration through interaction with the tumour suppressor PTEN, which is part of the PI3K/Akt signalling pathway, and knockdown of TIRR was found to enhance cell migration[34] (**Section 1.4**). This suggests that TIRR may influence cell migration at an RNA level as well as through PTEN interaction.

Broadly, this total RNA-Seq data suggests that TIRR does not dramatically influence RNA steady state levels, and this is also not the case in damage conditions. Comparing our RIP-Seq data with our RNA-Seq data showed that of the 729 RNA transcripts bound in non-damage conditions, only 8 were found to be significantly differentially expressed in our RNA-Seq after TIRR knockdown (8 out of a total of 65 differentially expressed genes in RNA-Seq), including BCAM, DCAF4L2, NTS, and RNF182, which can be seen in the PCA plot (**Figure 4.8.F**). Therefore, whilst it is possible that the levels of these specific RNAs are influenced by TIRR binding (with 8/65 (~12%) of all differentially expressed RNAs in RNA-Seq being bound to

TIRR in RIP-Seq), overall this suggests that TIRR binding to RNA does not dramatically influence the total steady-state levels of RNA globally, with only 8/729 (~1%) of RNAs bound to TIRR changing in their steady state levels after TIRR knockdown.

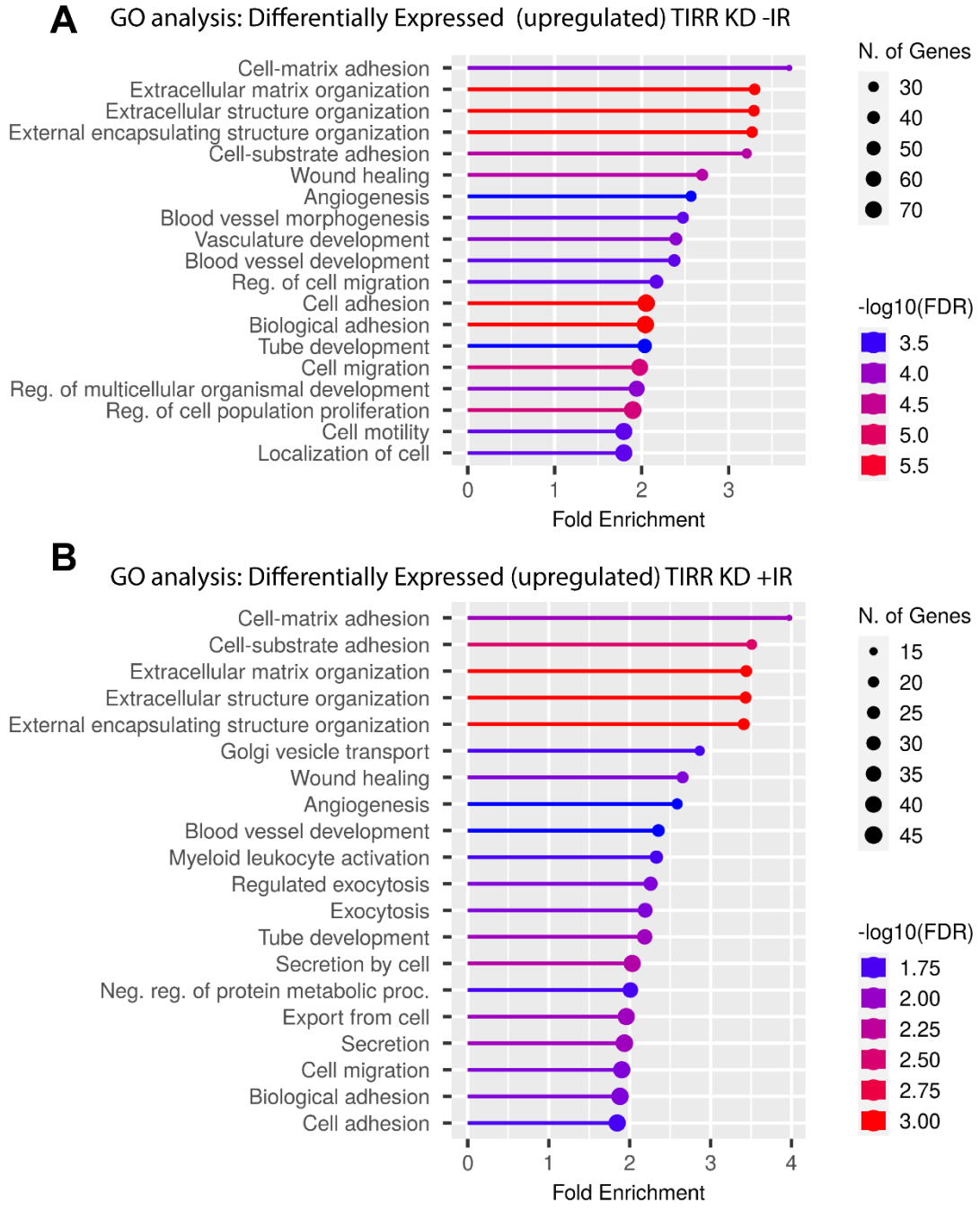


Figure 4.9: ***A)*** *GO analysis of differentially expressed (upregulated) RNAs in TIRR knockdown compared to the GFP control in non-damaged conditions.* ***B)*** *As in A, but in damage conditions.*

4.3.4 TIRR contains a predicted nuclear export signal and interacts with XPO1 in damage conditions

Given that we did not observe many changes to total RNA levels in TIRR KD, to try and understand the function of TIRR RNA binding, we looked at the sequence of TIRR to identify any known motifs which may suggest potential functionality. We used the Eukaryotic Linear Motif (ELM) program in order to identify short motifs which can be recognised by other proteins[35]. Of particular interest, ELM predicted a nuclear export sequence (NES) in TIRR. NES motifs can be bound by the protein chromosome region maintenance protein 1, also known as Exportin-1 (XPO1/CRM1), which is the main protein export receptor in human cells[36], regulating the export of different proteins and some RNAs, including miRNA, tRNA, and a subset of mRNAs, from the nucleus through the nuclear pore complex (NPC) into the cytoplasm[36,37]. Although not the major export mechanism of RNA in human cells, XPO1-dependent export is important for many RNA processes, such as translation and mRNA decay, including components of P-bodies and stress granules, for example DCP1 and 2, and LSM14[38]. To mediate RNA export, XPO1 does not bind directly to RNAs, but instead binds to proteins with a NES that can themselves bind RNA, such as EIF4E, HuR, NXF3, and LRPPRC[36,37]. TIRR is known to have functions in both the nucleus and the cytoplasm[1,3], although the regulation of TIRR localisation between these compartments is not understood (**Section 1.4**).

The NES in a target protein is bound directly by XPO1 in complex with RAN-GTP. The majority, but not all, NES motifs are defined by the pattern Φ-$X_{2,3}$-Φ-$X_{2,3}$-Φ-X-Φ, where Φ is a hydrophobic amino acid (Leu, Val, Met, Phe, and Ile), and X is any amino acid. To expand on the ELM prediction, we also employed other NES prediction programs, including NESmapper[39], Wregrex[40], and LocNES[41]. Using these programs, 5 potential candidate NES

motifs in TIRR were identified (**Figure 4.10.A**). The positions of these candidate NES in TIRR have been given an identifier (1-5), and are highlighted on the TIRR structure (**Figure 4.10.B**).

NES sequences are relatively commonly found across the proteome, especially in hydrophobic cores of proteins, which in reality are not available for targeting and binding of XPO1[42]. True NES sequences are mainly found in accessible regions of proteins, in regions of alpha helical secondary structure, and are more likely to be within or adjacent to regions which are more flexible or locally disordered[42]. Looking at the identified candidate NES sequences, we can see that candidate 4 is located within the TIRR core and is beta stranded, and candidates 1 and 3 also contain regions of beta stranded structure (**Figure 4.10.B**), and are therefore unlikely to be true functional NES motifs. Candidates 2 and 5 are both within alpha helical structures, and are also adjacent to locally disordered regions in TIRR as predicted by PONDR, a computational tool for predicting disorder (data not shown). Therefore, Candidates 2 and 5 appear to fit the defined criteria for a NES motif which is accessible for XPO1 binding, and if TIRR is bound by XPO1, then Candidates 2 and 5 are the most likely true positive NES motifs. However, these motifs would need to be experimentally validated using deletion/substitution mutations. It is also possible for a protein to contain more than one functional NES, for example, BRCA1 contains 2 NES motifs with functional activity[43].

We next assessed if TIRR associates with XPO1 in both non-damage and damage conditions, as many NES motifs in proteins are responsive to cell stress, and only available for XPO1 binding in specific cellular conditions, such as after modification[41]. Using PLA with TIRR and XPO1 antibodies, we were able to see an interaction with XPO1 which was significantly increased after DNA damage with either IR (**Figures 4.10.C and 4.10.D**), or Etoposide (**Figures 4.10.E and 4.10.F**). We also confirmed this result using Co-IP with TIRR-GFP,

observing an increase in XPO1 binding to TIRR after damage (**Figure 4.10.G**). This suggests that TIRR is an XPO1-interacting protein. We therefore hypothesise that upon damage a portion of TIRR may be actively exported from the nucleus into the cytoplasm. This export could potentially be of RNA-bound TIRR or TIRR which is not bound to RNA.

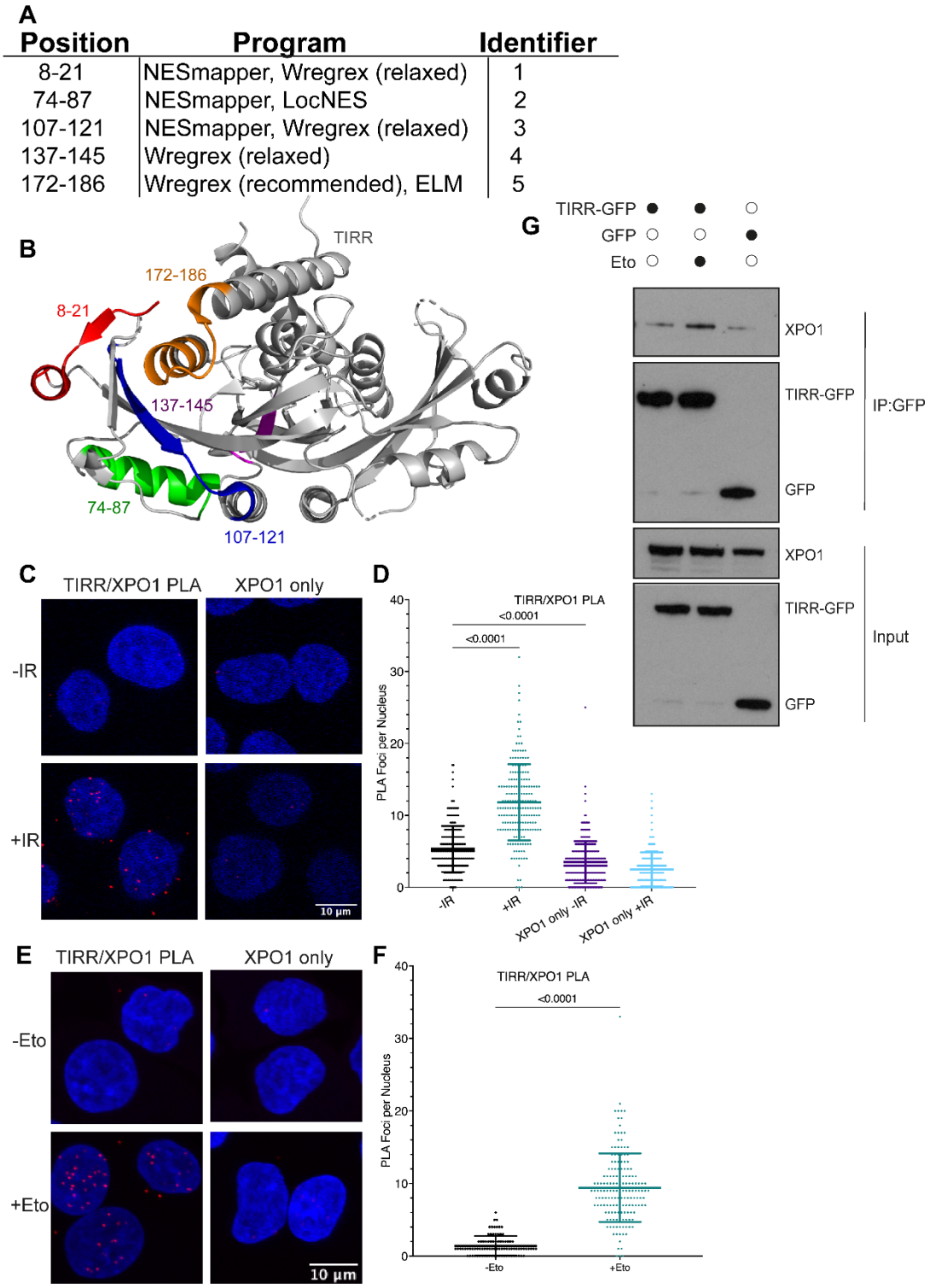


Figure 4.10: ***A)*** *Table of predicted NES on TIRR.* ***B)*** *TIRR (PDB: 6D0L) with the location of each predicted NES highlighted in one TIRR monomer.* ***C)*** *PLA of TIRR and XPO1 or XPO1 only with and without IR (10Gy, 1 hour).* ***D)*** *Quantification of C, n(TIRR/XPO1 -IR)=231, n(TIRR/XPO1 +IR)=192, n(XPO1 only -IR)=269, n(XPO1 only +IR)=265. (mean ± sd, n=2).* ***E)*** *PLA of TIRR and XPO1 or XPO1 only with and without Eto (10μM, 2 hour).* ***F)*** *Quantification of E, n(TIRR/XPO1 -Eto)=88, n(TIRR/XPO1 +Eto)=158. (mean ± sd, n=1).* ***G)*** *Co-IP of TIRR-GFP or GFP only and immunoblot for XPO1 with and without Eto (10μM, 2 hour) (n=1).*

4.3.5 TIRR regulates the formation of Stress Granules and P-Bodies

TIRR binding to RNA, including in damage conditions, coupled with an apparent preference for AU-rich RNA binding (**Figure 4.7.E**), the interaction with XPO1 after damage (**Figure 4.10**), and the function of other NUDIX proteins in RNA decapping and stability[44] (including TIRR paralogue NUDT16[45]), led us to consider whether TIRR has an RNA regulatory function in the cytoplasm after DNA damage, in particular in the regulation of RNA granules such as P-bodies, which are sites of RNA decay/storage. Previously, it has been shown that TIRR may localise into Stress Granules after Sodium Arsenite induced stress, however whether or not TIRR plays a regulatory role in SG formation, or may also regulate P-bodies in response to DSBs is not known.

We performed immunofluorescence microscopy in the presence of TIRR overexpression using a marker for P-bodies, LSM14A[11]. Overexpression of TIRR in non-damage conditions resulted in an increase in P-body numbers, even in the absence of IR (**Figures 4.11.A and 4.11.B**). This suggests that TIRR may promote PB formation even in the absence of DNA damage, and this may be slightly enhanced after DSB induction (**Figures 4.11.A and 4.11.B**). Interestingly, we saw that TIRR-GFP appears to colocalise with LSM14A, suggesting TIRR may associate with / be a component of PBs (**Figure 4.11.C**).

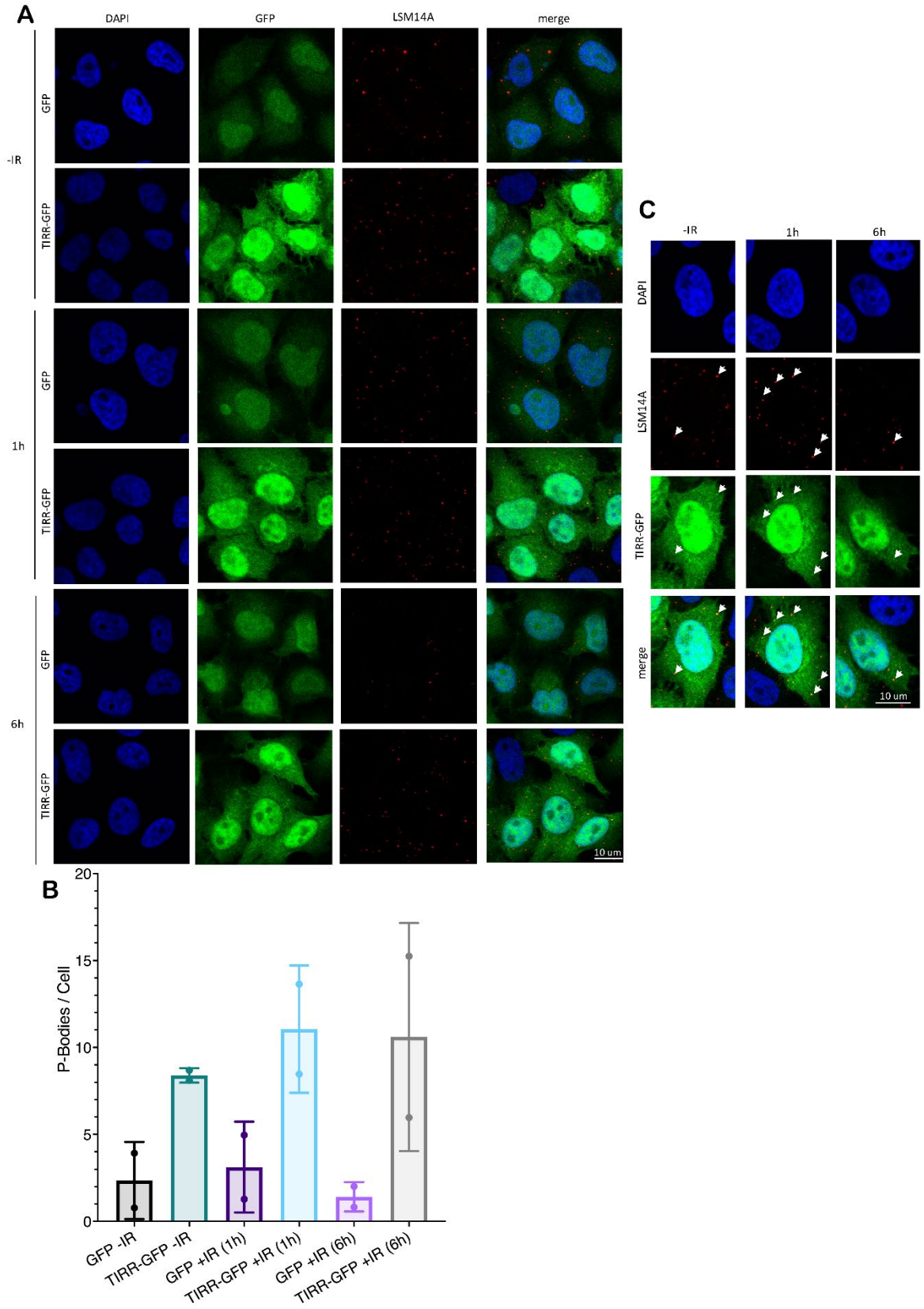


Figure 4.11: ***A)*** *Immunofluorescence microscopy of TIRR-GFP and GFP only expressing Hela cells without IR, or 1h or 6h post-IR (10Gy). LSM14A is used as a marker for P-body formation.* ***B)*** *Quantification of A (mean ± sd, n=2).* ***C)*** *Zoom of TIRR-GFP cells in -IR and*

+IR (1 and 6 hour) conditions, arrows highlight colocalisation between TIRR-GFP and LSM14A.

We then performed the same experiment using LSM14A as a PB marker, but this time using doxycycline inducible TIRR knockdown, or GFP knockdown as a control. In non-damage conditions, we did not observe any effect of TIRR knockdown on PB formation, suggesting TIRR is not essential for PB formation in resting conditions (**Figures 4.12.A and 4.12.B**). However, we saw an increase in PB numbers in TIRR knockdown after IR. Given that TIRR overexpression appears to result in an increase in PBs, including after IR (**Figures 4.11.A and 4.11.B**), it was unexpected that the knockdown of TIRR would also result in an increase in PBs after damage. The reasons for this increase in PBs after TIRR KD are not clear, but this suggests that TIRR is an important regulator of PB formation, including after DNA damage (discussed further in **Section 4.4.4**).

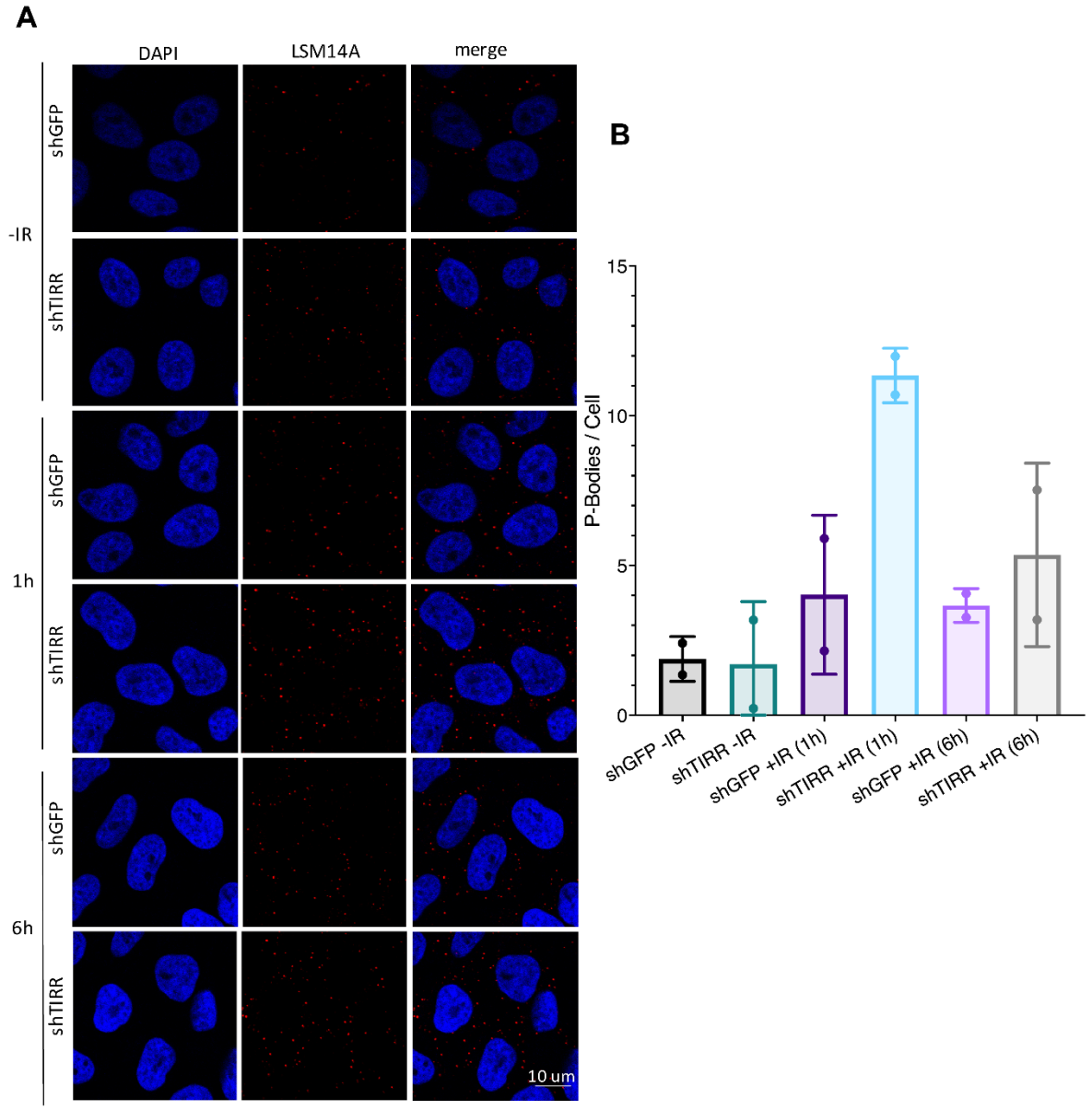


Figure 4.12: ***A)*** *Immunofluorescence microscopy of shTIRR and shGFP expressing Hela cells without IR, or 1h or 6h post IR (10Gy). LSM14A is used as a marker for P-body formation.* ***B)*** *Quantification of A (mean ± sd, n=2).*

We then assessed if TIRR might regulate the formation of another RNA-containing cytoplasmic compartment, stress granules. We performed immunofluorescence microscopy using G3BP1 as a marker of stress granule formation[12]. We performed the assay using IR, fixing cells 1 and 6 hours post exposure (10Gy), and additionally after Sodium Arsenite stress as a positive control for SG formation. Interestingly, we did not observe an increase in SG numbers after 10Gy IR at either 1 hour or 6 hours post-irradiation, in either the shGFP or the

shTIRR condition (data not shown). To the best of our knowledge the formation (or not) of SGs in response to IR has not been reported, and therefore the significance behind this observation is unclear. However, the apparent lack of SG formation could also be due to technical considerations. Most SGs require G3BP1 for their formation, including those induced by UV-damage, but osmotic or severe heat shock can result in SG formation by mechanisms independent of G3BP1[20]. Therefore, we cannot completely rule out the possibility that SGs induced by IR may not contain G3BP1, which could be confirmed by using another SG marker. However, this possibility seems unlikely given that the vast majority of SGs require G3BP1 for their formation. Additionally, while UV-induced stress granules were reported to be observed as early as 1 hour post-damage[20], another study did not observe SG formation until 18 hours post-damage, coinciding with arrest of the cell cycle in G1 phase[21]. Therefore, our time points of 1 hour and 6 hours post-irradiation may not be the correct time points to observe SG formation after IR, and a time course extended to 24 hours may allow visualisation of SGs. Additionally, SG formation in response to UV damage was shown to be dose dependent, so different Gy of IR could be tested[20,21].

Nevertheless, when we look at SGs which form under oxidative stress induced by SA treatment (1h of 0.5mM SA), we can see that TIRR overexpression results in an increase in SG formation (**Figure 4.13.A and 4.13.B**). Conversely, we can see that TIRR knockdown results in the reduced formation of SGs after SA stress (**Figures 4.13.C and 4.13.D**). Similarly to P-bodies, we can see that TIRR-GFP appears to localise with the G3BP1 stress granule marker (**Figure 4.13.E**), suggesting that TIRR may also localise to SGs. The reduced SG number after TIRR KD and increased number after TIRR overexpression after cell stress is similar to that observed with G3BP1 KD/overexpression respectively, which is (in general) critical for SG formation[46]. Together, this suggests that TIRR is important for the formation of RNA granules after stress.

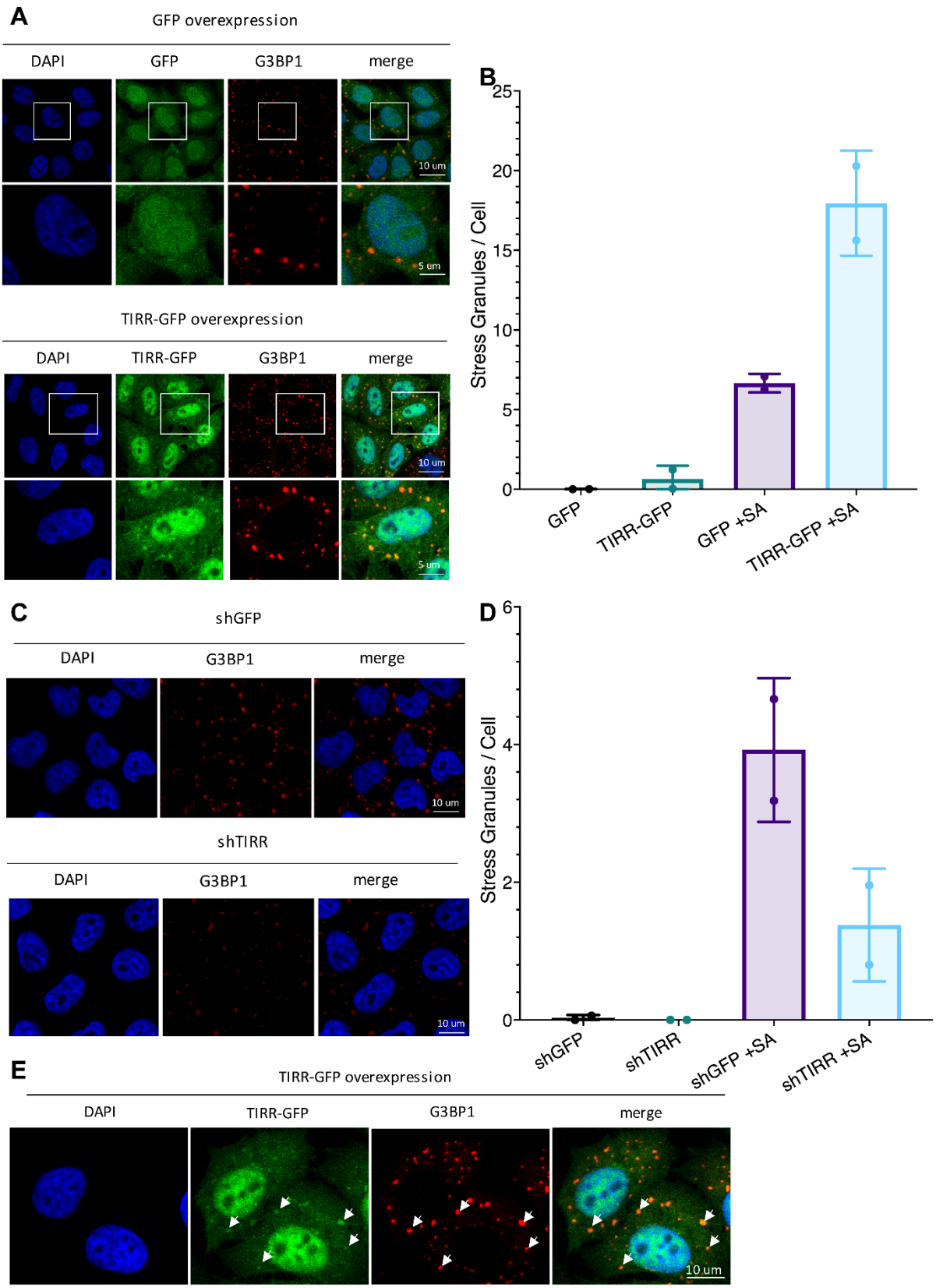


Figure 4.13: ***A)*** *Immunofluorescence microscopy of TIRR-GFP and GFP only expressing Hela cells after sodium arsenite treatment (1h, 0.5mM). G3BP1 is used as a marker for stress granule formation.* ***B)*** *Quantification of A (mean ± sd, n=2).* ***C)*** *Immunofluorescence microscopy of shTIRR and shGFP expressing Hela cells after sodium arsenite stress (1h,*

*0.5mM). **D)** Quantification of C (mean ± sd, n=2). **E)** Zoom of TIRR-GFP cells after sodium arsenite stress, arrows highlight colocalisation between TIRR-GFP and G3BP1.*

4.3.6 TIRR can regulate the protein levels of proteins involved in RNA metabolism and DNA damage

To assess if TIRR may influence the levels of total protein, such as through regulating translation after DNA damage, we performed a whole cell mass spectrometry experiment in TIRR knockdown conditions and GFP knockdown as a control, using the same doxycycline shRNA cell lines as in the RNA-Seq. DNA damage was induced using IR at 10Gy, and protein from whole cell lysates was collected 6 hours after damage induction. TIRR knockdown and induction of DNA damage was confirmed by western blot (**Figure 4.14**).

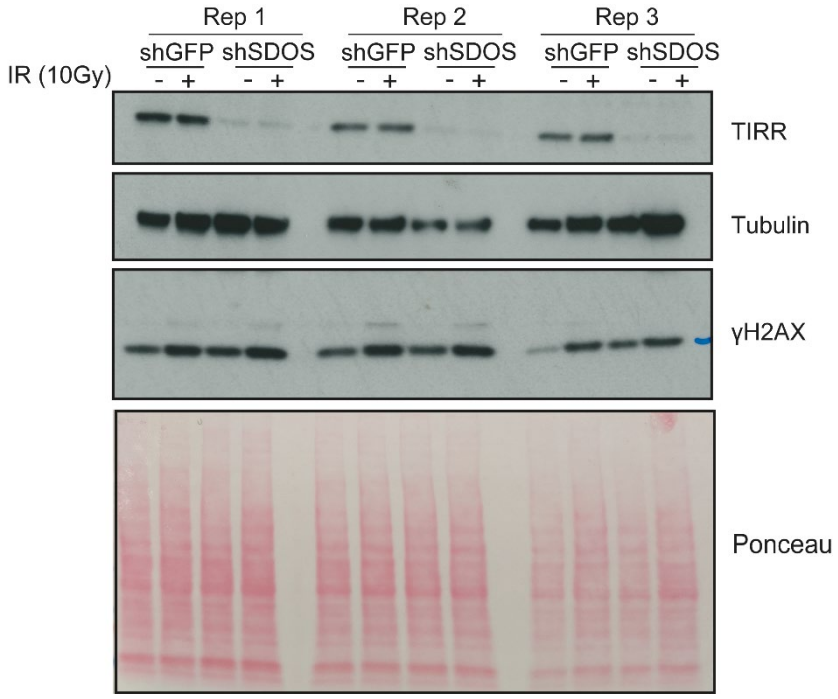


Figure 4.14: *Western blot of shGFP and shTIRR samples with and without IR (10Gy, 6 hour post) sent for mass spectrometry analysis (shSDOS = shTIRR).*

Trypsin digestion and Quantitative label free proteomics was performed on the samples. We were able to detect proteins up to a depth of around ~3500 proteins across 3 replicates with a FDR cutoff of 1%. A complex mixture of peptides, such as a whole cell lysate, would be

expected to typically yield a depth of around 3000 proteins identified (Dr Marjorie Fournier, personal communication), however, in a cell there are upwards of ~20,000 proteins[47], so our coverage of the full proteome is incomplete. Therefore, our whole cell mass spectrometry dataset represents a 'snapshot' of what is happening across the entire proteome.

Comparing identified proteins after TIRR knockdown in non-damage conditions revealed 14 proteins which are significantly downregulated after TIRR knockdown, and 18 proteins which are upregulated after TIRR knockdown (**Figure 4.15.A**). After damage, we identified 17 downregulated proteins and 25 upregulated proteins after TIRR knockdown (**Figure 4.15.B**).

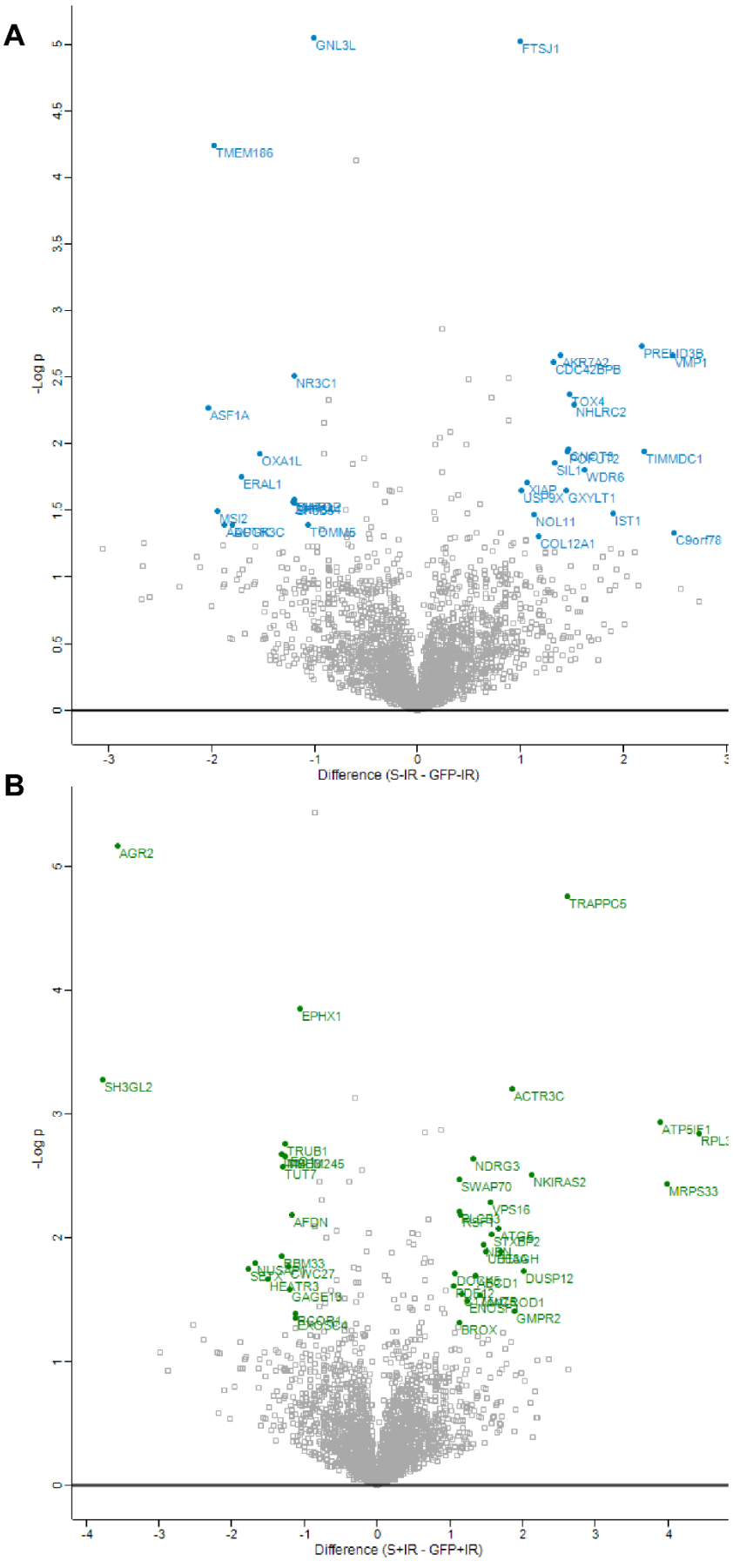

A
GNL3L
FTSJ1
TMEM186
NR3C1
ASF1A
OXA1L
ERAL1
MSI2
TOMM5
PREX1
AKR7A2
CDC42BPB
VMP1
TOX4
NHLRC2
TIMMDC1
SIL1
WDR6
USP9X
GXYLT1
NOL11
IST1
COL12A1
C9orf78
-Log p
Difference (S-IR - GFP-IR)
B
AGR2
TRAPPC5
EPHX1
SH3GL2
ACTR3C
ATP5IF1
TRUB1
NDRG3
SWAP70
NKIRAS2
MRPS33
VPS16
AFDN
DUSP12
GMPR2
BROX
-Log p
Difference (S+IR - GFP+IR)

Figure 4.15: ***A)*** *Volcano plot of mass spectrometry data showing differences (difference = fold change) between GFP knockdown and TIRR knockdown in non-damage conditions.* ***B)*** *As in A, in damage conditions (IR, 10Gy). S=shSDOS (shTIRR).*

Of the 729 RNAs which were identified as bound to TIRR in non-damage by RIP-Seq, only ~80 of those were detected reliably in our mass spectrometry data. Similarly, of the 1208 RNAs identified in damage conditions, only ~110 were detected in the mass spectrometry. Therefore, only around 10% of our RNA targets can be assessed for changes at the total protein level. In damage conditions, ENOSF1 and TRAPPC5 which are bound by TIRR were differentially expressed at the protein level, while in non-damage conditions, only WDR6 and TOMM5 were differentially expressed at the protein level. WDR6 protein was upregulated after TIRR knockdown, similarly to both ENOSF1 and TRAPPC5, whilst TOMM5 was downregulated. Therefore, it would be interesting to perform ribosome profiling in damage conditions, to understand if TIRR RNA binding and sequestration into PBs or SGs may facilitate translational repression of TIRR-bound RNA (**Section 4.4.7**).

Whilst it is disappointing to not be able to measure more changes at the protein level of more RNAs identified in TIRR RIP-Seq, we can use our mass spectrometry data to get a global overview of either direct or indirect changes in proteins as a result of TIRR knockdown. This may reflect the function of TIRR RNA binding, or highlight how TIRR may impact RNA regulatory processes and DNA repair. GO analysis of upregulated proteins in either non-damage or damage conditions showed an enrichment for cellular metabolic pathways, including Protein deubiquitination and Intracellular protein transport (**Figures 4.16.A and 4.16.B**). GO analysis of proteins which were downregulated after TIRR knockdown showed an enrichment for protein insertion into the membrane (**Figure 4.16.C**). Interestingly, GO analysis of downregulated proteins after IR showed an enrichment in processes related to RNA

processing, suggesting these proteins are downregulated as a consequence of TIRR knockdown after IR (**Figure 4.16.D**).

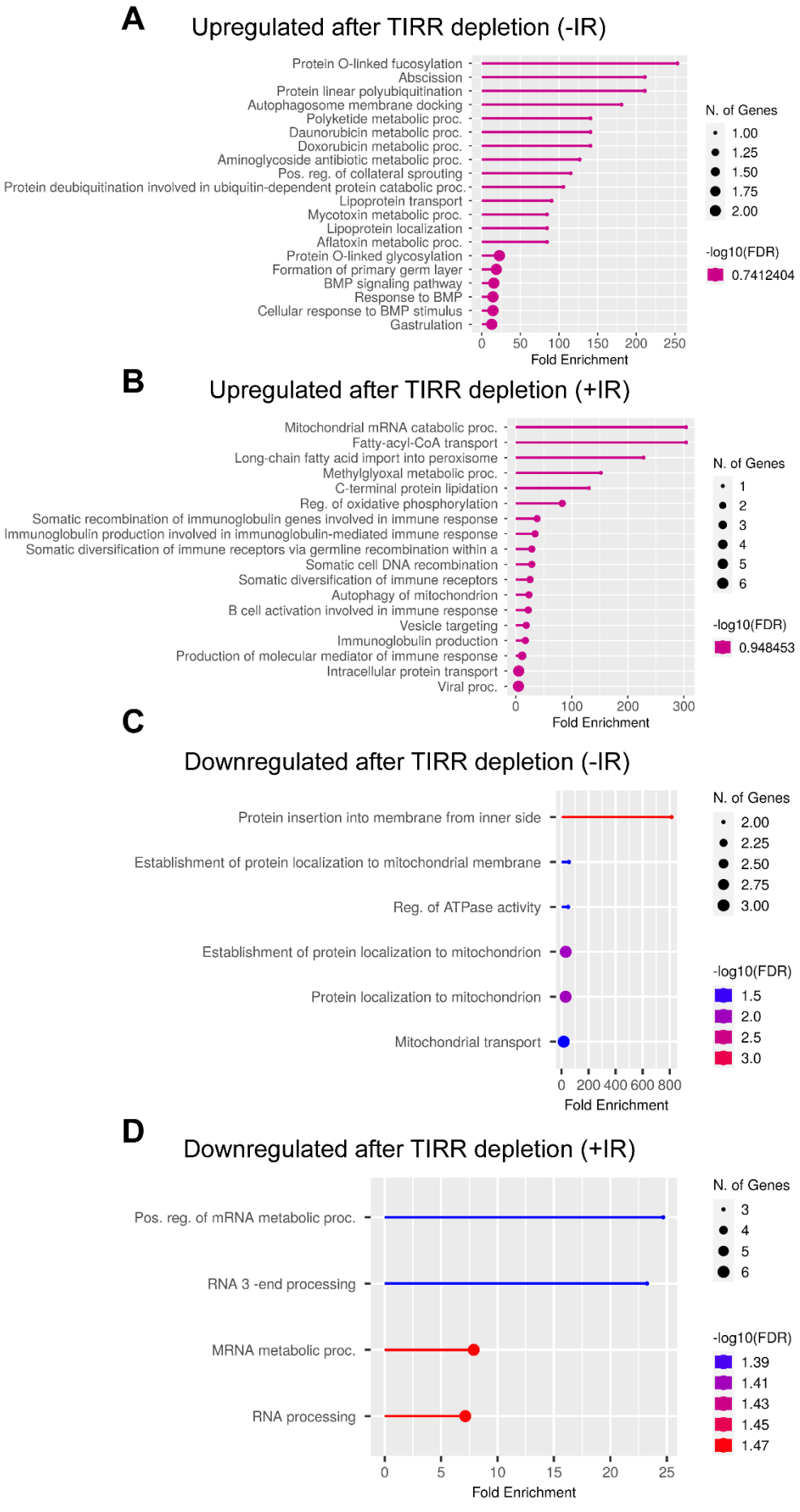

A
Upregulated after TIRR depletion (-IR)
Protein O-linked fucosylation
Abscission
Protein linear polyubiquitination
Autophagosome membrane docking
Polyketide metabolic proc.
Daunorubicin metabolic proc.
Doxorubicin metabolic proc.
Aminoglycoside antibiotic metabolic proc.
Pos. reg. of collateral sprouting
Protein deubiquitination involved in ubiquitin-dependent protein catabolic proc.
Lipoprotein transport
Mycotoxin metabolic proc.
Lipoprotein localization
Aflatoxin metabolic proc.
Protein O-linked glycosylation
Formation of primary germ layer
BMP signaling pathway
Response to BMP
Cellular response to BMP stimulus
Gastrulation
0 50 100 150 200 250
Fold Enrichment
N. of Genes
1.00
1.25
1.50
1.75
2.00
-log10(FDR)
0.7412404
B
Upregulated after TIRR depletion (+IR)
Mitochondrial mRNA catabolic proc.
Fatty-acyl-CoA transport
Long-chain fatty acid import into peroxisome
Methylglyoxal metabolic proc.
C-terminal protein lipidation
Reg. of oxidative phosphorylation
Somatic recombination of immunoglobulin genes involved in immune response
Immunoglobulin production involved in immunoglobulin-mediated immune response
Somatic diversification of immune receptors via germline recombination within a
Somatic cell DNA recombination
Somatic diversification of immune receptors
Autophagy of mitochondrion
B cell activation involved in immune response
Vesicle targeting
Immunoglobulin production
Production of molecular mediator of immune response
Intracellular protein transport
Viral proc.
0 100 200 300
Fold Enrichment
N. of Genes
1
2
3
4
5
6
-log10(FDR)
0.948453
C
Downregulated after TIRR depletion (-IR)
Protein insertion into membrane from inner side
Establishment of protein localization to mitochondrial membrane
Reg. of ATPase activity
Establishment of protein localization to mitochondrion
Protein localization to mitochondrion
Mitochondrial transport
0 200 400 600 800
Fold Enrichment
N. of Genes
2.00
2.25
2.50
2.75
3.00
-log10(FDR)
1.5
2.0
2.5
3.0
D
Downregulated after TIRR depletion (+IR)
Pos. reg. of mRNA metabolic proc.
RNA 3 -end processing
MRNA metabolic proc.
RNA processing
0 5 10 15 20 25
Fold Enrichment
N. of Genes
3
4
5
6
-log10(FDR)
1.39
1.41
1.43
1.45
1.47

Figure 4.16: *GO analysis of differentially expressed proteins in TIRR knockdown conditions compared to GFP control.* ***A)*** *Upregulated after TIRR KD in -IR conditions.* ***B)*** *Upregulated in TIRR KD in +IR conditions.* ***C)*** *Downregulated after TIRR KD in -IR conditions.* ***D)*** *Downregulated after TIRR KD in +IR conditions.*

Looking at specific proteins which were differentially expressed in our dataset (**Table 4.1**), we can see several proteins of interest relevant to RNA processing and DNA damage. In non-damage conditions, upregulated proteins include C9orf78 and CNOT3, and downregulated proteins include SF3B5, CHTOP, and ASF1A. C9orf78 is involved in splicing[48], while CNOT3 is involved in RNA deadenylation/decay as part of the CCR4-NOT complex[49]. SF3B5 is part of the SF3B splicing complex[50], CHTOP plays a role in RNA export from the nucleus[51], and ASF1A is a histone chaperone, with additional roles in promoting NHEJ[52].

In damage conditions after TIRR KD, upregulated proteins include NBN and RSF1, and downregulated proteins include RCOR1, CWC27, TUT7, LEO1, and SETX. Interestingly, NBN and RSF1 are both known to play roles in DNA repair, with RSF1 remodelling chromatin around DSBs via an interaction with ATM to promote repair[53], while NBN (Nibrin/NBS1) is part of the MRN complex (**Section 1.2**). This suggests that in TIRR knockdown conditions after IR, levels of certain DNA repair factors involved in early DSB repair and chromatin remodelling were increased. The reasons for this are unknown, although could potentially reflect the reduced regulation of 53BP1 in TIRR knockdown conditions. For example, increased 53BP1 occupancy at DSBs due to TIRR knockdown (**Table 1.1**) may result in an upregulation of end resection factors, such as NBN, to counteract increased 53BP1 activity. Several proteins involved in RNA processing are downregulated after TIRR knockdown in response to IR. TUT7 is involved in RNA decay by uridinylating mRNA and miRNA[54], LEO1 is part of the PAF1C complex involved in RNAPII transcription elongation[55], CWC27 participates in pre-mRNA splicing[56], RCOR1 is involved in transcriptional repression[57], and

SETX is an RNA helicase which can unwind RNA:DNA hybrids, which also plays a role in DNA repair (**Section 1.5**). Taken together, this suggests that TIRR may influence DNA repair and RNA processing by regulating the levels of proteins in these pathways, or conversely, these proteins are indirectly regulated as a consequence of TIRR knockdown.

Lastly, given that many of these differentially expressed proteins across TIRR knockdown in both damage and non-damage conditions are known to play roles in splicing (such as C9orf78, SF3B5, and CWC27), and RIP-Seq in non-damage conditions suggests TIRR binds RNA which is involved in splicing regulation (**Figure 4.6.C**), we also assessed if TIRR knockdown would result in changes in RNA splicing. However, we did not observe any significant effect of TIRR knockdown on splicing in either damage or non-damage conditions from analysis of our total RNA-Seq dataset (data not shown).

Downregulated TIRR KD -IR	Upregulated TIRR KD -IR	Downregulated TIRR KD +IR	Upregulated TIRR KD +IR
ACTR3C	AKR7A2	AFDN	ABCD1
ADPGK	C9orf78	AGR2	ACTR3C
ASF1A	CDC42BPB	CWC27	ATG5
CHTOP	CNOT3	EPHX1	ATP5IF1
ERAL1	COL12A1	EXOSC4	BROX
GNL3L	GXYLT1	GAGE13	C17orf75
MAIP1	IST1	HEATR3	DOCK5
MSI2	NHLRC2	LEO1	DUSP12
NR3C1	NOL11	MBD3	ENOSF1
OXA1L	POFUT2	NUSAP1	GMPR2
SF3B5	PRELID3B	RBM33	HAGH
TMEM186	SIL1	RCOR1	MACROD1
TOMM5	TIMMDC1	SETX	MRPS33
ZNF644	TOX4	SH3GL2	NBN
	USP9X	TMEM245	NDRG3
	VMP1	TRUB1	NKIRAS2
	WDR6	TUT7	PDE12
	XIAP		PLCB3
			RPL36A
			RSF1
			STXBP2
			SWAP70
			TRAPPC5
			UBE3A
			VPS16

Table 4.1: *Differentially expressed proteins identified in whole cell mass spectrometry analysis of TIRR knockdown in damage and non-damage conditions.*

4.4 Discussion

4.4.1 Considerations when selecting appropriate knockdown methods for a protein of interest

During the course of our investigation into TIRR functionality, we employed the use of RNA interference (RNAi) mediated knockdown, using an inducible shRNA and transient transfection of different siRNAs. Conflicting data surrounding the effect of TIRR knockdown on cell viability led us to investigate the possibility of siRNA induced off target effects. In our studies, we observe that 3 out of the 6 siRNA/shRNA tested led to a significant reduction in cell viability. These 3 non-specific siRNAs encompassed two individual siRNAs targeting different regions of TIRR, with one (Sigma) in the 3'UTR and the other (Thermo) in the CDS, and a pool of siRNAs targeting along the transcript (siTools).

SiRNAs can elicit off-target effects in a number of different ways[58]. Off-target effects can arise from the unintentional targeting through sequence complementarity with another RNA, either with the guide (antisense) strand of the siRNA, or with the non-guide/passenger strand (sense)[58]. Off-target effects can also occur through other mechanisms, including the saturation of the RISC complex which prevents proper miRNA loading, through interferon responses, and through certain sequences which induce toxic effects[58], such as UGGC in the guide strand of the siRNA[58]. Effects of RISC saturation and interferon response activation can mostly be excluded in our experiments due to the transfection of other siRNAs (including both negative control siRNA and other TIRR-targeting siRNAs) at the same concentrations without inducing any cell death. In the two individual siRNAs used, we also did not find any common motifs associated with off-target cell death, including those which are known to activate an interferon response[59]. A phenomenon known as death induced by survival gene elimination (DISE) has also been reported, where the seed region of an siRNA shows complementarity to off-target

genes needed for survival, and therefore induces cell death[60]. Interestingly, many different siRNAs targeting CD95 (>80% of 22 tested) induce off-target effects through a DISE mechanism[61].

Whilst we cannot draw any concrete conclusions about exactly why 50% of our RNAi methods used to target TIRR resulted in nonspecific cell death, we speculate that a DISE-like mechanism may be occurring, for two main reasons. Firstly, the cell death phenotype appeared to be highly similar between the different siRNAs we used and did not show much variation between different cell lines tested. Secondly, sequencing of cells after transfection of a nonspecific siRNA targeting TIRR (Thermo), showed very dramatic changes in the transcriptome, and down regulation of factors needed for cell survival, such as those involved in cell cycle progression and DNA repair, and an upregulation of pro-apoptotic factors (**Appendix Figures 3 and 4**). We also considered the possibility that the siRNAs may target different isoforms of TIRR other than the main isoform, which may have a pro-survival role. However, we can exclude this possibility as there is very little evidence that a functional second isoform of TIRR is expressed, and the sequences of the different possible transcripts (as identified using Ensembl Genome Browser) are highly similar, and therefore would be targeted by all the siRNAs and shRNA used in this study.

In general, performing experiments with 2 different siRNAs is usually considered sufficient proof of specific phenotypes resulting from the knockdown of a protein of interest. Here, we find that multiple siRNAs to TIRR showed off-target effects resulting in cell death (**Figures 4.1 and 4.2**). Rescue experiments performed using exogenous expression of siRNA resistant TIRR showed that re-expression of TIRR was unable to rescue cell death, indicating that the loss of viability does not result from TIRR knockdown, but rather nonspecific effects (**Figure**

4.4). Furthermore, additional siRNAs and an inducible shRNA did not result in any observable change in cell viability, despite reducing TIRR protein to comparable levels (>90% knockdown efficiency at the protein level) (**Figures 4.3.E and 4.3.F**). It is therefore important to validate phenotypes observed as a result of the knockdown of a protein of interest, in particular when knockdown results in the loss of cellular viability.

4.4.2 TIRR binds to many different RNA in damaged cells

In both damage and non-damage conditions we find that TIRR can bind to different RNA, particularly mRNAs. We find that TIRR binds to RNAs which are predominantly involved in regulatory processes after damage, including transcription factors which regulate RNAPII transcription (**Figures 4.6.D and 4.7.A**), as assessed by GO analysis. These RNAs also have significantly lower GC content when compared to the rest of the genome (**Figure 4.7.E**). Given the observed influence of TIRR on RNA granule formation (**Section 4.3.5**), and the suggested role of TIRR in translation repression[1], we hypothesise that TIRR may bind specifically to these RNAs in order to regulate their sequestration into RNA granules, and influence their translation.

In agreement with this, analysis of RNAs which are targeted to PBs revealed that PB-associated RNAs tend to be involved in regulatory pathways which would require dynamic regulation, such as RNA-processing, cell division, and RNA Polymerase II transcription[11], whereas those which are excluded from PBs tend to be more related to constitutive functions, such as translation, metabolic pathways, and the extracellular matrix[11]. Therefore, TIRR may localise RNAs involved in dynamic regulatory processes into PBs. The observation of regulatory RNAs being preferentially associated with RNA granules was also seen under different stresses, with broadly similar RNAs sequestered into stress granules in response to ER stress, heat shock, and arsenite stress[9]. After ER stress, RNAs which encode transcription factors and genes involved

in cell survival and proliferation were targeted to RNA granules, and therefore RNA granule sequestration may be a mechanism of dynamically regulating the cellular response to response to different stress stimuli[9].

4.4.3 TIRR can interact with XPO1 after damage

The mechanism of XPO1-dependent nuclear export, where XPO1 binds to proteins with a leucine-rich NES motif in complex with RAN-GTP, followed by export through the NPC and RAN-GTP to RAN-GDP hydrolysis resulting in release of XPO1 from the NES-containing protein, regulates the export of certain proteins and RNA from the nucleus[37]. Over 1000 proteins in human cells are estimated to be regulated by XPO1-dependent export[38], including proteins involved in translation and mRNA degradation, such as LSM14 which directly interacts with XPO1, DDX6, which interacts with LSM14 rather than XPO1 directly, and DCP1/2[38].

There are many examples of proteins which are involved in the DNA damage response which can be regulated by XPO1-mediated nuclear export, such as BRCA1. BRCA1 has been shown to be regulated at least in part by XPO1-dependent nuclear export after DNA damage[43,62]. BRCA1 is a predominantly nuclear protein, but was identified to contain two functional NES motifs, and can move between the nucleus and the cytoplasm[63]. At 4-8 hours post-IR, BRCA1 in the cytoplasm was found to increase (although the majority of BRCA1 still resides in the nucleus), and this cytoplasmic localisation was more prominent at later time points after IR (24 hours), which was reduced by the inhibition of XPO1[62]. The nuclear export of BRCA1 is prevented by the interaction with the BRCA1 binding partner BARD1, masking the NES motif in BRCA1[64], while p53 binding to BRCA1 promotes nuclear export by XPO1 by preventing the interaction with BARD1. The p53-BRCA1 interaction promotes cell death in response to IR, therefore the interaction of p53 and BRCA1 and BRCA1 export is important for cell death

induced by IR[65]. XPO1-mediated BRCA1 export also promotes BRCA1 localisation to centrosomes to regulate centrosome number[66]. Furthermore, p53 itself is also exported from the nucleus via XPO1 binding to a NES motif in p53[67], and this NES motif can be phosphorylated to reduce export after DNA damage to promote p53 functions in the nucleus[68]. Therefore, a network of PTMs, protein-protein interactions, and repair progression can regulate XPO1-mediated export in response to DNA damage.

In our work we identify a previously unknown interaction of TIRR with XPO1, and identify candidate NES sequences within TIRR. TIRR is both a nuclear and cytoplasmic protein[1,3], with functions in both compartments. However, it is not clear how this localisation is regulated, and if cell stress such as DNA damage can influence the subcellular localisation of TIRR. We find that TIRR interacts with XPO1 after DNA damage induced by either IR or Etoposide (**Figure 4.10**), suggesting a portion of TIRR may be exported from the nucleus after damage via an XPO1-mediated pathway. We suggest that this is a direct interaction due to the identification of candidate NES motifs within TIRR, although these NES motifs will need to be validated as part of future work. Nevertheless, we provide evidence that the nuclear export of TIRR could be relevant for TIRR function after DNA damage, in a manner similar to what has been observed for other DNA damage repair proteins such as BRCA1 and p53[65,68].

It is not presently clear what would trigger the interaction with XPO1 after DNA damage. It is tempting to speculate that the release of TIRR from 53BP1 after DNA damage could act as a trigger for XPO1 binding to TIRR. Comparing the locations of the identified candidate NES motifs on TIRR with the site of 53BP1 binding (**Figure 4.17**), reveals that candidate 2 spanning residues 74-87 is somewhat distal to the site of 53BP1 binding, and therefore it seems unlikely that 53BP1 would preclude XPO1 binding to this site in non-damage conditions. On the other

hand, the second prioritised candidate NES, candidate 5, spanning residues 172-186, faces the 53BP1 Tudor domain, and full-length 53BP1 binding to TIRR could potentially block the interaction of TIRR with XPO1 in non-damage conditions.

We hypothesise that TIRR bound to RNA may facilitate the export of certain RNAs from the nucleus, in a manner analogous to other RNA binding proteins, such as HuR and NFX3[36]. NFX3 contains a NES motif and is bound by XPO1, and can transport RNA out of the nucleus to the cytoplasm[69]. We interestingly observe that RNAs bound to TIRR are typically more AU-rich, which has been shown to influence the dependence of RNA on particular export factors for nuclear export[30], for example RNA with a higher GC content may be more dependent on TREX for nuclear export, whereas NXF1 may be required for the export of RNAs with lower GC content[30]. Given that RNA binds on TIRR to the same site as 53BP1 (**Figure 3.19**), RNA binding to TIRR may also preclude XPO1 binding to TIRR at NES candidate 5. However, this could be reconciled with two possible scenarios. Firstly, TIRR exists stably as a dimer, as many NUDIX proteins do[70], and binds to 53BP1 in a 1:1 ratio[25], with one TIRR dimer binding to one 53BP1 dimer, with 53BP1 bridging over the C terminal regions of each TIRR monomer unit[25]. Therefore, both TIRR RNA-binding interfaces (one from each monomer of the dimer) are occupied when TIRR is bound to 53BP1. However, TIRR could engage other proteins using one monomer, and bind other substrates such as RNA with the second monomer. Therefore, XPO1 interaction with candidate 5 NES on TIRR does not necessarily preclude RNA-binding. Secondly, XPO1 may bind TIRR at candidate 2 NES, and would likely not interfere with RNA binding. It also is important to consider the possibility that TIRR is exported from the nucleus without being bound to RNA, and may potentially engage RNA once in the cytoplasm after XPO1 dissociation following RAN-GTP hydrolysis. Further work on validating the location of

the NES within TIRR and relevance of the TIRR and XPO1 interaction would shed light on the details of this mechanism.

It is also interesting to note that the location of candidate 2 NES on TIRR overlaps with the location of the NUDIX box, where catalytic glutamic acid residues are replaced with glycine/leucine residues on TIRR. Additionally, the candidate 5 NES on TIRR is present at the C-terminus. NUDT16 displays a truncated C-terminus relative to TIRR, and so only part of the candidate 5 NES would be present at the corresponding residues in NUDT16. It is therefore interesting to speculate that, if either candidate 2 or 5 is the functional NES on TIRR, the presence of the NES may confer additional damage specific functions to TIRR compared to NUDT16. This parallels the additional function of TIRR over NUDT16 for 53BP1 binding, due to the presence of H106 in TIRR[25].

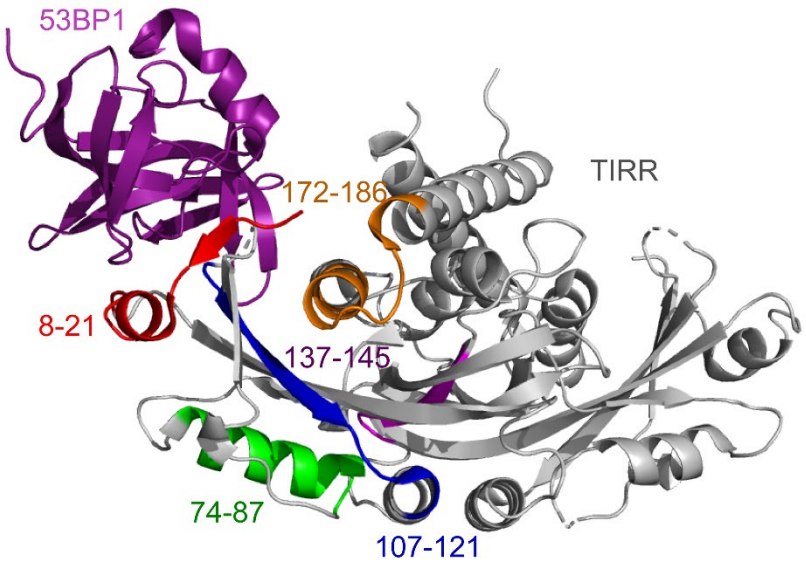


Figure 4.17: *Overlay of 53BP1 Tudor (from PDB:6CO1) with TIRR (PDB: 6D0L) annotated with candidate NES sequences.*

4.4.4 TIRR can regulate the formation of cytoplasmic RNA granules after stress

We have shown that TIRR can localise to both SGs and PBs in response to cell stress or DNA damage. TIRR can also localise to PBs in non-stressed conditions, and this appears to be enhanced by IR, although this could reflect the general increase in PBs observed after IR and TIRR overexpression (**Figure 4.11**). We observe that TIRR overexpression enhances the formation of SGs in response to oxidative stress induced by sodium arsenite, and reciprocally TIRR knockdown reduces SG formation (**Figure 4.13**). We did not observe any formation of SGs after IR at the dosage and time points used in our study (data not shown), although we can't completely exclude the possibility that they may form at later time points or at different IR doses, as is the case with UV induced damage[21]. TIRR may therefore target specific RNAs to SGs for translational repression and/or stabilisation, and TIRR itself may form part of the stress granule compartment.

To our knowledge, no investigation has evaluated the contribution of P-body or SG formation for DSBs repair by NHEJ or HR. However, in response to replication stress, LSM1 regulates YOX1 mRNA in P-bodies, targeting YOX1 for degradation and preventing YOX1-mediated transcriptional repression of genes important for survival after replication stress[22]. P-body numbers also increase after replication stress induced by HU[23]. Therefore, PBs are important for cell survival after replication stress. It is likely that similar control of certain transcripts would exist in response to other types of DNA damage, including DSBs. In our studies we observe that the number of PBs slightly increases after exposure to IR, which suggests an increase in the number of RNAs which are either targeted for stabilisation or degradation in response to IR. We found that TIRR overexpression enhanced the formation of PBs in non-damage conditions, and this increase persisted over the GFP control after IR-induced DNA damage, suggesting that TIRR could targets RNA to PBs either for stabilisation or degradation

in response to IR (**Figures 4.11 and 4.12**), in a manner similar to that observed with TIRR-mediated stress granule formation after stress. This would also agree with the observed role of TIRR in translational repression[1]. We found that TIRR binds to different RNAs after DSB induction (**Figure 4.6.A**), which could suggest that TIRR may target different RNAs to RNA granules after stress/damage compared to non-damage conditions. In agreement with this, we can see that TIRR binds to RNAs involved in transcription and related to cell stress programs after DSBs (**Figure 4.6.D**), which suggests TIRR may regulate the processing or stability of these transcripts by enhancing their sequestration into RNA granules.

TIRR knockdown did not appear to influence the formation of PBs in non-damage conditions (**Figure 4.12**), suggesting TIRR may not be an essential component for the formation of PBs in resting conditions. However, upon DSB-induction by IR, TIRR knockdown enhanced the formation of PBs over the GFP control. This was unexpected as TIRR overexpression also enhances PB formation, even in non-damage conditions. There are several possible explanations for this observed increase in PBs in both TIRR knockdown and overexpression. Firstly, TIRR may target RNAs into PBs, and this is enhanced after TIRR overexpression and/or IR, resulting in the increased formation of PBs. The knockdown of TIRR may therefore result in the formation of PBs due to the need to sequester these transcripts after damage and the lack of regulation of these transcripts by TIRR, in a compensatory mechanism. Secondly, dynamic regulation exists between SGs and PBs, with some proteins and RNAs able to move between polysomes, SGs, and PBs (**Section 4.2**). Given that TIRR may play a role in targeting RNAs to both SGs and PBs (**Figures 4.11.C and 4.13.E**), and TIRR can associate with polysomes[1], TIRR appears to be a protein which can dynamically regulate SGs, PBs, and polysomes. Given that TIRR knockdown results in reduced SG formation after stress, it is tempting to speculate that TIRR knockdown may result in channelling these transcripts to PBs,

and may therefore result in a reciprocal increase in the number of PBs after stress. However, we did not test if TIRR regulates PB formation in response to oxidative stress induced by SA, and we also did not observe SG formation after IR, so this possibility would warrant further investigation. Thirdly, we also see that the knockdown of TIRR can influence the levels of proteins which can either associate with SGs and PBs, are involved in RNA processing, or are known RNA-binding proteins (**Section 4.4.6**). Therefore, TIRR may be involved in the targeting of RNAs to PBs, but may also indirectly influence the number of PBs through regulation of proteins which are targeted to RNA granules and influence their formation.

Aside from TIRR, other NUDIX proteins are also involved in RNA processing and RNA granule formation. NUDT16 is a close paralogue of TIRR and is involved in decapping U8 snoRNA and mRNA in both the nucleus and the cytoplasm in mammalian cells[45]. NUDT16, in a redundant fashion with DCP2 (which is also a NUDIX protein (NUDT20)), plays a role in the degradation of AU-rich element (ARE)-containing mRNA and in miRNA-mediated RNA degradation via 5' → 3' RNA decay. However, knockdown of NUDT16 in steady-state/non-damage conditions does not impact the formation of P-bodies[44]. On the other hand, NUDT3 has also been implicated in decapping of mRNAs which are involved in cell motility[71]. A chemical inhibitor of NUDT3 resulted in an increase in P-body numbers, likely due to stabilisation of NUDT3 target mRNAs[72]. TIRR lacks the catalytic activity of other NUDIX proteins due to the absence of key glutamic acid residues in the NUDIX motif (**Section 1.4**), and also does not display decapping activity *in vitro*, unlike NUDT16[73], however it is feasible that TIRR could also play a role in RNA stability/degradation through RNA binding, rather than a catalytic role. There is also an interesting suggestion that TIRR and NUDT16 could form a heterodimer[6], and therefore it is possible that a TIRR/NUDT16 heterodimer could influence RNA decapping. However, we have not yet found any evidence to suggest this is the case.

Given that we observe an interaction of TIRR with XPO1 after DNA damage, and an increased number of RNA granules after cell stress/damage which appear to be regulated by TIRR, we speculate that the interaction of TIRR with XPO1 and RNA granule targeting may be linked. PB formation is known to be coordinated with XPO1-mediated nuclear export. Human PAT1B, a component of P-bodies, can interact with XPO1 via a NES motif and is shuttled out of the nucleus into the cytoplasm[74]. Furthermore, treatment of cells with an XPO1 inhibitor, Leptomycin B (LMB), reduces the number of PBs in cells, suggesting XPO1-mediated export may be important for proper PB formation[74]. Stress granule formation and nuclear export have also been shown to be closely linked. RAN, part of the export complex with XPO1, localises into SGs, as can XPO1 itself[75]. Additionally, HuR can mediate the export of several different mRNA into the cytoplasm via XPO1. It was observed that heat shock increased the interaction of HuR with XPO1, and HuR was responsible for the export of hsp70 mRNA after heat shock[76]. HuR can also localise into stress granules after stress induced by sodium arsenite[77]. Therefore, the known links between nuclear export and RNA granule formation could suggest an interesting hypothesis that TIRR-mediated export could influence RNA sequestration into RNA granules. However, several points may argue against this model. Firstly, even in non-damage conditions we can see that TIRR can localise into PBs (**Figure 4.11.C**). Nevertheless, this could be explained by the existence of TIRR already in the cytoplasm in non-damage conditions, and after damage TIRR may regulate RNA granule formation via enhanced export from the nucleus. Additionally, even in non-damage conditions some low levels of endogenous DNA damage will be present. Secondly, we do not know if the TIRR/XPO1 interaction is enhanced after other types of cell stress other than DSBs/DNA damage, such as oxidative stress, where we observe that TIRR regulates SG formation. It would be important to address this question, such as by PLA or Co-IP with TIRR and XPO1 after sodium arsenite treatment,

in order to add support to this model. Lastly, we would need to examine if TIRR can act as an adaptor protein for RNA export via XPO1, or if TIRR which is not bound to RNA is the main target of XPO1 after DNA damage.

4.4.5 TIRR broadly does not influence steady state levels of RNA

Performing total RNA-Seq after TIRR knockdown showed that broadly TIRR knockdown does not induce wide-spread changes in steady state RNA levels at the time point tested (48 hours after induction of TIRR knockdown using doxycycline) (**Figure 4.8.C**). Similarly, this was also the case after IR, as when RNA was collected 6 hours post-IR (10Gy) after TIRR knockdown, very few changes were observed that were dependent on both TIRR and IR (**Figure 4.8.D**). Therefore, TIRR does not appear to broadly regulate steady state RNA levels in either non-damage or post-damage conditions. RNAs which were differentially expressed between shTIRR and shGFP control conditions were also not well represented in RNAs identified as bound to TIRR (**Figures 4.5.D and 4.5.E**), suggesting TIRR binding to different RNAs does not broadly influence their steady-state levels.

Interestingly, proteins which target RNAs in PB or SG RNA granules may also not influence the steady state levels of these RNAs. DDX6 is a key component of PBs, and DDX6 knockdown results in impaired PB formation[11]. Whilst DDX6 knockdown results in a modest increase in translation of PB-targeted RNAs, indicating a general role of PBs in translational repression and subsequent resumption of translation, DDX6 knockdown does not result in accumulation of transcripts at the RNA level which are targeted to PBs[11]. Furthermore, targeting of RNAs to SGs after stress does not result from a general increase in the total levels of these RNAs[9]. Therefore, it is possible that TIRR may not generally influence the levels of particular transcripts, but may rather influence their cellular location, such as through

sequestration in RNA granules. Additionally, TIRR may only act on a subset of RNA transcripts, in a similar manner to NUDT16 and NUDT3[78].

It is also possible that our studies on the influence of TIRR on total RNA levels could be expanded to fully explore if TIRR can regulate RNA at the transcript level. We harvested RNA 48 hours post addition of doxycycline to induce TIRR knockdown, when we know knockdown at the protein level is >90% (**Figure 4.8.A**). Given the ability of TIRR to localise into RNA granules, it may be beneficial to look at time points later than 48 hours, to assess if TIRR may influence RNA stability, which may become more apparent after an extended period of knockdown. To further explore the influence of TIRR on RNA stability, performing RNA-Seq in the presence of RNAPII transcriptional arrest would further help address if TIRR may influence RNA stability/half-life, in a similar manner to NUDT16, whose knockdown followed by transcriptional arrest resulted in the ability to measure the increased half-life/stability of a subset of mRNA due to reduced decapping activity[79]. It may also be useful to sequence the RNA content of RNA granules specifically[11,80], rather than total RNA-Seq which may mask changes in the RNA content of granules. This would also help to overcome any effect of 'transcript buffering', a phenomenon observed where depletion of RNA decay proteins leads to a decrease in RNA decay but does not lead to dramatic changes in steady-state RNA levels due to a reciprocal decrease in transcription[81].

4.4.6 TIRR can regulate the protein levels of proteins involved in RNA metabolism and DNA damage

By performing mass spectrometry analysis on whole cell lysates in TIRR knockdown conditions with and without damage, we identified several proteins which are regulated either directly or indirectly by TIRR at the protein level (**Figures 4.15.A and 4.15.B**) and are known to be involved in the DNA damage response. These proteins include NBN, RSF1, and ASF1A,

which are involved in DSB repair via end resection as part of the MRN complex, through chromatin remodelling[53], and through promoting RNF168 recruitment via MDC1 binding, respectively[52]. This could be a result of deregulation of 53BP1 due to lack of TIRR binding, or could suggest TIRR may play additional roles in regulating repair pathway choice either directly or indirectly through regulation of other proteins.

TIRR appears to also regulate a number of proteins involved in RNA processing, including components of the PB and SG proteomes. TIRR knockdown resulted in increased levels of CNOT3 in non-damage conditions, part of the CNOT deadenylation complex. Previous studies have found that the CNOT complex is present in P-bodies, and knockdown of CNOT1 or CNOT2 resulted in reduced P-body numbers[82,83]. DUSP12 was upregulated in TIRR KD after IR, which is part of the RNA granule proteome[12] and localises into SGs, with DUSP12 knockdown preventing stress granule disassembly[84]. Meanwhile, TUT7, involved in RNA decay, and RBM33, were downregulated after IR, and MSI2 was downregulated after TIRR KD without damage, which are all identified as part of the RNA granule proteome[12]. Overall, 5/73 proteins altered in TIRR knockdown in either -IR or +IR in the WCL mass spectrometry dataset were identified as PB or SG proteome components in Tier 1 or Tier 2 (highest confidence, weighted mainly on microscopy evidence for localisation, evidence for physical association, or genetic evidence) in the RNA Granule database[12]. An additional 43 proteins identified through WCL mass spectrometry were present in the RNA granule database with low weighted evidence (Tier 4, RNA binding evidence with as yet no evidence for SG or PB localisation/regulation)[12]. This could suggest that TIRR may influence RNA granule assembly through multiple mechanisms, including RNA binding and regulation of the levels of proteins involved in RNA processing / granule formation.

Interestingly, TIRR knockdown also resulted in the downregulation of proteins which are known to play a role in RNA export via the main RNA export machinery, the TREX complex and NFX1 pathway[85]: CHTOP in non-damage conditions, and RBM33 after damage. RBM33 binds to RNAs and mediates their export through interaction with NFX1[85], and CHTOP, part of the TREX complex, interacts with NFX1 to promote NFX1 RNA binding activity and RNA export[51]. It is therefore possible that TIRR may influence RNA export also through regulation of other RNA export pathways.

It is important to keep in mind that the mass spectrometry data reflects only around 15-20% of the whole cell proteome (~3500 proteins identified out of ~20,000 total proteins), and therefore the dataset will have intrinsic bias (more abundant proteins will be represented whilst proteins present at low levels will not be reliably identified). However, the data are useful to capture an overview of the influence of TIRR knockdown in non-damage and damage, and highlight how TIRR may regulate DNA repair and/or RNA processing through multiple direct and indirect mechanisms.

4.4.7 Future work

Future work should focus on understanding the significance of the observations detailed in this chapter. Firstly, does TIRR binding to RNA influence their sequestration into RNA granules? To address this question, experiments looking at specific RNA candidates identified using RIP-Seq and their fate after DNA damage, such as RNA granule localisation or translation into protein, in the presence and absence of TIRR, would shed light on the function of TIRR RNA binding. Expanding on this, ribosome profiling experiments with TIRR knockdown / overexpression after cell stress would highlight the role of TIRR in promoting/repressing translation of specific RNAs, potentially those which are bound to TIRR after damage. In addition, as mentioned in **Section 4.4.5**, experiments centred on addressing the exact role of

TIRR sequestration in RNA granules, such as to influence RNA stability/degradation like NUDT16, would help understand why exactly TIRR may localise into RNA granules.

Mapping of the functional export sequence on TIRR, starting with the prioritised candidates identified in **Figures 4.10.A and 4.10.B**, would then allow functional studies on the relevance of TIRR binding to XPO1. Interesting questions to address include; what would be the consequence of mutating the functional NES in TIRR on SG and/or PB formation after DNA damage/cell stress? Is the functional NES one which would be precluded from XPO1 binding by 53BP1 binding, or is TIRR which binds to XPO1 distinct from TIRR which binds 53BP1? Does TIRR binding to XPO1 facilitate RNA export from the nucleus? Transcriptomics of nuclear and cytoplasmic RNA in TIRR KD conditions after damage would be important to address the relevance of XPO1 interaction after damage. Lastly, it would be interesting to address the contribution of different TIRR functions (53BP1 binding vs RNA binding / export) on DNA repair outcomes. Does TIRR RNA regulation also contribute to the reduced HR efficiency observed in TIRR knockdown (**Figure 3.21**)? Rescue experiments using 53BP1-binding null (K10E) TIRR and WT TIRR would help address this question.

In summary, TIRR is a damage-responsive RNA binding protein, which can localise to and regulate the formation of RNA granules in response to DNA damage/stress. TIRR can interact with XPO1 after DNA damage, in an as yet uncharacterised mechanism and can also regulate the levels of proteins involved in RNA processing and DNA repair (**Figure 4.18**). Together this highlights how TIRR may further augment the DNA damage response in addition to 53BP1 binding. In particular, RNA processing and RNA granule deregulation are known to be associated with cancers and other diseases[9], which could be potentially relevant given that TIRR is amplified in a subset of cancer, in particular breast cancers (**Figure 3.22**). How TIRR

coordinates its RNA binding/regulatory function with its 53BP1 binding function, and the extent to which TIRR influences DNA repair through RNA regulation is currently unclear, but will be an interesting area for future studies. Collectively, this work provides a preliminary foundation for understanding the role of TIRR outside of 53BP1 binding in the DNA damage response.

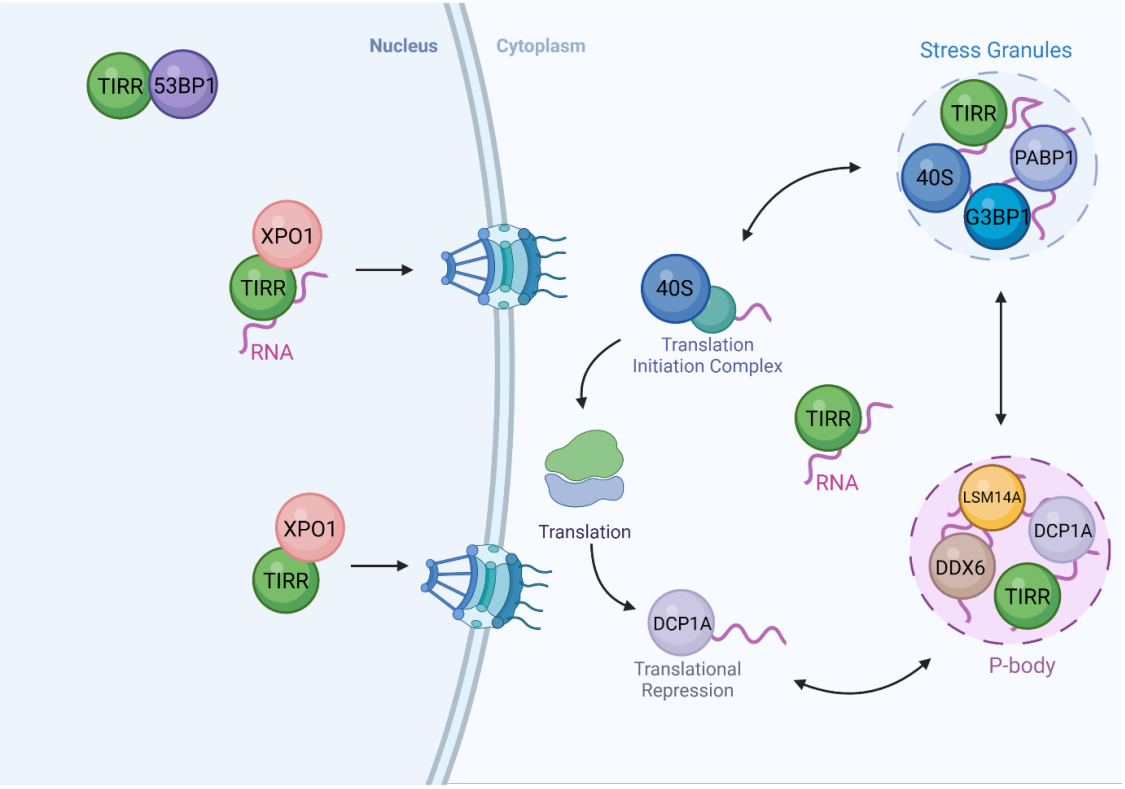


Figure 4.18: *Potential functions of TIRR in RNA export and RNA processing*[14]*. Image created with BioRender.com.*

4.5 References

1. Avolio, R. *et al.* Protein Syndesmos is a novel RNA-binding protein that regulates primary cilia formation. *Nucleic Acids Res.* (2018) doi:10.1093/nar/gky873.
2. Avolio, R. Characterization of novel RNA binding proteins in cancer. (UNIVERSITY OF NAPLES "FEDERICO II", 2017).
3. Drané, P. *et al.* TIRR regulates 53BP1 by masking its histone methyl-lysine binding function. *Nature* **543**, 211–216 (2017).
4. Parnandi, N. *et al.* TIRR inhibits the 53BP1-p53 complex to alter cell-fate programs. *Mol. Cell* **81**, (2021).
5. Dai, Y., Zhang, A., Shan, S., Gong, Z. & Zhou, Z. Structural basis for recognition of 53BP1 tandem Tudor domain by TIRR. *Nat. Commun.* **9**, (2018).
6. Wang, J. *et al.* Molecular basis for the inhibition of the methyl-lysine binding function of 53BP1 by TIRR. *Nat. Commun.* **9**, (2018).
7. He, C. *et al.* High-Resolution Mapping of RNA-Binding Regions in the Nuclear Proteome of Embryonic Stem Cells. *Mol. Cell* **64**, (2016).
8. Treiber, T. *et al.* A Compendium of RNA-Binding Proteins that Regulate MicroRNA Biogenesis Molecular Cell Resource A Compendium of RNA-Binding Proteins that Regulate MicroRNA Biogenesis. *Mol. Cell* **66**, 270-281.e13 (2017).
9. Namkoong, S., Ho, A., Woo, Y. M., Kwak, H. & Lee, J. H. Systematic Characterization of Stress-Induced RNA Granulation. *Mol. Cell* **70**, 175-187.e8 (2018).
10. Chantarachot, T. & Bailey-Serres, J. Polysomes, Stress Granules, and Processing Bodies: A Dynamic Triumvirate Controlling Cytoplasmic mRNA Fate and Function. *Plant Physiol.* **176**, 254–269 (2018).
11. Hubstenberger, A. *et al.* P-Body Purification Reveals the Condensation of Repressed mRNA Regulons. *Mol. Cell* **68**, 144-157.e5 (2017).
12. Youn, J.-Y. *et al.* Properties of Stress Granule and P-Body Proteomes. *Mol. Cell* **76**, 286–294 (2019).
13. Decker, C. J. & Parker, R. P-bodies and stress granules: possible roles in the control of translation and mRNA degradation. *Cold Spring Harb. Perspect. Biol.* **4**, a012286 (2012).
14. Buchan, J. R. & Parker, R. Eukaryotic stress granules: the ins and outs of translation. *Mol. Cell* **36**, 932–941 (2009).
15. Zheng, D., Chen, C.-Y. A. & Shyu, A.-B. Unraveling regulation and new components of human P-bodies through a protein interaction framework and experimental validation. *RNA N. Y. N* **17**, 1619–1634 (2011).
16. Kedersha, N. *et al.* Stress granules and processing bodies are dynamically linked sites of mRNP remodeling. *J. Cell Biol.* **169**, 871–884 (2005).
17. Wang, C. *et al.* Context-dependent deposition and regulation of mRNAs in P-bodies. *eLife* **7**, e29815 (2018).
18. Campos-Melo, D., Hawley, Z. C. E., Droppelmann, C. A. & Strong, M. J. The Integral Role of RNA in Stress Granule Formation and Function. *Front. Cell Dev. Biol.* **9**, 621779 (2021).
19. Courel, M. *et al.* GC content shapes mRNA storage and decay in human cells. *eLife* **8**, e49708 (2019).
20. Ying, S. & Khaperskyy, D. A. UV damage induces G3BP1-dependent stress granule formation that is not driven by translation arrest via mTOR inhibition. *J. Cell Sci.* jcs.248310 (2020) doi:10.1242/jcs.248310.
21. Moutaoufik, M. T. *et al.* UVC-Induced Stress Granules in Mammalian Cells. *PLoS ONE* **9**, e112742 (2014).
22. Loll-Krippleber, R. & Brown, G. W. P-body proteins regulate transcriptional rewiring to promote DNA replication stress resistance. *Nat. Commun.* **8**, 558 (2017).
23. Tkach, J. M. *et al.* Dissecting DNA damage response pathways by analysing protein localization and abundance changes during DNA replication stress. *Nat. Cell Biol.* **14**, 966–976 (2012).
24. Hannus, M. *et al.* siPools: highly complex but accurately defined siRNA pools eliminate off-target effects. *Nucleic Acids Res.* **42**, 8049–8061 (2014).
25. Botuyan, M. V. *et al.* Mechanism of 53BP1 activity regulation by RNA-binding TIRR and a designer protein. *Nat. Struct. Mol. Biol.* **25**, 591–600 (2018).
26. Briggs, E. M. *et al.* RIP-seq reveals LINE-1 ORF1p association with p-body enriched mRNAs. *Mob. DNA* **12**, 5 (2021).
27. Holmes, Z. E. *et al.* The Sox2 transcription factor binds RNA. *Nat. Commun.* **11**, (2020).
28. Zhao, J. *et al.* Genome-wide Identification of Polycomb-Associated RNAs by RIP-seq. *Mol. Cell* **40**, 939–953 (2010).
29. Wheeler, E. C., Van Nostrand, E. L. & Yeo, G. W. Advances and challenges in the detection of transcriptome-wide protein–RNA interactions. *WIREs RNA* **9**, (2018).
30. Palazzo, A. F. & Kang, Y. M. GC-content biases in protein-coding genes act as an "mRNA identity" feature for nuclear export. *BioEssays* **43**, 2000197 (2021).
31. Higgs, M. R. *et al.* BOD1L Is Required to Suppress Deleterious Resection of Stressed Replication Forks. *Mol. Cell* **59**, 462–477 (2015).

32. Lin, Y. *et al.* PIK3R1 negatively regulates the epithelial-mesenchymal transition and stem-like phenotype of renal cancer cells through the AKT/GSK3β/CTNNB1 signaling pathway. *Sci. Rep.* **5**, 8997 (2015).
33. Wang, H. *et al.* DCAF4L2 promotes colorectal cancer invasion and metastasis via mediating degradation of NFκb negative regulator PPM1B. *Am. J. Transl. Res.* **8**, 405–418 (2016).
34. Gunaratne, J. *et al.* Protein interactions of phosphatase and tensin homologue (PTEN) and its cancer-associated G20E mutant compared by using stable isotope labeling by amino acids in cell culture-based parallel affinity purification. *J. Biol. Chem.* **286**, 18093–18103 (2011).
35. Van Roey, K. *et al.* Short Linear Motifs: Ubiquitous and Functionally Diverse Protein Interaction Modules Directing Cell Regulation. *Chem. Rev.* **114**, 6733–6778 (2014).
36. Wickramasinghe, V. O. & Laskey, R. A. Control of mammalian gene expression by selective mRNA export. *Nat. Rev. Mol. Cell Biol.* **16**, 431–442 (2015).
37. Azizian, N. G. & Li, Y. XPO1-dependent nuclear export as a target for cancer therapy. *J. Hematol. Oncol.J Hematol Oncol* **13**, 61 (2020).
38. Kırlı, K. *et al.* A deep proteomics perspective on CRM1-mediated nuclear export and nucleocytoplasmic partitioning. *eLife* **4**, e11466 (2015).
39. Kosugi, S., Yanagawa, H., Terauchi, R. & Tabata, S. NESmapper: Accurate Prediction of Leucine-Rich Nuclear Export Signals Using Activity-Based Profiles. *PLoS Comput. Biol.* **10**, e1003841 (2014).
40. Prieto, G., Fullaondo, A. & Rodriguez, J. A. Prediction of nuclear export signals using weighted regular expressions (Wregex). *Bioinformatics* **30**, 1220–1227 (2014).
41. Xu, D. *et al.* LocNES: a computational tool for locating classical NESs in CRM1 cargo proteins. *Bioinforma. Oxf. Engl.* **31**, 1357–1365 (2015).
42. Lee, Y., Pei, J., Baumhardt, J. M., Chook, Y. M. & Grishin, N. V. Structural prerequisites for CRM1-dependent nuclear export signaling peptides: accessibility, adapting conformation, and the stability at the binding site. *Sci. Rep.* **9**, 6627 (2019).
43. Thompson, M. E. BRCA1 16 years later: nuclear import and export processes. *FEBS J.* **277**, 3072–3078 (2010).
44. Li, Y., Song, M. & Kiledjian, M. Differential utilization of decapping enzymes in mammalian mRNA decay pathways. *RNA* **17**, (2011).
45. Lu, G. *et al.* hNUDT16: A universal decapping enzyme for small nucleolar RNA and cytoplasmic mRNA. *Protein Cell* **2**, 64–73 (2011).
46. Matsuki, H. *et al.* Both G3BP1 and G3BP2 contribute to stress granule formation. *Genes Cells* **18**, 135–146 (2013).
47. Ponomarenko, E. A. *et al.* The Size of the Human Proteome: The Width and Depth. *Int. J. Anal. Chem.* **2016**, 1–6 (2016).
48. Bergfort, A. *et al.* A multi-factor trafficking site on the spliceosome remodeling enzyme BRR2 recruits C9ORF78 to regulate alternative splicing. *Nat. Commun.* **13**, 1132 (2022).
49. Shirai, Y.-T., Suzuki, T., Morita, M., Takahashi, A. & Yamamoto, T. Multifunctional roles of the mammalian CCR4-NOT complex in physiological phenomena. *Front. Genet.* **5**, (2014).
50. Sun, C. The SF3b complex: splicing and beyond. *Cell. Mol. Life Sci.* **77**, 3583–3595 (2020).
51. Chang, C.-T. *et al.* Chtop is a component of the dynamic TREX mRNA export complex. *EMBO J.* **32**, 473–486 (2013).
52. Lee, K. Y., Im, J.-S., Shibata, E. & Dutta, A. ASF1a Promotes Non-homologous End Joining Repair by Facilitating Phosphorylation of MDC1 by ATM at Double-Strand Breaks. *Mol. Cell* **68**, 61-75.e5 (2017).
53. Pessina, F. & Lowndes, N. F. The RSF1 Histone-Remodelling Factor Facilitates DNA Double-Strand Break Repair by Recruiting Centromeric and Fanconi Anaemia Proteins. *PLoS Biol.* **12**, e1001856 (2014).
54. Lim, J. *et al.* Uridylation by TUT4 and TUT7 Marks mRNA for Degradation. *Cell* **159**, 1365–1376 (2014).
55. Chu, X. *et al.* Structural insights into Paf1 complex assembly and histone binding. *Nucleic Acids Res.* **41**, 10619–10629 (2013).
56. Bertrand, R. E. *et al.* Cwc27, associated with retinal degeneration, functions as a splicing factor *in vivo*. *Hum. Mol. Genet.* **31**, 1278–1292 (2022).
57. Rivera, C. *et al.* Unveiling RCOR1 as a rheostat at transcriptionally permissive chromatin. *Nat. Commun.* **13**, 1550 (2022).
58. Putzbach, W. *et al.* DISE: A Seed-Dependent RNAi Off-Target Effect That Kills Cancer Cells. *Trends Cancer* **4**, 10–19 (2018).
59. Fedorov, Y. *et al.* Off-target effects by siRNA can induce toxic phenotype. *RNA N. Y. N* **12**, 1188–1196 (2006).
60. Putzbach, W. *et al.* Many si/shRNAs can kill cancer cells by targeting multiple survival genes through an off-target mechanism. *eLife* **6**, e29702 (2017).
61. Patel, M. & Peter, M. E. Identification of DISE-inducing shRNAs by monitoring cellular responses. *Cell Cycle Georget. Tex* **17**, 506–514 (2018).
62. Feng, Z., Kachnic, L., Zhang, J., Powell, S. N. & Xia, F. DNA damage induces p53-dependent BRCA1 nuclear export. *J. Biol. Chem.* **279**, 28574–28584 (2004).

63. Rodríguez, J. A. & Henderson, B. R. Identification of a functional nuclear export sequence in BRCA1. *J. Biol. Chem.* **275**, 38589–38596 (2000).
64. Fabbro, M., Rodriguez, J. A., Baer, R. & Henderson, B. R. BARD1 induces BRCA1 intranuclear foci formation by increasing RING-dependent BRCA1 nuclear import and inhibiting BRCA1 nuclear export. *J. Biol. Chem.* **277**, 21315–21324 (2002).
65. Jiang, J. *et al.* p53-dependent BRCA1 nuclear export controls cellular susceptibility to DNA damage. *Cancer Res.* **71**, 5546–5557 (2011).
66. Brodie, K. M. & Henderson, B. R. Characterization of BRCA1 protein targeting, dynamics, and function at the centrosome: a role for the nuclear export signal, CRM1, and Aurora A kinase. *J. Biol. Chem.* **287**, 7701–7716 (2012).
67. Stommel, J. M. *et al.* A leucine-rich nuclear export signal in the p53 tetramerization domain: regulation of subcellular localization and p53 activity by NES masking. *EMBO J.* **18**, 1660–1672 (1999).
68. Zhang, Y. & Xiong, Y. A p53 Amino-Terminal Nuclear Export Signal Inhibited by DNA Damage-Induced Phosphorylation. *Science* **292**, 1910–1915 (2001).
69. Yang, J., Bogerd, H. P., Wang, P. J., Page, D. C. & Cullen, B. R. Two closely related human nuclear export factors utilize entirely distinct export pathways. *Mol. Cell* **8**, 397–406 (2001).
70. Ray, A. & Frick, D. N. Fluorescent probe displacement assays reveal unique nucleic acid binding properties of human nudix enzymes. *Anal. Biochem.* **595**, 113622 (2020).
71. Grudzien-Nogalska, E., Jiao, X., Song, M.-G., Hart, R. P. & Kiledjian, M. Nudt3 is an mRNA decapping enzyme that modulates cell migration. *RNA N. Y. N* **22**, 773–781 (2016).
72. Sahu, S. *et al.* InsP7 is a small-molecule regulator of NUDT3-mediated mRNA decapping and processing-body dynamics. *Proc. Natl. Acad. Sci.* **117**, 19245–19253 (2020).
73. Taylor, M. J. & Peculis, B. A. Evolutionary conservation supports ancient origin for Nudt16, a nuclear-localized, RNA-binding, RNA-decapping enzyme. *Nucleic Acids Res.* **36**, 6021 (2008).
74. Marnef, A., Weil, D. & Standart, N. RNA-related nuclear functions of human Pat1b, the P-body mRNA decay factor. *Mol. Biol. Cell* **23**, 213–224 (2012).
75. Zhang, K. *et al.* Stress Granule Assembly Disrupts Nucleocytoplasmic Transport. *Cell* **173**, 958-971.e17 (2018).
76. Gallouzi, I. E., Brennan, C. M. & Steitz, J. A. Protein ligands mediate the CRM1-dependent export of HuR in response to heat shock. *RNA N. Y. N* **7**, 1348–1361 (2001).
77. David, P. S., Tanveer, R. & Port, J. D. FRET-detectable interactions between the ARE binding proteins, HuR and p37AUF1. *RNA N. Y. N* **13**, 1453–1468 (2007).
78. SGrudzien-Nogalska, E. & Kiledjian, M. New insights into decapping enzymes and selective mRNA decay. *Wiley Interdiscip. Rev. RNA* **8**, (2017).
79. Song, M.-G., Li, Y. & Kiledjian, M. Multiple mRNA Decapping Enzymes in Mammalian Cells. *Mol. Cell* **40**, 423 (2010).
80. Matheny, T., Rao, B. S. & Parker, R. Transcriptome-Wide Comparison of Stress Granules and P-Bodies Reveals that Translation Plays a Major Role in RNA Partitioning. *Mol. Cell. Biol.* **39**, e00313-19 (2019).
81. Timmers, H. Th. M. & Tora, L. Transcript Buffering: A Balancing Act between mRNA Synthesis and mRNA Degradation. *Mol. Cell* **72**, 10–17 (2018).
82. Ito, K. *et al.* CNOT2 depletion disrupts and inhibits the CCR4-NOT deadenylase complex and induces apoptotic cell death. *Genes Cells Devoted Mol. Cell. Mech.* **16**, 368–379 (2011).
83. Ito, K., Takahashi, A., Morita, M., Suzuki, T. & Yamamoto, T. The role of the CNOT1 subunit of the CCR4-NOT complex in mRNA deadenylation and cell viability. *Protein Cell* **2**, 755–763 (2011).
84. Geng, Q., Xhabija, B., Knuckle, C., Bonham, C. A. & Vacratsis, P. O. The Atypical Dual Specificity Phosphatase hYVH1 Associates with Multiple Ribonucleoprotein Particles. *J. Biol. Chem.* **292**, 539–550 (2017).
85. Thomas, A. *et al.* RBM33 directs the nuclear export of transcripts containing GC-rich elements. *Genes Dev.* **36**, 550–565 (2022).

Chapter 5: Identifying novel binding partners of TIRR in non-damage and damage conditions

5.1 Summary

TurboID, a proximity-based biotin labelling method, and affinity pulldown experiments were carried out on TIRR to identify novel binding partners in non-damage and damage conditions, to enhance our understanding of the function of TIRR in the wider DDR. Here, we optimise a TurboID protocol for TIRR, identifying a total of 67 interactors in non-damage conditions, around ~50% of which are found in previously published datasets as TIRR interactors, suggesting TurboID allows the identification of reproducible TIRR interactors, while also identify novel proteins. We also find 23 damage-specific interactors of TIRR, of which 9 have previously characterised roles in DNA damage and DSB repair. In addition, we find that TIRR interacts with a diverse array of RNA binding and regulatory proteins, a large portion of which are also known to regulate RNA granule formation, further confirming a role of TIRR in RNA processing. To expand on this, we also perform affinity pull-down experiments on TIRR in damage and non-damage, to compare between different methods of interaction capture. We see broadly good overlap between affinity pull-down and TurboID experiments, although TurboID was superior in identifying more TIRR interactors.

5.2 Introduction

Protein-protein interactions (PPIs) are a fundamental part of cell biology. PPIs govern cellular processes and signalling, controlling all aspects of normal cellular function and the responses to environmental cues and stressors, such as DNA damaging agents. Therefore, elucidating PPIs and interaction networks is critical to understanding how biological processes occur and are regulated. However, dissecting these complex interaction networks is not trivial, and poses many technical challenges.

Several methods exist to study PPIs, including *in vitro* methods such as FRET-based assays like HTRF, and cellular assays such as Co-IP and PLA, however these methods are often low-throughput and require at least some previous knowledge of the PPI under investigation. To address these issues, more high-throughput unbiased methods have been extensively used, such as affinity purification mass spectrometry (AP-MS). In AP-MS, a protein of interest (POI) can be immunoprecipitated from cells using either an antibody for the endogenous protein, or by fusing a tag to the POI followed by immunoprecipitation using a tag-specific antibody. AP-MS has been used to study the interactomes of many different proteins. For example, TIRR was discovered as a 53BP1 interaction partner through tandem AP-MS of Flag and HA tagged 53BP1[1]. However, whilst AP-MS is a useful technique, many drawbacks exist including: difficulties in identifying weak, dynamic, and transient interactions which may not be able to withstand harsh lysis or wash conditions resulting in false negatives; mislocalisation of the POI due to affinity tags; and protein mixing in cellular lysates may allow interactions to occur which normally would not in the compartmentalised cellular environment, which could result in false positives[2,3]. To overcome some of these challenges, various proximity labelling assays have been developed.

Proximity labelling followed by mass spectrometry is the process of fusing a POI to a labelling enzyme, which promiscuously labels proteins which directly interact with the POI, as well as proteins in the close vicinity[3]. Currently, the major proximity labelling systems are the APEX system and the BioID system, which allow biotin labelling of interaction partners followed by streptavidin pull-down and identification by mass spectrometry (**Figure 5.1**)[4].

The APEX system uses the ascorbate peroxidase APEX, a ~28kDa enzyme which can catalyse the production of a short-lived biotin-phenoxyl intermediate (~1ms) from H_2O_2 and biotin-phenol. When a POI is fused to APEX, exogenous H_2O_2 and biotin-phenol can be added, and APEX covalently labels surrounding electron rich amino acids, predominantly tyrosine (95-98%)[4,5], but also tryptophan, histidine, and cysteine[3,4]. The labelling radius of APEX is approximately 10-20nm, and the labelling time can be tightly controlled through short incubation times (~1 minute) with H_2O_2. After H_2O_2 incubation, biotinylated proteins can be purified from cells using streptavidin beads and analysed using mass spectrometry. Disadvantageously, H_2O_2 is toxic to cells and could impact normal cellular processes, although short H_2O_2 incubations should not profoundly influence cell signalling[5].

The proximity dependent biotin identification (BioID) system also utilises the covalent biotin modification of proteins in close proximity to the POI. BioID uses the *E. coli* BirA enzyme, a 35kDa protein which usually functions in cells to biotinylate acetyl-CoA carboxylase. BirA catalyses the generation of biotinoyl-5'-AMP (bioAMP) from biotin and ATP, which is then covalently added to the substrate at a primary amine (a lysine residue). The BirA enzyme was modified to be a more promiscuous biotin ligase (R118G, BirA*), to enable the biotinylation of any protein[6]. In BioID, BirA* is fused to the POI, and after addition of exogenous biotin, will covalently label proteins in proximity (10-20nm) to the POI. These biotinylated proteins

can then be purified using streptavidin beads and analysed by mass spectrometry, similarly to the APEX system (**Figure 5.1)**. In contrast to the short labelling times of the APEX system, BioID requires much longer incubation times with biotin, around 18-24 hours, which significantly reduces the temporal resolution of the BioID and would not allow the study of more rapid processes, such as DNA damage repair. As a result of these slow labelling kinetics, other versions of the BioID utilising different biotin ligases generated from BirA have been developed to improve the speed of the labelling window[3]. Directed evolution of BioID resulted in the generation of the more rapid TurboID and miniTurboID biotin ligases[7]. TurboID is a 35kDa protein with biotinylation kinetics which are greatly improved in comparison to the original BioID, with a labelling window of as little as 10 minutes. MiniTurboID is a version of BirA without the N-terminus, generating a smaller 28kDa biotin ligase. MiniTurboID also displays more rapid biotinylation kinetics than BioID, although is slower than TurboID. The labelling radius of TurboID and miniTurboID is comparable to BioID at around 10-20nm, although with much shorter labelling kinetics (10 minutes compared to 18 hours biotin incubation, respectively). However, extended biotin incubation times with TurboID and miniTurboID may result in an increased labelling radius, and therefore more false positive hits, due to saturation of neighbouring lysines with biotin which would allow biotin-AMP to biotinylate proteins a greater distance away. TurboID may also display increased background biotinylation, that is biotinylation without the addition of exogenous biotin, due to its increased activity, and may also sequester endogenous biotin, which could lead to cellular toxicity[7]. Nevertheless, TurboID and miniTurboID are useful tools for studying more rapid cellular processes which occur on the order of minutes or a few hours[7].

Key advantages of proximity labelling systems include the ability to identify PPIs in ‘native’ conditions, without relying on lysis buffers to maintain physiological interactions.

Furthermore, in theory proximity labelling should allow the identification of weak and transient interactions, as interactors with which the interaction would not normally be preserved during lysis and washing steps will be biotinylated. The strong interaction of biotin and streptavidin should then allow weak interactors to be identified. Furthermore, the strength of the biotin-streptavidin interaction allows the use of stringent lysis and wash conditions to reduce false positives.

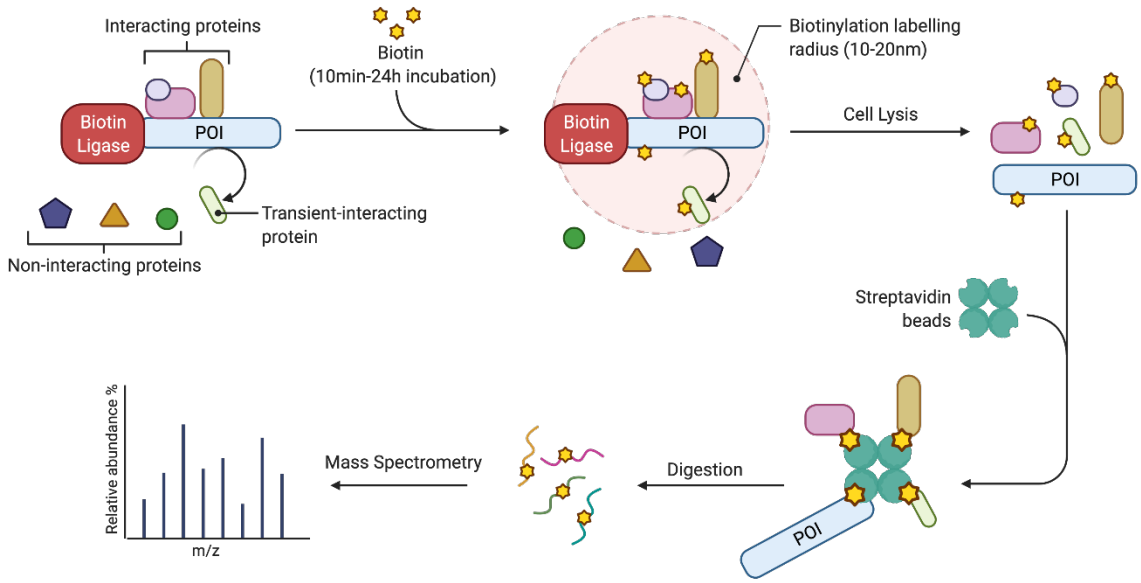


Figure 5.1: *Principles of the biotin proximity labelling assay (BioID/TurboID). A POI is fused to a promiscuous biotin ligase and after the addition of exogenous biotin, proteins in close proximity to the POI are labelled with biotin at lysine residues. Due to the short labelling radius of biotinylation (10-20nm), biotinylated proteins are likely interaction partners with the POI. Biotinylated proteins are enriched using streptavidin beads, digested on-bead, and are then analysed by mass spectrometry. Image created with BioRender.com.*

Our knowledge of the interactome of TIRR, especially in damage conditions, is somewhat limited. Avolio *et al* used an inducible C-terminal GFP tagged version of TIRR in AP-MS in non-damage conditions to identify 39 interaction partners of TIRR in Hela cells[8], while Drané *et al,* also in non-damage conditions, used C-terminally Flag and HA tagged TIRR stably expressed in U2OS cells in tandem AP-MS to identify 757 interaction partners[1], with an

overlap of 18 proteins between the two lists. The BioGRID database of protein interactors also contains 71 protein interactors of TIRR in humans across different experiments (overlap of all available datasets shown in **Figure 5.2**). As discussed in **Chapter 4**, outside of 53BP1 binding, our understanding of the functions of TIRR is also somewhat unexplored. Identifying the interactome of TIRR would therefore aid our understanding of previous observations, such as those in **Chapter 4**, as well as highlighting novel roles of TIRR in cells. Additionally, no interactome for TIRR has been determined in damage conditions. Given that TIRR dissociates from 53BP1 after damage, and the fate of TIRR after dissociation is unknown, determining the TIRR interactome after damage could highlight novel roles of TIRR in the DNA damage response, as well as potentially giving further insight into the mechanism of TIRR-53BP1 dissociation.

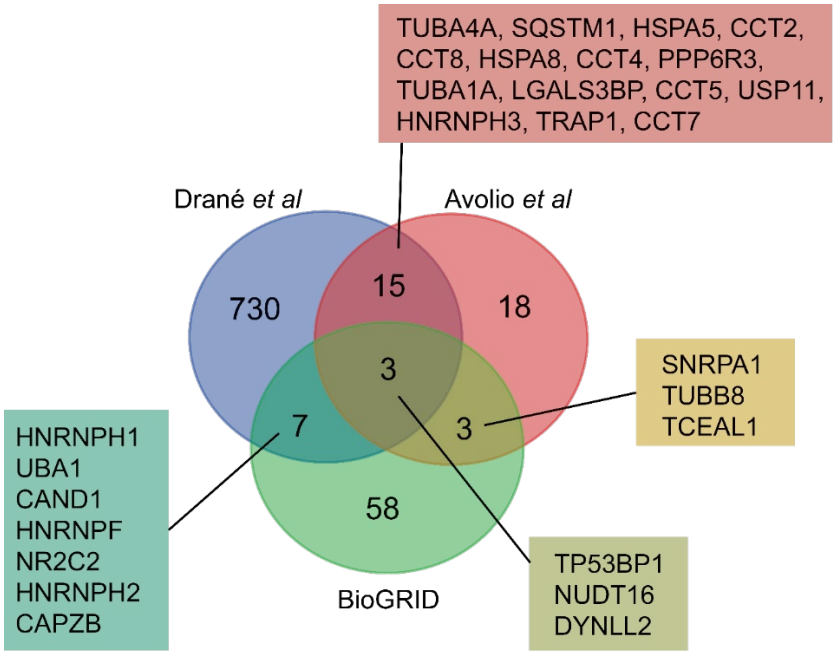


Figure 5.2: *Overlap of three available datasets/databases of TIRR interactors from Drané et al (2017), Avolio et al (2018), and the BioGRID database.*

Therefore, the aim of this chapter is to determine the interactome of TIRR using a proximity labelling technique, TurboID, in both non-damage and damage conditions. We additionally

compare this to an AP-MS performed on TIRR-GFP in damage and non-damage conditions. Using both methods, we hope to get a full picture of the TIRR interactome, including in damage conditions, and also highlight the benefits/drawbacks of each technique.

5.3 Results

5.3.1 Optimising the expression of TIRR with a Biotin Ligase

Initial considerations when designing the TIRR TurboID experiment included the N or C terminal labelling of TIRR with the biotin ligase, the choice of the biotin ligase itself (TurboID or miniTurboID), and the length of the linker between TIRR and the biotin ligase (increasing the length of the linker is reported to increase the radius of biotinylation[9]). Fusion constructs of TIRR tagged at both the N and the C terminus with normal functionality have been published, however since both AP-MS studies were performed with C-terminally tagged TIRR, we decided to initially tag TIRR at the C-terminus with the biotin ligase (**Figure 5.3.A**). We selected the TurboID ligase because despite its slightly larger size over miniTurboID (35kDa vs 28kDa), the TurboID is reported to have shorter biotinylation kinetics which would be useful for looking at specific time points after irradiation (1 hour). The linker between TIRR and TurboID was composed of 13xGly and 3xSer. It has also been suggested that transient expression of the fusion construct results in large cell-to-cell variations in biotinylation. For this reason, we also included an antibiotic resistance gene for stable cell selection. Additionally, careful controls should be selected in BioID/TurboID experiments to allow background biotinylation from the biotin ligase or endogenously biotinylated proteins (some carboxylases) to be distinguished from real interaction partners. For this purpose, we selected the biotin ligase without TIRR (Turbo ID only) as a control.

The resulting Flag-TIRR-TurboID plasmid with bleomycin resistance was transiently transfected into Hela cells, with a construct lacking TIRR as a control. Immunoblotting against the Flag tag demonstrated that the Turbo only plasmid was expressed well, however the TIRR-Turbo construct was not expressed to a readily detectable level (**Figure 5.3.B**). After adding

exogenous biotin to transiently transfected cells, we observed that the Turbo only expressing cells showed detectable biotinylation after 10 minutes of labelling, but as expected from the very low levels of TIRR-Turbo expression, no biotinylation activity could be detected in the TIRR-Turbo expressing cells (**Figure 5.3.C**).

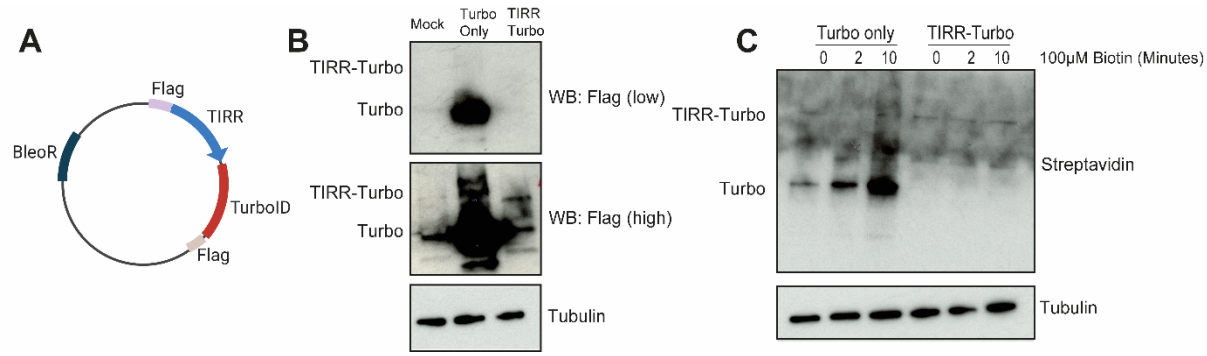


Figure 5.3: ***A)*** *Design of the Flag-tagged TIRR-TurboID (C-terminal) construct.* ***B)*** *Western blot to detect transient expression of TurboID only or TIRR-TurboID in Hela cells as assessed by Flag immunoblot. Tubulin is used as a loading control.* ***C)*** *Transient expression of TurboID only or TIRR-TurboID with addition of 100µM of exogenous biotin for 0 (no biotin control), 2, or 10 minutes. Biotin labelling of proteins is assessed by probing with streptavidin.*

To address this issue, the construct was redesigned (**Figure 5.4.A**). Even though TIRR has been C-terminally expressed with both GFP and NeonGreen which are comparable in size to the TurboID, and appeared to be fully functional, we reasoned that TIRR-Turbo may not express well because either the TurboID was interfering with TIRR folding due to its larger size, or the C-terminal location was problematic for TIRR folding. Therefore, we designed a construct expressing the smaller miniTurboID at the TIRR N-terminus. We also swapped the Flag tags for a V5 tag, as the Flag tag is more lysine-rich and could potentially interfere with biotinylation[10]. Additionally, the linker was made shorter (6xGly, 2Ser) to reduce the radius of biotinylation. Transient expression of both miniTurboID alone or miniTurboID-TIRR was detectable by immunoblot for the V5 tag (**Figure 5.4.B**). Incubation of cells transiently expressing the miniTurboID constructs showed detectable biotinylation activity after 10 minutes of exogenous biotin expression, although this appeared to be comparably lower than

the activity observed with the TurboID only construct, as has been previously reported (**Figure 5.4.C**)[7].

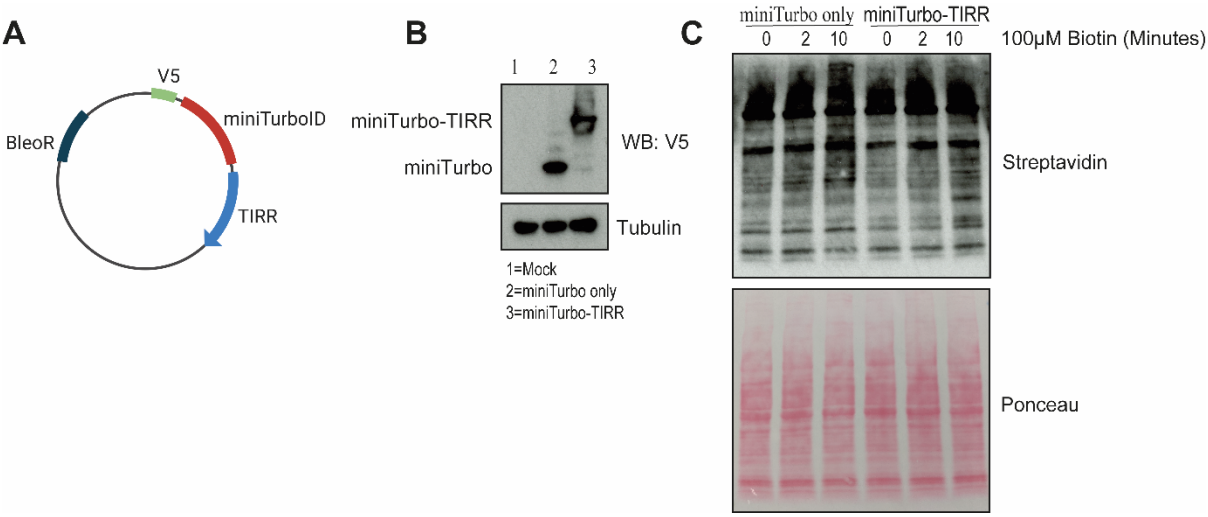


Figure 5.4: ***A)*** *Design of the V5-tagged miniTurboID-TIRR (N-terminal) construct.* ***B)*** *Western blot to detect transient expression of miniTurboID only or miniTurboID-TIRR in Hela cells as assessed by V5 immunoblot. Tubulin is used as a loading control.* ***C)*** *Transient expression of miniTurboID only or miniTurboID-TIRR with addition of 100µM of exogenous biotin for 0 (no biotin control), 2, or 10 minutes. Biotin labelling of proteins is assessed by probing with streptavidin. Ponceau is used as a loading control.*

As miniTurbo-TIRR expressed well, we continued with this construct for stable selection. Stable selection is preferable in BioID/TurboID experiments for multiple reasons. Firstly, by stably selecting cells and then single-cell sorting and screening individual colonies, the expression of the fusion construct can be selected to be closer to endogenous levels. This is more likely to result in near-physiological interactions and minimise false positives from overexpression or mislocalisation of the POI. Secondly, stable selection and single cell sorting will result in a cell line where each cell will express the POI-Biotin Ligase and have the same biotinylation activity, as opposed to transient expression where each cell will vary in expression and biotinylation. This will generate a more reproducible data set without the cell-to-cell variation[10]. Initially transfection of Hela cells with constructs and selection with Zeocin at 100µg/ml after 10 days yielded cell populations which expressed both miniTurbo and miniTurbo-TIRR (**Figure 5.5**), although miniTurbo expression was significantly reduced

compared to miniTurbo-TIRR expression. However, continued selection with Zeocin before single cell sorting resulted in no miniTurbo or miniTurbo-TIRR expression after 2-3 weeks of selection (data not shown).

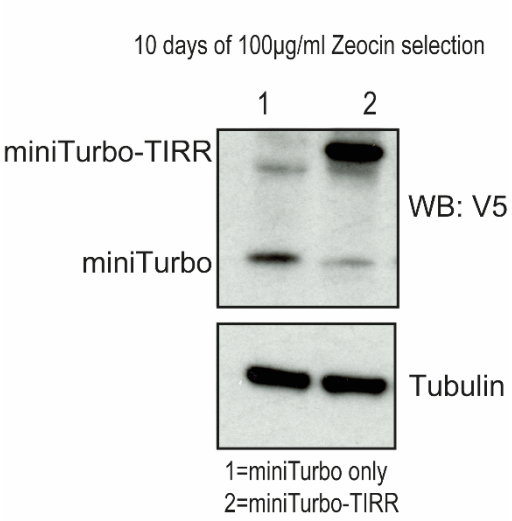


Figure 5.5: *Antibiotic selection of miniTurboID and miniTurboID-TIRR expressing Hela cells with 100µg/ml Zeocin. Immunoblot for V5 is performed after 10 days of Zeocin selection. Tubulin is used as a loading control.*

In an attempt to overcome this, Hela cells were transfected again with miniTurbo or miniTurbo-TIRR and selected with 100µg/ml or 200µg/ml Zeocin for 3 weeks. Immunoblot analysis with V5 revealed that after 200µg/ml selection with Zeocin for 3 weeks, miniTurbo-TIRR cells were no longer expressing the construct, and after addition of exogenous biotin, showed no biotinylation activity (**Figure 5.6.B**). Cells selected with 100µg/ml Zeocin displayed some miniTurbo-TIRR expression, although this was significantly downregulated compared to initial expression and did not result in significant biotinylation activity after addition of exogenous biotin even after 5 hours of biotin incubation, and therefore would likely not be amenable to analysis by mass spectrometry after streptavidin pull down (**Figure 5.6.A**). The reasons for the lack of miniTurbo-TIRR expression despite cells being Zeocin resistant are not clear, but could be either due to cellular toxicity caused by background biotinylation of miniTurbo-TIRR, or,

although anecdotal, could be due to the fact that Zeocin selection appears to result in the downregulation of TIRR expression, as similar difficulties were experienced when attempting to stably select Neongreen-TIRR expressing cells with Zeocin (data not shown). Additionally, although miniTurbo alone was stably expressing after both 100µg/ml and 200µg/ml Zeocin selection, the kinetics of biotinylation were much slower than previously observed, and biotinylation was only really detectable after 5 hours of biotin incubation. Because a 5 hour labelling window is not particularly useful to look at earlier time point in the DSB response, and miniTurbo-TIRR expression was not stable over continuous cell passages, it was apparent that the miniTurbo system was not appropriate for determining the interactome of TIRR after DNA damage.

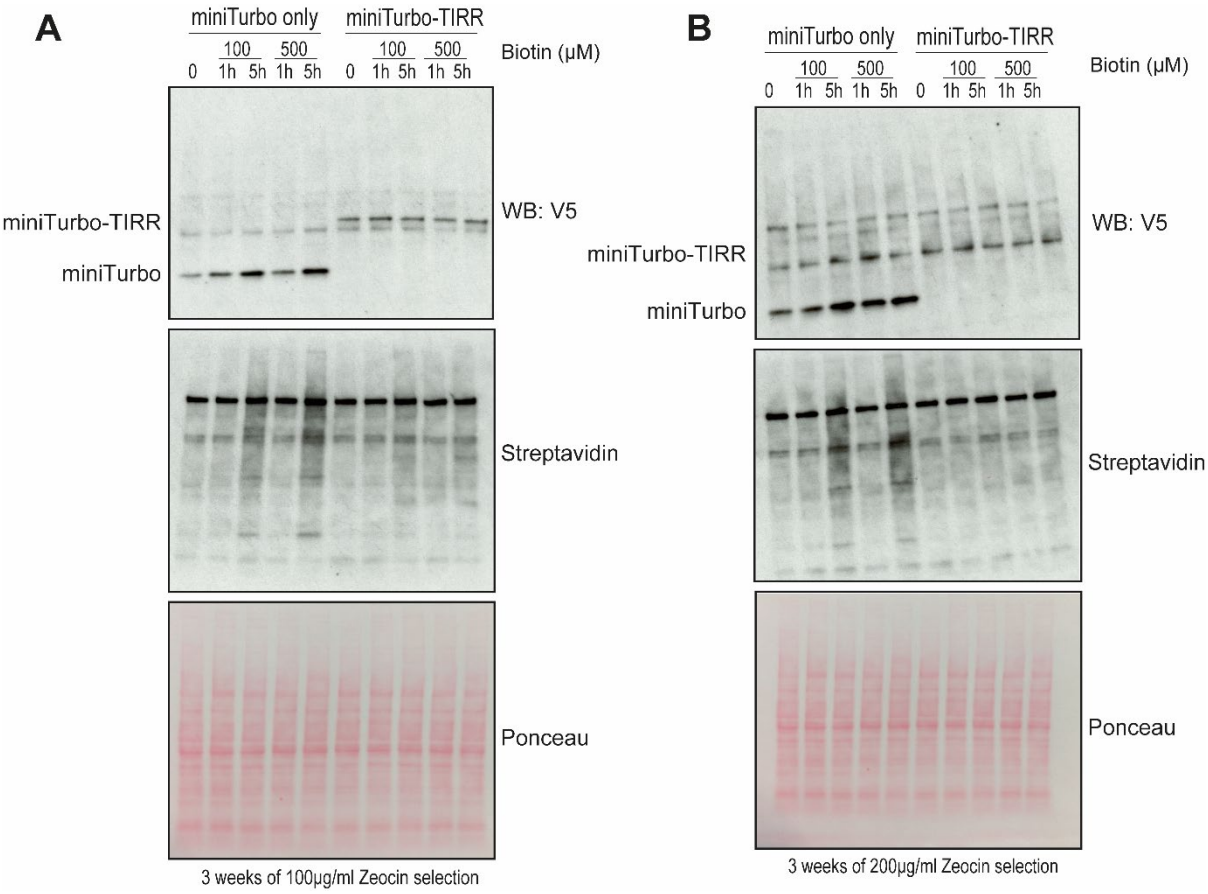


Figure 5.6: ***A)*** *Stable selection of miniTurboID and miniTurboID-TIRR expressing Hela cells with 100µg/ml Zeocin after 3 weeks of Zeocin selection. Immunoblot for V5 and probing with*

streptavidin is performed after addition of 100µM or 500µM exogenous biotin for 1 hour or 5 hours. ***B)*** *Same as in the left panel, but after selection with 200µg/ml Zeocin for 3 weeks.*

For the next iteration of the TIRR construct, TurboID was selected over miniTurbo as the kinetics of miniTurbo were too slow, this time in the N-terminal position as miniTurbo-TIRR expressed well transiently. The hygromycin resistance gene was used to replace the Zoecin resistance, as obtaining a TIRR expressing stable cell line using Hygromycin had previously been successful (siResistant TIRR) (**Figure 5.7.A**). The TurboID-TIRR and TurboID only constructs were again transiently transfected into Hela cells and the expression checked by immunoblot for V5. Both Turbo-TIRR and Turbo only expressed well to comparable levels (**Figure 5.7.B**). After incubation with exogenous biotin for 30 minutes, clear induction of biotinylation was observed, again at comparable levels for both Turbo-TIRR and Turbo only, indicating that this construct was highly active and would be suitable for monitoring TIRR interactions partners at shorter time frames after damage (**Figure 5.7.B**). However, a high level of background biotinylation was observed which reduces the temporal resolution and does not give a tight labelling window. Nevertheless, this construct was carried forward an increase in biotinylation was still observed after exogenous biotin addition.

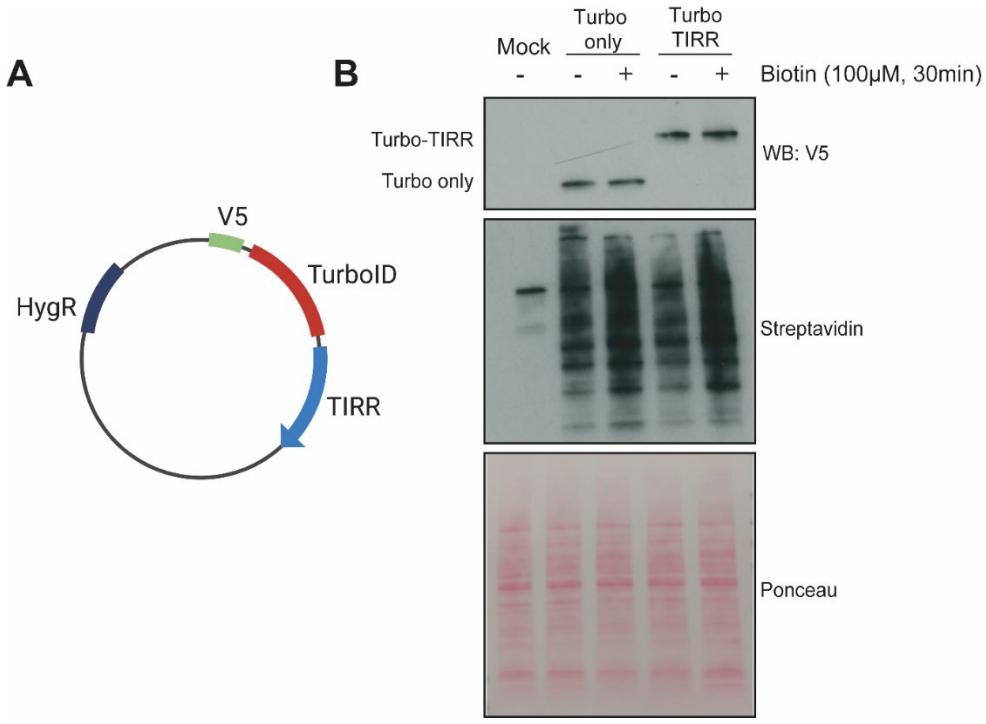


Figure 5.7: ***A)*** *Design of the V5-tagged TurboID-TIRR (N-terminal) construct.* ***B)*** *Western blot to detect transient expression of TurboID only or TurboID-TIRR in Hela cells as assessed by V5 immunoblot. Biotin labelling of proteins is assessed by probing with streptavidin after addition of 100μM of exogenous biotin for 30 minutes. Ponceau is used as a loading control.*

5.3.2 Generating stable cell lines expressing TurboID-TIRR and TurboID only

Having determined that the Turbo-TIRR construct expressed and had sufficiently rapid biotinylation kinetics, the constructs were transfected into Hela cells and stably selected with Hygromycin and the expression monitored over time. After 2 weeks of Hygromycin selection both Turbo only and Turbo-TIRR were still expressing, although the TurboID only construct appeared to be significantly less well expressed than the TurboID-TIRR construct, suggesting that Turbo only expression may induce some cellular toxicity, potentially due to the higher level of background biotinylation in the absence of exogenous biotin that was observed after transient transfection (**Figure 5.8.A**). After 3 weeks of Hygromycin selection, Turbo-TIRR was still well expressed as determined by V5 immunoblot, and exhibited robust induction of biotinylation after 30 minutes of exogenous biotin addition (**Figure 5.8.B**). Turbo only was

still expressed, although to a much lower level than Turbo-TIRR, but did display some modest yet detectable biotinylation activity after 30 minutes of labelling (**Figure 5.8.B**).

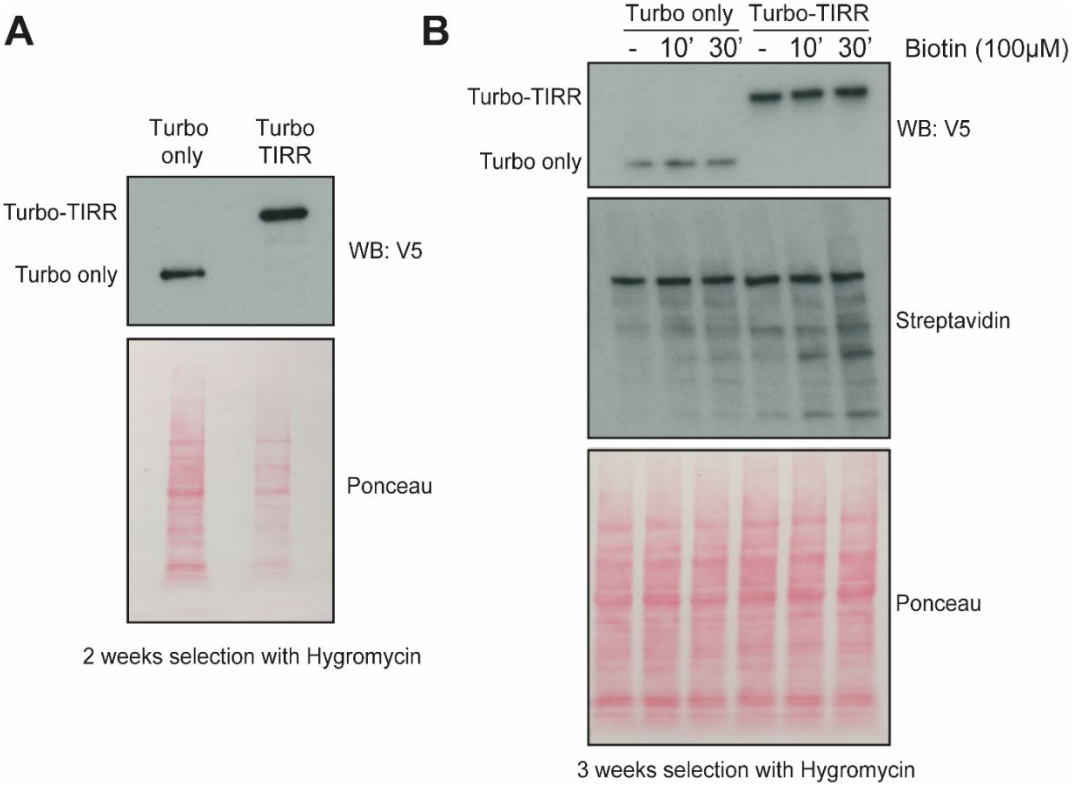


Figure 5.8: ***A)*** *Stable selection of TurboID only and TurboID-TIRR expressing Hela cells after 2 weeks of selection with 300µg/ml Hygromycin. Immunoblot for V5 is used to detect TurboID or TurboID-TIRR expression.* ***B)*** *After 3 weeks of selection with 300µg/ml Hygromycin, stable TurboID or TurboID-TIRR expression is monitored using immunoblotting for V5. Probing with streptavidin is performed after addition of 100µM exogenous biotin for 10 or 30 minutes. Ponceau is used as a loading control.*

Cells stably expressing Turbo only and TIRR-Turbo were then single cell sorted and individual clones screened for expression and biotinylation activity. For TIRR-Turbo, all colonies screened apart from one colony displayed expression of TIRR-Turbo. The choice of colony selected was based on two key factors; expression of TIRR-Turbo, and induction of biotinylation activity after addition of exogenous biotin. Many of the colonies displayed comparable TIRR-Turbo expression, and therefore Colony 20 was selected on the basis of having robust induction of biotinylation after 30 minutes of biotin incubation (**Figure 5.9.A**).

Interestingly, some colonies which expressed TIRR-Turbo did not show a measurable increase in biotin labelling after biotin incubation, such as colonies 10, 27, and 38, highlighting the importance of screening individual cells to achieve the same biotin ligase activity across all cells, which would not be the case in a polyclonal cell population, even one which is stably expressing the biotin ligase. In contrast to TIRR-Turbo, only 4 of the colonies screened on western blot had detectable Turbo-only expression, in line with the observed reduction in Turbo-only expression over time in the polyclonal cell population (**Figure 5.9.B**). Of the Turbo-only colonies which did express Turbo, colonies did not display robust induction of biotinylation after exogenous biotin addition (**Figure 5.9.B**). Coupled with the low number of Turbo-expressing colonies, this suggests that Turbo-only expression may be toxic to cells. It is not clear why exactly the fusion of TIRR to Turbo limits this toxicity, although one explanation could be that Turbo-only may biotinylate more extensively throughout the cell and continued biotinylation of proteins may impair normal protein function[11], and fusion to a POI (in this case TIRR) may restrain this biotinylation. In *in vivo* models, toxicity when expressing Turbo-only was observed, due to sequestration of endogenous biotin which prevented biotinylation of metabolic enzymes needed for survival[7,11]. An ideal control for a TurboID/BioID experiment would have comparable biotinylation activity to the fused POI and biotin ligase, to enable the identification of false positives which may appear due to the presence of non-interaction partners in the same cellular location[5]. False positives can also occur due to the interaction of nonspecific proteins with the streptavidin beads, or from endogenously biotinylated proteins. Therefore, the low biotinylation activity of the Turbo only cells can still control for background due to the beads and endogenously biotinylated proteins, but will not be an ideal spatial control, and therefore the possibility of more false positives and a greater need for manual validation of candidates in the TIRR-TurboID needs to be kept in mind. We selected colony 21 for Turbo-only experiments, as this colony exhibited the highest level of Turbo expression.

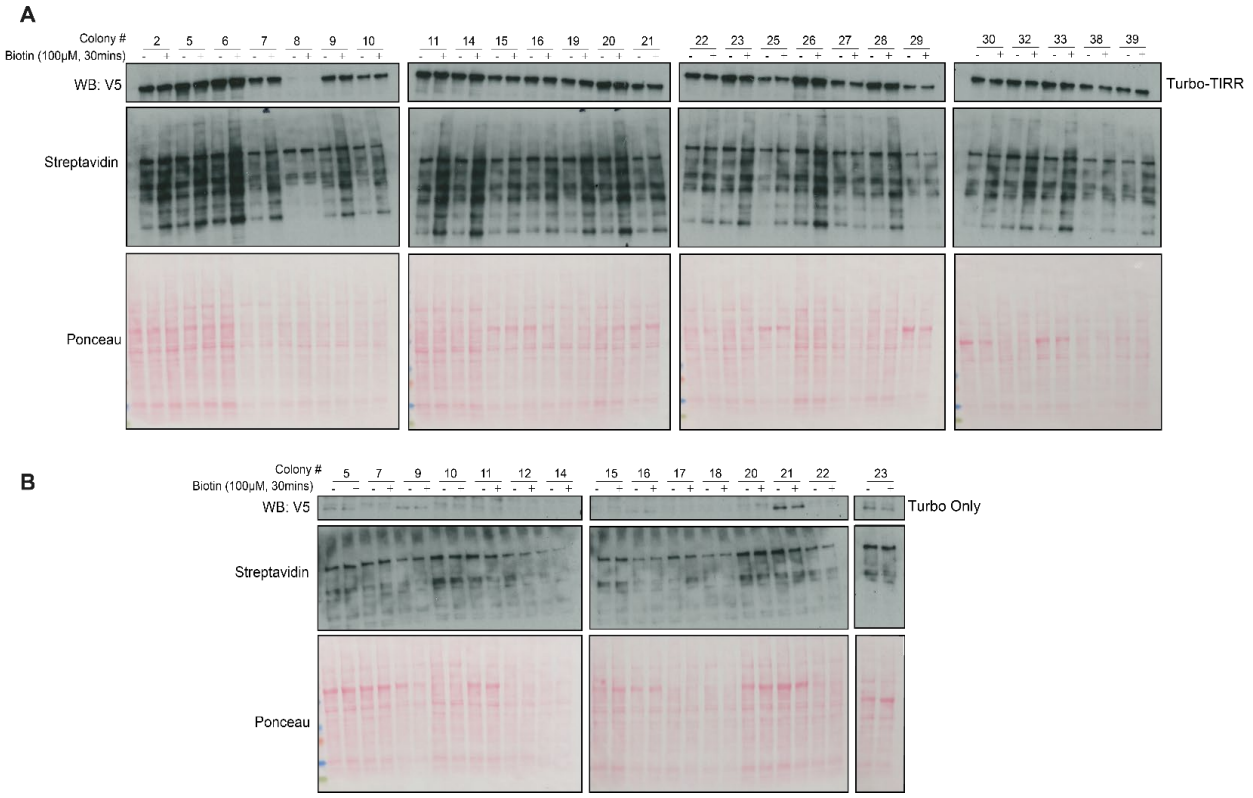


Figure 5.9: ***A)*** *Hygromycin selected Hela cells stably expressing Turbo-TIRR are single cell sorted and individual cells are cultured. Individual colonies were probed for Turbo-TIRR expression using immunoblotting for V5. Biotinylation activity of each colony was also assessed by incubation with 100µM biotin for 30 minutes and probing with streptavidin.* ***B)*** *Same as in A, but for cells stably expressing Turbo only. Ponceau is used as a loading control.*

5.3.3 Optimisation of TurboID experimental conditions

After selecting individual colonies, the duration of exogenous biotin addition and concentration was optimised to find the shortest duration of biotin incubation which would result in an observable increase in biotinylated protein on a western blot. The maximum duration of biotinylation tested was 1 hour, as we wanted to look at shorter time points after DNA damage induction. Two concentrations of biotin were used, either 100µM, a 'typical' concentration based on a literature search, or 500µM. Incubation times of 10 minutes, 30 minutes, and 1 hour were tested for TIRR-Turbo. A small increase in biotinylation could be detected after 10 minutes of exogenous biotin incubation, which was more pronounced after 30 minutes, and further increased after 1 hour of incubation (**Figure 5.10**). Whilst 1 hour resulted in the highest

level of biotinylation, increased incubation with biotin can result in more false positives due to a greater labelling radius as a result of saturation of nearby lysine residues allowing labelling of more distal sites (upwards of ~35nm)[11]. Therefore, 30 minutes was selected as a compromise between biotin ligase activity and minimising the labelling radius to limit false positives. There was no observable difference between 100µM and 500µM of biotin, and therefore 100µM was selected.

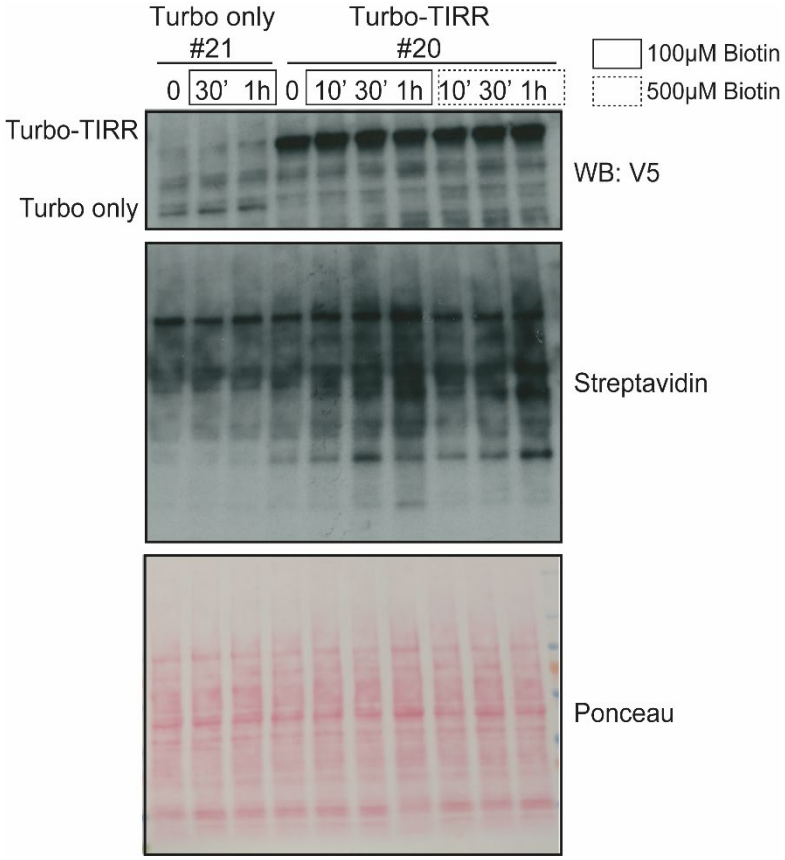


Figure 5.10: *Optimisation of biotin concentration and labelling time for Turbo only colony 21 and Turbo-TIRR colony 20. Biotin was added at a concentration of 100µM for 30 minutes or 1 hour for Turbo only cells, or either 100µM or 500µM for 10 minutes, 30 minutes, or 1 hour for Turbo-TIRR cells. Expression of Turbo and Turbo-TIRR was detected by immunoblotting for V5, and biotin labelling was detected by probing with streptavidin. Ponceau was used as a loading control.*

Additionally, to ensure TIRR was not mislocalising due to the addition of the TurboID biotin ligase[10], the correct localisation of the Turbo-TIRR fusion protein was determined using IF. Turbo-TIRR Colony 20 cells showed predominantly nuclear localisation with some

cytoplasmic staining, and the biotin signal overlapped with this Turbo-TIRR signal (**Figure 5.11**). This indicated that Turbo-TIRR was correctly localised, and that the biotin labelling activity is restricted to the sites of Turbo-TIRR localisation.

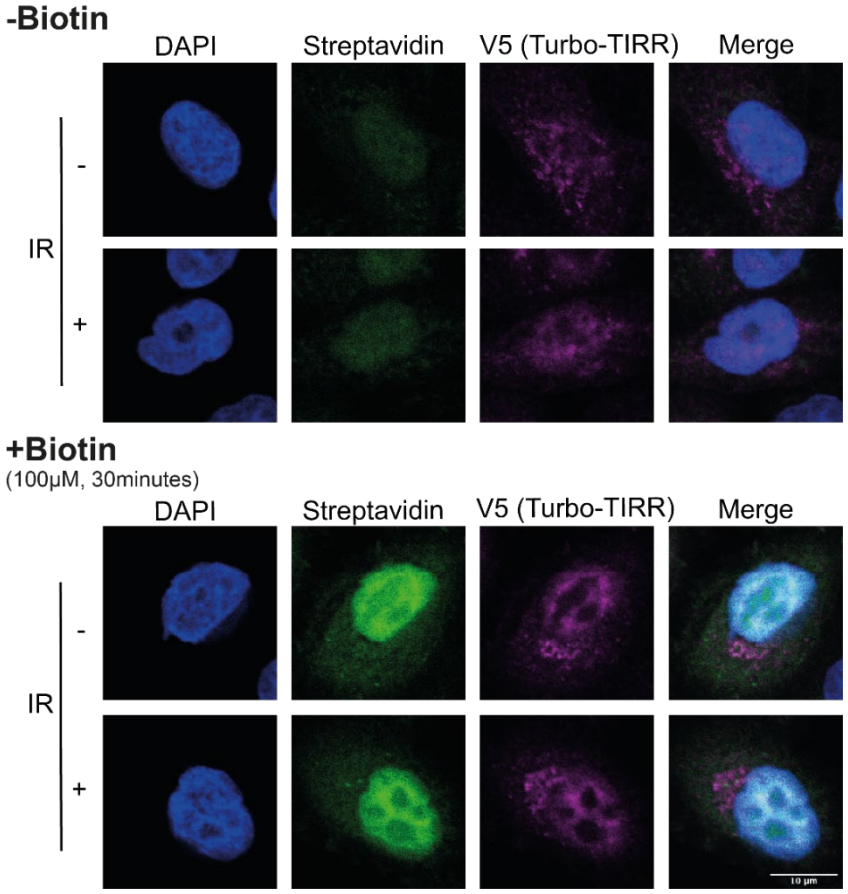


Figure 5.11: *Correct localisation of Turbo-TIRR in colony 20 cells was assessed by IF. Predominantly nuclear localisation of Turbo-TIRR was detected by proving with V5, and induction of biotin labelling was monitored after the addition of biotin at 100µM for 30 minutes by probing with streptavidin. Turbo-TIRR and Streptavidin can be seen to colocalise in the nucleus (DAPI).*

Having established the Turbo-TIRR cell line for biotin proximity labelling of TIRR interaction partners, the streptavidin pull-down was then optimised. TurboID-only and TurboID-TIRR cells were seeded in 15cm dishes (~3.5million cells seeded per condition) and 24 hours later cells were irradiated with 10Gy ionising radiation or not. 45 minutes after damage, 100µM of exogenous biotin was added for 30minutes, until cells were harvested at 75 minutes post-IR.

After cell lysis, 2.5mg of total protein per condition was added to streptavidin beads and incubated overnight. The strength of the biotin-streptavidin interaction makes it challenging to efficiently elute biotinylated proteins from the streptavidin beads, and therefore a trypsin digest directly from the beads before mass spectrometry should be performed[5]. Performing an on-bead digestion can increase the background due to non-specific proteins bound to the beads, and therefore the bead volume was optimised to achieve maximum recovery of biotinylated proteins at the lowest bead volume possible. Additionally, it should be noted that washing of cells with cold PBS after incubation with biotin-containing media is sufficient to remove free biotin which could bind to the streptavidin beads and reduce the efficiency of the pull down, although in other experimental systems, such as *Arabidopsis*, this is not the case and extra steps are needed to remove free biotin[2,3]. After overnight incubation of the streptavidin beads and extensive washing steps, bound material was eluted for western blot using Laemmli buffer. Immunoblot for V5 showed a clear enrichment of Turbo-TIRR in the streptavidin pull-down of Turbo-TIRR cells after the addition of biotin (**Figure 5.12.A**). The Turbo-TIRR, as detected by V5 immunoblot, was visible in the input and flowthrough of the sample without biotin addition, however following biotin addition the Turbo-TIRR was enriched in the streptavidin pulldown and almost absent from the flowthrough. This indicates that there was substantial self-biotinylation of Turbo-TIRR after biotin addition, as would be expected as proteins which are in close proximity to the TurboID biotin ligase should be biotinylated. Probing for streptavidin showed a similar trend, with the biotin signal being significantly increased in the streptavidin pulldown of Turbo-TIRR after the addition of exogenous biotin. At all bead volumes tested (200µl, 100µl, and 50µl) there was enrichment of biotin signal in the pulldown, and this was almost completely depleted in the flowthrough, suggesting that 50µl of beads was sufficient to deplete almost all biotinylated proteins from 2.5mg of total protein. Additionally, 53BP1 was detected in the streptavidin pulldown by western blot in non-damage conditions,

but was not detected after IR, nor in the Turbo-only pulldown or Turbo-TIRR pulldown without biotin addition, indicating that this system is effective at labelling TIRR interaction partners specifically. A silver stain of the streptavidin pull down samples showed a somewhat similar pattern for all conditions, indicating that there is a significant amount of background from the streptavidin beads, despite harsh and thorough washing conditions (including 1M KCl and 2M Urea) (**Figure 5.12.B**). Nevertheless, this method successfully enriched for Turbo-TIRR itself, and captured all biotinylated proteins in the sample, suggesting that this method can be used to enrich for TIRR interaction partners for detection and identification by mass spectrometry.

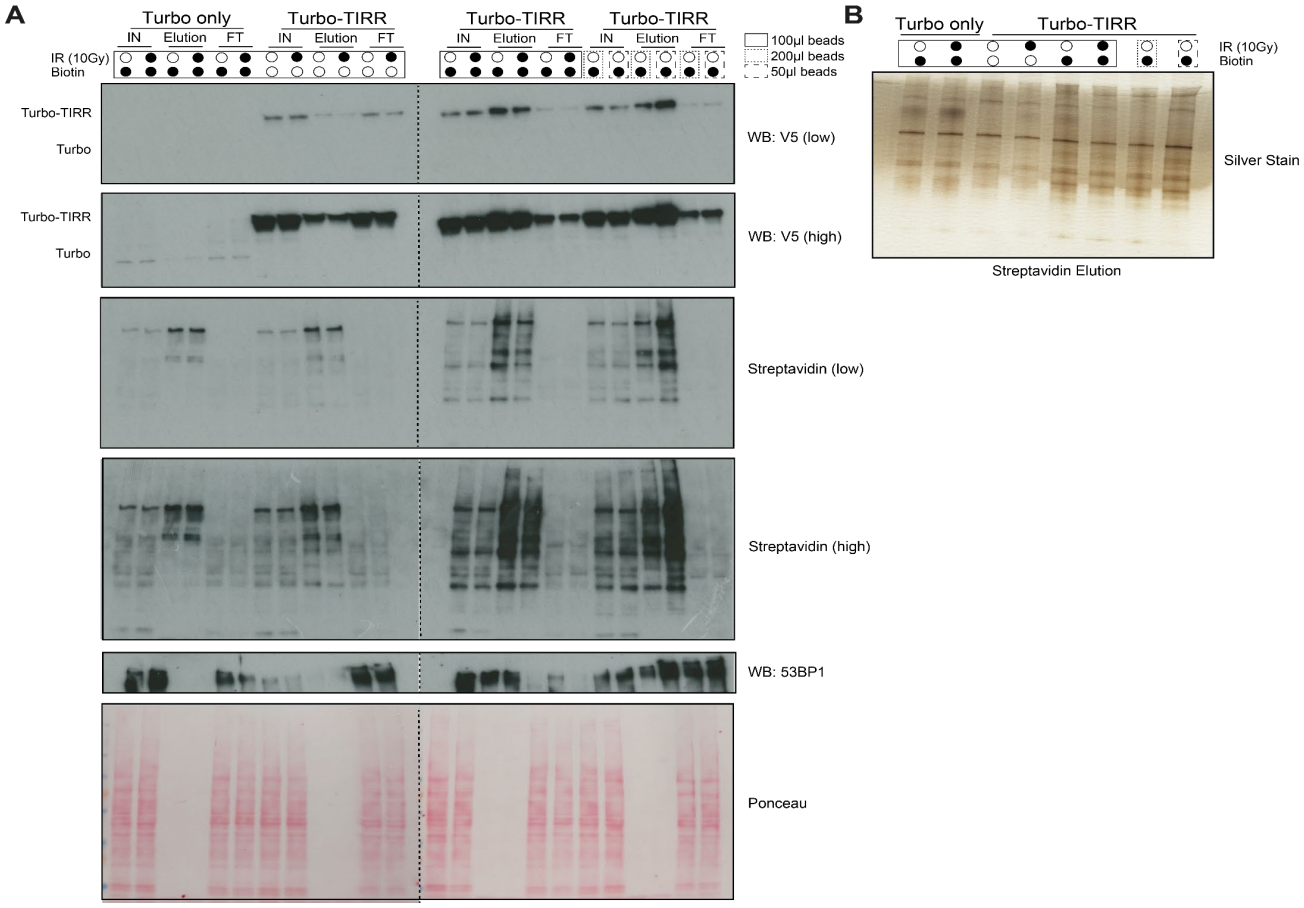


Figure 5.12: *Optimisation of TurboID pull down with streptavidin beads.* ***A)*** *Streptavidin pull down of TurboID only samples with 100µM Biotin for 30 minutes, or Turbo-TIRR with or without Biotin. IR damage was induced to indicated samples (~1 hour after 10Gy IR). Streptavidin bead volumes were varied as indicated (200µl, 100µl, or 50µl). Input, streptavidin elution, and flowthrough fractions were taken from each sample and immunoblotting for V5 and 53BP1 performed. Enrichment of biotinylated proteins in the streptavidin pulldown was assessed by probing with streptavidin. Ponceau was used as a loading control.* ***B)*** *Silver stain of Streptavidin elutions for TurboID with Biotin, and Turbo-TIRR with and without Biotin (+/- IR).*

5.3.4 Mass Spectrometry of Turbo-TIRR

Having established the experimental conditions for the TurboID, samples were prepared for mass spectrometry analysis in triplicate for each condition, TurboID only with biotin (+/- IR), TurboID-TIRR without biotin (+/-IR), and TurboID-TIRR with biotin (+/- IR). Quality control was performed on a small sample of the streptavidin beads for mass spectrometry, and once again showed an increased presence of TurboID-TIRR and increased biotinylated proteins in pull down samples after the addition of biotin as seen from V5 immunoblot and streptavidin blot respectively (**Figure 5.13.A**). A silver stain of the streptavidin pull down samples once again showed a similar pattern for all conditions (**Figures 5.13.B, 5.13.C, and 5.13.D**).

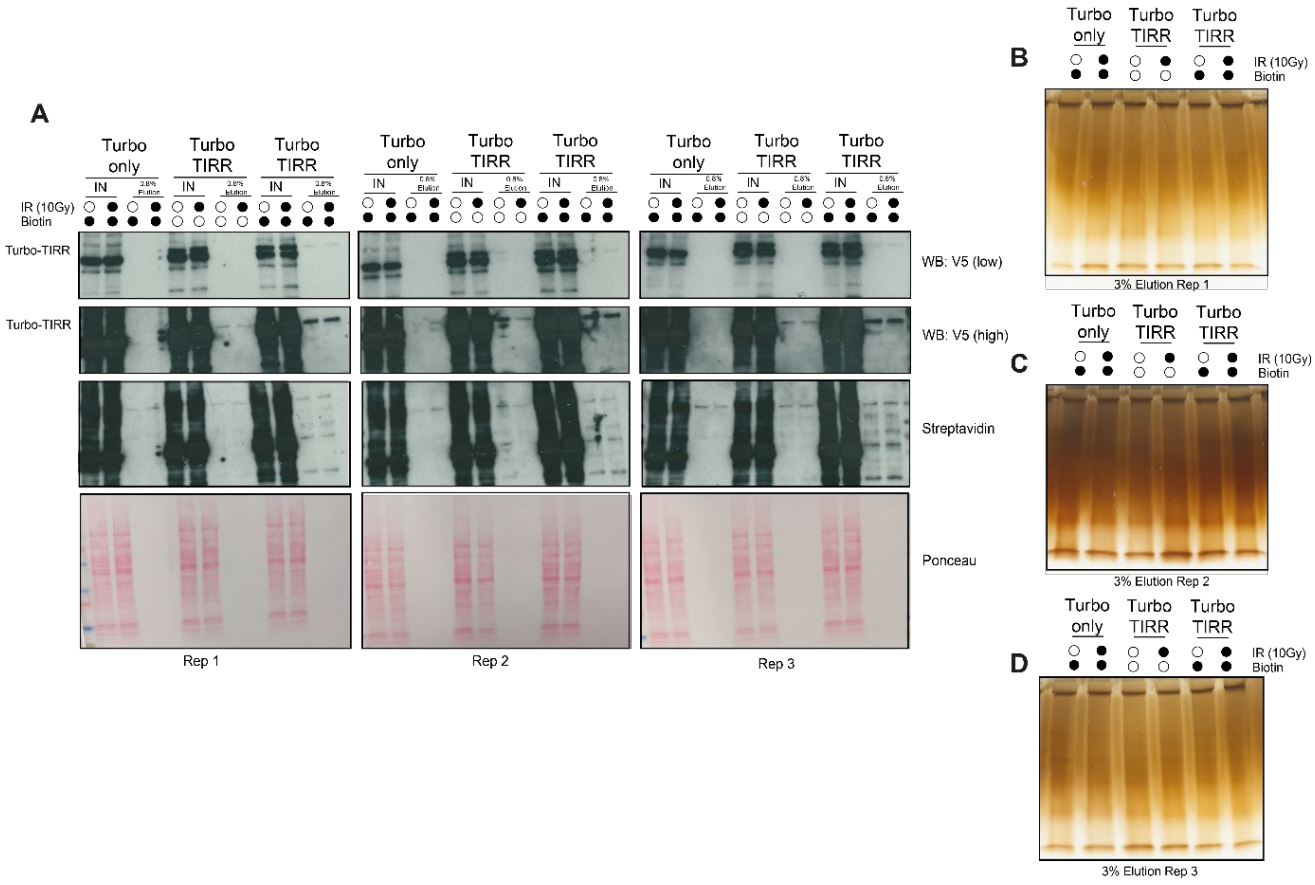


Figure 5.13: *Enrichment of biotin labelled proteins with streptavidin beads for mass spectrometry.* ***A)*** *Streptavidin pull down of TurboID only samples with 100μM Biotin for 30 minutes, or Turbo-TIRR with or without Biotin for replicate 1 (left), replicate 2 (middle), and replicate 3 (right). IR damage was induced to indicated samples (~1 hour after 10Gy IR). Input and streptavidin elution fractions were taken from each sample and immunoblotting for V5*

performed. Enrichment of biotinylated proteins in the streptavidin pulldown was assessed by probing with streptavidin. Ponceau was used as a loading control. ***B)*** *Silver stain of Streptavidin elutions for TurboID with Biotin, and Turbo-TIRR with and without Biotin (+/- IR) for replicate 1,* ***C)*** *replicate 2,* ***D)*** *and replicate 3.*

Mass spectrometry and label free quantitative proteomics analysis of the elution from streptavidin beads identified a total of 67 proteins in -IR conditions which were significantly enriched over the TurboID only control, and 53 proteins in +IR conditions (**Figures 5.14.A and 5.14.B**). In both -IR and +IR conditions, TIRR-Turbo was reassuringly identified as the most abundant protein, which is consistent with TIRR being the closest protein to the TurboID biotin ligase, and therefore would be most biotinylated and enriched in the sample (**Figures 5.14.A and 5.14.B**).

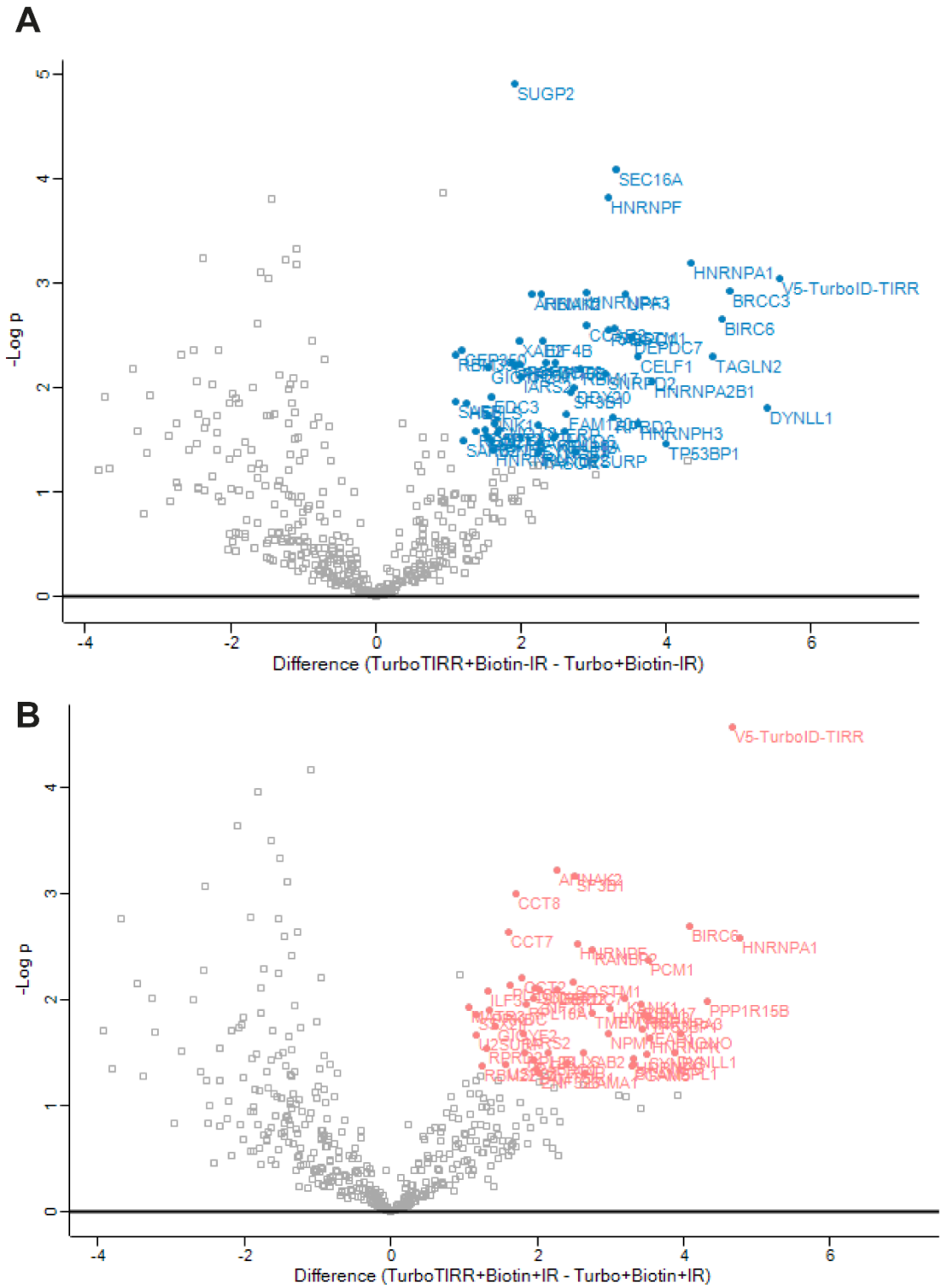


Figure 5.14: *Volcano plot representation of TurboID samples in **A)** -IR conditions and **B)** +IR conditions. TIRR-TurboID samples are shown relative to TurboID only samples.*

We next sought to compare the interactors of TIRR with and without damage. In our TurboID analysis, a specific -IR interactor is classified as a protein which showed a minimum 2-fold

decrease in abundance upon IR, and a specific +IR interactor is defined as a protein which showed a minimum 2-fold increase in abundance after damage. Firstly, we compared the levels of 53BP1 in -IR and +IR conditions. As expected 53BP1 levels were lower after IR, consistent with 53BP1 and TIRR separating after damage (**Figure 5.15.A**), however this decrease was not significant, likely due to the high levels of background biotinylation in 'normal/steady-state' conditions before exogenous biotin addition after IR, and therefore 53BP1 is classed in this analysis as both a -IR and +IR interactor. This suggests that it may be more difficult to identify interactors which only change their association with TIRR minimally after damage. Nevertheless, when comparing the identified interactors in -IR with +IR conditions, we found 37 specific non-damage interactors, and 23 specific damage interactors, with an overlap of 30 proteins between the two conditions (**Figure 5.15.B**).

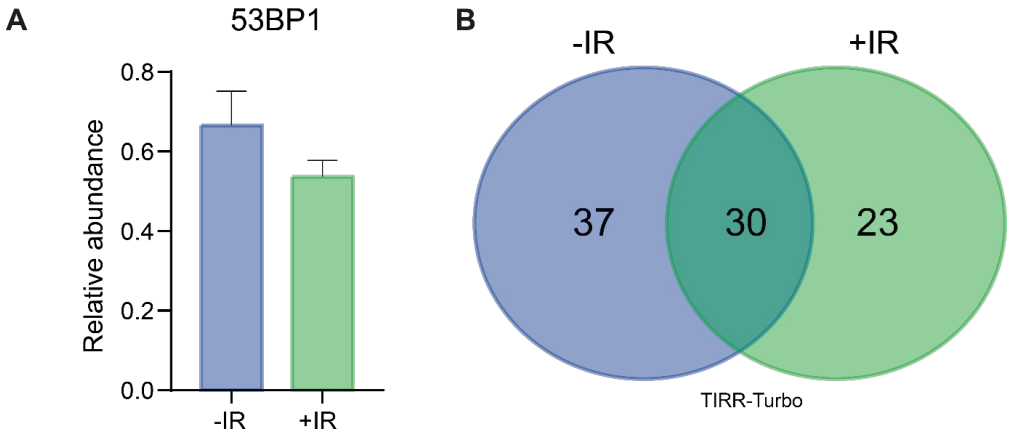


Figure 5.15: ***A)*** *Levels of 53BP1 in TIRR-TurboID samples before and after IR.* ***B)*** *Venn Diagram of the identified TIRR interactors in TurboID in -IR or +IR conditions, which were significantly enriched over the TurboID only control.*

The list of identified interactors can be found in **Table 5.1**. Of these interactors, in non-damage conditions we see overlap with published mass spectrometry data. Of our 67 proteins identified in either -IR alone or both -IR and +IR (therefore interactors of TIRR in non-damage conditions), 32 were identified in previously published mass spectrometry datasets (datasets

found in **Figure 5.2**). These included 53BP1, DYNLL1, components of the T-complex protein 1 complex, CCT6A and CCT8, and Heterogeneous nuclear ribonucleoproteins (HNRNPs); HNRNPA2B1, HNRNPA3, HNRNPF, HNRNPH3, HNRNPK, and HNRNPU. The HNRNP protein family is of interest, as they have wide-spread roles in RNA processing (**Section 5.4.4**).

Of the 23 proteins identified as enriched in +IR samples, NONO, XIAP, HNRNPC, LAMA1, NPM1, PRKDC, STAMBPL1, USP28, and ZNF281 play known roles in the DDR and DSB repair. XIAP, a member of the Inhibitors of Apoptosis (IAP) family, has been shown to be overexpressed in BRCA mutant cancers and increased XIAP expression is associated with PARPi sensitivity[12]. XIAP was also identified in our mass spectrometry data (**Chapter 4**) as a protein which is upregulated after TIRR knockdown, suggesting a possible mechanism whereby TIRR may promote the degradation of XIAP through their proximity/interaction. Interestingly, TIRR contains a predicted IAP-binding motif as assessed by ELM (data not shown), and BIRC6, which like XIAP also contains a baculovirus IAP repeat (BIR), was identified in proximity with TIRR, in both -IR and +IR conditions. Furthermore, NONO is recruited to DSB sites and has been implicated in NHEJ mediated DSB repair via interaction with LIG4 and KU[13,14]. The recruitment of NONO to DSBs has been suggested to be regulated by MATR3[14], which was also identified in our TurboID as a TIRR interactor in damage and non-damage conditions. HNRNPC can interact with RAD51 and regulates RAD51 nucleofilament formation[14], NPM1 is recruited to DSB sites and is required for proper DNA repair[15], STAMBPL1 depletion leads to reduced RAD51 and BRCA1 foci[16], and ZNF281 is recruited to DSBs and interacts with XRCC4 to promote NHEJ[17]. LAMA1 and USP28 are also known 53BP1 interactors, regulating 53BP1 recruitment to chromatin and stability[18,19], and the p53 stress response respectively[20,21]. The relevance of TIRR proximity/interaction with these

proteins is currently unclear, however this should be investigated in future studies (**Sections 5.4.4 and 5.4.5**).

-IR	+IR	Both -IR and +IR
AHNAK	CCT2	AHNAK2
BRCC3	CCT7	BIRC6
CCAR2	DDX46	CCT8
CCT6A	HNRNPC	DEPDC7
CELF1	ILF3	DYNLL1
CEP350	KANK1	FLNA
CHERP	LAMA1	GIGYF2
CNOT8	LAMTOR1	HELLS
CPSF7	NONO	HNRNPA1
DDX20	NPM1	HNRNPA3
EDC3	PCM1	HNRNPF
EIF4B	PGAM5	HNRNPH3
FAM120A	PRKDC	HNRNPK
FLNB	RBM22	IARS2
GSPT1	RPL28	KEAP1
HNRNPA2B1	SSX2IP	MATR3
HNRNPU	STAMBPL1	NUDT16L1
HSPA1A	SYNRG	PABPC1
IMMT	TMEM160	PLEC
JPT2	USP28	PPP1R15B
KPNB1	XIAP	RANBP2
MEPCE	ZNF281	RBM17
MYH9	ZNF326	RPL18A
MYO6		RPRD2
PUF60		SF3B1
RBM10		SNRPD2
RBM39		SQSTM1
RCN2		TP53BP1
SAFB		U2SURP
SAFB2		XAB2
SEC16A		
SUGP2		
SYNCRIP		
TAGLN2		
TASOR		
TNK1		
UPF1		

Table 5.1: *Interactors with TIRR identified using TurboID in damage and non-damage conditions. Listed in alphabetical order.*

5.3.5 Affinity Pulldown Mass Spectrometry with TIRR-GFP

To compare the TurboID method with the 'traditional' AP-MS method, we performed a GFP pull down on cells overexpressing either GFP or TIRR-GFP in damage and non-damage conditions. GFP and TIRR-GFP Flp-IN cells were induced with doxycycline, and pull down was performed either in non-damage conditions, or 1 hour after 10Gy IR. Quality control for GFP pull down showed enrichment of GFP or TIRR-GFP in the elution, with no TIRR or GFP protein present in the flowthrough in both replicates (**Figure 5.16.A**). Two repeats were performed and silver stains of samples sent for mass spectrometry showed a clear enrichment of either GFP or TIRR-GFP, with comparable pulldown efficiency across all samples (**Figure 5.16.B**).

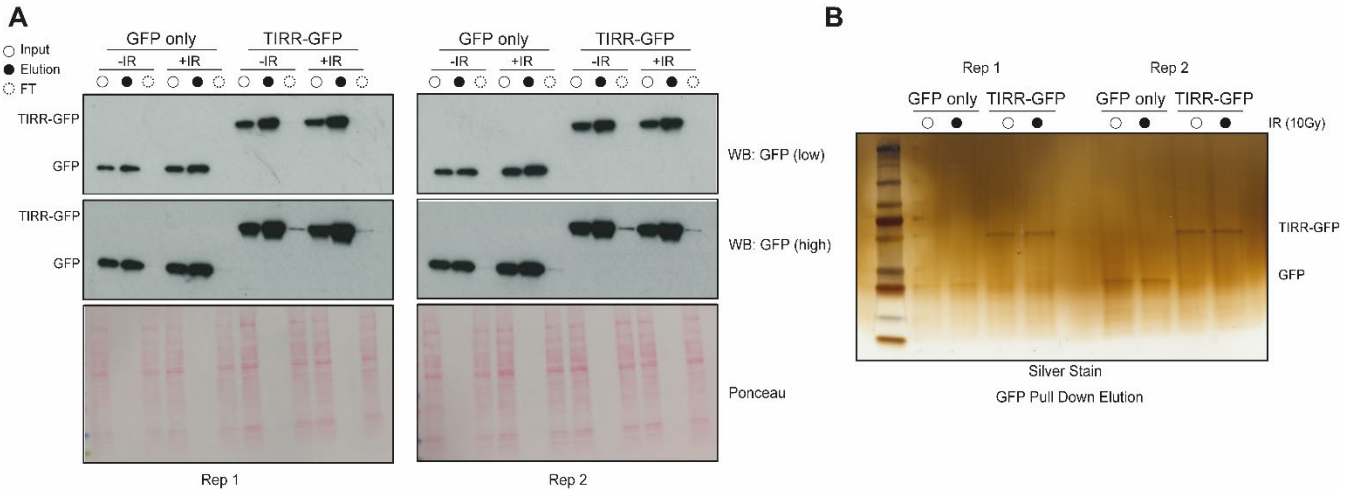


Figure 5.16: *GFP pulldown on GFP and TIRR-GFP Hela cells to identify interactors.* ***A)*** *Western blot confirming successful GFP pull down.* ***B)*** *Silver stain of samples (5%) sent for mass spectrometry.*

In the AP-MS, after filtering for proteins which were at least 2-fold enriched in TIRR-GFP samples over the corresponding GFP controls, with a p-value cut-off of 0.05, we identified a

total of 15 proteins bound to TIRR in non-damage, and 23 proteins bound in damage, with an overlap of 9 proteins (**Figure 5.17.A** and **Table 5.2**). As a control, we can see that 53BP1 abundance was reduced in +IR samples compared to -IR samples as expected, although this did not reach statistical significance, likely due to two repeats being performed instead of three (**Figure 5.17.B**). Nevertheless, many proteins identified in AP-MS in non-damage conditions overlapped with those identified in TurboID in non-damage, confirming the specificity of the TurboID (**Section 5.4.2**).

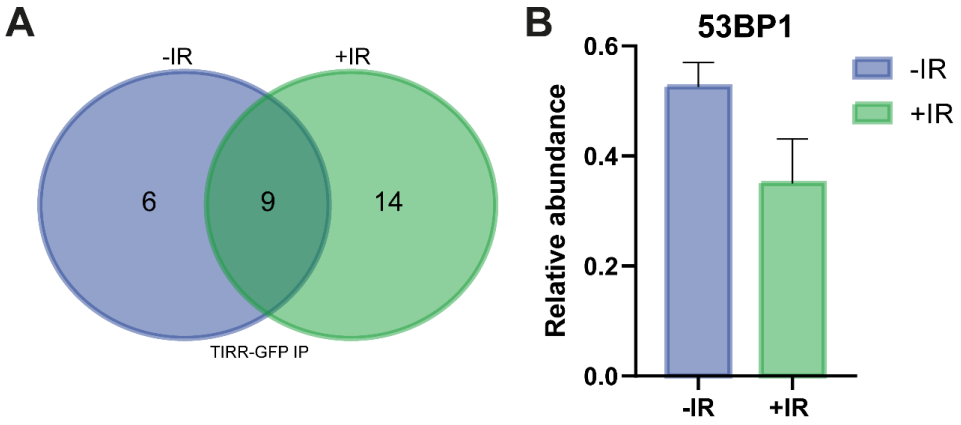


Figure 5.17: A) *Overlap of proteins identified by TIRR-GFP pull-down and mass spectrometry in damage and non-damage conditions.* ***B)*** *Comparison of 53BP1 abundance in non-damage and damage conditions.*

-IR	+IR	Both -IR and +IR
HNRNPA2B1	AKAP8	GFP-TIRR
HNRNPF	ATP5ME	H4-16
HNRNPM	CALM3	HNRNPC
RBMX	CCT3	HNRNPH1
RBMXL1	DNAJA3	HNRNPH2
RPL27	ELAVL1 (HuR)	HNRNPH3
	HSP90AB1	PRDX1
	HSPA1A	TRAP1
	HSPA5	TUBB
	NDUFA4	
	RALY	
	RPS16	
	RPS23	
	RPS24	

Table 5.2: *Proteins identified as TIRR interactors in non-damage and damage conditions by GFP affinity pulldown of TIRR-GFP, using GFP only as a control. Listed in alphabetical order.*

5.4 Discussion

5.4.1 Considerations when designing a biotin proximity labelling assay to identify interaction partners

There are several key parameters which should be considered when designing a biotin proximity labelling assay in order to identify proteins which interact with a POI. Firstly, the choice of the biotin ligase is critical, principally determined by the acceptable labelling window (i.e. how quickly the biotinylation of interacting proteins needs to take place). In the case of TIRR, BirA* was not screened due to the slow (~18h) labelling kinetics, which would not allow for identification of binding partners shortly after DNA damage. In addition, in our hands miniTurbo displayed very slow biotinylation kinetics, on the order of 5-6 hours to achieve a signal above background levels. A labelling window of ~5 hours would not allow the identification of interactors at shorter time points after damage, such as 1 hour, and is therefore inappropriate for this experimental set-up.

Secondly, the appropriate controls are required in order to be able to distinguish between specific 'real' interactors, and background from either nonspecific binding to the beads, or random spatial proximity to the biotin ligase. Therefore, ideally controls for the POI fused to the ligase without the addition of biotin and a spatial control (e.g. TurboID fused to a NLS) would be used[5]. In our hands TurboID showed significant downregulation by the cell after stable selection, indicating a degree of toxicity of either TurboID expression or background biotinylation by TurboID. Surprisingly this was not observed to the same extent with TIRR-TurboID, which suggests that fusion to a protein may somehow restrain TurboID spatially, which then limits toxicity. In our experiments we chose TurboID without fusion to another sequence, like an NLS, as TIRR is present in many cellular compartments including on the chromatin, in the nucleus, associated with the ER, in the cytoplasm, and at the plasma

membrane (see **Section 1.4**). Therefore we didn't restrict our control to one specific cellular compartment. However, the downregulation of TurboID due to suspected toxicity is in itself problematic, as an ideal control would biotinylate substrates within the cell to the same degree of the TurboID-POI fusion, in order to control for nonspecific biotinylation. Nevertheless, TurboID in our hands still displays some biotinylation activity, and we can see is enrichment of biotinylated proteins in the TurboID only sample by the streptavidin beads (**Figure 5.12.A**), and a similar amount of total protein was enriched by streptavidin pull-down in all conditions (**Figure 5.12.B**), which suggests TurboID only in our set-up is still useful as a background control. Having said that, one should be mindful of an increased possibility of false positive results due to the increased biotinylation capacity of TIRR-TurboID over TurboID only.

Furthermore, for capturing interactors in specific time windows, for example after DNA damage, a high level of temporal control and resolution over background is needed. This means that without the addition of exogenous biotin, the background level of biotinylation should be minimal, therefore a short labelling window (i.e. 1 hour post damage), would enable one to distinguish between background (i.e. pre-damage), and actual condition specific interactors (i.e. during / post-damage). This could explain why in our dataset we see the inclusion of 53BP1 in both a -IR and +IR in TIRR proximity labelling. Although 53BP1 relative enrichment in streptavidin pull downs after IR is lower when compared to non-damage conditions, this did not reach statistical significance. Whilst it is possible that TIRR and 53BP1 may occupy spatially similar regions after damage, and therefore 53BP1 would still be labelled by biotin after IR, it appears more likely that this is due to the stable interaction of TIRR with 53BP1 in non-damage, which then leads to a high degree of 53BP1 labelling even without exogenous biotin in non-damage conditions, due to the background of the TurboID. This would likely lead to a reduced capacity to identify damage specific interactors in general.

5.4.2 Comparing TurboID and AP-MS

In our AP-MS experiments, we identified a total of 15 non-damage interactors and 23 interactors of TIRR in damage (**Figure 5.17.A**). In non-damage, the proteins identified as bound to TIRR showed a significant PPI enrichment by STRING analysis (p-value<1.0E-16) (**Figure 5.18.A**). STRING analysis allows the visualisation of a network of predicted functional associations for an individual protein or a group of input proteins (https://string-db.org/) (further details on STRING analysis can be found in **Section 2.2.45**). A significant PPI enrichment suggests the proteins in the network have more interactions than would be expected for a random dataset, indicating they are more likely to be biologically functionally linked. GO analysis of proteins identified in non-damage (including those bound both in non-damage and damage) showed an enrichment for biological processes including regulation of mRNA metabolic process (FDR=4.19E-03) and regulation of RNA splicing (FDR=7.88E-07). Furthermore, molecular functions including RNA binding (FDR=1.47E-08), and cellular components including ribonucleoprotein complex (FDR=1.82E-08) were also enriched. Proteins identified in only damage conditions in our AP-MS experiment showed a significant PPI enrichment on STRING analysis (p-value = 1.19E-07) (**Figure 5.18.B**, shown in figure with +/-IR overlap, analysis performed on proteins identified only in +IR). The GO analysis on proteins identified only in damage conditions yielded an enrichment for biological processes including chaperone-mediated protein folding (FDR=4.86E-02), as well as molecular functions including RNA binding (FDR=1.65E-03), and cellular components including cytosolic small ribosomal subunit (FDR=3.41E-03).

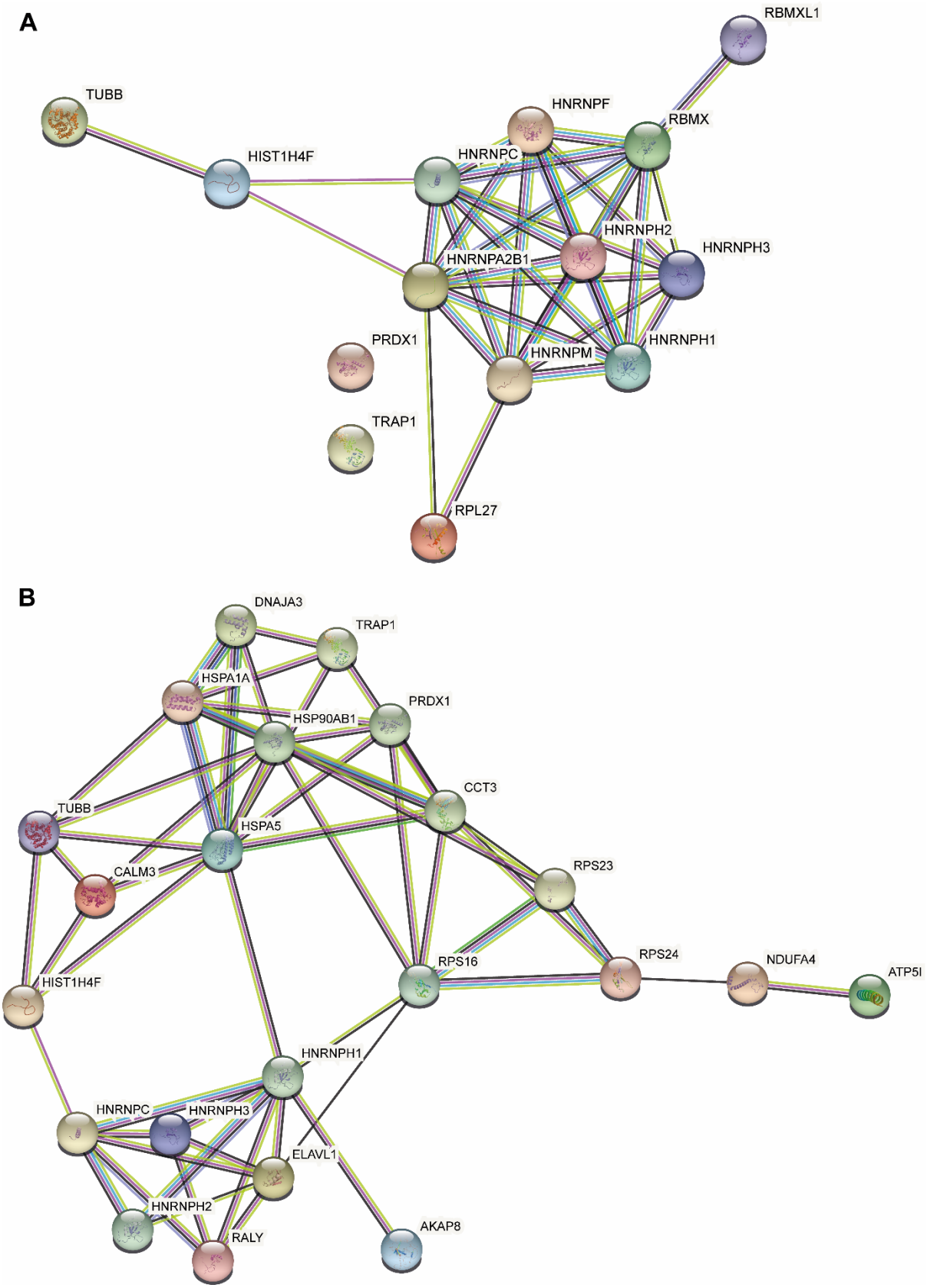


Figure 5.18: ***A)*** *String network for proteins bound to TIRR in non-damage in AP-MS (including overlap between damage and non-damage, 15 proteins in total).* ***B)*** *As in A, for proteins identified bound to TIRR in damage (including overlap, 23 proteins in total).*

The intersection between TurboID and AP-MS datasets shows clear overlap of proteins and protein complexes. Whilst different HRNPs were identified in TurboID vs AP-MS, there is an overlap of HNRNPH3, HNRNPA2B1, HNRNPC, and HNRNPF, indicating that TIRR interacts with the HNRNP RNA-binding protein family. While a lot of HNRNP proteins are relatively abundant in cells and could be false positives as a result, we see that they were significantly enriched over the GFP only control, suggesting that this interaction is specific to TIRR. Similarly, TurboID identified many components of the chaperone T-complex protein Ring Complex (TRiC), including CCT6A, CCT2, CCT7, and CCT8. Whilst our AP-MS did not identify these specific TRiC components, we do identify CCT3, indicating that TIRR can interact with the TRiC complex. Additionally, other proteins which were identified in TurboID were seen in AP-MS, although just below statistical significance, including DYNLL1 and FAM120A. Taken together, we confirm using AP-MS that TurboID can identify specific TIRR interactors. Interestingly, TurboID identified more statistically significant TIRR interacting proteins than AP-MS, suggesting that TurboID may be superior to traditional affinity pulldown methods for identifying novel interactors. However, this could be caveated with the fact that TurboID may also be more likely to yield more false positive results due to nonspecific biotinylation. It is also important to consider the fact that proteins identified in the AP-MS dataset are more likely to be stable, direct interactors of TIRR, whereas proteins identified in TurboID could also include those which are transient or part of larger protein complexes. Therefore, TurboID may identify more TIRR interactors by virtue of the fact that proteins which may not directly or stably interact with TIRR but instead are in close proximity will also be biotinylated. Aside from confirming the reliability of our TurboID dataset, in our AP-MS, we were also able to identify novel interactors of TIRR in damage conditions, including RALY, 40S ribosomal subunits, and ELAVL1 (**Section 5.4.4**).

5.4.3 Identification of novel binding partners of TIRR in non-damage and damage using TurboID

In our non-damage TurboID interactome, we identified 67 proteins (including those which interact in both damage and non-damage conditions). Of these 67 identified proteins, 32 were identified in previously published mass spectrometry datasets (datasets found in **Figure 5.2**), which alongside our AP-MS data (**Section 5.4.2**), confirms that our TurboID approach is able to successfully identify TIRR interactors. As detailed above, previously known TIRR interactors which we were able to identify in our TurboID include 53BP1, DYNLL1, components of the TRiC complex, and the HNRNP family of proteins. STRING analysis (**Figure 5.19**) of the 67 identified interactors revealed a network enriched for RNA processing factors, similarly to our AP-MS (**Figure 5.18.A**), with a significant PPI enrichment (p-value: <1.0E-16). Enriched GO biological process terms include; mRNA destabilisation (FDR: 2.07E-02), Ribonucleoprotein complex assembly (FDR: 1.55E-04), Regulation of mRNA stability (FDR: 4.21E-05), and Nucleocytoplasmic transport (FDR: 2.72E-02). In agreement with a known role of TIRR in translation[8], regulation of translation (FDR 3.49E-04) was also enriched. Interestingly, GO analysis of cellular components revealed an enrichment in a number of GO categories, including CRD-mediated mRNA stability complex (FDR: 1.13E-02), chaperonin-containing T-complex (FDR: 3.59E-02), cytoplasmic stress granule (FDR: 1.08E-03), and P-body (FDR: 1.62E-02). This adds further support to our observations in **Chapter 4**, suggesting that TIRR has many previously uncharacterised roles in RNA metabolism and RNA regulatory processes.

Aside from many known TIRR interactors from previously published datasets (**Figure 5.2**), and from our AP-MS data (**Table 5.2**), many novel TIRR interactors/proteins in proximity were identified by TurboID in non-damage conditions, including CNOT8, UPF1, TASOR,

SNRPD2, PPP1R15B, KEAP1, EIF4B, GIGYF2, and EDC3. Therefore, TurboID may be advantageous in identifying previously unknown functions of TIRR (**Section 5.4.4**).

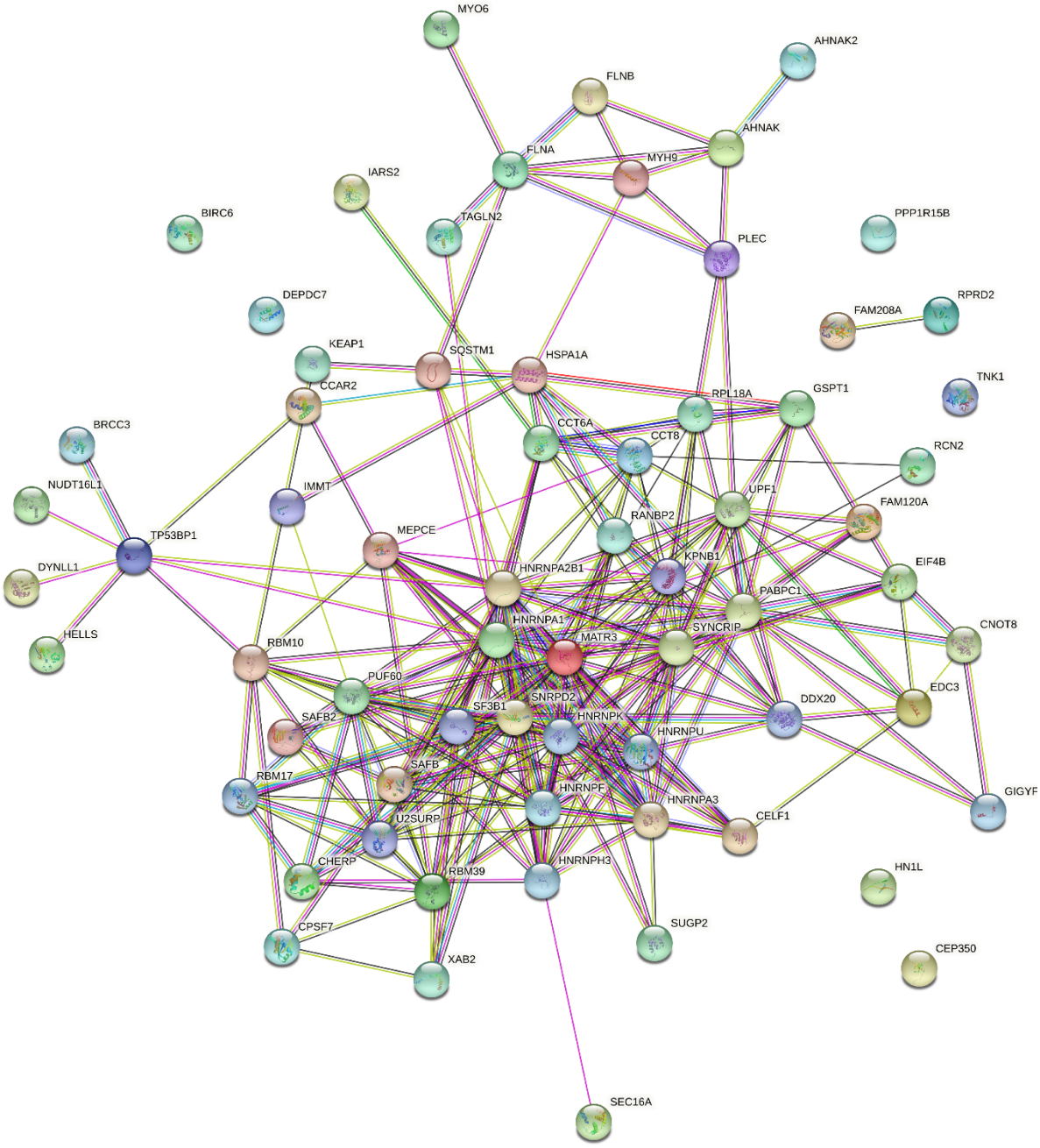


Figure 5.19: *STRING interaction network for proteins identified to interact with TIRR in non-damage conditions (including overlap between non-damage and damage, 67 in total).*

In damage conditions in our TurboID experiment, we identified 23 proteins (not including the overlap from those also identified in non-damage conditions), which are novel interactors of

TIRR in damage conditions. Interestingly, 9 of these 23 proteins have established roles in the DNA damage response and in DSB repair: NONO, XIAP, HNRNPC, LAMA1, NPM1, PRKDC, STAMBPL1, USP28, and ZNF281. STRING analysis also showed a PPI enrichment (p value: 3.01E-07) (**Figure 5.20**). However, GO analysis did not reveal an enrichment of any biological processes, likely due to the small number of queried proteins, but did show an enrichment of the cellular component ribonucleoprotein complex (FDR: 0.00955). Therefore, many novel proteins involved in DNA damage and RNA binding/processing were found in the TIRR interactome after IR.

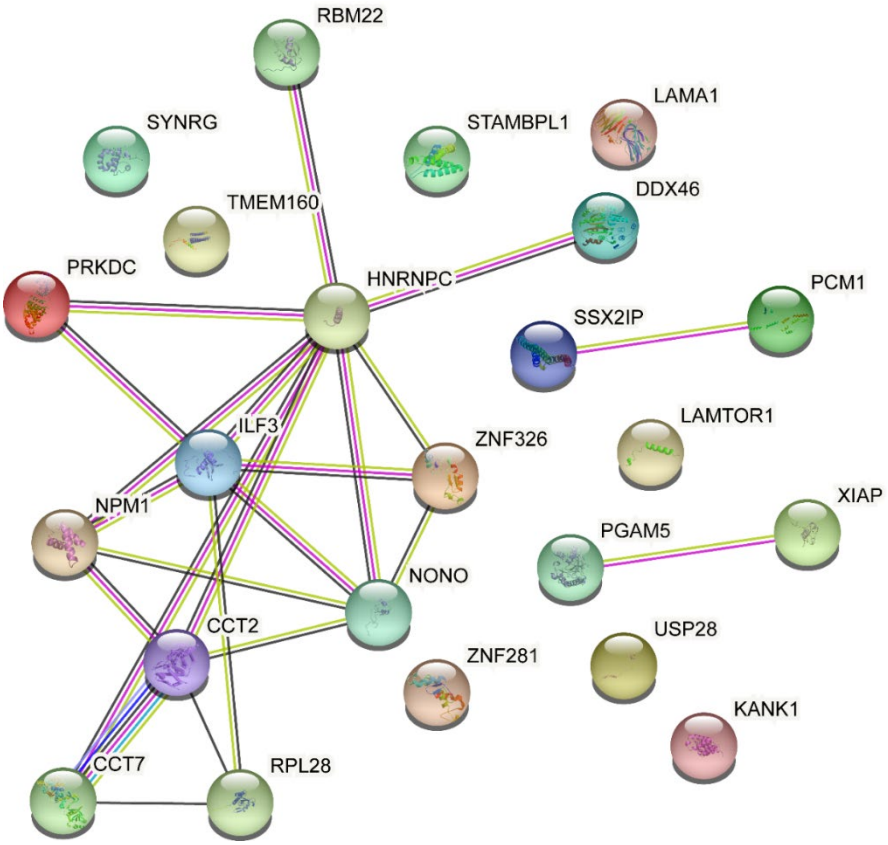


Figure 5.20: *STRING interaction network for proteins identified to interact with TIRR only in damage conditions (23 in total).*

5.4.4 What do the identified binding partners or proteins in proximity tell us about TIRR functions in non-damage and damage?

Whilst the data in this chapter will mainly form the basis of future studies on TIRR, it is apparent that many of the proteins which we identify in both TurboID and AP-MS may help us understand potential mechanisms in which TIRR plays a role, such as DSB repair (**Chapter 3**), and RNA processing (**Chapter 4**).

Many novel TIRR interactors were identified by TurboID in non-damage conditions. In the context of our observations in **Chapter 4**, CNOT8, UPF1, PPP1R15B, EIF4B, GIGYF2, PABPC1, and EDC3 are particularly interesting due to their roles in the regulation of RNA processing and stability. CNOT8 is part of the CCR4-NOT complex and has diverse functions in the regulation of RNA deadenylation and decay/stability[22,23]. In addition, the CCR4-NOT complex can associate with polysomes and regulate translation, and is associated with the repression of translation of RNAs which localise to PBs[22]. CNOT8 may also contribute to nonsense-mediated RNA decay (NMD) through UPF1 mediated recruitment, and the CCR4-NOT complex may regulate RNA export from the nucleus[23]. We also found that another component of the CCR4-NOT complex, CNOT3, was upregulated after TIRR knockdown in non-damage conditions (**Table 4.1**), suggesting TIRR may associate with and/or regulate CCR4-NOT functions. UPF1 is another component of P-bodies and is involved in nonsense-mediated decay of RNAs which contain premature termination codons, although PBs are not necessarily required for NMD[24]. GIGYF2 interacts with the cap binding protein 4EHP and is involved in translational repression of RNA[25]. GIGYF2 can also interact with the CCR4-NOT complex and repress mRNA translation, dependent on the deadenylation activity of CCR4-NOT[25]. GIGYF2 is also involved in NMD and miRNA repression of gene expression[25,26], and is also associated with RNA granules[27]. EDC3 is a decapping activator and is also a core component of P-bodies[28]. Additionally, CREP/PPP1R15B is a subunit of phosphatase PP1,

which regulates the phosphorylation of EIF2A needed for stress granule formation[29] (**Section 4.2**) and EIF4B is part of the translation initiation complex and can localise in SGs[30,31]. Lastly, PABPC1 is a poly(A) tail binding protein binds RNA tails and interacts with 5' RNA ends via proteins involved in translation, such as EIF4G, to form the RNA closed loop needed for translation initiation[32]. PABPC1 is also a key component of stress granules[32]. Taken together, this suggests that TIRR can interact with, or is in close proximity to, many different proteins which play important roles in the regulation of RNA export, translation, stability, and decay. Although it is still not clear exactly where TIRR functions in these pathways and what the role of TIRR is, our interactome data point to a role of TIRR in RNA processing, in agreement with our results in **Chapter 4**.

In addition, it is clear from both previously published datasets (**Figure 5.2**), our AP-MS (**Table 5.2**), and our TurboID data (**Table 5.1**), that TIRR interacts with many different HNRNP proteins, including HNRNPA2B1, HNRNPF, HNRNPH3. The HNRNP family can have a wide variety of functions in RNA regulation, from regulation of transcription and splicing, to RNA export and translation[33]. As the functions of this family of proteins are so broad, and we identify over 10 different HNRNP family members from the union of our AP-MS and TurboID datasets, it is difficult to determine exactly what the function of TIRR is in relation to this family of proteins. However, it is possible that this interaction/proximity is part of the mechanism of TIRR RNA function suggested above and in **Chapter 4**, as many HNRNP proteins, including HNRNPA2B1, HNRNPU, and HNRNPA3, are identified to be part of the RNA granule proteome[27]. Interestingly, the HNRNP protein family has also been implicated widely in the repair of DSBs[14].

Additionally, whilst we did not detect XPO1 in our TurboID analysis, we could identify RANBP2, associated with the nuclear pore complex, which hydrolyses RAN-GTP into RAN-GDP to facilitate XPO1-mediated nuclear export[34]. We could also identify RAN, the binding partner of XPO1, in our AP-MS after DNA damage, although this was below the statistical thresholds. In our AP-MS after damage we can also identify an XPO1-dependent nuclear/cytoplasmic protein ELAVL1/HuR[35], which binds AU-rich element in 3' UTRs and can regulate the export of RNA from the nucleus[35], including after stress[36], and can also localise into SGs[37] (**Section 4.4.4**).

By performing TurboID in damage conditions, we also identified RNA binding proteins as part of the TIRR interactome, including NPM1, RBM22, and DDX46. NPM1 has a wide variety of functions, including in the regulation of ribosomal subunit export from the nucleus[38]. NPM1, as well as being an RNA-binding protein, has also been implicated in the repair of DSBs[39]. We also identified many different proteins with known roles in DNA repair enriched in our TIRR TurboID +IR samples, such as NONO, LAMA1, USP28, and ZNF281. Some of these proteins have also been directly implicated in the regulation or functionality of 53BP1 in DNA damage, such as USP28 and LAMA1[18,20,21]. Therefore, as well as other RNA-binding proteins, TIRR appears to interact with/be in proximity to many proteins involved in 53BP1 regulation and DSB repair after damage.

5.4.5 Future work

Future work looking at the relevance of TIRR interaction partners should integrate findings from **Chapter 3** and **Chapter 4**. Proteins identified in TIRR TurboID include those known to play a role in DSB repair, such as USP28 and NPM1. Understanding if these interactions contribute to 53BP1 regulation would help further expand our understanding of TIRR-mediated 53BP1 regulation, for example, the fate of TIRR after separation from 53BP1.

Additionally, when we look at TIRR interaction partners identified in this chapter, we can see that TIRR interacts with a variety of different RNA binding proteins, including a number which are known to be involved in RNA processing, decay, and regulation of translation, such as CNOT3, GIGYF2, and PABPC1. In addition, many of the identified RNA regulatory proteins are known to be involved in the regulation/formation of RNA granules. This could potentially help illuminate the mechanism behind the observed regulation of SGs and PBs by TIRR seen in **Chapter 4**.

Manual validation of TIRR interactors in damage and non-damage, such as by pull-down and western blot or PLA, is essential for validating the interaction of TIRR with the identified proteins, as a small number of proteins, such as HNRNPC, showed a discrepancy between being -IR or +IR interactors in AP-MS vs TurboID, where HNRNPC was identified as a +IR interactor in TurboID, but both a +IR and a -IR interactor in AP-MS. This should be clarified using manual validation.

Our results presented here could be further expanded upon using variations of the TurboID or AP-MS approaches. Performing mass spectrometry for TIRR interactors in the presence or absence of RNases would allow us to assess if some of these interactions may be RNA-mediated. Similarly, performing mass spectrometry with the 53BP1-binding null TIRR (K10E) would highlight if any of the interactions with TIRR, such as those with DNA damage proteins like USP28, are 53BP1-dependent. It would also be interesting to see if the knockdown of any of the identified proteins of interest, such as the RNA regulatory proteins (**Section 5.4.4**), would impact the TIRR-driven phenotypes, which are presumably related to RNA processing, seen in **Chapter 4**.

We also see that TIRR appears to respond to other types of cell stress, such as oxidative stress which induces stress granules (**Chapter 4**). It would therefore be highly interesting to perform interaction assays with TIRR in different damage/stress conditions. This could be performed low throughput to look at interactors of interest already identified in this chapter, such as by using Co-IP and western blotting, or high throughput by mass spectrometry.

In summary, we identify many novel TIRR interactors in non-damage and damage conditions, which can help expand our understanding of TIRR as both a 53BP1-regulator and a damage-responsive RNA binding protein.

5.5 References

1. Drané, P. *et al.* TIRR regulates 53BP1 by masking its histone methyl-lysine binding function. *Nature* **543**, 211–216 (2017).
2. Mair, A., Xu, S.-L., Branon, T. C., Ting, A. Y. & Bergmann, D. C. Proximity labeling of protein complexes and cell-type-specific organellar proteomes in Arabidopsis enabled by TurboID. *eLife* **8**, e47864 (2019).
3. Xu, Y., Fan, X. & Hu, Y. In vivo interactome profiling by enzyme-catalyzed proximity labeling. *Cell Biosci.* **11**, 27 (2021).
4. Santin, Y. G. Uncovering the In Vivo Proxisome Using Proximity-Tagging Methods. *BioEssays* **41**, 1900131 (2019).
5. Ummethum, H. & Hamperl, S. Proximity Labeling Techniques to Study Chromatin. *Front. Genet.* **11**, 450 (2020).
6. Roux, K. J., Kim, D. I., Raida, M. & Burke, B. A promiscuous biotin ligase fusion protein identifies proximal and interacting proteins in mammalian cells. *J. Cell Biol.* **196**, 801–810 (2012).
7. Branon, T. C. *et al.* Efficient proximity labeling in living cells and organisms with TurboID. *Nat. Biotechnol.* **36**, 880–887 (2018).
8. Avolio, R. *et al.* Protein Syndesmos is a novel RNA-binding protein that regulates primary cilia formation. *Nucleic Acids Res.* **46**, 12067 (2018).
9. Kim, D. I. *et al.* An improved smaller biotin ligase for BioID proximity labeling. *Mol. Biol. Cell* **27**, (2016).
10. Cho, K. F. *et al.* Proximity labeling in mammalian cells with TurboID and split-TurboID. *Nat. Protoc.* **15**, 3971–3999 (2020).
11. May, D. G., Scott, K. L., Campos, A. R. & Roux, K. J. Comparative Application of BioID and TurboID for Protein-Proximity Biotinylation. *Cells* **9**, (2020).
12. Cremona, M. *et al.* BRCA mutations lead to XIAP overexpression and sensitise ovarian cancer to inhibitor of apoptosis (IAP) family inhibitors. *Br. J. Cancer* **127**, 488–499 (2022).
13. Salton, M., Lerenthal, Y., Wang, S.-Y., Chen, D. J. & Shiloh, Y. Involvement of Matrin 3 and SFPQ/NONO in the DNA damage response. *Cell Cycle* **9**, 1568–1576 (2010).
14. Klaric, J. A., Wüst, S. & Panier, S. New Faces of old Friends: Emerging new Roles of RNA-Binding Proteins in the DNA Double-Strand Break Response. *Front. Mol. Biosci.* **8**, 668821 (2021).
15. Koike, A. *et al.* Recruitment of Phosphorylated NPM1 to Sites of DNA Damage through RNF8-Dependent Ubiquitin Conjugates. *Cancer Res.* **70**, 6746–6756 (2010).
16. Yu, H. *et al.* Tumor suppressor and deubiquitinase BAP1 promotes DNA double-strand break repair. *Proc. Natl. Acad. Sci.* **111**, 285–290 (2014).
17. Nicolai, S. *et al.* ZNF281 is recruited on DNA breaks to facilitate DNA repair by non-homologous end joining. *Oncogene* **39**, 754–766 (2020).
18. Gibbs-Seymour, I., Markiewicz, E., Bekker-Jensen, S., Mailand, N. & Hutchison, C. J. Lamin A/C-dependent interaction with 53BP1 promotes cellular responses to DNA damage. *Aging Cell* **14**, 162–169 (2015).
19. Etourneaud, L. *et al.* Lamin B1 sequesters 53BP1 to control its recruitment to DNA damage. *Sci. Adv.* **7**, eabb3799 (2021).
20. Cuella-Martin, R. *et al.* 53BP1 Integrates DNA Repair and p53-Dependent Cell Fate Decisions via Distinct Mechanisms. *Mol. Cell* **64**, 51–64 (2016).
21. Parnandi, N. *et al.* TIRR inhibits the 53BP1-p53 complex to alter cell-fate programs. *Mol. Cell* **81**, (2021).
22. Gillen, S. L. *et al.* Differential regulation of mRNA fate by the human Ccr4-Not complex is driven by coding sequence composition and mRNA localization. *Genome Biol.* **22**, 284 (2021).
23. Chalabi Hagkarim, N. & Grand, R. J. The Regulatory Properties of the Ccr4–Not Complex. *Cells* **9**, 2379 (2020).
24. Stalder, L. & Mühlemann, O. Processing bodies are not required for mammalian nonsense-mediated mRNA decay. *RNA N. Y. N* **15**, 1265–1273 (2009).
25. Amaya Ramirez, C. C., Hubbe, P., Mandel, N. & Béthune, J. 4EHP-independent repression of endogenous mRNAs by the RNA-binding protein GIGYF2. *Nucleic Acids Res.* **46**, 5792–5808 (2018).
26. Zinshteyn, B., Sinha, N. K., Enam, S. U., Koleske, B. & Green, R. Translational repression of NMD targets by GIGYF2 and EIF4E2. *PLOS Genet.* **17**, e1009813 (2021).
27. Youn, J.-Y. *et al.* Properties of Stress Granule and P-Body Proteomes. *Mol. Cell* **76**, 286–294 (2019).
28. Decker, C. J., Teixeira, D. & Parker, R. Edc3p and a glutamine/asparagine-rich domain of Lsm4p function in processing body assembly in Saccharomyces cerevisiae. *J. Cell Biol.* **179**, 437–449 (2007).
29. Moujaber, O. *et al.* Dissecting the molecular mechanisms that impair stress granule formation in aging cells. *Biochim. Biophys. Acta Mol. Cell Res.* **1864**, 475–486 (2017).
30. Decker, C. J. & Parker, R. P-bodies and stress granules: possible roles in the control of translation and mRNA degradation. *Cold Spring Harb. Perspect. Biol.* **4**, a012286 (2012).
31. Buchan, J. R. & Parker, R. Eukaryotic stress granules: the ins and outs of translation. *Mol. Cell* **36**, 932–941 (2009).

32. Burgess, H. M. & Gray, N. K. An integrated model for the nucleo-cytoplasmic transport of cytoplasmic poly(A)-binding proteins. *Commun. Integr. Biol.* **5**, 243–247 (2012).
33. Geuens, T., Bouhy, D. & Timmerman, V. The hnRNP family: insights into their role in health and disease. *Hum. Genet.* **135**, 851–867 (2016).
34. Azmi, A. S., Uddin, M. H. & Mohammad, R. M. The nuclear export protein XPO1 — from biology to targeted therapy. *Nat. Rev. Clin. Oncol.* **18**, 152–169 (2021).
35. Delaleau, M. & Borden, K. L. B. Multiple Export Mechanisms for mRNAs. *Cells* **4**, 452–473 (2015).
36. Gallouzi, I. E., Brennan, C. M. & Steitz, J. A. Protein ligands mediate the CRM1-dependent export of HuR in response to heat shock. *RNA N. Y. N* **7**, 1348–1361 (2001).
37. David, P. S., Tanveer, R. & Port, J. D. FRET-detectable interactions between the ARE binding proteins, HuR and p37AUF1. *RNA N. Y. N* **13**, 1453–1468 (2007).
38. Maggi, L. B. *et al.* Nucleophosmin Serves as a Rate-Limiting Nuclear Export Chaperone for the Mammalian Ribosome. *Mol. Cell. Biol.* **28**, 7050–7065 (2008).
39. Box, J. K. *et al.* Nucleophosmin: from structure and function to disease development. *BMC Mol. Biol.* **17**, 19 (2016).

Chapter 6: Overall discussion and perspectives

6.1 A diverse array of different RNAs and RNA binding proteins can function in the DNA damage response

A diverse and highly regulated network of RNAs and RNA binding proteins has a profound influence on dynamic regulatory processes. The pool of RNA within a cell is vast, with many different classes of RNA existing in human cells. The population of RNAs includes: the highly abundant ribosomal RNAs, of which there are only a few species, but contribute around 80% of the total RNA within cells, mRNA, of which there are estimated to be over 20,000 different species (comprising around 5% of total cellular RNA), lncRNAs, of which there are tens of thousands (<2% of total RNAs), and shorter RNAs such as miRNA which also number around 1000 (<2%), amongst many others[1]. RNAs exert their functions in cells largely through interactions with many different RNA binding proteins, with over 1000-2000 proteins estimated to have RNA binding functionality[1,2], around ~8% of the proteome[2]. The diversity in the number of RNA transcripts, the sequence of the RNA, RNA structures, and regulation of both RNA-RNA and RNA-protein interactions, confers specific functions of RNA[1]. The complexity of the RNA pool can be even further extended, by the modification of RNA bases, such as m^6A and m^5C, influencing RNA stability, localisation, and interactions with RNA binding proteins[3]. New functions of RNAs are constantly emerging, from RNA *de novo* transcribed at DSBs[4–6], to the striking discovery of RNA on the surface of cells[7,8].

Many proteins involved in RNA processing, such as RNA transcription, export, splicing, and translation, have been identified in genome wide screens as regulators of DNA repair and genome stability, including in the regulation of HR repair[9], in the regulation of genome stability as measured by γH2AX induction[10], and as phosphorylation targets of ATM/ATR after IR[11].

Increasingly, RNA binding proteins are emerging as important factors influencing DNA repair, and conversely, proteins which were considered 'core' DNA repair factors are now been identified to have RNA-binding functionality[12]. An example of such a protein is DDX1. DDX1 is an RNA-binding protein which binds to and stabilises an array of RNAs involved in cell stress responses and DNA damage. DDX1 is localised into stress granules after oxidative and ER stress and contributes to their resolution/disassembly[13]. In response to DNA DSBs, DDX1 is also localised to sites of DNA damage[14]. In fact, simultaneous exposure of cells to IR and sodium arsenite results in localisation of DDX1 at both ɣH2AX foci in the nucleus and stress granules in the cytoplasm[13]. At DSBs, DDX1 functions to remove RNA:DNA hybrids formed at resected DNA ends to promote HR and is important for survival after IR[14]. Therefore, DDX1 displays dual functionality in both RNA stability regulation in the cytoplasm and DSB repair in the nucleus. Furthermore, NUDT16, previously characterised as a protein functioning mainly in U8 snoRNA and mRNA decapping and IDP/ITP hydrolysis[15,16], is now also known to function in the promoting 53BP1 stability, by removing ADP-ribosylation on 53BP1 after IR[17]. In addition, RBMX/HNRNPG, a protein which was identified as a TIRR interactor in our AP-MS (**Table 5.2**), is an RNA binding protein which plays a role in RNA splicing through recognition of m^6A modified RNA[18], and has also been characterised as a protein which is recruited to DSBs and promotes HR-mediated DSB repair[9,12]. It is therefore apparent that the regulation of DNA repair and RNA processing are closely linked, with many proteins acting in both pathways.

6.2 Summary of experimental findings

In this thesis, we work towards characterising the role of RNA in the separation of TIRR and 53BP1 after DSBs, as well as further exploring the significance of TIRR as an RNA binding protein in the wider response to DNA damage and cell stress.

In **Chapter 3**, we find that RNA derived from DNA DSBs, transcribed by RNAPII, contributes to the dissociation of 53BP1 and TIRR after DSBs. This RNA appears to originate from the DSB sites themselves, and the formation of RNA secondary structure, namely an RNA hairpin, was influential in TIRR and 53BP1 dissociation. We suggest that this dissociation occurs in proximity to the break, with TIRR and 53BP1 both recruited to DSBs likely as a complex, dependent on RNAPII transcription. We also find that Dicer and Drosha, independently of their miRNA processing roles, are needed for dissociation, although the exact mechanistic details of this are as yet unclear. We also show through modelling and molecular dynamics simulations that RNA binding to TIRR would be incompatible with 53BP1 binding, suggesting a direct competition between RNA and 53BP1 for TIRR binding. We also show that TIRR is important for repair of DSBs by HR, as the knockdown of TIRR impairs HR.

In **Chapter 4**, we further characterise the RNA binding function of TIRR in response to DSBs, finding that TIRR can bind to many different RNAs, including those involved in RNAPII transcription regulation. We also find that TIRR can localise to RNA granules and regulate their formation. Firstly, TIRR can localise to P-bodies, and the overexpression of TIRR enhances PB formation. In response to DNA damage, TIRR knockdown also results in an increase in PB numbers, indicating that TIRR is both a component of PBs and can also influence their formation under DNA damage conditions. Additionally, we see that TIRR can localise to stress granules and promote their formation in response to sodium arsenite stress.

We also identified a nuclear export sequence in TIRR, and find that TIRR can interact with XPO1 after DNA damage. Although the mechanism of this interaction requires further validation, we speculate that TIRR may localise specific RNAs into RNA granules to either regulate their translation or stability.

In **Chapter 5**, we establish a TurboID system to study TIRR interactors in non-damage and damage conditions. We find that TIRR interacts with a connected network of RNA binding proteins and DNA repair factors, some of which have known roles in 53BP1 regulation or in the regulation of RNA processing. This raises the interesting possibility that the proteins identified in our TurboID may contribute to the regulatory properties of TIRR.

6.3 Remaining Questions

Although most outstanding questions relating to this work are addressed in Chapters 3, 4, and 5, some overarching questions regarding the regulation of TIRR in response to DNA damage remain.

A particularly interesting question pertains to the coordination between TIRR binding to 53BP1 vs TIRR binding to RNA. The binding of RNA to TIRR is incompatible with 53BP1 binding, and we know that in non-damage conditions TIRR exists which is bound to RNA, and therefore there must be distinct populations of RNA-bound and 53BP1-bound TIRR. Additionally, TIRR can localise both within the nucleus and the cytoplasm. The TIRR and 53BP1 interaction is entirely nuclear[19], while it is unknown if RNA bound TIRR exists in both the nucleus or the cytoplasm, or both. We assume that TIRR bound to RNA exists in both cellular compartments, although this is an interesting point for future studies. Nevertheless, understanding the regulation of how a certain portion of TIRR is directed for 53BP1 binding, while another population is free to bind and regulate RNA, will be important to fully understand the coordination of TIRR in response to DNA damage.

One possibility which we considered is that TIRR may be post-translationally modified, which could influence the ability of TIRR to localise to certain cellular compartments, or to bind RNA for example. When we look at the Eukaryotic Linear Motif resource[20], which we used to identify a NES motif in TIRR, we see that TIRR contains a number of other motifs. This includes an S/TQ motif for ATM/ATR phosphorylation at residues 146-152, as well as a number of other potential phosphorylation sites for other kinases (data not shown). TIRR is also constitutively ubiquitinated[19], although the relevance of this is not understood. Using our AP-MS dataset, we tried to identify if TIRR may contain any PTMs, specifically

phosphorylation, ubiquitination, and methylation, however we were unable to detect any modifications on TIRR (data not shown). Nevertheless, it is possible that more sensitive methods to detect PTMs may need to be employed, such as gel extraction of TIRR rather than an affinity pull-down, or expansion of the analysis for a wider range of modifications.

Furthermore, to the best of our knowledge, this RNA-mediated dissociation of TIRR and 53BP1 represents a new functionality of RNA transcribed at DSBs. It is therefore interesting to speculate that RNA, including DSB-derived RNAs, may perform this function in regulating other protein-protein interactions. Some examples of conceptually similar 'competition' functionality of RNA at DSBs include the lncRNA PRLH1, which binds to RNF169 to prevent 53BP1 chromatin binding[21], or the binding of scaRNA2 to DNA-PKc, reducing the interaction with Ku70 and the formation of the DNA-PK complex[22] (**Section 1.5.2**). However, a direct competition function of RNA derived from DSBs in separating a protein-protein interaction has not previously been described, and could potentially be a more widespread function of DSB-derived RNA.

Moreover, while we see that TIRR can bind to different RNAs, and regulate the formation of RNA granules, questions still remain regarding what the function of TIRR binding to RNA is and how does this influence RNA fate? Does TIRR function in regulating RNA stability like NUDT16, albeit without a catalytic role, or through other mechanisms, such as regulating the levels of proteins involved in RNA processing and stability, a possibility which arises from our WCL mass spectrometry analysis? We speculate that TIRR may play a role in translation, RNA stability, or decay, however further experiments, such as those discussed in **Section 4.4.7**, are needed to define the exact role of TIRR in RNA processing. Other questions which arise from this work include; is RNA binding to TIRR a prerequisite for RNA granule localisation? We

expect that TIRR binding to RNA is important for its RNA granule localisation, however not every protein requires RNA binding for localisation to granules. For example, DDX1 RNA binding is not required for DDX1 localisation to SGs[13]. It would also be interesting to further explore if TIRR binds particular RNA structural motifs or sequences. We found that TIRR can bind to both hairpin and ssRNA, and the dissociation of TIRR and 53BP1 appeared to be independent of RNA sequence and rely more on RNA structure, so it would be interesting to see if the RNA which TIRR binds contains certain structural motifs.

Finally, can TIRR also contribute to the repair of DSBs through a separate RNA binding/processing function, not just through RNA-mediated 53BP1 regulation? We see that the depletion of TIRR impairs HR using reporter constructs (**Figure 3.21**), which we mainly attribute to 53BP1 regulation, however it is certainly possible that TIRR could contribute to DSB repair through other functions, which would be addressed by performing rescue experiments with TIRR mutants.

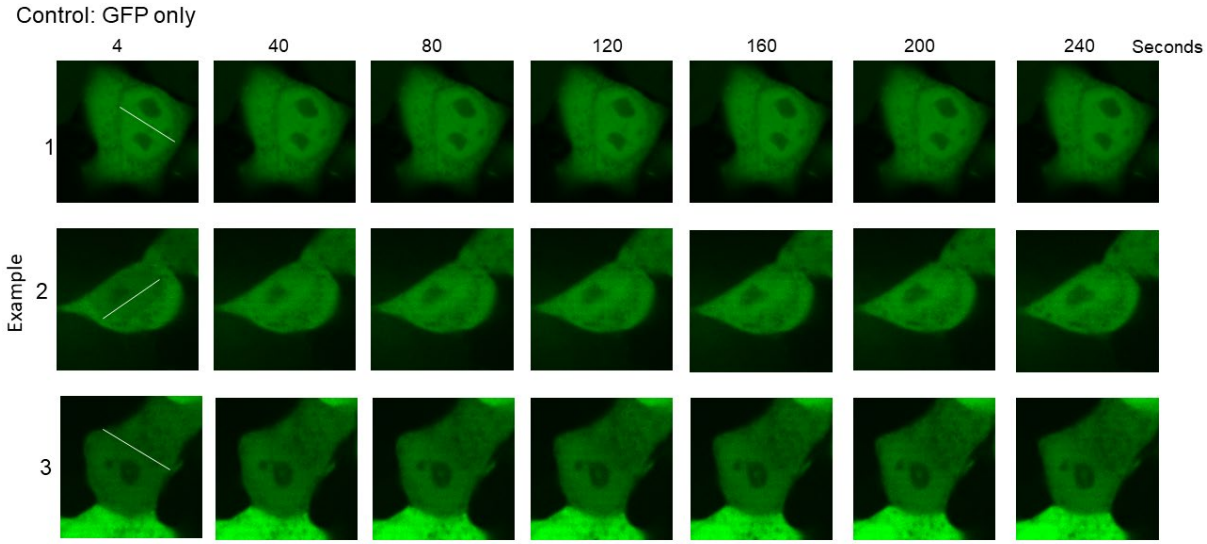
6.4 Final remarks

Overall, this thesis identifies a role for RNA in the regulation of TIRR and 53BP1, and further explores a role for TIRR in RNA processing in response to DNA damage. Understanding exactly how TIRR acts in these processes has therapeutic implications, as TIRR is frequently amplified in breast cancers (**Section 3.4.8**), and has been implicated in the development of PARP inhibitor resistance[19]. Additionally, cancer cells also experience high levels of cell stress, such as ER stress, and RNA granules may be implicated in cancer progression, and have been found to form in response to various chemotherapeutic agents[23]. Therefore, understanding the mechanism of TIRR regulation of both 53BP1 and RNA processing has important implications in our understanding of the mechanism of cancer progression and provides new avenues for the development of anticancer therapies.

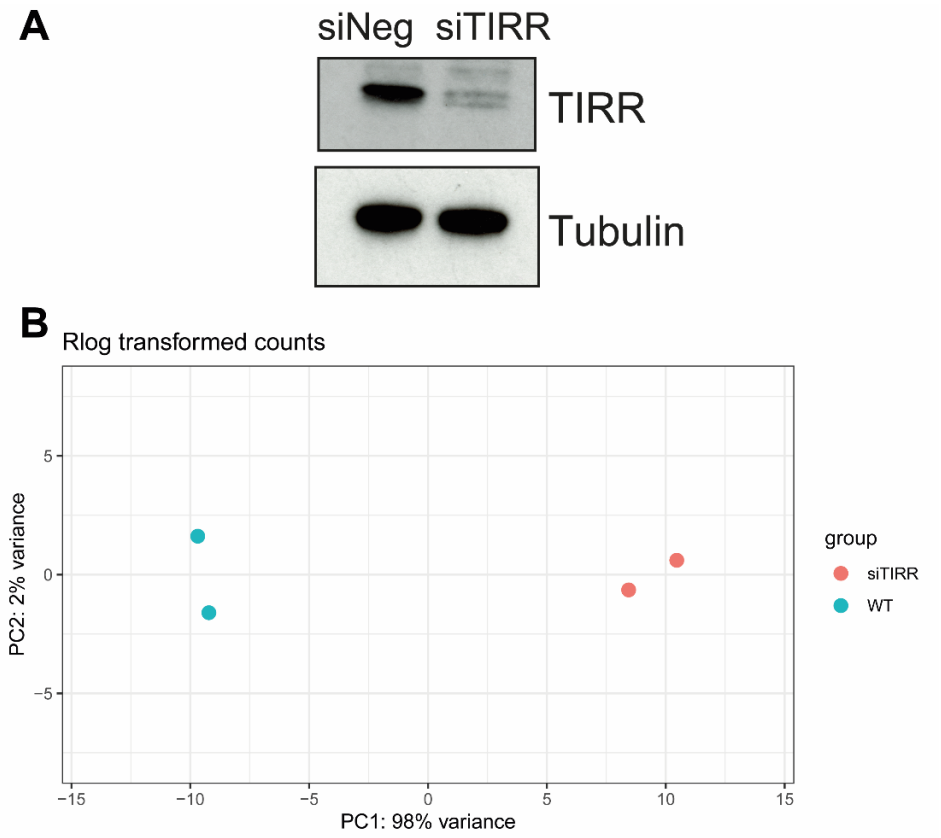
6.5 References

1. Jankowsky, E. & Harris, M. E. Specificity and nonspecificity in RNA-protein interactions. *Nat. Rev. Mol. Cell Biol.* **16**, (2015).
2. Balcerak, A., Trebinska-Stryjewska, A., Konopinski, R., Wakula, M. & Grzybowska, E. A. RNA-protein interactions: Disorder, moonlighting and junk contribute to eukaryotic complexity. *Open Biol.* **9**, (2019).
3. Ketley, R. F. & Gullerova, M. Jack of all trades? The versatility of RNA in DNA double-strand break repair. *Essays Biochem.* **64**, 721–735 (2020).
4. Bonath, F., Domingo-Prim, J., Tarbier, M., Friedländer, M. R. & Visa, N. Next-generation sequencing reveals two populations of damage-induced small RNAs at endogenous DNA double-strand breaks. *Nucleic Acids Res.* **46**, (2018).
5. Michelini, F. *et al.* Damage-induced lncRNAs control the DNA damage response through interaction with DDRNAs at individual double-strand breaks. *Nat. Cell Biol.* **19**, 1400–1411 (2017).
6. Burger, K., Schlackow, M. & Gullerova, M. Tyrosine kinase c-Abl couples RNA polymerase II transcription to DNA double-strand breaks. *Nucleic Acids Res.* (2019) doi:10.1093/nar/gkz024.
7. Huang, N. *et al.* Natural display of nuclear-encoded RNA on the cell surface and its impact on cell interaction. *Genome Biol.* **21**, 225 (2020).
8. Flynn, R. A. *et al.* Small RNAs are modified with N-glycans and displayed on the surface of living cells. *Cell* **184**, 3109-3124.e22 (2021).
9. Adamson, B., Smogorzewska, A., Sigoillot, F. D., King, R. W. & Elledge, S. J. A genome-wide homologous recombination screen identifies the RNA-binding protein RBMX as a component of the DNA-damage response. *Nat. Cell Biol.* **14**, 318–328 (2012).
10. Paulsen, R. D. *et al.* A genome-wide siRNA screen reveals diverse cellular processes and pathways that mediate genome stability. *Mol. Cell* **35**, 228–239 (2009).
11. Matsuoka, S. *et al.* ATM and ATR Substrate Analysis Reveals Extensive Protein Networks Responsive to DNA Damage. *Science* **316**, 1160–1166 (2007).
12. Klaric, J. A., Wüst, S. & Panier, S. New Faces of old Friends: Emerging new Roles of RNA-Binding Proteins in the DNA Double-Strand Break Response. *Front. Mol. Biosci.* **8**, 668821 (2021).
13. Li, L., Garg, M., Wang, Y., Wang, W. & Godbout, R. DEAD box 1 (DDX1) protein binds to and protects cytoplasmic stress response mRNAs in cells exposed to oxidative stress. *J. Biol. Chem.* **298**, 102180 (2022).
14. Li, L. *et al.* DEAD Box 1 Facilitates Removal of RNA and Homologous Recombination at DNA Double-Strand Breaks. *Mol. Cell. Biol.* **36**, 2794–2810 (2016).
15. Iyama, T., Abolhassani, N., Tsuchimoto, D., Nonaka, M. & Nakabeppu, Y. NUDT16 is a (deoxy)inosine diphosphatase, and its deficiency induces accumulation of single-strand breaks in nuclear DNA and growth arrest. *Nucleic Acids Res.* **38**, (2010).
16. Lu, G. *et al.* hNUDT16: A universal decapping enzyme for small nucleolar RNA and cytoplasmic mRNA. *Protein Cell* **2**, 64–73 (2011).
17. Zhang, F. *et al.* Nudix hydrolase NUDT16 regulates 53BP1 protein by reversing 53BP1 ADP-ribosylation. *Cancer Res.* canres.2205.2019 (2020) doi:10.1158/0008-5472.can-19-2205.
18. Zhou, K. I. *et al.* Regulation of Co-transcriptional Pre-mRNA Splicing by m6A through the Low-Complexity Protein hnRNPG. *Mol. Cell* **76**, 70-81.e9 (2019).
19. Drané, P. *et al.* TIRR regulates 53BP1 by masking its histone methyl-lysine binding function. *Nature* **543**, 211–216 (2017).
20. Van Roey, K. *et al.* Short Linear Motifs: Ubiquitous and Functionally Diverse Protein Interaction Modules Directing Cell Regulation. *Chem. Rev.* **114**, 6733–6778 (2014).
21. Deng, B. *et al.* An LTR retrotransposon-derived lnc RNA interacts with RNF 169 to promote homologous recombination. *EMBO Rep.* **20**, (2019).
22. Bergstrand, S. *et al.* Small Cajal body-associated RNA 2 (scaRNA2) regulates DNA repair pathway choice by inhibiting DNA-PK. *Nat. Commun.* **13**, 1015 (2022).
23. Anderson, P., Kedersha, N. & Ivanov, P. Stress granules, P-bodies and cancer. *Biochim. Biophys. Acta* **1849**, 861–870 (2015).

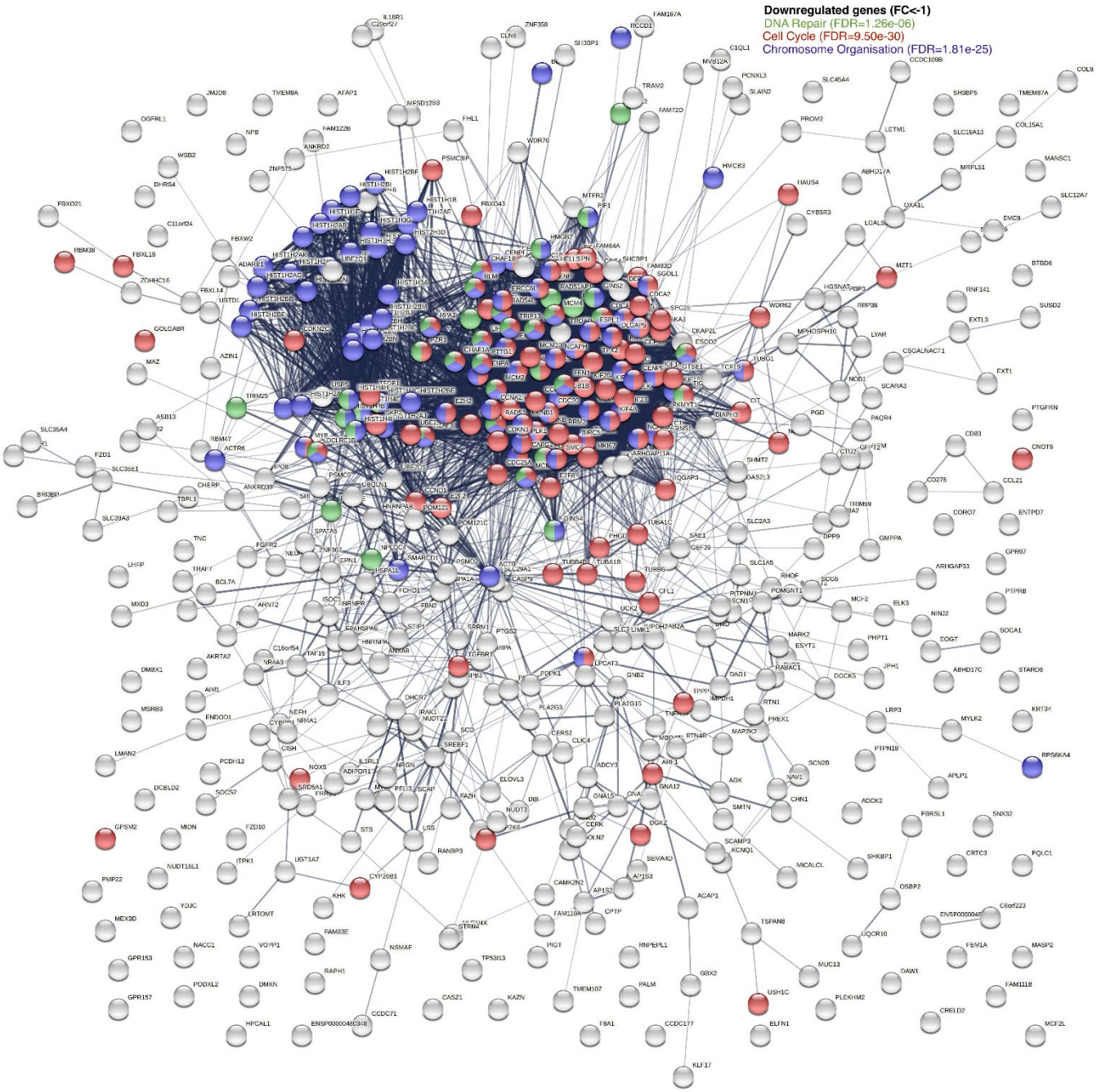
Appendix



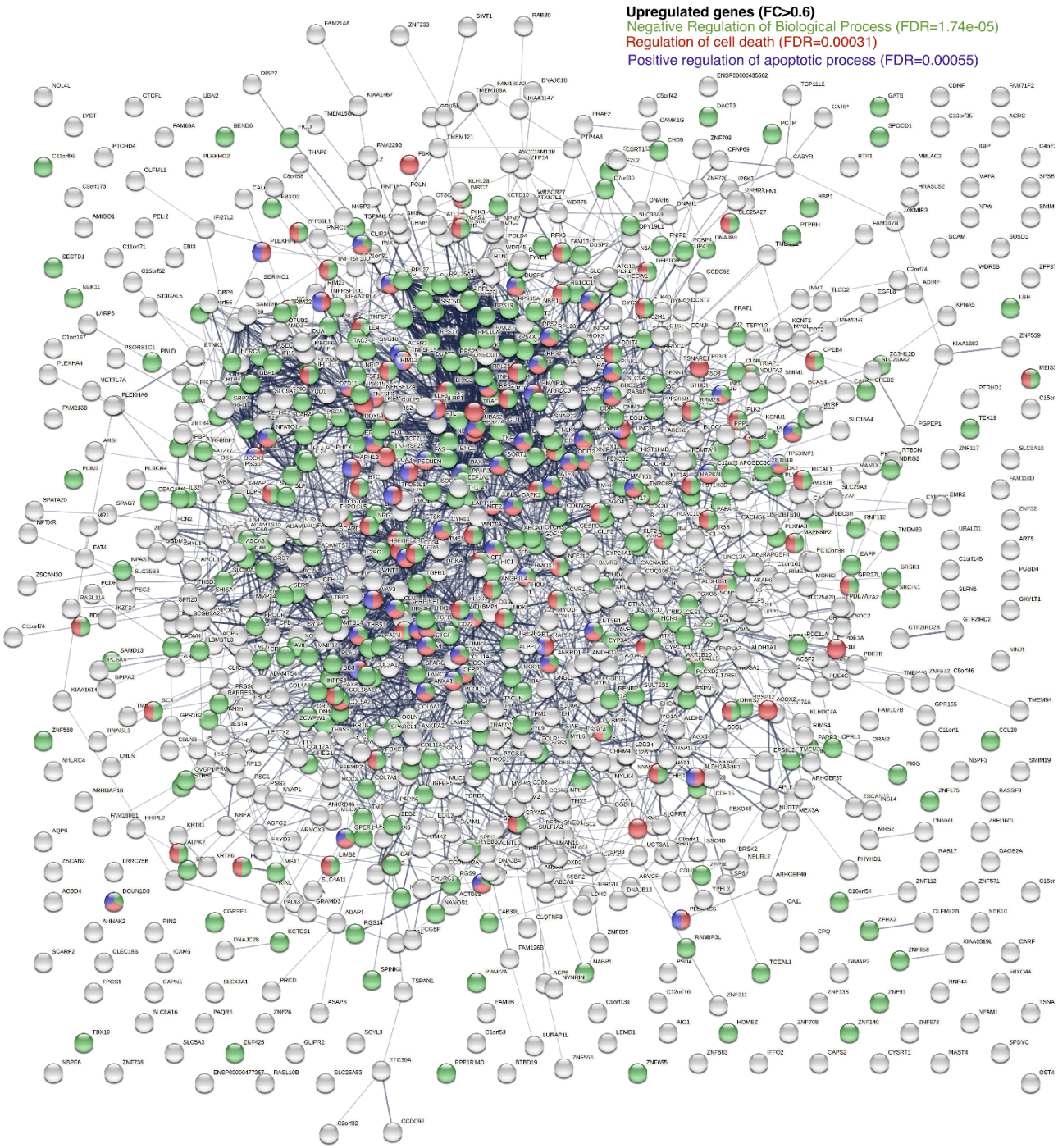
Appendix Figure 1: *Control for live laser striping using doxycycline inducible Hela cells expressing GFP only.*



Appendix Figure 2: ***A)*** *Western blot showing knockdown of TIRR using Thermo siRNA for RNA-Seq.* ***B)*** *PCA plot of siNeg (WT) control samples and TIRR knockdown (Thermo siRNA) samples in RNA-Seq.*



Appendix Figure 3: *STRING analysis on downregulated RNAs in siTIRR (Thermo) RNA-Seq. GO analysis showed significant enrichment of Biological processes including DNA repair (highlighted in green), Cell Cycle (Red), and Chromosome organisation (blue).*



Appendix Figure 4: *STRING analysis on upregulated RNAs in siTIRR (Thermo) RNA-Seq. GO analysis showed significant enrichment of Biological Processes including negative regulation of biological process (highlighted in green), regulation of cell death (Red), and positive regulation of apoptotic process (blue).*